Jefferson Laboratory

Physics Division

Annual Report

April, 2001

Contents

1 Hall A

1.1 Hall A Overview

Commissioning of Hall A began in May 1997 and by the end of 2000 sixteen experiments have been completed. Five of those experiments were completed during 2000: E89-044, E93-049, E91-011, E97-111 and E99-007. E89-044 investigated the single nucleon structure of ^{3}He via separation of the longitudinal (R_L), transverse (R_T) and interference (R_{LT}) response functions in the reaction $^3He(e,e'p)$ at high momenta using "perpendicular" kinematics, the four-momentum transfer dependence of R_T and R_L in "parallel" kinematics and two-nucleon correlations in the continuum region. E93-049 used the polarization transfer technique to search for medium modifications of the proton elastic form factors in the reaction $^4He(\vec{e},e'\vec{p})^3He$ as a function of four-momentum transfer and missing momentum. E91-011 also used the polarization transfer technique to study the transition $p \to \Delta$ and characterize the deviations from a spherically symmetric Δ wavefunction. E97-111 searched for short-range correlations in the reaction $^4He(e,e'p)^3He$, and E99-007 measured the ratio of the proton electric to magnetic elastic form factors up to a four-momentum transfer of 5.6 $(GeV/c)^2$ via the polarization transfer technique. For E99-007, it was required to interchange the detector packages of the two Hall A High Resolution spectrometers so that the focal plane polarimeter would be located in the spectrometer and be capable of reaching the highest momentum ($\sim$ 4 Gev/c).

Both the Møller and the Compton polarimeters were used during the year 2000 by those experiments which used the polarization transfer technique for their measurements. Both polarimeters were also involved in a special program of simultaneous polarization measurements (so called "spin dance") by all five polarimeters at JLab (the two Hall A polarimeters, a Møller polarimeter in each of Hall B and C, and a Mott polarimeter at the injector). The goal of the program was to cross-calibrate the polarimeters and to obtain additional information on the beam energy. The results from the Hall A polarimeters were consistent with the results from the other polarimeters. During the year 2000, a new and a more precise method to measure the magnetization of the ferromagnetic foil used as the target in the Møller polarimeter was also developed.

Both the “Ep” and the “ARC” energy measurement systems were used by the experiments to determine the incident beam energy. Over the range from 600 MeV to above 5 GeV, the “ARC” system has a total error of $\pm 0.02\%$. Measurements by the “Ep” and “ARC” systems agree within $\pm$ 0.03% except around 3 GeV (0.15%). The disagreement is very likely due to an incorrectly positioned/measured ($\sim$ 200 μm error) silicon microstrip in the “Ep” electron detector subsystem.

Optics calibration data accumulated over the past few years have been used to calibrate the two Hall A High Resolution spectrometers over their complete momentum ranges. Resolutions close to the spectrometer design values have been achieved (i.e. the momentum resolution is 0.02% (FWHM)). Both spectrometers are capable of measuring absolute momenta to the 0.05% level.

In terms of new experimental equipment, a stand alone lead-glass calorimeter was built and used by experiment E99-007 to detect the scattered electrons. Two “diffuse” aerogel Čerenkov counters were also built for experiments to be performed in early 2001. The design and/or construction of several major pieces of equipment also proceeded well: (a) Ring Imaging Čerenkov (RICH) counter (to be used in 2001), (b) stand-alone Real Compton calorimeter, (c) septum magnets and related support hardware (i.e. cryogenics transfer lines and support platforms), and (d) the detector system and support platform of a third magnetic spectrometer for Hall A (so-called “ Big Bite”).

In summary, Hall A has been running efficiently since 1997 and it has a broad physics program covering the nucleon, few-body and transition electromagnetic form factors, electroweak form factors, few-body systems and heavier nuclei. The user collaboration is very active with many invited talks and numerous conference contributions. Publication of experimental results is coming along well.

1.2 E89-003

A Study of the Quasielastic $(e, e'p)$ Reaction in ^{16}O at High Recoil Momenta
W. Bertozzi, R. Lourie, A. Saha, L. Weinstein, and the Hall A Collaboration

1.2.1 Introduction

Exclusive and semi-exclusive quasielastic $(e, e'p)$ knockout reactions have been used successfully to study both nuclear structure and reaction mechanisms. In general, the single-particle aspect of nuclear structure was studied using valence-proton removal, while other aspects of the structure and the reaction mechanism were studied at higher missing energies. Unfortunately, the theories used to describe these two regions are very different. Hence, in our present understanding, the regions are related mainly by the transfer of valence strength to higher missing energies [Mu94].

^{16}O has long been a favorite nucleus for theorists, and thus, it has been investigated extensively. The knockout of $1p$-shell protons in ^{16}O$(e, e'p)$ was previously studied at Saclay [Be82, Ch91], NIKHEF [Sp93, Le94], and Mainz [Bl95] at $Q^2 < 0.4$ (GeV/c)^2. Kelly demonstrated that there are inconsistencies in these data sets, particularly in the normalization of the Mainz data [Ke97], and the values for R_{lt} for the $1p_{3/2}$-state extracted by Spaltro [Ke99]. Not many data are available for ^{16}O$(e, e'p)$ at higher missing energies; however, above the two-nucleon emission threshold, excess transverse strength is observed for many nuclei [Ul87, St88, La90, Du99]. Attempts to explain the data at high-E_{miss} using two-body knockout models [Ta89, Gi97, Ry97] and tensor and short-range correlations [Mu94] fail. Even for quasielastic kinematics, significant contributions from non-single-particle processes are made to the high-E_{miss} cross sections.

1.2.2 Experiment Status

During the summer of 1997, in the first physics experiment performed in Hall A [Be89], the ^{16}O$(e, e'p)$ reaction was used to study nucleon removal from the valence $1p$-shell [Ga00] and the $1s_{1/2}$-state and higher residual excitations [Li00]. The Hall A waterfall target [10] served as a convenient and self-normalizing ^{16}O target. All measurements were made at a fixed four-momentum transfer, $Q^2 = 0.8$ (GeV/c)^2, and in quasielastic kinematics at $\omega = 0.445$ GeV. Cross sections and response functions were measured as a function of missing energy at several different missing momenta up to $P_{\text{miss}} = 345$ MeV/c. This was the first ever response function separation measurement performed on a complex nucleus at large E_{miss} and P_{miss}.

1.2.3 Results

Differential cross sections were measured in perpendicular kinematics for proton removal from the $1p_{1/2}$- and $1p_{3/2}$-states at eight P_{miss} values in the range $-345 < P_{\text{miss}} < +345$ MeV/c (see Fig. 1). The cross section is well-described by fully relativistic DWIA calculations [Ud99] which solve the Dirac equation and include Dirac spinor distortions of both the bound and scattered states. It is also well-described by relativistic DWIA calculations which solve a relativized Schrödinger equation and use the Effective Momentum Approximation (EMA) to include the lower components of the Dirac spinors [Ke99]. However, the EMA breaks down at $P_{\text{miss}} > 275$ MeV/c, and hence the latter calculations are less successful in reproducing the data in this P_{miss} range. Both calculations use the NLSH [Sh93] bound-state wave function which yields values for ^{16}O for the binding and single-particle energies, as well as a charge radius, which are in good agreement with data.

The $R_l + (v_{tt}/v_l)R_{tt}$, R_t, and R_{lt} response functions (see [Ga00]) as well as the left-right asymmetry, A_{lt} (see Fig. 2), were also extracted for the $1p$-shell proton knockout and compared to the relativistic DWIA calculations. The most striking result is a structure in A_{lt} which is predicted and well-reproduced by the calculations only when spinor distortions are fully included. While A_{lt} is very sensitive to this dynamic enhancement of the lower components of the Dirac spinors (especially at $P_{\text{miss}} > 275$ MeV/c), the inclusion of these spinor distortions is also needed to reproduce R_{lt} at $P_{\text{miss}} < 275$ MeV/c. Note that neither DWIA calculation includes contributions from two-body effects such as Meson Exchange Currents (MEC) or Isobar Configurations (IC), or from initial-state correlations. Hence, we conclude that up to a P_{miss} of 345 MeV/c, well above the Fermi-momentum, these effects are not important.

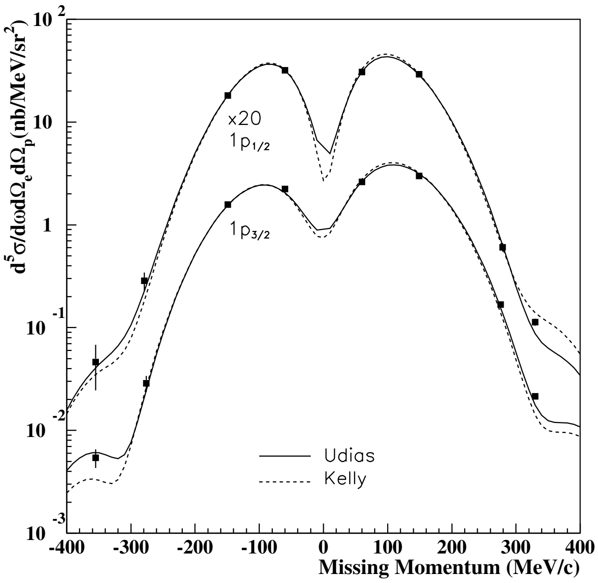

Figure 1: Cross sections for the knockout of $1p$-shell protons from ^{16}O.

The reaction was also studied at higher missing energies. Spectra for $0 < E_{\rm miss} < 120$ MeV were obtained for four missing momenta in the range 50 - 345 MeV/c (see Fig. 3). Also extracted were the R_l and R_t responses for $P_{\rm miss} \approx 60$ MeV/c, and the $R_l + (v_{tt}/v_l)R_{tt}$, R_t, and R_{lt} responses for $P_{\rm miss} = 145$ MeV/c and 280 MeV/c (see [Li00]). The data were compared to the same DWIA calculations [Ke99, Ud00] that successfully predicted the $1p$-shell removal data. These calculations assume the dominance of $1s_{1/2}$-state knockout in the region $20 < E_{\rm miss} < 60$ MeV. The data were also compared to calculations by Ryckebusch *et al.* [Ry88, Ry89, Ry97, Sl97, Ja99] which include a single-particle non-relativistic Hartree-Fock (HF) component which uses the same potential for the bound state and the ejectile nucleon. Ryckebusch also calculated the contributions from both $(e, e'pp)$ and $(e, e'pn)$ due to pion-exchange currents, intermediate $\Delta(1232)$ creation, central short-range correlations, and tensor correlations (see Fig. 3).

These observables are also well-described by all calculations [Ja99, Ke99, Ud00] with a reasonable occupancy in the calculation of Kelly of 0.73. However, at higher $P_{\rm miss}$, the $1s_{1/2}$-state peak is increasingly masked by strength at higher and lower missing energies, and

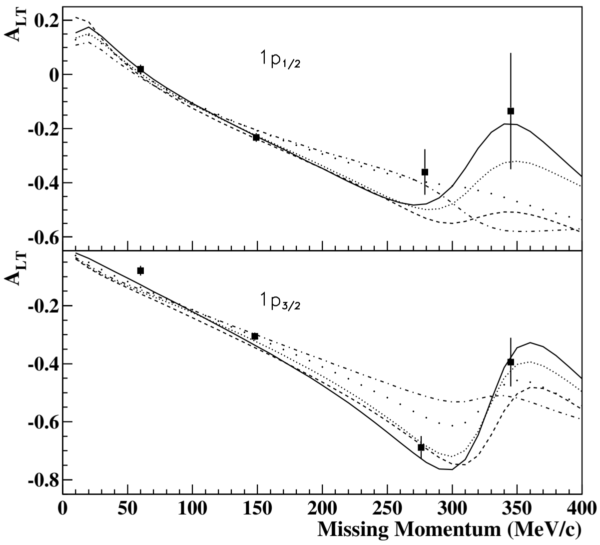

Figure 2: A_{lt} in comparison to DWIA calculations. The dashed line is the Kelly [Ke99] calculation, while all others have been provided by Udias [Ud99]. In particular, the solid line is a fully relativistic calculation, while the densely (loosely) dotted line has only the bound- (scattered-) state spinor distortion included. The dotted-dashed line does not include any spinor distortions, making it essentially identical to factorized calculations.

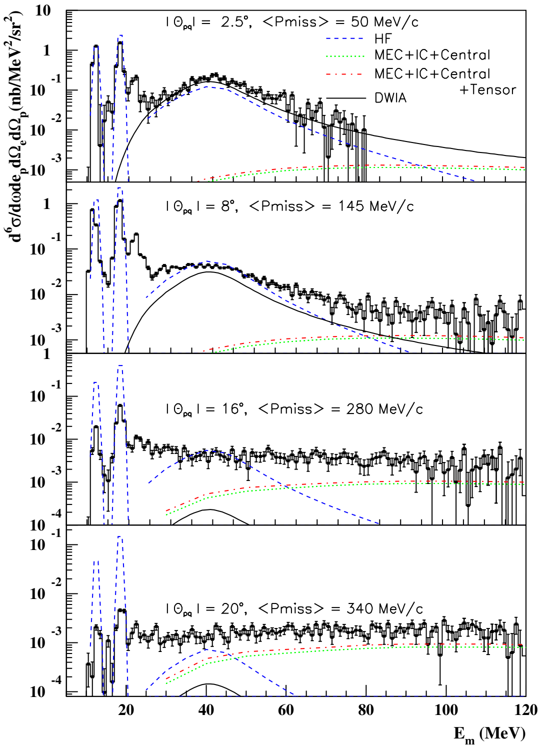

Figure 3: Cross sections for different average values of missing momentum. The solid (dashed) lines represent the Kelly [Ke99] (Ryckebusch *et al.* [Ry88, Ry89, Ry97, Sl97, Ja99]) single-nucleon knockout calculations folded with the Lorentzian parameterization of Mahaux [Je83].

for $P_{\rm miss} > 280$ MeV/c, the missing energy spectrum is completely flat. The $1s_{1/2}$-state peak is decreasingly noticeable with increasing $P_{\rm miss}$ in the measured response functions as well.

Note that the HF calculations of Ryckebusch *et al.* qualitatively reproduce the strength of the $1s_{1/2}$-state for the entire $P_{\rm miss}$ range. However, this is due to the non-absorptive potential used which yields strength at $P_{\rm miss} > 250$ MeV/c that is a decade larger than that yielded by the DWIA calculations. The HF calculations thus overpredict the $1p$-shell cross sections by the same amount for $P_{\rm miss} > 250$ MeV. Hence, neither the DWIA nor the HF calculations are able to reliably reproduce the $1s_{1/2}$-state behavior because at large $P_{\rm miss}$, the single-particle aspect of proton removal is increasingly masked by other processes or components of the wave function.

1.2.4 Summary

To summarize, $1p$-shell proton knockout appears to be very well-described up to $P_{\rm miss} = 345$ MeV/c by a fully relativistic, single-nucleon knockout DWIA calculation that includes the effects of spinor distortions. The single-particle aspect of the $1p$-shell structure is dominant in this momentum range. However, this is not true for $E_{\rm miss} > 25$ MeV. Here, the reaction is well-described by single-nucleon knockout calculations only at $P_{\rm miss} < 100$ MeV/c. At higher $P_{\rm miss}$, the single particle aspects are increasingly masked by more complicated states and processes. And at even higher $E_{\rm miss}$, other aspects of the wave function (such as NN correlations) and/or of the reaction mechanism (such as MEC and IC) mask the single-particle picture.

References

[Be82] M. Bernheim *et al.*, Nucl. Phys. **A375**, 381 (1982).

[Je83] J.P. Jeukenne and C. Mahaux, Nucl. Phys. **A394**, 445 (1983).

[Ul87] P. E. Ulmer *et al.*, Phys. Rev. Lett. **59**, 2259 (1987).

[Ry88] J. Ryckebusch *et al.*, Nucl. Phys. **A476**, 237 (1988).

[St88] G. van der Steenhoven *et al.*, Nucl. Phys. **A480**, 547 (1988).

[Be89] W. Bertozzi, R. W. Lourie, A. Saha, and L. B. Weinstein, JLAB proposal 89-003, 1989; see also K.G. Fissum, MIT-LNS Internal Report #02, 1997 and `http://www.jlab.org/~fissum/e89003.html`

[Ry89] J. Ryckebusch *et al.*, Nucl. Phys. **A503**, 694 (1989).

[Ta89] T. Takaki, Phys. Rev. **C39**, 359 (1989).

[La90] J. B. J. M. Lanen *et al.*, Phys. Rev. Lett. **64**, 2250 (1990).

[Ch91] L. Chinitz *et al.*, Phys. Rev. Lett. **67**, 568 (1991).

[Ga92] F. Garibaldi *et al.*, Nucl. Instrum. Methods **A314**, 1 (1992).

[Sh93] M. M. Sharma, M. A. Nagarajan, and P. Ring, Phys. Lett. **B312**, 377 (1993).

[Sp93] C. M. Spaltro *et al.*, Phys. Rev. **C48**, 2385 (1993).

[Le94] M. Leuschner *et al.*, Phys. Rev **C49**, 955 (1994).

[Mu94] H. Müther *et al.*, Phys. Rev. **C49**, R17 (1994).

[Bl95] K. I. Blomqvist *et al.*, Phys. Lett. **B344**, 85 (1995).

[Gi97] A. Gil *et al.*, Nucl. Phys. **A627**, 599 (1997).

[Ke97] J. J. Kelly, Adv. Nucl. Phys. **23**, 75 (1996); see also Phys. Rev. **C56**, 2672 (1997).

[Ry97] J. Ryckebusch *et al.*, Nucl. Phys. **A624**, 581 (1997).

[Sl97] V. Van der Sluys *et al.*, Phys. Rev. **C55**, 1982 (1997).

[Du99] D. Dutta, Ph.D. thesis, Northwestern University, 1999 (unpublished).

[Ke99] J. J. Kelly, Phys. Rev. **C60**, 044609 (1999).

[Ja99] S. Janssen *et al.*, Nucl. Phys. **A672**, 285 (2000).

[Ud99] J. M. Udias *et al.*, Phys. Rev. Lett. **83**, 5451 (1999).

[Ga00] J. Gao *et al.*, Phys. Rev. Lett. **84**, 3265 (2000).

[La00] L. Lapikas *et al.*, LANL preprint nucl-ex/9905009 v2 (2000).

[Li00] N. Liyanage *et al.*, submitted to Phys. Rev. Lett. in 2000.

[Ud00] J. M. Udias, private communications.

Appended list of E89-003 experiment-related publications

K. Fissum *et al.*,
Study of the Quasielastic $(e, e'p)$ Reaction in ^{16}O at High Recoil Momentum,
MIT-LNS Internal Report #02, 1997.

P. Ulmer,
Requirements on the Determination of the Beam Energy for E89-003,
Old Dominion University Internal Report, 1997.

J. Gao *et al.*,
Beam Energy Measurement at JLab Using the Hall A Spectrometers,
MIT-LNS Internal Report #04, 1998.

N. Liyanage *et al.*,
Optics Commissioning of the Hall A High Resolution Spectrometers,
MIT-LNS Internal Report #05, 1998.

P. Ulmer,
Beam Charge Measurements for Hall A Experiment E89-003 at JLab,
Old Dominion University Internal Report, 1998.

J. Gao,
Study of Quasielastic $1p$-shell Proton Knockout in the $^{16}\mathrm{O}(e, e'p)$ Reaction at $Q^2 = 0.8$ $(\mathrm{GeV}/c)^2$,
MIT Ph.D. thesis, 1999.

N. Liyanage,
A Study of the $^{16}\mathrm{O}(e, e'p)$ Reaction at Deep Missing Energies,
MIT Ph.D. thesis, 1999.

J. Gao *et al.*,
Dynamical Relativistic Effects in Quasielastic $1p$-Shell Proton Knockout from ^{16}O,
Phys. Rev. Lett. **84**, 3265 (2000).

N. Liyanage *et al.*,
The dynamics of the ^{16}O$(e, e'p)$ reaction at high missing energies,
submitted to Physical Review Letters.

K. Fissum *et al.*,
in preparation for Physical Review Section C.

1.3 E89-019

Measurement of Proton Polarization in the $D(\gamma, p)n$ Reaction

R. Gilman, R. Holt, Z.-E. Meziani
and the Hall A Collaboration

1.3.1 Introduction

The deuteron structure is conventionally understood in terms of baryon and meson degrees of freedom. At sufficiently high momentum transfer, however, we expect that it will be necessary to use quark and gluon degrees of freedom to describe the deuteron. Deuteron photodisintegration cross sections have been intensively studied in this regard, for indications of a transition to quark and gluon degrees of freedom at high momentum transfer. The most recent cross section data appear consistent with quark models, but do not entirely rule out a conventional baryon and meson based description of the reaction process [Bo98].

Experiment 89-019 was proposed to use the greater sensitivity of polarization degrees of freedom to better understand the underlying reaction mechanism. All calculations to date using baryon and meson degrees of freedom show that the induced polarization should be large; this results largely from the interference of Born terms and nucleon resonances in the intermediate state. In contrast, high energy quark and gluon theories, such as perturbative quantum chromodynamics (pQCD), generally assume helicity conservation and predict vanishing polarizations.

1.3.2 Experiment Status

The experiment ran during fall 1999, and obtained 10 data points for $\theta_{\rm cm} = 90°$ at energies between 0.5 and 2.5 GeV. The polarization transfer components C_x and C_z were measured along with the induced polarization; there are no previous data and no calculations for the polarization transfer observables. Analysis of the data is complete, and an initial publication

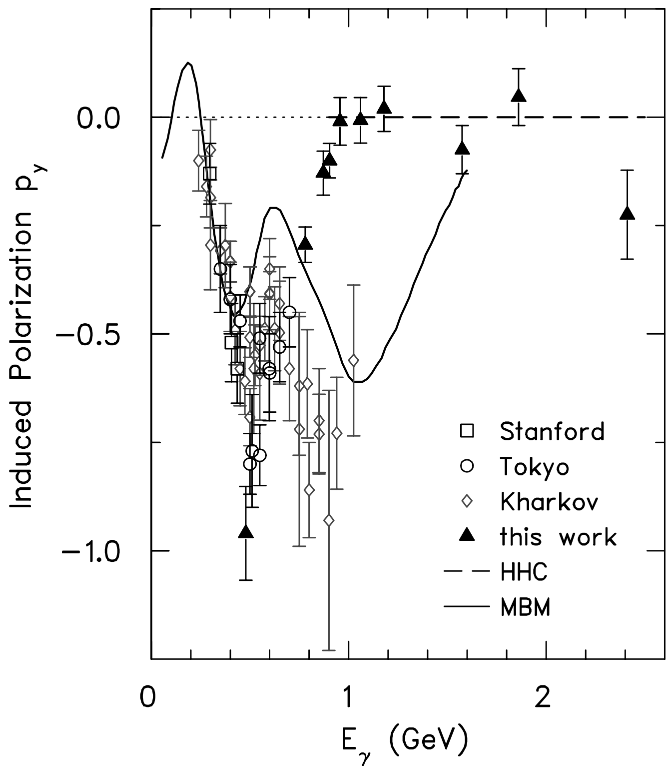

Figure 1: The induced polarization as a function of energy for deuteron photodisintegration at $\theta_{\rm cm} = 90°$. A conventional meson baryon calculation is shown labelled MBM, while the helicity conservation prediction is labelled HHC.

has been accepted by Physical Review Letters [Wi01]; the Letter includes a fuller discussion of the results shown below.

1.3.3 Results

The induced polarization is shown in Figure 1. The most significant result is the vanishing of the induced polarization above about 1 GeV photon energy, in stark contrast with the highest energy previous data and the predictions of the Bonn calculation. Based on expectations before the experiment ran, this observation would tend to rule out models based on baryons and mesons. However, these calculations include a number of approximations, and it remains to be seen if it is possible to construct a more exact and more modern model that reproduces the data.

While p_y vanishes, we find that C_x does not vanish, and thus helicity conservation does not hold. This observation firmly rules out explaining these data with pQCD; it may be consistent with recent ideas about the importance of including orbital angular momenta in quark based descriptions of reaction processes [Go96]. One new model that appears to explain the trend of the induced polarization data is the QCD rescattering model [Fr00, Sa00]. In this model, the photodisintegration process is related to proton – neutron scattering; the pn scattering is believed to be dominated by quark exchange between the nucleons, while in the photodisintegration the photon is absorbed by the exchanged quarks.

References

[Bo98] C. Bochna *et al.*, Phys. Rev. Lett. **81**, 4576 (1998).

[Wi01] K. Wijesooriya *et al.*, to be published in Phys. Rev. Lett.

[Go96] T. Gousset, B. Pire, and J.P. Ralston, Phys. Rev. D **53**, 1202 (1996).

[Fr00] L.L. Frankfurt, G.A. Miller, M.M. Sargsian, and M.I. Strikman, Phys. Rev. Lett. **84**, 3045 (2000).

[Sa00] M.M. Sargsian, private communication.

1.4 E89-028

P. E. Ulmer, J. M. Finn and M. K. Jones , Spokespersons,

and

K. Baker, E. Chudakov, A. Cochran, J. Calarco S. Dumalski, R. Ent, S. Frullani, F. Garibaldi, S. Gilad, R. Gilman, C. Glashausser, V. Gorbenko, J. Hovebo, B. Hu, X. Jiang, T. Keppel, A. Klein, S. Kuhn, G. Kumbartski, P. Markowitz, D. Meekins, J. Mitchell, Z. Papandreou, C. Perdrisat, V. Punjabi, R. Roche, D. Rowntree, L. Todor, G. Urciuoli, K. Wijesooriya, R. Woo.

The goal of this experiment is to provide a test of the validity of deuteron models by providing data on the recoil polarization observables in d($\vec{e}, e'\vec{p}$)n. In addition to enhancing our understanding of the deuteron structure and reaction mechanisms in $(e, e'p)$, the information gained here will be critical in interpreting the G_{En} experiment of Madey *et al.*. The Madey experiment employs an analogous reaction, d($\vec{e}, e'\vec{n}$)p, to extract the ratio of the neutron form factors G_{En}/G_{Mn}, assuming that the deuteron provides a source of essentially free neutrons. Various calculations suggest that polarization transfer at quasifree kinematics is expected to be free from the effects which have frustrated extraction of form factors in Rosenbluth L/T separations, most notably final state interactions (FSI). However, the G_{En} measurement cannot test the quasifree assumption. Experiment E89-028 can test this assumption by comparing measurements on hydrogen and deuterium targets.

E89-028 measured the recoil polarization observables of the ^{1}H($\vec{e}, e'\vec{p}$) reaction and the ^{2}H($\vec{e}, e'\vec{p}$) reaction in quasifree kinematics (*i.e.* centered at zero recoil momentum) at the three Q^2 points of the Madey experiment: 0.43, 1.0 and 1.61 (GeV/c)^2.

In Fig. 1, the G$_{Ep}$/G$_{Mp}$ ratio measured for ^{1}H($\vec{e}, e'\vec{p}$) in this experiment is plotted and compared to previous measurement of e93027 [Jo-79]. The agreement with the previous experiment is excellent.

In Fig. 2, preliminary results for the double ratio of the ratio of transverse, P$_T$, to longitudinal, P$_L$, polarization for ^{2}H($\vec{e}, e'\vec{p}$) to the ratio for ^{1}H($\vec{e}, e'\vec{p}$) are plotted.

Only statistical error bars are shown. The ^{1}H($\vec{e}, e'\vec{p}$) and ^{2}H($\vec{e}, e'\vec{p}$) data were taken at exactly the same spectrometer settings, so that systematic errors would be minimized when measuring the ratio of polarization variables. Previous measurements [2] of the ^{2}H($\vec{e}, e'\vec{p}$) reaction, from an experiment at Bates, are plotted in Fig. 2.

Where the two data sets overlap at low Q^2, they agree. The new JLab data exhibit a significant reduction of the statistical error bar.

Since the Madey experiment will need to sample a fairly large range of recoil momenta (in order to achieve the required statistical precision), it is also important to test the quasifree assumption away from zero recoil momentum. Measurements were made of the three polarization components of ^{2}H($\vec{e}, e'\vec{p}$) at $Q^2 = 1$ (GeV/c)^2 and centered at recoil momentum of 160 MeV/c which spans the range of the Madey experiment. The longitudinal and transverse components of the polarization were measured to a precision of 5% .

At this recoil momentum, the measurement of the normal polarization, which is zero in the absence of FSI, will provide another constraint for this important aspect of the theory. At this point, we need to make comparsions to theoretical calculations before any conclusions can be drawn and a paper submitted.

References

[1] M. K. Jones *et al.*, Phys. Rev. Lett. **84**, 1398 (2000).

[2] B. Milbrath *et al.*, Phys. Rev. Lett. **80**, 452 (1998); erratum, Phys. Rev. Lett. **82**, 2221 (1999).

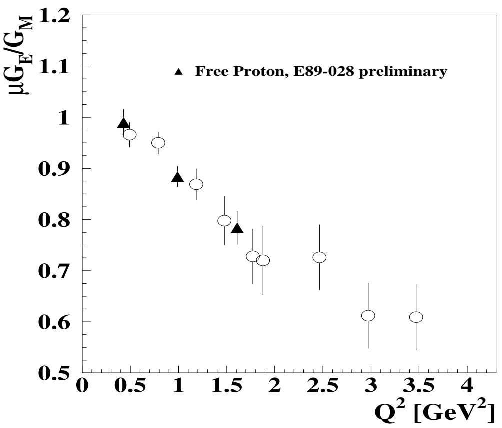

Figure 1: *Comparison between G_{Ep}/G_{Mp} for the $^1H(\vec{e}, e'\vec{p})$ reaction measured in E89-028 and in E93-027 (open circles) [Jo-79].*

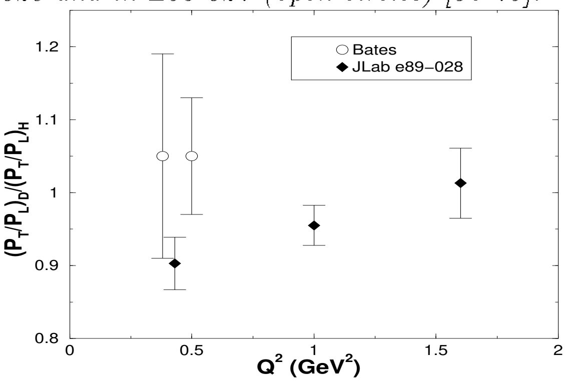

Figure 2: *Preliminary results for the double ratio, $(P_T/P_L)_D/(P_T/P_L)_H$, of the ratio of transverse to longitudinal polarization for $^2H(\vec{e}, e'\vec{p})$ to the ratio for $^1H(\vec{e}, e'\vec{p})$. The open circles are measurements from Ref. [2]*

1.5 E89-044

Selected Studies of the ^{3}He and the ^{4}He Nuclei through Electrodisintegration at High Momentum Transfer

Spokespersons: M. Epstein, E. Voutier, and A. Saha

Coincidence experiments have proven to be very useful tools in studying specific aspects of the nucleus. In particular the (e,e'p) reaction has been used not only to study the single-nucleon structure of nuclei but also to study the behavior of nucleons embedded in the nuclear medium. At JLAB, this will be accomplished by extending the domain of momentum transfers towards higher values where short- range effects and possibly the internal structure of the nucleons are manifested, by exploring nuclear structure in its extreme conditions, and by investigating the high momentum part of the wave functions. We also will increase the specificity of the probe by separating the response functions associated with different polarization states of the virtual photon.

The E89-044 collaboration plans to exploit these new possibilities by undertaking a series of (e,e'p) measurements on the Helium isotopes. Next to the deuteron, the A=3 and A=4 nuclei are the simplest systems in which all the basic ingredients of a complex nucleus exist. Sophisticated methods to solve the Schrödinger equation almost exactly have been applied to the A=3 nuclei and have been extended to ^{4}He. Microscopic calculations of FSI and MEC contributions have been developed and applied to reactions on few-nucleon systems. The data provided by the E89-044 experiment will test the validity of these models in the high Q^2 and high missing momentum regime.

The collaboration completed the ^{3}He(e,e'p) portion of this study in March 2000 after receiving nearly three months of beam time. In perpendicular kinematics, with a constant momentum transfer of 1.5 GeV/c and a constant energy transfer of 0.837 GeV, cross sections were measured at missing momentum 0, 150, 300, 425, 550, 750, and 1000 MeV/c, as shown in Figure 1.5. The R_{L+TT}, R_T, and R_{LT} response functions will be extracted for missing momenta of 0, 150, 300, 425, and 550 MeV/c. In parallel kinematics, where the proton is

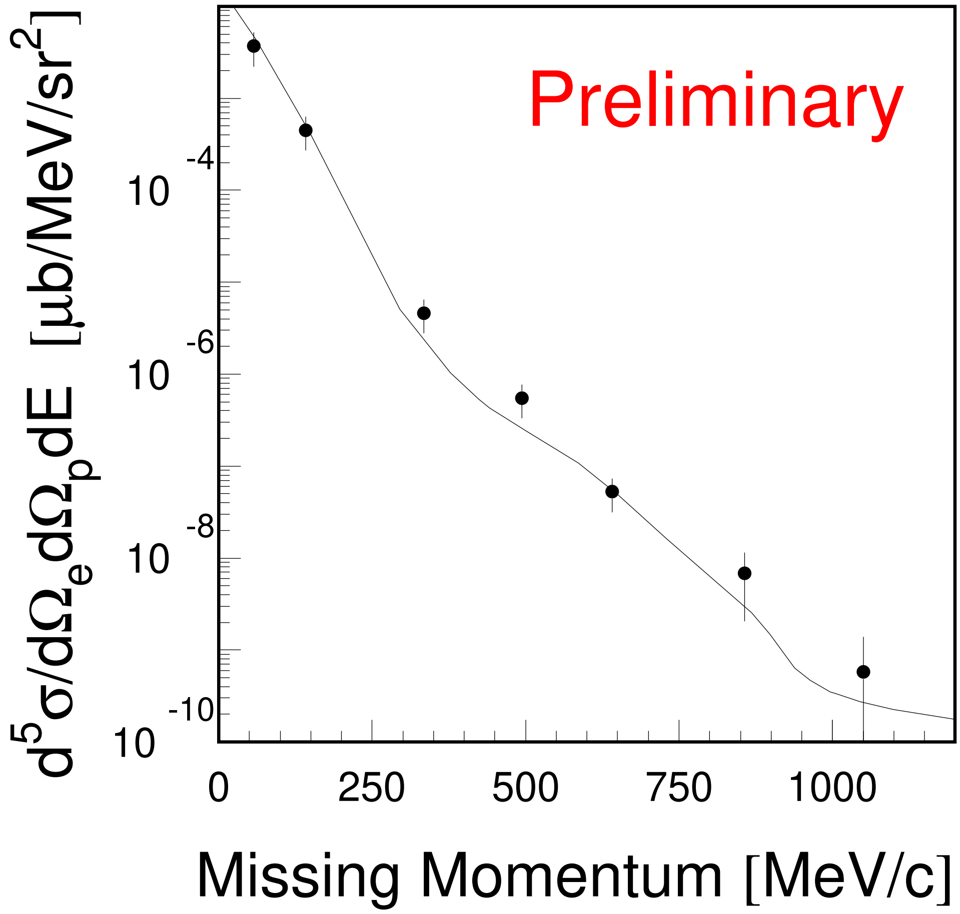

Figure 1: Shown are preliminary cross sections as a function of missing momentum with a beam energy of 4807 MeV with fixed q = 1500 MeV/c and ω = 840 MeV. The theory curve was generated using the full calculation of Jean Marc Laget [La87, La94]. While the data shown is only a sample of the full data set, the agreement with the theory even at large missing momentums is striking.

emitted in the direction of the momentum transfer vector, the Q^2 dependence from 0.8 to 4.1 $[\mathrm{GeV/c}]^2$ will be determined by performing longitudinal/transverse separations. These measurements were performed for -300, 0, 300 MeV/c missing momentum and for momentum transfers 1.0, 1.9 and 3.0 GeV/c. In addition, the experiment measured cross sections in the continuum region to study correlated nucleon pairs.

The analysis of the data is being performed primarily by four groups, CalState, Grenoble, MIT, and Rutgers. Three graduate students, Fatiha Benmokhtar (Rutgers), Emilie Penel (Grenoble), Marat Rvachev (MIT), will receive their dissertation data from this experiment. Also, several undergraduates at CalState have been working with the elastic scattering data to get their first experience analyzing nuclear physics data. Preliminary results of these analysis efforts were presented at the Fall 2000 DNP meeting [An00, Be00, Pe00, Rv00].

References

[An00] K. Aniol, Luminosity Determination for the ^{3}He(e,e'p)d Experiment in Hall-A at JLab, APS-DNP Conference, Williamsburg VA, (2000).

[Be00] F. Benmokhtar, Perpendicular Kinematics in ^{3}He(e,e'p)d at $Q^2 = 1.54$ $[\mathrm{GeV/c}]^2$, APS-DNP Conference, Williamsburg VA, (2000).

[La87] J.M. Laget, Phys. Lett. B199 (1987) 493.

[La94] J.M. Laget, Nucl. Phys. A579 (1994) 333.

[Pe00] E. Penel, High Precision ^{3}He Elastic Electron Scattering Cross Sections up to $Q^2 = 20\ fm^{-2}$, APS-DNP Conference, Williamsburg VA, (2000).

[Rv00] M. Rvachev, Study of the ^{3}He Nuclei through Electrodisintegration at High Momentum Transfer, APS-DNP Conference, Williamsburg VA, (2000).

1.6 E91-011

Investigation of the $N \to \Delta$ Transition via Polarization Observables in Hall A

S. Frullani, J.J. Kelly, and A.J. Sarty, Spokespersons,
and
the Hall A Collaboration

1.6.1 Introduction

Recoil polarization observables can provide new insight into properties of nucleon resonances and the reaction mechanisms for electroproduction of mesons by providing access to interference between small amplitudes and dominant amplitudes. The dominant amplitude for pion electroproduction at the Δ resonance is the M_{1+} multipole, but there is much current interest in the smaller S_{1+} amplitude that arises from configuration mixing within the quark core [Is82], often described as quadrupole deformation, or from meson and gluon exchange currents between quarks [Bu99], or coupling to the pion cloud outside the quark core [Fi96, Ka99]. Observables which depend upon real parts of interference products are sensitive to these quadrupole amplitudes, but reliable interpretation of such data requires understanding background contributions from nonresonant production mechanisms and from underlying nondominant resonances. Sensitivity to background amplitudes is provided by observables which depend upon the imaginary parts of similar interference products. Experiment E91-011 was designed to measure both types of observables for the $p(\vec{e}, e'\vec{p})\pi^0$ reaction using the focal-plane polarimeter.

1.6.2 Experiment Status

The experiment ran between May 19 and July 31, 2000, and received an average current of 45 μA for 36.5 days, corresponding to about 64% of scheduled calendar time. The beam polarization for several cathode locations varied between 67 and 79% and was monitored almost continuously by the Compton polarimeter. Polarized beam was delivered to Hall A during the June 8 to July 1 period using two lasers and achieved a record current of 110 μA with high polarization, although the lifetime was relatively short.

The production kinematics are summarized in Table 1. The nominal beam energy, $E_0 = 4.535$ GeV, electron scattering angle, $\theta_e = 14.09°$, and scattered electron momentum, $k_f = 3.066$ GeV/c, were constant for the production data. The proton momenta and angles were chosen to give central values of $W = 1.232$ GeV and $Q^2 = 1.0$ (GeV/c)^2 while optimally covering the center-of-mass angular distribution. The table lists nominal center-of-mass angles θ_{cm} where positive (negative) angles refer to nucleon momenta forward (backward) with respect to the virtual photon momentum $\vec{q}$. The total charge collected for each setting is given in coulombs. For each setting, a portion of the data was collected with 6 msr collimators in each spectrometer, but for most settings the bulk of the data was acquired without collimators. Extensive measurements for optics, pointing, luminosity, and dead time were made also.

Table 1: *Kinematics summary for E91-011.*

θ_{cm} deg.	θ_{lab} deg.	p_{lab} GeV/c	charge C
-155	49.72	0.742	11.5
-135	53.64	0.819	20.2
-90	54.79	1.066	13.7
-50	50.18	1.270	10.5
-25	46.33	1.350	4.6
0	42.30	1.378	16.7
25	38.12	1.350	6.2
50	34.29	1.270	13.0
90	29.81	1.066	12.0
135	30.81	0.819	11.1
155	34.71	0.742	11.1
180	42.28	0.703	3.8

The high singles rates on the forward side of $\vec{q}$ and relatively large π^+ contamination necessitate careful particle identification and background rejection. Figure 1 illustrates the effectiveness of several selection criteria. A cut on the correlation between vertex position and coincidence time eliminates most of the accidental coincidences. A cut on mean pulse height in the scintillators versus β eliminates most of the pion contamination. An aerogel detector was used for most of the forward-angle running to reduce the trigger rate and dead time contributed by pions. An additional cut on missing energy versus missing mass also reduces background, particularly on the large-angle side of $\vec{q}$ where the elastic radiative tail is responsible for the strong peak at small missing mass; this peak is cut off on its lower side by acceptance. Very little background remains under the final missing-mass peak. Note that the missing-mass resolution is better on the large-angle than on the small-angle side of $\vec{q}$ where the sensitivity to angular resolution is greater.

1.6.3 Expected Results

Even though the hadron spectrometer is confined to a horizontal plane, Fig. 2 demonstrates that kinematic focusing of the reaction cone to a laboratory opening angle of about 13° provides considerable out-of-plane acceptance. The nearly complete coverage for $\theta_{cm} < 50°$ will permit extraction of response functions which require out-of-plane momenta. Therefore, we have developed an analysis procedure that exploits the various ϕ dependencies of cross section and polarization observables to extract most of the response functions that do not require Rosenbluth separation. This procedure was tested by Monte Carlo simulation before the experiment and will be applied to the data after the calibration analysis. The data analysis is proceeding smoothly and we expect to have preliminary data for polarized and unpolarized response functions by spring of 2001.

References

[Is82] N. Isgur, G. Karl, and R. Koniuk, Phys. Rev. D **25**, 2394 (1982).

[Bu99] A.J. Buchmann, hep-ph/9909385 (1999).

[Fi96] M. Fiolhais, B. Golli, and S. Sirca, Phys. Lett. **B373**, 229 (1996).

[Ka99] S.S. Kamalov and S.N. Yang, Phys. Rev. Lett. **83**, 4494 (1999).

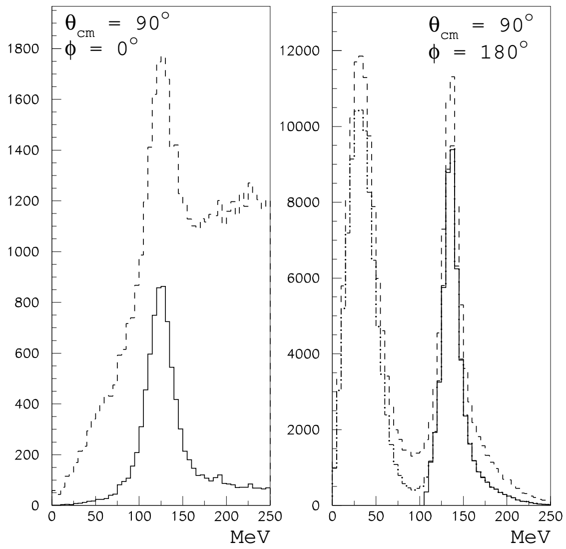

Figure 1: *The effectiveness of event selection criteria is illustrated for $\theta_{cm} = \pm 90°$. The dashed curves have only a loose cut on coincidence time; the dash-dotted curves have cuts applied to both coincidence time versus reaction-vertex and β versus pulse-height particle identification; and the solid curves add a cut to select pion production in E_m versus p_m.*

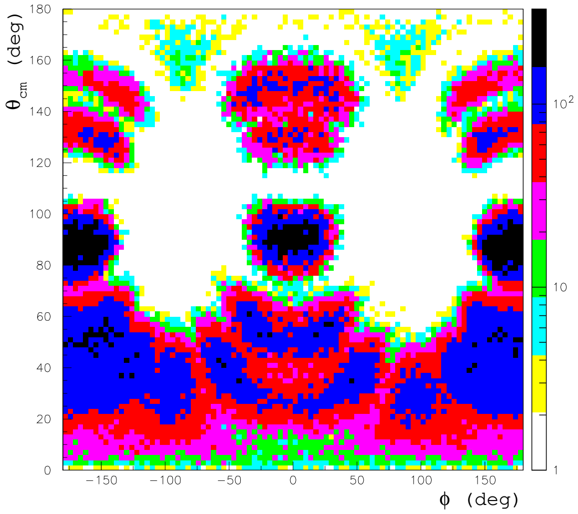

Figure 2: *Angular acceptance for* $1.207 \leq W \leq 1.257$ *GeV and* $0.9 \leq Q^2 \leq 1.1$ *(GeV/c)*^{2}*. Contours of normalized yield are shown for* (θ_{cm}, ϕ_{cm})*, combining the various spectrometer settings.*

1.7 E93-049

Polarization Transfer in the Reaction ^{4}He$(\vec{e}, e'\vec{p})\,^3$H in the Quasi-elastic Scattering Region
R. Ent and P.E. Ulmer, Spokespersons, and the E93-049 Collaboration.

1.7.1 Introduction

Whether nucleons undergo considerable change of their internal structure when bound in the nuclear medium is a long standing issue in nuclear physics. Polarization transfer in quasi-elastic nucleon knockout is sensitive to the properties of the nucleon in the nuclear medium, including possible modification of the nucleon form factor and/or spinor. Experiment E93-049 measured the polarization transfer coefficients over the range of Q^2 from 0.5 to 2.6 GeV^2, and as a function of missing momentum in the range 0 to 240 MeV/c, in order to determine the electric to magnetic form factor ratio for protons bound in the ^{4}He nucleus. ^{4}He was selected for study since its relative simplicity allows for realistic microscopic calculations and since its high density enhances any possible medium effects. Also, a variety of calculations indicate polarization observables for the $^4\mathrm{He}(\vec{e}, e'\vec{p})\,^3\mathrm{H}$ reaction have minimal influence from final state interactions (FSI) and meson exchange currents (MEC). It is precisely these effects (especially FSI) that have so far prevented a clean determination of nucleon medium modifications from unpolarized response functions in $(e, e'p)$ experiments.

A recent calculation by D.H. Lu *et al.* [1], shown in Figure 1, suggests a measurable deviation from the free space ratio over the Q^2 range of this experiment. Note that the calculation is consistent with present constraints on possible medium modifications for both the electric form factor (from the Coulomb Sum Rule, with $\mathrm{Q}^2 < 0.5$ GeV^2), and the magnetic form factor (from a y-scaling analysis) for $\mathrm{Q}^2 > 2$ GeV^2. The calculation seems to predict too large an effect for the magnetic form factor at higher Q^2; however, it has been suggested that in order to interpolate smoothly between confined and deconfined phases, the bag constant might decrease as the baryon density increases. Such an effect would reduce the Q^2-dependence of the medium modification of the magnetic form factor, while still having a measurable effect in the ratio of G_E/G_M. Similar measurable effects have been calculated in the model of Frank *et al* [2].

For free electron-nucleon scattering, the ratio of the electric to magnetic Sachs form factors, G_E and G_M, is given by [3]:

$$\frac{G_E}{G_M} = -\frac{P'_x}{P'_z} \cdot \frac{E_e + E_{e'}}{2m_p} \tan(\theta_e/2), \tag{1}$$

where P'_x and P'_z are the transverse and longitudinal transferred polarizations [4]. The beam energy is E_e, the energy (angle) of the scattered electron is $E_{e'}$ (θ_e) and m_p is the proton mass. The relation in Eq. (1) was recently used to extract G_E/G_M for the proton [11]. For quasielastic nucleon knockout of a bound proton this relation is only approximately correct, but polarization transfer remains sensitive to the properties of the nucleon in the nuclear medium: although proper interpretation of the results requires accounting for such effects as FSI and MEC, their effects on polarization transfer are, as mentioned, expected to be small.

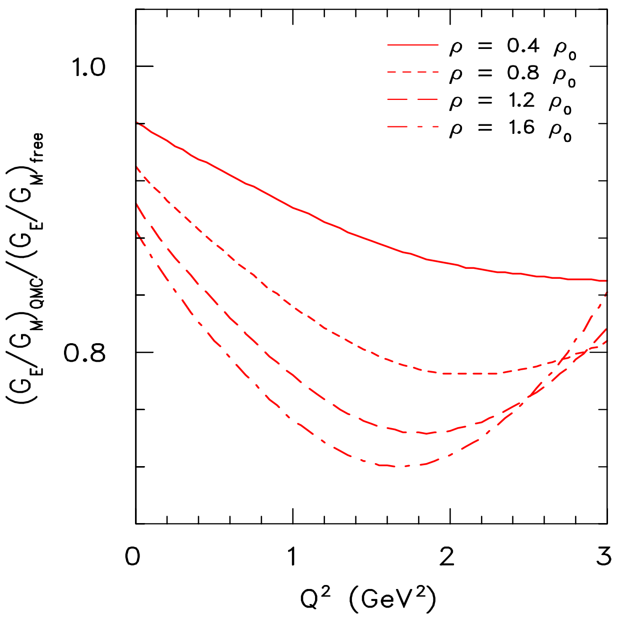

Figure 1: Ratio of in-medium to free space ratio of electric to magnetic form factors of the proton, as a function of nuclear densities in the range of the ^{4}He nucleus [1]. The free bag radius was taken to be 0.8 fm.

1.7.2 Experiment Status

Data taking for this experiment were completed in May 2000. The experiment used beam currents of 40 μA for the lower Q^2 values and up to 70 μA for the highest Q^2 value, combined with beam polarizations of 66% for the lowest Q^2 value and $\approx$ 77% for the other Q^2 values. The beam helicity was flipped pseudorandomly to reduce systematic uncertainties of the extracted polarization transfer observables. The proton spectrometer was equipped with a focal plane polarimeter (FPP). Polarized protons lead to azimuthal asymmetries after scattering in the carbon analyzer of the FPP. These distributions, in combination with information on the beam helicity, were analyzed by means of a maximum likelihood method to obtain the induced and transferred polarization components.

As the experiment was designed to detect differences between the in-medium polarizations compared to the free values, both ^{4}He and ^{1}H targets were employed (due to beam time constraints, at $Q^2 = 2.6$ GeV^2 only ^{4}He data was acquired). The statistical precision

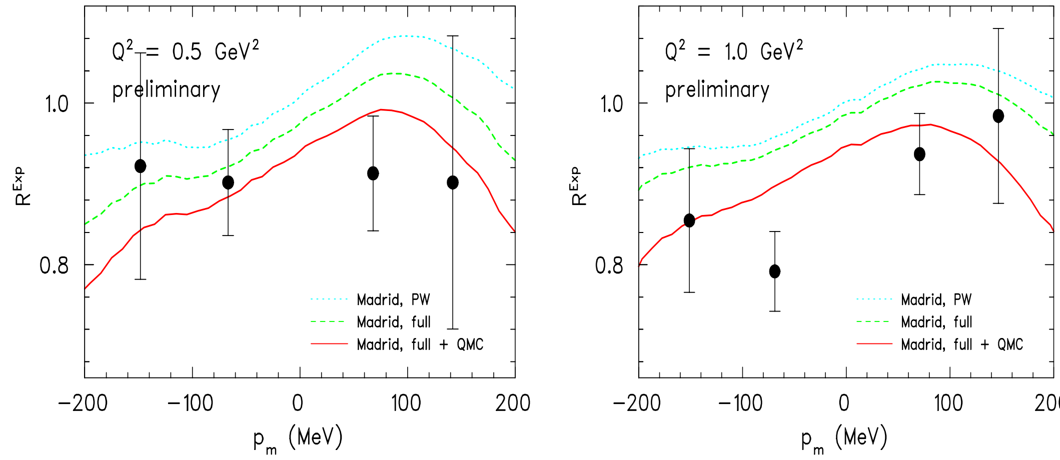

Figure 2: Measured values of the polarization double ratio R_{Exp} for $^4\mathrm{He}(\vec{e},e'\vec{p})^3\mathrm{H}$ at $Q^2 = 0.5$ GeV^2 (a) and $Q^2 = 1.0$ GeV^2 (b). The theoretical curves represent PWIA calculations (dotted), relativistic DWIA calculations (dashed) and relativistic DWIA calculations including QMC medium–modified form factors [1] by Udias *et al.* [6] (solid).

for the polarization double ratio is roughly 5%, 4%, 4% and 12% at Q^2 of 0.5, 1.0, 1.6, and 2.6 GeV^2 respectively (the dominant error at the high Q^2 point is from our interpolation of the existing Hall A G_E/G_M data for the proton from Jones *et al.* [11]). Systematic errors are expected to be significantly less than the statistical errors.

1.7.3 Results

Our results, binned versus missing momentum, are shown in Fig. 2 for two of the four kinematical settings along with theoretical results in terms of the polarization double ratio

$$R_{Exp} = \frac{(P'_x/P'_z)_{^4\mathrm{He}}}{(P'_x/P'_z)_{^1\mathrm{H}}}. \tag{2}$$

Here, the helium polarization ratio is normalized to the hydrogen polarization ratio measured in the identical setting. As a cross check, the hydrogen results were also used to extract the free proton form factor ratio G_E/G_M and found to be in excellent agreement with previous data [11]. Negative values of missing momentum correspond to the recoiling nucleus having a momentum component antiparallel to the direction of the three-momentum transfer.

The theoretical predictions are results of our acceptance-averaging of calculations by the Madrid group [6]. The plane-wave impulse approximation (PWIA) calculation is not able to describe the experimental results although it follows a similar trend. The relativistic distorted-wave impulse approximation (RDWIA) calculation gives a smaller value of R_{Exp} but still overpredicts the data. The inclusion of a medium modification of the proton form factor as predicted by Lu *et al.* [1] in the RDWIA calculation is in excellent agreement with both settings. All calculations shown use the Coulomb gauge, the CC1 current operator as defined in [Fo83], and the MRW optical potential of [8]. The CC2 current operator gives higher values of R_{Exp}, worsening agreement with the data. Our results at $Q^2 = 0.5$ GeV^2 closely coincide with the recent results at $Q^2 = 0.4$ GeV^2 of Mainz [9].

Presently the data analysis at $Q^2 = 0.5$ and 1.0 GeV^2 is complete apart from detailed comparisons of Monte Carlo and data, and extraction of the induced polarization transfer coefficient P_y. The latter is identically zero in the absence of FSI effects (in the one-photon exchange approximation) and would constitute a stringent test of various model calculations. For the data at $Q^2 = 1.6$ and 2.6 GeV^2 the theoretical analysis is still in progress.

References

[1] D.H. Lu, K. Tsushima, A.W. Thomas, A.G. Williams and K. Saito, Phys. Lett. **B417**, 217 (1998) and Phys. Rev. C **60**, 068201 (1999).

[2] M.R. Frank, B.K. Jennings and G.A. Miller, Phys. Rev. C **54**, 920 (1996).

[3] A.I. Akhiezer and M.P. Rekalo, Sov. J. Part. Nucl. **3**, 277 (1974); R. Arnold, C. Carlson and F. Gross, Phys. Rev. C **23**, 363 (1981).

[4] With the inital and final electron momentum $\vec{k}_i$ and $\vec{k}_f$, the coordinate system is given by the unit vectors $\hat{z} = (\vec{k}_i - \vec{k}_f)/|\vec{k}_i - \vec{k}_f|$, $\hat{y} = (\vec{k}_i \times \vec{k}_f)/|\vec{k}_i \times \vec{k}_f|$, and $\hat{x} = \hat{y} \times \hat{z}$.

[5] M.K. Jones *et al.*, Phys. Rev. Lett. **84**, 1398 (2000).

[6] J.M. Udias *et al.*, Phys. Rev. Lett. **83**, 5451 (1991); J.A. Caballero *et al.*, Nucl. Phys. **A632**, 323 (1998).

[7] T. de Forest, Nucl. Phys. **A392**, 232 (1983).

[8] J.A. McNeil, L. Ray, and S.J. Wallace, Phys. Rev. C **27**, 2123 (1983).

[9] S. Dieterich *et al.*, nucl-ex/0011008; accepted for publication in Phys. Lett. **B** (2001).

1.8 E93-050

VIRTUAL COMPTON SCATTERING FROM THE PROTON

P.-Y. Bertin, P.A.M. Guichon, C.E. Hyde-Wright, co-spokespersons,
for the Hall A VCS Collaboration

1.8.1 Introduction

The H$(e, e'p)\gamma$ reaction is a coherent superposition of radiation from the incident or scattered electron in elastic ep scattering (Bethe-Heitler–BH) and exclusive production of a photon on the proton, by absorption of a virtual photon (Virtual Compton Scattering–VCS). Experimentally, we separate the exclusive photon final state from π^0 electroproduction and other channels by reconstructing the missing mass of the unobserved particle(s). This experiment was the subject of three completed Ph.D. theses [To00b, Ja00, De01], with two more in progress: C. Jutier (ODU - Clermont-Ferrand), and G. Laveisière (Clermont-Ferrand). The experiment has been presented in several conference proceedings [Di99, Ja99, To00a]

The kinematics of the VCS reaction are characterized by the invariant momentum transfer squared from the electron: $Q^2 = -q^2 = (k - k')^2$, the invariant mass of the photon-proton system: $s = W^2 = (q + P)^2$, and the polar and azimuthal angles $\theta_{\gamma\gamma}$ and $\phi_{\gamma\gamma}$ of the outgoing photon relative to the direction $\vec{q}$ of the momentum transfered from the electron.

1.8.2 Experiment Status

We took the complete E93050 data set in the spring of 1998, with a 4 GeV beam (up to 100 μA) incident on a 15 cm liquid Hydrogen cell in Hall A. The scattered electron and recoil proton were detected in the HRS pair. Below pion threshold ($M_p^2 < s < (M_p + m_\pi)^2$) at $Q^2 = 1.0$ and 1.9 GeV^2, a single electron arm setting spanned the entire region, and we moved the proton arm to span a large range in $\theta_{\gamma\gamma}$. At $Q^2 = 1$, we also measured a resonance excitation scan for nine central values of s from 1.3 GeV^2 to 3.6 GeV^2, with the coincidence angular kinematics centered on $\theta_{\gamma\gamma} = \pi$.

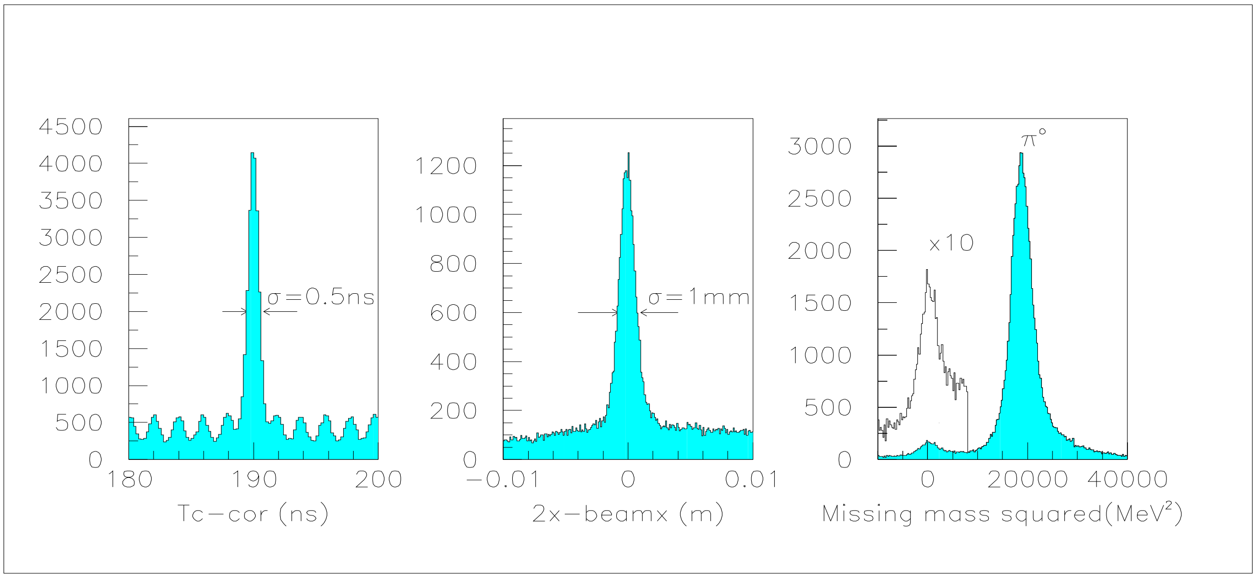

Figure 1: VCS Analysis for setting $s = 2.5$ GeV^2 and $Q^2 = 1.0$ GeV^2. Left: Coincidence time of flight (ns) between the electron and proton arms, corrected for the path length variation in the two spectrometers. Middle: Two-arm-x – Beam-x (m). This is the the horizontal vertex coordinate reconstructed from the two spectrometers minus the instantaneous beam position. Right: H$(e, e'p)X$ missing mass squared, illustrating the VCS and π^0 peaks.

In addition to physics data, we took extensive data in E93050 to calibrate the optics of the spectrometers at high momenta and with extended targets. The optics calibrations were done primarily with sieve slit data. To eliminate the depth of field problems from the extended target, we reconstructed the trajectories of elastically scattered electrons at the face of the colimator. An essential element in these calibrations was the phase shift and attenuation in the instantaneous readout of the beam position monitors in the Hall A beam-line. We calibrated the beam energy by requiring agreement between the simulated and observed position of the missing mass peak. Typical values of the calibrated beam energy are 15 ± 3 MeV lower than the nominal 4045 MeV beam energy. The analysis is illustrated in Fig. 1. Details of these analysis can be found on the VCS web page:
http://www.jlab.org/˜luminita/vcs.html.

1.8.3 Results

Below pion threshold, we extract the differential cross section by comparing the integrated yield in a bin with a simulated cross section including the Bethe-Heitler and Born terms and the radiative tail (second photon emission) of the complete VCS process.[Va00] Our preliminary cross sections at $Q^2 = 1.9$ GeV^2 are illustrated in Fig. 2. The gap in the angular distribution at $\theta_{\gamma\gamma}^{CM} \approx 100°$ corresponds to the two large BH peaks in the directions of the incident and scattered electrons. The broad peak at $\theta_{\gamma\gamma}^{CM} \approx -180°$ is dominated by the Born term (approximately a dipole radiation pattern from the recoil proton). As q' increases, the deviation of the data from the BH+Born terms determines a pair of Generalized Polarizabilities that measure the spatial variation of the electric and magnetic polarization induced in the proton by external electric and magnetic fields.[Gu95]

Fig. 3 shows the preliminary VCS cross sections in the nucleon resonance region, averaged over our ϕ-acceptance as a function of W in a bin of $\theta_{\gamma p}$ and Q^2. The Δ peak is shifted below 1230 MeV by the strong interference with the BH and Born amplitudes. The different symbols in the plot correspond to different spectrometer settings. The overlapping points are not necessarily expected to agree, since the ϕ-acceptance varies with W for each setting. Fig. 4 presents our cross sections for [virtual] photo-production of a π^0, averaged over our acceptance as a function of W in a bin in Q^2 and $\cos\theta_{\gamma\pi}^{CM}$. The solid line is the MAID[Dr99]

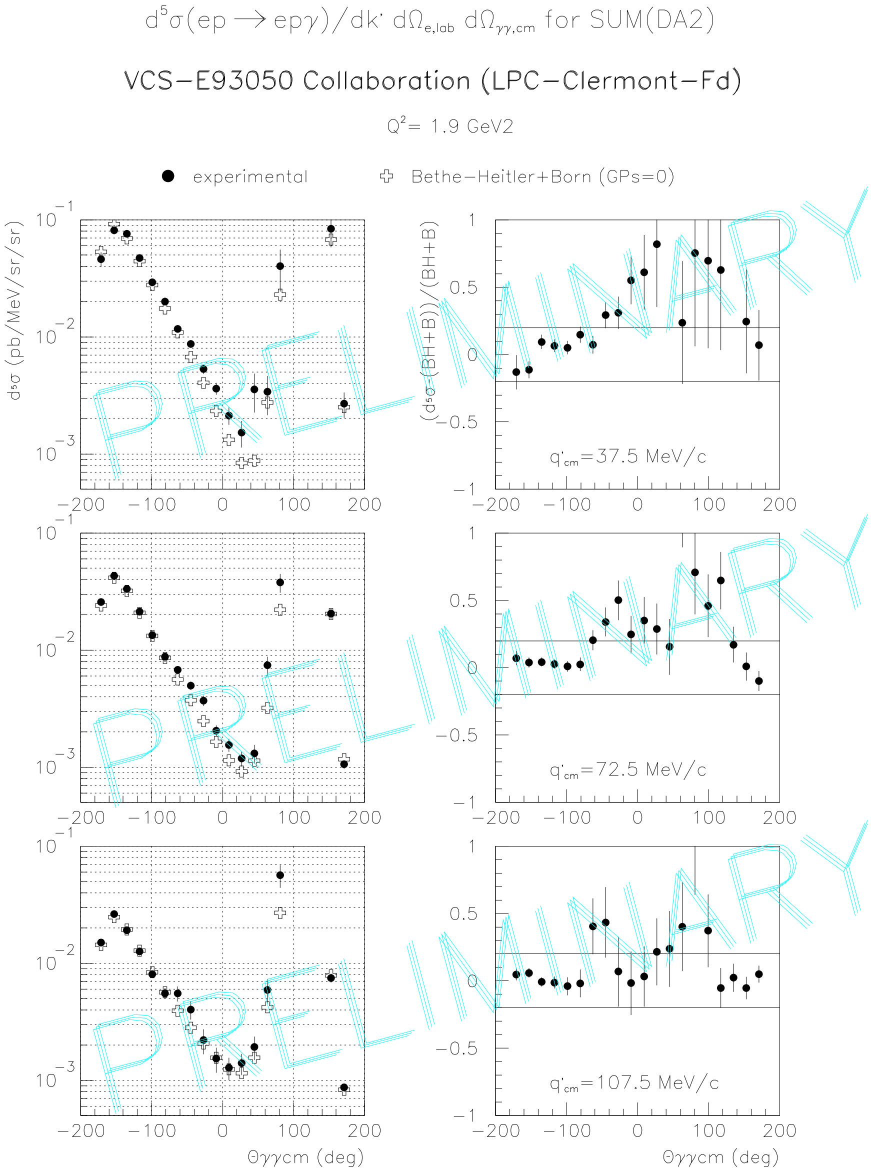

Figure 2: VCS cross section below pion threshold ($q'_{CM} = (s - M^2)/(2\sqrt{s}) = 37.5,\ 72.5\ 107.5$ MeV). The kinematics are defined for $Q^2 = 1.9$ GeV^2 and $E_0 = 4.028$ GeV. Positive values of $\theta_{\gamma\gamma}^{CM}$ correspond to $\phi_{\gamma\gamma} = 0$; negative values of $\theta_{\gamma\gamma}^{CM}$ correspond to $\phi_{\gamma\gamma} = \pi$. The solid dots are the experimental cross section with statistical error bars. The open crosses are the cross sections from the low energy theorem (Bethe-Heitler + Born only). The left hand plots show the differential cross section, the right hand plots show the fractional deviation of the experimental results from the BH + Born theory. The systematic errors are estimated to be 15% in the angular domain $[-180, -50] \cup [+150, +180]$ and 25-30% in the angular domain $[-50, +50]$.

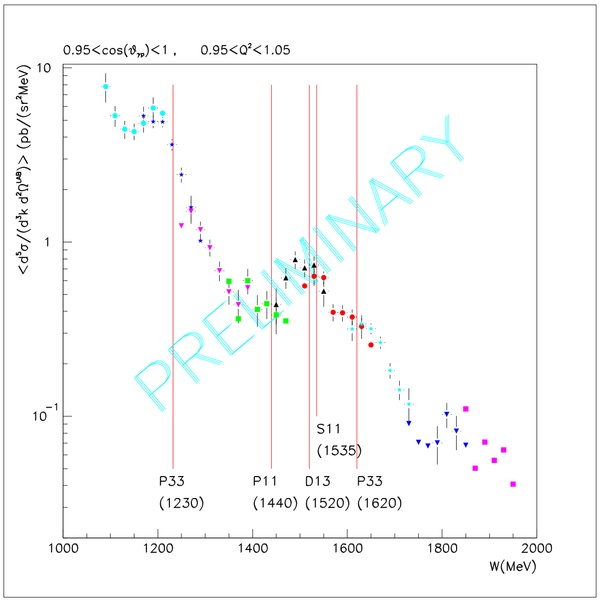

Figure 3: VCS differential cross section in the nucleon resonance region, averaged over the experimental acceptance in $\phi_{\gamma\gamma}$ as a function of W in a bin $0.95 < \cos\theta^{CM}_{\gamma p} \leq 1.0$ and $0.95 \leq Q^2 \leq 1.05$ GeV^2. $\theta^{CM}_{\gamma p}$ is the angle between the **q**-vector and the recoil proton, in the photon-proton CM frame.

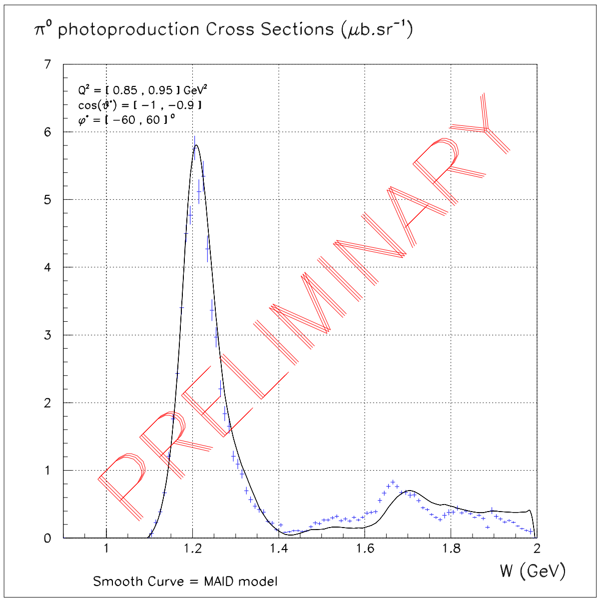

Figure 4: H$(\gamma^*, p)\pi^0$ virtual photo-production cross section $d\sigma/d\Omega^{CM}_{\gamma\pi}$ averaged over the experimental acceptance within $|\phi_{\gamma\gamma}| < 60°$, $-1.0 < \cos\theta' \leq -0.9$, and $0.85 \leq Q^2 \leq 0.95$ GeV^2, as a function of $W = \sqrt{s}$. θ' is the angle between the virtual photon and the detected recoil proton, in the photon-proton CM frame.

cross section model, averaged over the experimental acceptance. The integral of our result in the interval $1.15 < W < 1.35$ GeV agrees with the MAID model to within 7%.

References

[To00b] L. Todor, Ph.D., Old Dominion University, Norfolk VA, USA, Dec. 2000.

[Ja00] Stephanie Jaminion, Ph.D., Blaise Pascal Université, Clermont-Ferrand, France, Dec. 2000.

[De01] N. DeGrande, Ph.D., University of Gent, Gent, Belgium, Feb. 2001.

[Di99] R. Di Salvo *et al.*, Workshop on Symmetry and Spin,5–12 Sep. 1999, Prague, Czech Republic, Czech J. Phys. **49** (1999).

[Ja99] S. Jaminion, Proceedings, Electromagnetic Probes and the Structure of Hadrons and Nuclei, Erice, Italy, 17–25 September 1999, Prog. Part. Nucl. Phys. **44**, 451 (2000).

[To00a] L. Todor *et al.*, Proceedings, NSTAR2000: The Physics of Excited Nucleons, Newport News, VA, Feb 16–19, 2000.

[Gu95] P. A. Guichon, *et al.*,Nucl. Phys. **A591**, 606 (1995); P.A. Guichon, and M. Vanderhaeghen, Prog. Part. Nucl. Phys. **41**, 125 (1998).

[Va00] M. Vanderhaeghen *et al.*, Phys. Rev. **C62**, 025501 (2000)

[Dr99] D. Drechsel *et al.*, Nucl Phys **A645** (1999) 145, and http://www.kph.uni-mainz.de/MAID/

1.9 E94-012

Measurement of Photoproton Polarization in the $^{1}H(\gamma,p)\pi^{0}$ Reaction

R. Gilman, R. Holt, Z.-E. Meziani
and the Hall A Collaboration

1.9.1 Introduction

For photon energies from a few hundred MeV up to a few GeV, the photonuclear reaction exhibits strong baryon resonance production. Up to slightly over 1 GeV, there are a number of spin measurements which show structure corresponding to prominent peaks in the cross section data. However, there are little polarization data at higher energies and there are almost no spin measurements above the energy region of discrete resonances, up to $W \approx 2$ GeV, with the exception of a few measurements at very forward angles.

This experiment was proposed to survey recoil spin observables, using the focal plane proton polarimeter in Hall A, up to energies of nearly 5 GeV. The goal was to determine whether these spin observables above the resonance region approach the asymptotic limits expected from perturbative quantum chromodynamics (pQCD), or whether there are indications of underlying resonances that are not seen in the cross section data. The main feature of the pQCD prediction is helicity conservation, which leads to the induced polarization p_y and polarization transfer C_x vanishing. The longitudinal polarization transfer, C_z, would be expected to vary like polarization transfer to a single quark, though with some dilution factor [Af97].

1.9.2 Experiment Status

The experiment ran during fall 1999. Data were obtained in a total of 39 kinematic settings. Table 1 gives the π^0 angles in the c.m. system – the proton angles are given by $180° - \theta_{\pi^0}$ – versus electron beam energy in GeV. The experiment ran interleaved with E89-019, making it possible to obtain 10 more data points at 3 more energies than originally proposed. Angular distribution coverage at the highest energies was limited by the maximum central momentum of the Hall A spectrometer.

	60°	75°	90°	105°	120°	135°
0.86	$\surd$	$\surd$	$\surd$	$\surd$	$\surd$	$\surd$
1.15	$\surd$	-	$\surd$	-	-	-
1.27	$\surd$	$\surd$	$\surd$	$\surd$	-	-
1.67	$\surd$	$\surd$	$\surd$	$\surd$	$\surd$	$\surd$
1.95	$\surd$	$\surd$	$\surd$	$\surd$	$\surd$	$\surd$
2.50	$\surd$	$\surd$	$\surd$	$\surd$	$\surd$	$\surd$
3.12	$\surd$	$\surd$	$\surd$	$\surd$	-	-
4.11	$\surd$	$\surd$	$\surd$	$\surd$	-	-
4.80	-	$\surd$	-	-	-	-

Table 1: *Kinematic coverage of E94-012 measurements.*

1.9.3 Expected Results

The analysis of the raw data is now largely complete. As the data were taken using a singles proton measurement, they contain a background from the tail of the *ep* elastic peak. For forward proton angles, the tail is small, due to the relatively larger pion photoproduction cross sections. However, at larger proton angles, the elastic scattering dominates. The present analysis is concentrated on Monte Carlo simulations which will allow us to understand and reliably subtract the ep elastic tail. Estimated uncertainties on the spin observables are generally in the range 0.05 - 0.1, except for increases due to spin transport. Becuase the data are very preliminary, without a subtraction of the *ep* elastic tail, we do not show any results here. We anticipate that the final results will be submitted for publication during summer 2001 [Wi01].

References

[Af97] A.A. Afanasev, private communication.

[Wi01] K. Wijesooriya *et al.*, to be published.

1.10 E95-001

Precise Measurement of the Transverse Asymmetry in Quasielastic $^3\vec{\mathrm{He}}(\vec{e}, e')$ and the Neutron Magnetic Form Factor

H. Gao, J.-O. Hansen, Spokespersons
and
The Jefferson Lab E95-001 collaboration

1.10.1 Introduction

JLab experiment E95-001 was completed in the spring of 1999. The purpose of this experiment was two-fold. The first goal was to measure the transverse asymmetry $A_{T'}$ on top of the quasielastic peak of $^3\vec{\mathrm{He}}(\vec{e}, e')$ and then to extract the neutron magnetic form factor G_M^n from these data. $A_{T'}$ was measured at six kinematic points corresponding to $Q^2 = 0.1$ to 0.6 $(\mathrm{GeV/c})^2$ in steps of 0.1 $(\mathrm{GeV/c})^2$. G_M^n has been extracted for $Q^2 = 0.1$ and 0.2 $(\mathrm{GeV/c})^2$. The results were published in a letter [1], and were also presented in conferences PANIC '99 [2] and SPIN 2000 [3]. The second goal was to measure the quasielastic asymmetry in the threshold region of $^3\vec{\mathrm{He}}(\vec{e}, e')$. Two kinematic points corresponding to $Q^2 = 0.1$ and 0.2 $(\mathrm{GeV/c})^2$ were covered. The data analysis was completed by the end of 2000 and a letter is in preparation [4].

1.10.2 Experiment

The experiment was carried out in Hall A, using a longitudinally polarized continuous wave electron beam of 10 μA current incident on a high-pressure polarized ^{3}He gas target, which was developed for the Hall A Polarized ^{3}He Target Program [5]. The beam helicity was flipped at a rate of 1 Hz (30 Hz for part of the experiment). The target was polarized by spin-exchange optical pumping at a density of 2.5×10^{20} nuclei/cm^3. The target spin was oriented at 62.5° to the right of the incident electron momentum direction. The beam and target polarizations were approximately 70% and 30%, respectively.

Electrons scattered from the target were detected in the two Hall A high resolution spectrometers, HRSe and HRSh. Both spectrometers were configured to detect electrons in single-arm mode using nearly identical detector packages consisting of two vertical drift chambers, two scintillator planes, a CO_2 gas Cherenkov detector and a lead-glass shower counter. The HRSe was set for kinematics near the top of quasielastic peak while HRSh covered both elastic peak and elastic threshold region. The elastic measurement allows for a continuous monitoring of the product of the beam and target polarizations, $P_b P_t$. The average $P_t P_b$ of this experiment determined from the elastic polarimetry was $0.208 \pm 0.001 \pm 0.005$ [6], where the errors are statistical and systematic, respectively.

1.10.3 Results

The transverse asymmetry $A_{T'}$ was obtained from the raw asymmetry of HRSe data for all Q^2 values. To extract G_M^n for the two lowest Q^2 kinematics, the transverse asymmetry data were averaged over a 30 MeV bin around the quasi-elastic peak. A Faddeev calculation with both final state interactions(FSI) and meson exchange currents(MEC) [7] was employed to generate $A_{T'}$ as a function of G_M^n in the same ω region. By comparing the measured asymmetries with the predictions, the G_M^n values at $Q^2 = 0.1$ and 0.2 (GeV/c)^2 were extracted. The extracted values of G_M^n are shown in Fig. 1 along with results from previous measurements and several theoretical calculations. The uncertainties shown are the quadrature sum of the statistical and experimental systematic uncertainties.

Although $A_{T'}$ has also been obtained at higher Q^2 values (0.3 - 0.6 (GeV/c)^2), full calculations are at present not available for these values of Q^2 to allow the extraction of G_M^n with high precision. Theoretical efforts are currently underway to extend the full calculation to higher Q^2.

The physics asymmetry in the elastic threshold region was obtained from the raw asymmetry of HRSh data at $Q^2 = 0.1$ and 0.2 (GeV/c)^2. The results are shown in Fig. 2. The inner error bars on the data are statistical only, while the outer error bars are the statistical

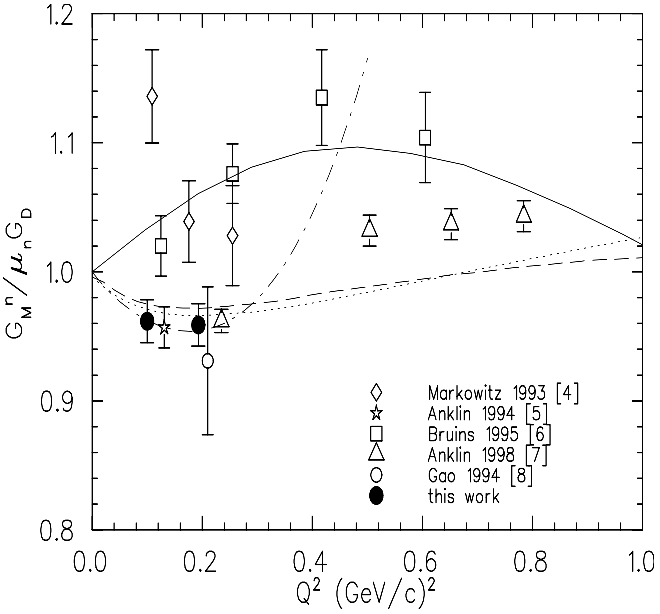

Figure 1: The neutron magnetic form factor G_M^n in units of the standard dipole form factor $(1 + Q^2/0.71)^{-2}$, as a function of Q^2, along with previous measurements and theoretical models. The Q^2 points of Anklin 94 [8] and Gao 94 [9] have been shifted slightly for clarity. The solid curve is a recent cloudy bag model calculation[10], the long dashed curve is a recent calculation based on a fit of the proton data using dispersion theoretical arguments [11], and the dotted curve is from the Höhler [12] parametrization. The dash-dotted curve is an analysis based on the relativistic baryon chiral perturbation theory [13].

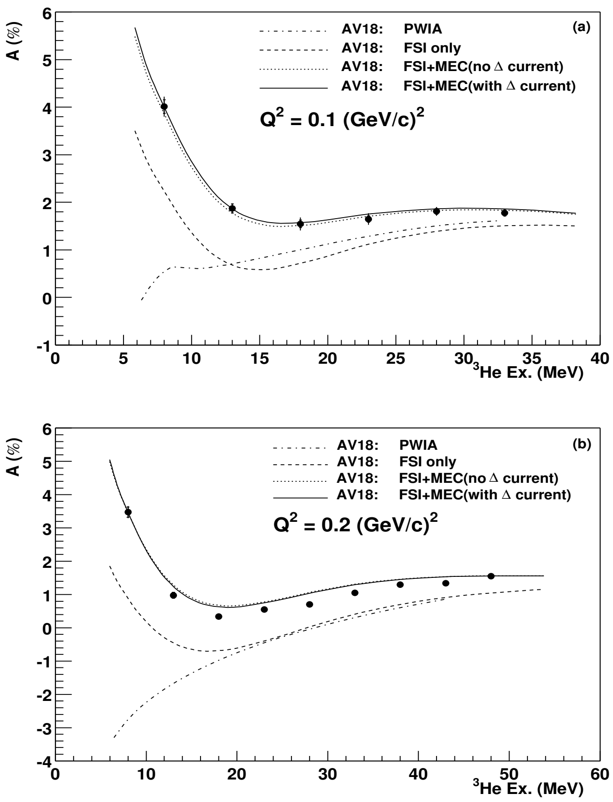

Figure 2: The physics asymmetry together with theoretical calculations for (a) $Q^2 = 0.1$ (GeV/c)^2 and (b) $Q^2 = 0.2$ (GeV/c)^2. The theoretical calculations are all performed using AV 18 potential, but with different reaction mechanisms.

and systematic errors added quadratically. As can be seen, the agreement between the full calculation and the data is quite good at $Q^2 = 0.1$ (GeV/c)^2. The discrepancy at $Q^2 = 0.2$ (GeV/c)^2 might be due to effects of three-nucleon force and relativity, which are not included in the present calculation. Theoretical work is currently underway to investigate these effects.

References

[1] W. Xu *et. al*, Phys. Rev. Lett. **85**, 2900 (2000).

[2] J.-O. Hansen, Proceedings of the 15th International Conference on Particles and Nuclei (PANIC '99), Uppsala, Sweden, 10-16 June 1999, Elsevier, Amsterdam, 2000. Nucl. Phys. A663 & 664, 409c (2000).

[3] J.-O. Hansen, to be published in Proceedings of the 14th International Spin Physics Symposium(SPIN 2000), Osaka, Japan, 16-21 October 2000, K. Hatanaka, ed., AIP Conference Proceedings, 2001.

[4] F. Xiong *et. al*, in preparation for publication.

[5] J.S. Jensen, Ph.D. Thesis, California Institute of Technology, 2000 (unpublished); P.L. Anthony *et al.*, Phys. Rev. D, **54** 6620 (1996); http://www.jlab.org/e94010/tech_notes.html.

[6] O.N. Ozkul, Senior Thesis, MIT (2000), unpublished.

[7] V.V. Kotlyer, H. Kamada, W. Glöckle, J. Golak, Few-Body Syst. **28**, 35 (2000).

[8] H. Anklin *et al.*, Phys. Lett. **B336**, 313 (1994).

[9] H. Gao *et al.*, Phys. Rev. C **50**, R546 (1994); H. Gao, Nucl. Phys. **A631**, 170c (1998).

[10] D.H. Lu, A.W. Thomas, A.G. Williams, Phys. Rev. C **57**, 2628 (1998).

[11] P. Mergell, U.-G. Meißner, D. Drechsel, Nucl. Phys. **A596**, 367 (1996).

[12] G. Höhler *et al.*, Nucl. Phys. **B114**, 505 (1976).

[13] B. Kubis, U.-G. Meißner, hep-ph/0007056.

2 Hall B

2.1 Hall B Overview

Hall B's mission is to carry out experiments that require the efficient detection of multi-particle final states, or experiments that can only be performed at low luminosity. Final states with several particles are typical in reactions involving the production of excited mesons and baryons, or in nuclear break-up reactions. The luminosity may have to be limited to keep accidental coincidences low, e.g. for a tagged bremsstrahlung photon beam or for experiments requiring the coincident detection of particles that are only loosely correlated. Solid-state polarized targets can only be operated at low luminosity. High detection efficiency for multi-particle events and a useful event rate at limited luminosity both require a detection system with a large acceptance.

To carry out this program, Hall B is equipped with a large acceptance magnetic detector, the CEBAF Large Acceptance Spectrometer (CLAS). CLAS is a magnetic toroidal multi-gap spectrometer. Its magnetic field is generated by six super-conducting coils arranged around the beam line to produce a field which is pointing primarily in the ϕ-direction. The particle detection system consists of drift chambers to determine the track of charged particles, gas Cerenkov counters for electron identification, scintillation counters for the trigger and for measuring time-of-flight, and electromagnetic calorimeters to detect showering particles (electrons and photons) and neutrons. The segments are individually instrumented to form six independent magnetic spectrometers. This facilitates pattern recognition and track reconstruction at high luminosity.

For electron scattering experiments, a small normal-conducting toroid ("mini-torus") surrounding the target keeps (low momentum) charged electromagnetic background from reaching the innermost drift chamber.

A two-stage trigger system is used to initiate data conversion and readout. The Level I trigger makes use of the fast information from the time-of-flight counters, the Cerenkov counters, and the electromagnetic calorimeters. Level 2 adds crude track finding using the hit pattern in the drift chambers.

For tagged bremsstrahlung experiments, a six-element start counter will provide a fast input for the Level I trigger, and the start for the time-of-flight measurements.

The data acquisition system collects the digitized information and stores the information for later off-line analysis. For an event rate of 1,500 events/sec, the system has to handle a data rate of approximately 10 Mbytes/sec.

A Møller polarimeter to measure the polarization of the incident electron beam is located in the upstream beam tunnel. For electron scattering experiments the primary electron beam - after passing through the target - is stopped in a Faraday cup to measure the beam current.

For tagged photon experiments, a radiator is inserted in front of the bremsstrahlung tagging spectrometer which occupies an enlarged tunnel section at the entrance of the hall. The primary electron beam is deflected vertically into a low-power beam dump. Equipment to monitor the tagged photon beam is located behind CLAS in the downstream tunnel section.

Commissioning of the CLAS was completed in November 1997, and physics research began in December of that year. Since then, CLAS has taken partial data on a total of 42 experiments CLAS is now operating at its design luminosity, and typical figures-of-merit used to characterize the device, such as energy resolution, position reconstruction accuracy, and time-of-flight resolution are close to their design values. Data acquisition speed has exceeded the design values of 1,500 events/sec by more than a factor of two.

2.2 e1 Run Group Overview

V. Burkert - for the CLAS Collaboration

2.2.1 Introduction

The E1 run group comprises experiments with common run conditions such as energy, target, and magnetic field setting that take data simultaneously using the CLAS detector in Hall B. While each experimental collaboration within the run group defines its own physics goals, and has the responsibility to analyse and publicize the physics results of specific reactions, the run groups are optimizing their operation and physics output by utilizing the capabilities of CLAS in an efficient way. The E1 run group comprises now 16 individual experiments studying reactions with single pion and eta production, two pion production, hyperon excitation, vector meson production, etc., using unpolarized or polarized electron beams.

While some experiments address nuclear physics problems in the deuteron, the primary thrust of this program is to obtain a better understanding of nucleon structure in the transition region from small to large distances where perturbative methods of QCD are not applicable. The experiments of the E1 run group will provide precise data on the helicity structure of nucleon resonance transitions, they search for “missing” baryon resonances in an effort to probe fundamental symmetry properties related to the internal structure of baryons, and then study strangeness production mechanisms and hyperon excitations. As these measurements are being done with varying spatial resolution of the virtual photon probe, we will obtain detailed information on the nucleon structure as a function of the distance scale. This program will provide the experimental information to answer questions such as “What are the relevant degrees of freedom at different distance scales?”, and help connect successful models such as the quark model, to the fundamentals of QCD.

2.2.2 Experiment Status

The total beam time allocated to the E1 run group is 122 beam days at energies ranging from 1.5 GeV to 5 GeV, with liquid hydrogen and deuterium as production targets. To date

61 days of effective beam time or 50% of the total time have been used, mostly on hydrogen targets and at lower energies. E1 data have been collected so far with an open trigger that enriches events with an electron scattered into the active area of CLAS. The entire event is kept for further analysis independent of the hadronic event topology. Electron thresholds are set using the total energy sum in the electromagnetic calorimeter. So far there were 3 run periods in winter/spring 1998, 1999, and 2000, with energies of 1.5/1.6 GeV, 2.4/2.5 GeV, 3.1 GeV, and several energies from 4.0 - 4.8 GeV. The reason for the many different energy settings is due to the requirement of compatibility with high electron polarization in all experimental Halls. Data were taken with several different current settings for the torus magnet, typically 1500A, 2250A, and 3375A, dependent on the resolution and acceptance requirements of the individual experiments.

Polarized electrons were available for most of the data with polarization degrees in the range from 60 to 75%. The lower energy data were taken with luminosities of 2-3×10^{33}cm^{-2}sec^{-1}, and for the higher energy runs of up to 10^{34}cm^{-2}s^{-1}.

Data taking at 1.6 and 2.4 GeV with hydrogen has been completed, while only a small fraction of data have been taken at the higher energies. Figure 1 shows an example of the simultaneous coverage of electron kinematics for a 4 GeV incident electron beam impinging upon a hydrogen target.

The total number of electron events collected exceeds 1.5 10^9 with all possible hadronic topologies. Most experiments make use of the missing mass technique to identify one undetected particle in the final state. As an example, Figure 2 shows the phase space covered in $ep \to epX$ reaction, where π^o, η and ω mesons are clearly visible.

The excellent resolution of the time-of-flight system of $\approx$ 150psec allows separation of pions, kaons, and protons over a large momentum range. Figure 3 shows the mass spectrum as determined from time-of-flight and particle momentum summed over the entire phase space measured in CLAS.

The next E1 run period is expected for early 2002 and will focus on the higher energies as well as on data taking using a deuterium target.

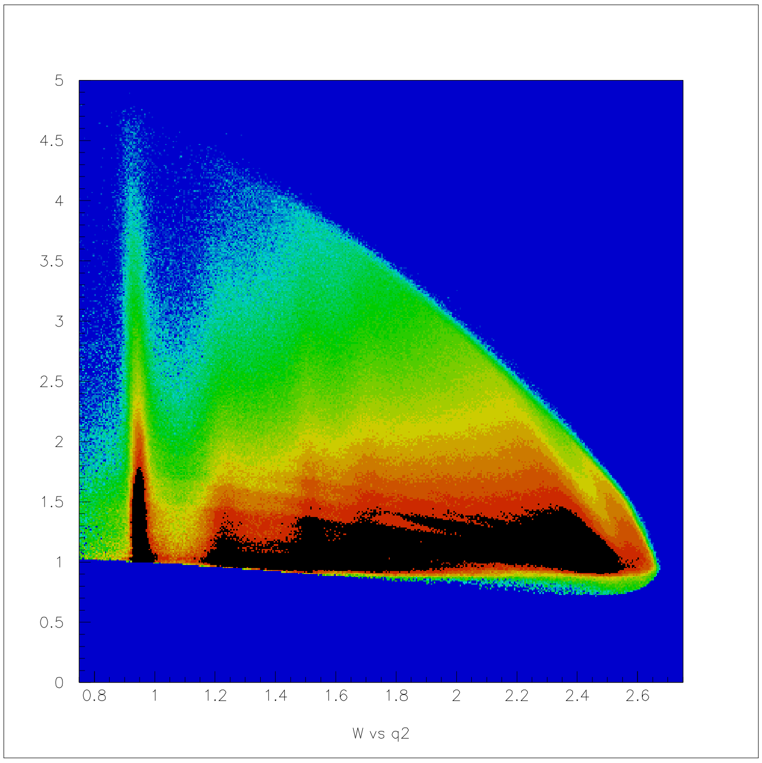

Figure 1: Simultaneous coverage in W(GeV) and Q^2(GeV^2) for CLAS E1 experiments at 4 GeV beam energy. The elastic scattering peak as well as the three resonance regions are evident. The low Q^2 cut-off is due to limitations in forward angle electron detection for high magnetic field and electron bending towards the beam axis. This region is covered in lower field operation or with reversed field polarity (electrons bending away from the axis).

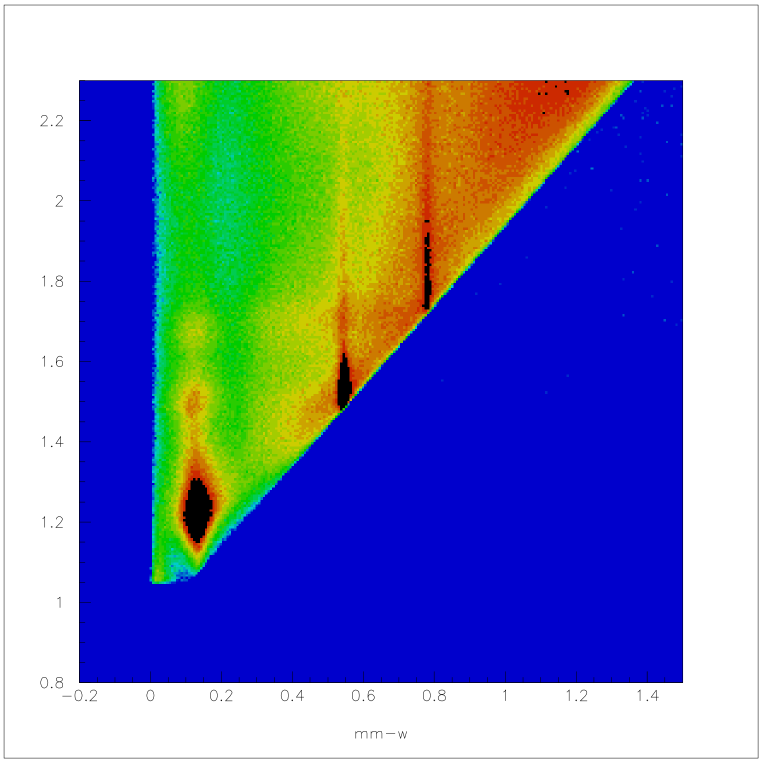

Figure 2: W vs (missing mass)^2 in GeV^2 for $ep \rightarrow epX$ at a 4 GeV beam energy. Strong correlations between specific final states and resonance production are evident.

2.2.3 Results - or Expected Results

A fraction of all data have been fully analysed and the results are published [1] or submitted for publication [2]. Several more analyses have been completed and draft papers are under collaboration review [3, 4, 5], or will be reviewed within the first half of 2001 [6, 7, 8, 9, 10].

The first results already have significant impact in several areas:

- The eta electroproduction results together with previous JLab results at higher Q^2 now show a consistent picture of the Q^2 dependence of the $S_{11}(1535)$ transition form factor. This behavior is not understood in any model.

- The results on the $N- > \Delta(1232)$ transition basically rule out quark models that do not explicitly include pion cloud contributions. Also, specific chiral soliton models of the nucleon structure do not reproduce the data on E_{1+}/M_{1+}.

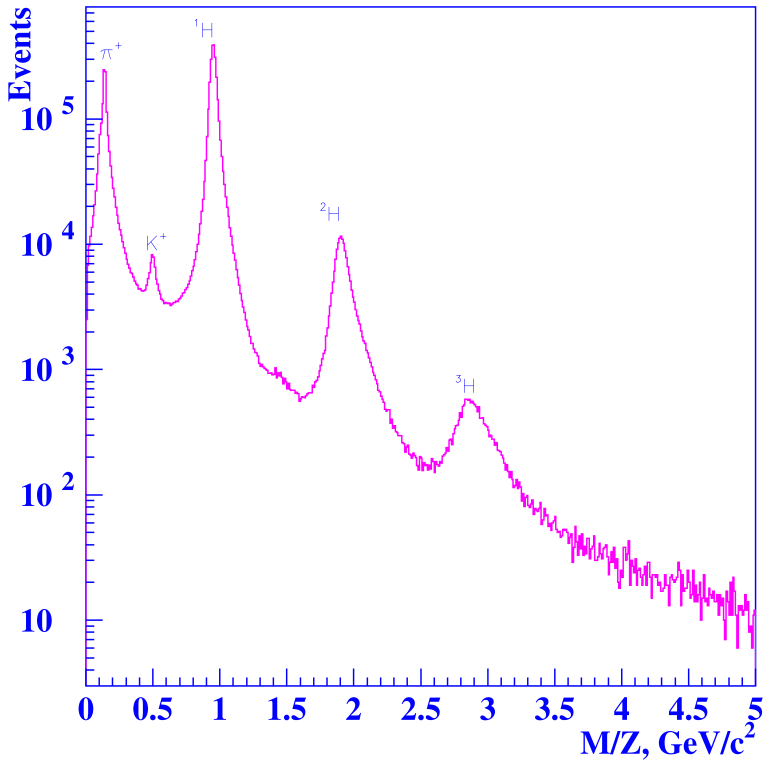

Figure 3: Mass spectrum of positive particles as determined by time-of-flight and momentum emerging from a carbon target. The presence of pions, kaons, protons, deuterons, and tritons is evident .

- Two-pion production data show clear resonance behavior in at least two regions of the invariant hadronic mass, not seen before in this channel.

- The $n\pi^+$ production channel, for the first time, provides the data needed for a more complete isospin decomposition, and is especially sensitive to the higher mass I=1/2 state such as the Roper $P_{11}(1440)$, or $D_{13}(1520)$ resonances.

- Measurement of hyperon production, such as the ground state $\Lambda(1115)$ and the excited state $\Lambda(1520)$ exhibit an intriguingly similar behavior in their Q^2 dependencies, which suggests a common production mechanism. This is in stark contrast to the Q^2 dependence of $K^+\Sigma^0(1193)$.

- Also for the first time, beam asymmetries have been measured in single π^o and π^+ production, that will help determine non-resonant amplitudes in the $\Delta(1232)$ region. Polarization obervables have also been measured in $K^+\Lambda$ and $K^+\Sigma$ production which show intriguing energy dependences with few indications of resonant behavior.

  Results of these measurements will put models that predict reactions at the amplitude level to serious tests, and further our understanding of nucleon structure.

- The exclusive process of "Deep Virtual Compton Scattering" has been unambiguously observed in beam asymmetry measurements for the first time in the E1 run. Not only does it provide the data to test models for the Generalized Parton Distributions, but it also shows the power of a large acceptance detector operating at high luminosity.

References

[1] R. Thompson, S. Dytman, K. Kim, J. Mueller, *et al.*, hep-ex/0011029, accepted by Phys. Rev. Letts.

[2] C. Lukashine, E. Smith, *et al.*, hep-ex/0101030, submitted to Phys. Rev. C

[3] S. Barrow, L. Dennis, S. McAleer, et al., Angular distributions in $ep \rightarrow eK^+\Lambda(1520)$ production

[4] K. Joo, L.C. Smith, V. Burkert, R. Minehart, *et al.*, "Measurement of the Q^2 dependence of E_{1+}/M_{1+}, S_{1+}/M_{1+} for the $\gamma N\Delta(1232)$ transition.

[5] M. Ripani, V. Burkert *et al.*, Two-pion Decay of electroproduced Light Quark Baryon Resonances.

[6] V. Burkert, L. Elouadrhiri, S. Stepanyan, et *al.*, First observation of the Deep Virtual Compton Scattering Process in $ep \to ep\gamma$.

[7] H. Egiyan, V. Burkert, R. Minehart, et al., Single $\pi+$ production off protons in the nucleon resonance region.

[8] K. Joo, L.C. Smith, V. Burkert, R. Minehart, *et al.*, Beam single spin asymmetry in single pion production

[9] R. Feuerbach, G. Niculescu, K. Hicks, M. Mestayer, *et al.*, Electroproduction of $K^+\Lambda$ on protons.

[10] D. Carman, K. Joo, B. Raue, et al., Polarization observables in $K^+\Lambda$ and $K^+\Sigma$ electroproduction off protons.

2.3 E89-037

Electroproduction of the $P_{33}(1232)$ Resonance

V. Burkert and R. Minehart (Spokespersons)
K. Joo, L.C. Smith
and the CLAS Collaboration

2.3.1 Introduction

Experiment 89-037 is part of a program using the CLAS detector to study the transition form-factors for production of single pions in the scattering of electrons on protons. These measurements cover a range in Q^2 from about 0.3 to 3.0 GeV^2 and span the resonance region up to W=2 GeV, and in some cases beyond. The experiment has been incorporated into the E1 running group. The electrons from energies of 1.6 to 4 GeV are scattered from the CLAS liquid hydrogen target, and electron scattering angles from as low as 8° (using the torus magnet to bend the scattering electrons away from the beam) to 45° can be measured. Since we can obtain a very large number of events, the exclusive reactions can be measured with high precision with small bins in W and Q^2 over an essentially complete kinematical range. We expect these data will yield new information with unprecedented precision on resonant and non-resonant transition amplitudes in the non-perturbative regime. Special focal points of the experiment are a precision determination of the transition amplitudes for the $\Delta(1232)$ for Q^2 ranging from near the photon point to the maximum values accessible at CEBAF.

2.3.2 Experiment Status

The E1 running group has had three major run periods, E1a, E1b and E1c, with the first one taking place in the spring of 1998. So far about 50% of the approved data set for 89-037 has been taken, with beam energies of 1.6, 2.4 and 4.0 GeV. About one billion electron events have been recorded on tape. We have finished calibrations and most of the analysis of the E1a data, with emphasis on extracting multi-pole parameters for the $\Delta(1232)$ resonance in exclusive π^+ and π^0 production. The analyses of the π^+ data set will form the basis for the

Ph.D. thesis of Hovanes Egiyan (William and Mary). The data reduction for the π^0 data set has been carried out primarily by Cole Smith and Kyungseon Joo. A detailed analysis report is being written, and a first draft of a PRL letter for π^0 production will shortly be submitted to the Structure of the Nucleon Working Group for its review. It is expected that the letter will be submitted for publication this spring. Preliminary results from these analyses have been presented in many invited and contributed talks at conferences around the world. The next E1 running period is scheduled for the fall of 2001, at which time we will obtain data for beam energies of 6 GeV.

2.3.3 Results

We have analyzed the 1.6 and 2.5 GeV data from E1a running period, using this set to develop the analysis techniques which we believe can be applied with only a small amount of fine-tuning to the rest of the data set. The analysis required extensive modeling of the CLAS acceptance, tracking efficiency, and resolution, using a GEANT model. Software fiducial cuts were used to define the solid angle for electrons and hadrons. Radiative corrections were calculated using a Monte-Carlo integration of the Mo-Tsai[4] formula not using the peaking approximation. Calculations with various values of cuts and other parameters have been made to estimate the magnitude of systematic errors.

For this first stage, we have concentrated on the region of the $\Delta(1232)$ resonance. A longstanding question is the origin of the quadrupole strength experimentally observed in the $\gamma N \rightarrow \Delta$ transition. Besides the dominant magnetic dipole (M_{1+}) excitation mode, in which a single quark spin is flipped, a small but non-zero electric (E_{1+}) and Coulomb (S_{1+}) quadrupole are seen, indicating strong tensor correlations among the hadronic constituents and an intrinsic nucleon deformation. A crucial experimental test for models of nucleon deformation is the Q^2 dependence of the multipole ratios $R_{EM} = E_{1+}/M_{1+}$ and $R_{SM} = S_{1+}/M_{1+}$. Recent precision measurements of the $p(\gamma,\pi^o)p$ and $p(\gamma,\pi^+)n$ reaction channels at LEGS and MAMI found $R_{EM} \approx -2.5 - 3.0\%$ at $Q^2 = 0$. A $p(e,e'p)\pi^o$ experiment in Hall C at JLAB found $R_{EM} = -2.0\%$ at $Q^2=4$ (GeV/c)^2, while R_{SM} was 5-6 times larger and increasingly negative with Q^2. These results clearly rule out the influence of perturbative QCD, which favors helicity conserving amplitudes for which $E_{1+} \rightarrow M_{1+}$ and

$S_{1+} \rightarrow constant$ as $Q^2 \rightarrow \infty$. At the same time, QCD-inspired constituent quark models account for $< 10\%$ of the value of R_{EM} obtained by the new measurements at $Q^2 = 0$. Although recent dynamical models incorporating chiral symmetry breaking or pion final state interactions[3] are more successful, they make different predictions for the Q^2 evolution of R_{EM} and R_{SM}.

Under the one-photon-exchange approximation, the electroproduction cross section factorizes as follows:

$$\frac{d^5\sigma}{dE_{e'}d\Omega_{e'}d\Omega^*_\pi} = \Gamma_v \frac{d^2\sigma_u}{d\Omega^*_\pi} \tag{1}$$

where Γ_v is the virtual photon flux. For unpolarized beam and target the center-of-mass (c.m.) differential cross section $d^2\sigma_u$ depends on the transverse ϵ and longitudinal ϵ_L polarization of the virtual photon through four structure functions: σ_T, σ_L and their interference terms σ_{LT} and σ_{TT}:

$$\begin{aligned}\frac{d^2\sigma_u}{d\Omega^*_\pi} = \frac{p^*_\pi}{k^*_\gamma}(\sigma_T \quad &+ \quad \epsilon_L\sigma_L + \epsilon\,\sigma_{TT}\,sin^2\theta^*_\pi\,cos\,2\phi^*_\pi \\ &+ \quad \sqrt{2\epsilon_L(\epsilon+1)}\,\sigma_{LT}\,sin\,\theta^*_\pi\,cos\,\phi^*_\pi)\end{aligned} \tag{2}$$

where $(p^*_\pi, \theta^*_\pi, \phi^*_\pi)$ are the π^o c.m. momentum, polar and azimuthal angles, $\epsilon_L = (Q^2/|k^*|^2)\epsilon$, and the virtual photon c.m. momentum and equivalent energy are $|k^*|$ and k^*_γ. Multipoles are obtained from a partial wave expansion of the structure functions, where M_{1+} dominance is assumed and the $p\pi^o$ final state is fitted up to l_π=1:

$$\begin{aligned}\sigma_T + \epsilon_L\sigma_L &= A_o + A_1\,cos\,\theta^*_\pi + A_2\,P_2(cos\,\theta^*_\pi) \\ \sigma_{TT} &= C_o \\ \sigma_{LT} &= D_o + D_1\,cos\,\theta^*_\pi\end{aligned} \tag{3}$$

To simplify the analysis, only terms which interfere directly with M_{1+} are retained. Thus, $|M_{1+}|^2$ and its projection onto the other s- and p-wave multipoles $E_{1+}, S_{1+}, M_{1-}, E_{0+}, S_{0+}$ are given in terms of the six partial-wave coefficients by [1]:

$$\begin{aligned}|M_{1+}|^2 &= A_0/2 \\ Re(E_{1+}\,M^*_{1+}) &= (A_2 - 2\,C_0/3)/8 \\ Re(M_{1-}\,M^*_{1+}) &= -(A_2 + 2\,(A_0 + C_0))/8 \\ Re(E_{0+}\,M^*_{1+}) &= A_1/2 \\ Re(S_{0+}\,M^*_{1+}) &= D_0 \\ Re(S_{1+}\,M^*_{1+}) &= D_1/6\end{aligned} \tag{4}$$

More extensive general analyses extending beyond the Δ region are also being applied. These include a method based on the AO program to fit amplitudes of resonances and background terms at each energy, as well as a dispersion theoretic method developed by Aznauryan and Stepanyan.

Figure 1 shows a typical set of angular distributions for the cross section at Q^2=0.525 GeV and W=1.26 GeV.

Preliminary results for the structure functions obtained in the region of the $\Delta(1232)$ for Q^2 = .525 GeV are shown in Figure 2 along with the predictions of the MAID98 and MAID2000 [6] models and a model of Sato and Lee [Sa-00]. The resulting fits are shown in Figure 3 as a function of W for this value of Q^2.

References

[1] A.S. Raskin and T.W. Donnelly, Ann. Phys., **191**, 78 (1989).

[2] A. Silva, D. Urbano, T. Watabe, M. Fiolhais and K. Goeke, hep- ph/9905326.

[3] S.S. Kamalov and Shin Nan Yang, Phys. Rev. Lett., **83**, 4494 (1999); S.S. Kamalov. S.N. Yang, D. Drechsel, O. Hanstein, L. Tiator, nucl-th/0006068.

[4] L.W. Mo and Y.S. Tsai, Rev. Mod. Phys., **45**, 205 (1969).

[5] O. Hanstein *et al*, Nucl. Phys., **A632**, 561 (1998); L. Tiator *et al*, nucl-th/0012046.

[6] D. Drechsel, O. Hanstein, S.S. Kamalov, L. Tiator, Nucl. Phys., **A645**, 145 (1999). Cross sections were calculated from $p\pi^o$ multipoles (up to L=5) downloaded from the MAID98 web page: http://www.kph.uni-mainz.de/T/maid/maid.html

[7] T. Sato and T.-S.H. Lee, Phys. Rev., **C54**, 2660 (1996) and T.-S.H. Lee, private communication, 2000.

[8] M. Warns, H. Schroder, W. Pfeil and H. Rollnik, Z. Phys. C, **45**, 627 (1990).

[9] V.V. Frolov *et al*, Phys. Rev. Lett., **82**, 45 (1999).

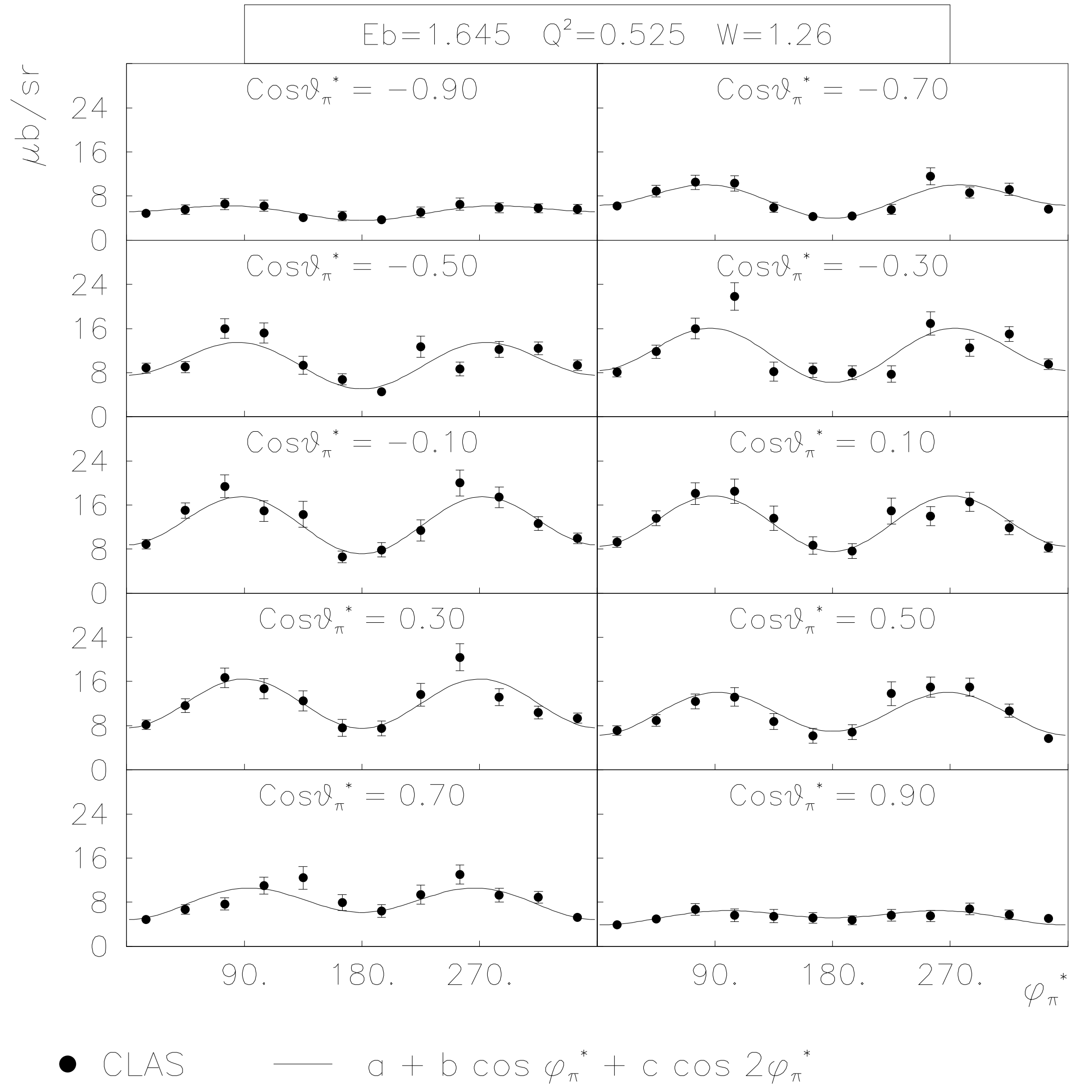

Figure 1: Cross sections plotted as functions of the hadronic center of mass angle, ϕ, for W=1.26 GeV, Q^2 =0.525 GeV^2, for a beam energy of E=1.645 GeV, and 8 bins in $\cos\theta^*_\pi$. The lines are a fit to $a + b\ \cos\phi^*_\pi + c\ \cos(2\phi^*_\pi)$.

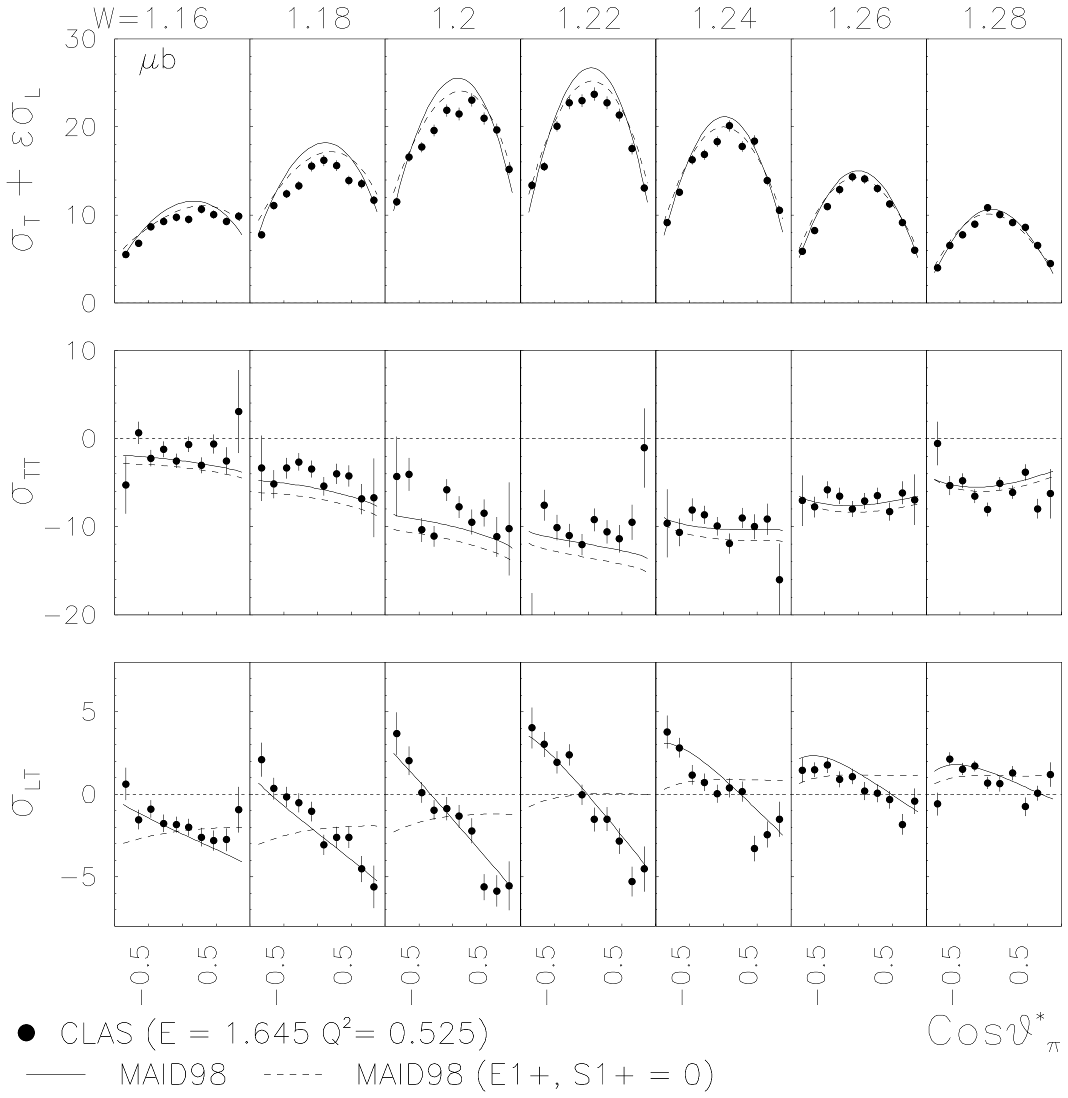

Figure 2: Structure functions extracted from $p(e, e'p)\pi^o$ data at $Q^2 = 0.525\,(\mathrm{GeV/c})^2$. Each data point represents a fit of Eq. 2 to ϕ^*_π distributions at a fixed W and $cos\,\theta^*_\pi$ bin, such as shown in Fig.1. Solid line shows MAID98 prediction with E_{1+} and S_{1+} multipoles turned on (solid line) and off (dashed line). To first order σ_{LT} is exclusively sensitive to S_{1+}.

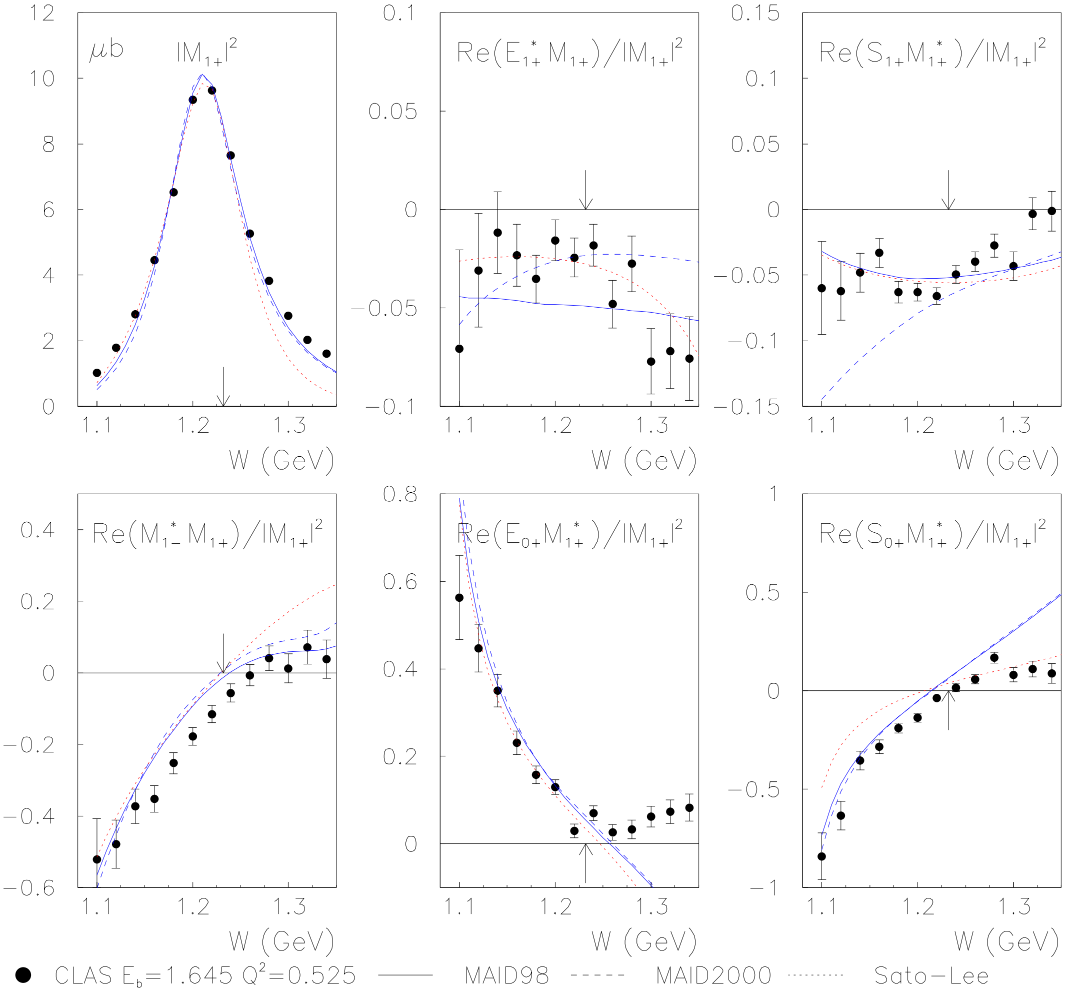

Figure 3: W dependence of $|M_{1+}|^2$ and its interference terms in the $\Delta^+ \rightarrow \pi^o p$ charge channel at Q^2= 0.525 (GeV/c)^2, extracted from fits to experimental structure functions using Eqs. 3,4. A separate fit was made for each W bin. Model predictions for $\pi^o p$ multipoles shown for MAID98 (solid line), MAID2000 (dashed line) and dynamical pion model of Sato and Lee (dotted line). Arrow indicates Δ resonance position at W=1.232 GeV

[10] R. Beck *et al*, Phys. Rev. Lett., **78**, 606 (1997).

[11] G. Blanpied *et al*, Phys. Rev. Lett. **79**, 4337 (1997).

[12] C. Mertz *et al*, nucl-ex/9902012.

[13] H. Schmieden, nucl-ex/9909006.

2.4 E89-038

Measurements of $p(e,e'\pi^+)n$, $p(e,e'p)\pi^o$, and $n(e,e'\pi^-)p$
in the Second and Third Resonance Regions

V. Burkert, R. Minehart, and the CLAS collaboration

2.4.1 Introduction

The goal of the experiment is to measure the transition form factors of several of the higher resonances that populate the mass region near 1.5 GeV and 1.7 GeV. States with masses near 1.5 GeV are the "Roper" $N(1440)P_{11}$, $N(1520)D_{13}$, and $N(1535)S_{11}$, while there are seven well known states near 1.7 GeV, the most prominent ones in electromagnetic interactions being the the $N(1680)F_{15}$, $N(1650)S_{11}$, and $\Delta(1700)D_{33}$. As many of these states have isospin 1/2 it is very important to measure not only the "easy" $\gamma^* p \rightarrow p\pi^o$ but the charged $n\pi^+$ final state as well. Note that the I=1/2 states couple preferentially to the charged pion final state. A combined analysis of both final states as well as the channel $\gamma n \rightarrow p\pi^-$ from deuterium targets gives the complete isospin information for single pion production from nucleons.

2.4.2 Experiment Status

Data have been taken mostly at 1.5 GeV and 2.5 GeV during the E1c and E1d run periods in spring 1999 and 2000 with a hydrogen target. Data on deuterium were also taken at 2.5 GeV during the E1d run period but have not been analyzed yet. This report deals only with the data from the E1c run period.

Two field settings were used to optimize the acceptance and cover a Q^2 range from 0.3 to 0.65 GeV^2. Data taken at different torus field settings will also help to determine systematic uncertainties in the acceptance calculation. Some complications in the analysis came from the performance of the liquid hydrogen target which, due to insufficient thermal shielding when using a new cell, was never completely full, and emptied itself at numerous occasions

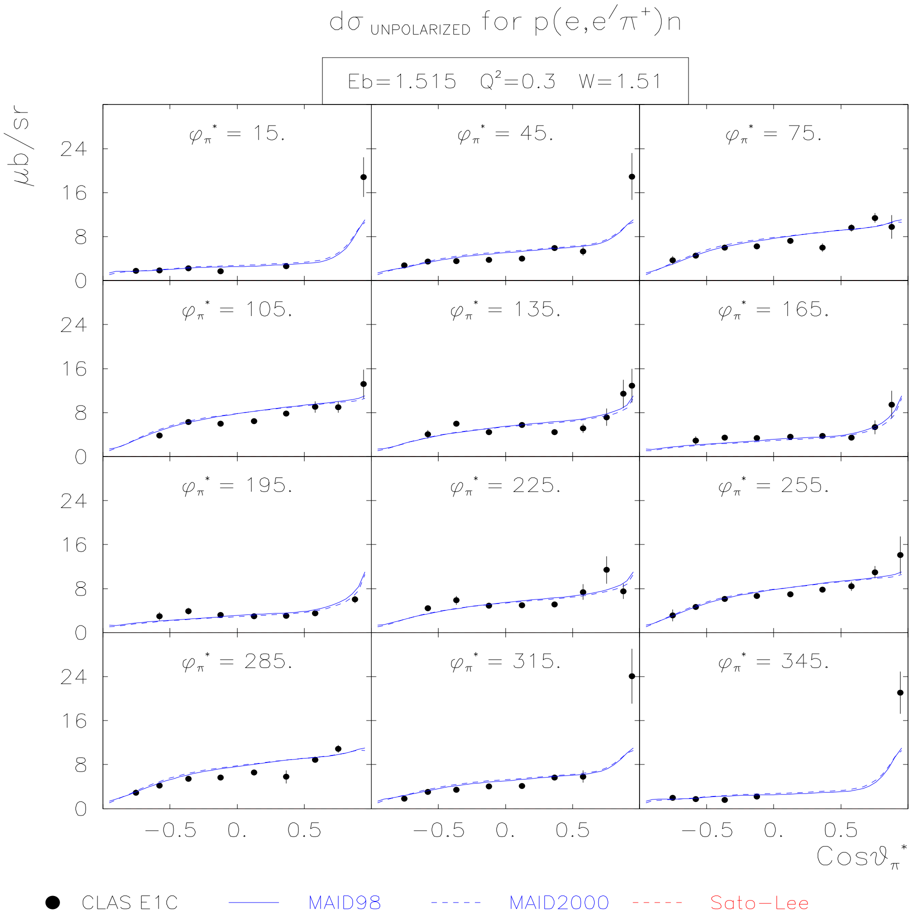

Figure 1: Preliminary angular distributions for $n\pi^+$ electroproduction at fixed invariant mass W off protons at different azimuthal angles. The curve represent the MAID parametrization.

in the course of the run. Although this behavior can be fully accounted for when analyzing the data, it introduced some delay in the analysis.

To complete data taking for this experiment, additional runs with the hydrogen target at higher energies and with the deuterium target at 1.5 GeV will be needed.

2.4.3 Expected Results

The 1.5 GeV data have been nearly completely analyzed for the $n\pi^+$ channel. Hovanes Egiyan, a graduate student from the College of William and Mary is writing his PhD thesis based on the analysis of these data. The data cover mainly the 1.5 GeV mass range for $Q^2 = 0.3 - 0.6\mathrm{GeV}^2$. Full GSIM simulations have been carried out using MAID2000 and AO as parametrization of the process. Radiative corrections have been applied using the procedure by Mo and Tsai in a full Monte Carlo simulation without applying the "peaking" approximation. In conjunction with I. Akushevich [1] a new approach for radiative corrections has been developed that applies to exclusive reactions. This approach is currently being tested. Differential cross sections have been extracted over nearly the complete center-of-mass angular distribution. A set of differential cross section data in the 2nd resonance region are shown in Figure 1.

Since the acceptance covers the full azimuthal angle for π^+ production, we can also determine the response functions $\sigma_t + \epsilon\sigma_L$, σ_{TT} and σ_{LT} using a fit to a function $a + b\cos(\phi) + c\cos(2\phi)$. The response functions have been further analyzed using a power expansion in $\cos\theta$. Preliminary results is shown in Figure 2. This is the first time that this information could be extracted from electroproduction experiments.

In collaboration with Inna Aznauryan, a theorist from Yerevan, and Stepan Stepanyan from CNU, a Fortran code (JANR) [2] was developed that allows fitting of all single pion production data in an energy-dependent fashion. The analysis implements basic features of MAID2000 and allows fitting of cross section data. The code was tested on π^o production in the $\Delta(1232)$ region. In the future, JANR will be used to analyze π^o and π^+ in a coupled channel analysis, including polarization observables. In addition, the GWU group is analyzing these data together with the world data to assess their impact on the extraction of resonance parameters.

We are currently in the process of finalizing the data analysis and hope to complete the physics analysis before the summer of 2001.

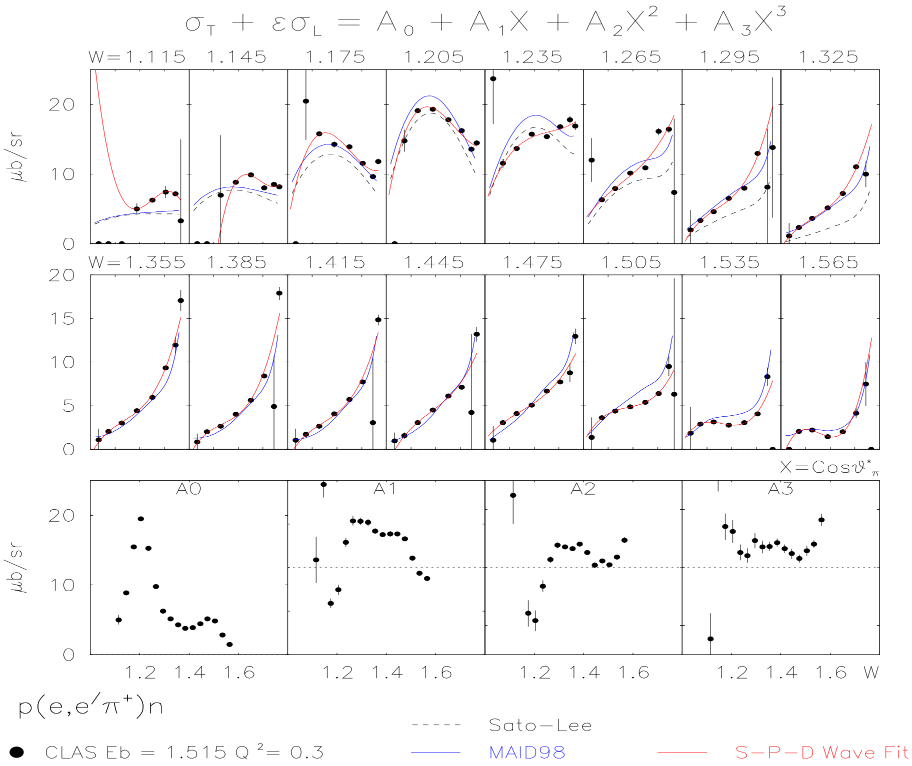

Figure 2: Response function $\sigma_T + \epsilon\sigma_L$ with fit to the angular distribution. The bottom panel shows preliminary angle coefficients from the fit. The angle- independent term A_0 shows a strong resonance behavior from the $\Delta(1232)$ and higher resonances. The A_1 term shows strong effects due to possible s-p-wave interference in the region of the $N(1440)P_{11}$ and $N(1535)S_{11}$ resonances.

References

[1] A. Afanasev, I. Akhushevich, V. Burkert, K. Joo, to be published

[2] I. Aznauryan, V. Burkert, S. Stepanyan, JANR - Jlab Analysis of Nucleon Resonances, internal report.

2.5 E89-039

Eta Electroproduction

S.A. Dytman, J.A. Mueller and the CLAS COLLABORATION

2.5.1 Introduction

This experiment is measuring quantities based on electroproduction experiments where there is at least one eta meson in the final state. These include cross sections and single polarization observables for eta electroproduction. There can be a nucleon or an N^* resonance in coincidence with the eta. The first results have been recently accepted for publication in Physical Review Letters [Th01].

The first interest is in the reaction $ep \to e'p\eta$. Near threshold, W=1.485 GeV, previous experiments have seen a strong inelastic excitation that has most often been associated with a *single* N^* state, the $S_{11}(1535)$. This brings a significant advantage in uniquely identifying an individual resonance signal. Further, this state has the unique properties of a very strong (50%) branching fraction to ηN and a very slow decrease of the transition form factor for $\gamma N \to N^*$, $A_{1/2}(Q^2)$. These data further elucidate the microscopic structure of $S_{11}(1535)$.

The second interest is to examine the reaction at energies above threshold where the previous data are far less complete. Before this experiment, eta production data has produced no strong signals for resonances other than $S_{11}(1535)$.

Interplay between this experiment and complementary photoproduction results is of great interest. Recent photoproduction experiments[Aj98] have shown the value of precise data in seeing the signs of interference between the dominant $S_{11}(1535)$ and other resonances. That theme has continued in this experiment.

2.5.2 Experiment Status

Data for this reaction have been taken in each of the 3 e1 run periods. The first e1 run period (February-March, 1998) data are reported here. Cross sections have been measured for W from threshold to about 1.86 GeV and at Q^2 from 0.25 to 1.5 $(\mathrm{GeV}/c)^2$. The second e1 run period data are presently being analyzed with results expected later in 2001. These data extend to lower Q^2 and add beam polarization data.

The great advance of CLAS is to simultaneously collect data over a broad kinematical range. For this reaction, cross sections are presented for the full range of meson decay angles (θ_η^* and ϕ_η^*).

2.5.3 Results

Unless an isolated resonance is seen, a partial wave amplitude fit is most often required before a physics analysis can be done. With only cross section data, that cannot be done uniquely without simplifying assumptions. Since these data are dominated by a single resonance and a limited number of partial waves are expected to contribute close to threshold, we do *both* a truncated PWA analysis and a single resonance analysis.

The exact virtual photon cross section is

$$\frac{d^2\sigma}{d\Omega_\eta^*} = \frac{|p_\eta^*|}{K_{cm}}\left[R_T + \epsilon R_L + R_{LT}\cdot\sqrt{\frac{\epsilon}{2}(\epsilon+1)}\cos\phi_\eta^* + R_{TT}\cdot\epsilon\cos 2\phi_\eta^*\right]. \tag{1}$$

The angular distributions were fit to a form,

$$\begin{aligned}\approx\ & \frac{|p_\eta^*|}{K_{cm}}\big[A + B\cdot\cos\theta_\eta^* + C\cdot P_2(\cos\theta_\eta^*) \\ & +(D\cdot\sin\theta_\eta^* + E\cdot\sin\theta_\eta^*\cdot\cos\theta_\eta^*)\ \cdot\cos\phi_\eta^* + F\cdot\sin^2\theta_\eta^*\cdot\cos 2\phi_\eta^*,\end{aligned} \tag{2}$$

This form has contributions from all four response functions. The response functions are bilinear products of multipoles (where the specific information about each resonance resides). Only terms that contain the S_{11} partial wave multipoles (E_{0+} and S_{0+}) and total angular momentum less than $\frac{5}{2}$ are included in the fit. This fit is unique and is expected to contain the primary physics dependencies.

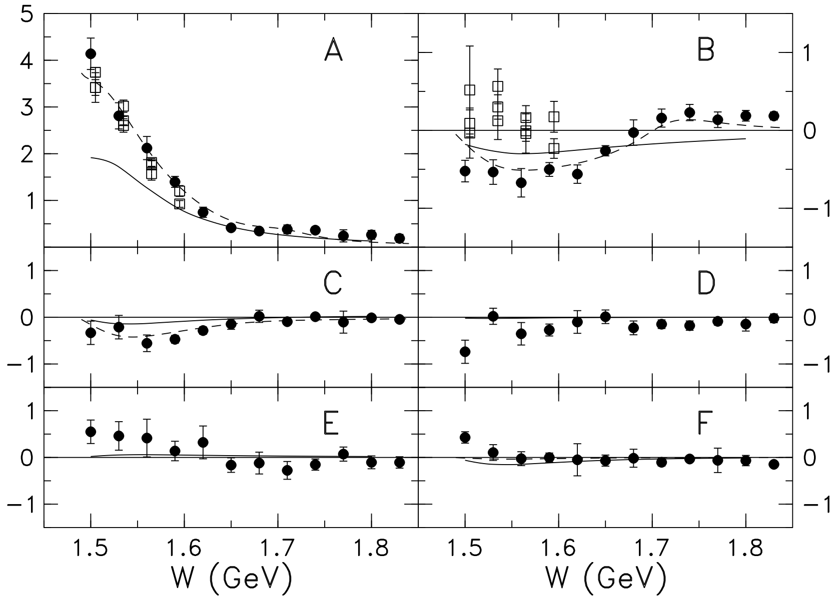

Figure 1: Fit results according to Eqn. 2 for Q^2=0.75(GeV/c)^2. The data include all systematic errors. See text for details.

The first line of Eqn. [2] contains terms that have been used to fit photoproduction data [Kr95] where only R_T contributes. The parameter A is mostly due to the dominant S_{11} excitation while B-F parameterize the interference between that partial wave and the others. B is mostly due to interference between S_{11} and P_{11} waves while C and F come from S_{11}-D_{13} interference. Results are shown in Fig. 1.

The largest parameter is A. The interference response functions in D-F are seen to be small and consistent with predictions [Kn95] with the statistics of this data set. Improvements with the larger data sets in the later run periods are anticipated. C is consistent with photoproduction data and reflects the small $D_{13}(1520)\rightarrow \eta N$ coupling. The combination of C and F give information about the ratio of $A_{3/2}$ to $A_{1/2}$ complementary to that seen in the polarized photon data [Aj98]. New information is seen in B in the sharp energy dependence seen at $W \sim 1.65$ GeV. (At the same W, the inclusive data [Th01] shows a sharp change in slope. The two phenomena are likely to have the same cause.) Our simple isobar fit (dashed line in the figure) supports the idea that the structure is due to interference with the $P_{11}(1710)$. The theoretical prediction of the Mainz group [Kn95] doesn't show this

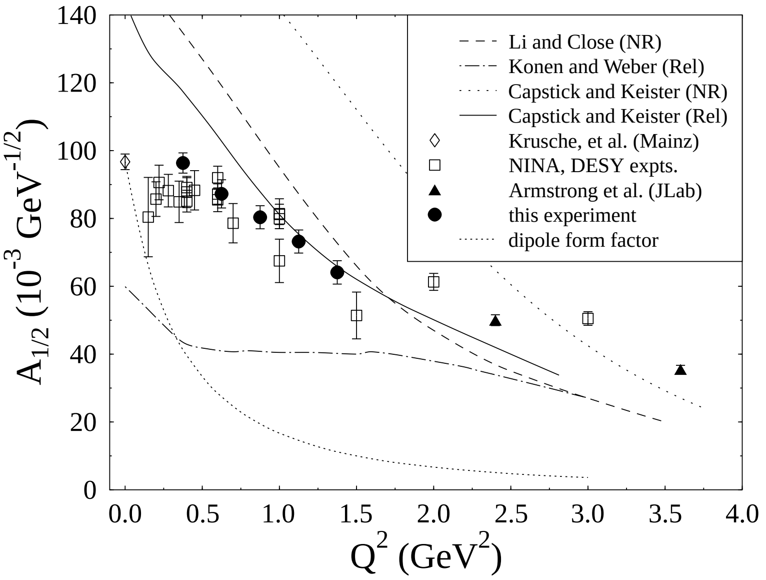

Figure 2: Values for the photon coupling amplitude calculated in a single resonance model. All previous experiments have been reanalyzed. The data points include statistical and systematic errors, but no errors in the theoretical parameters required in the calculation.

structure and doesn't include the $P_{11}(1710)$.

A single resonance analysis for the properties of $S_{11}(1535)$ was also done. $A_{1/2}$ was calculated by the standard formula [Kn95] for this and all previous electromagnetic experiments. The slow falloff seen in previous experiments is confirmed, but with much greater clarity. These data along with that of Refs. [Kr95] and [3] give a smooth falloff. Older data seen in both figures of this report are inconsistent in a number of ways.

In recent years, there has been a lot of controversy about the properties of $S_{11}(1535)$. Values of the Breit-Wigner width between 100 and 250 MeV and values of the photocoupling amplitude $A_{1/2}(0)$ from 0.060 to 0.150 $GeV^{-1/2}$ have been reported. Recent data and more careful Breit-Wigner analyses are now giving a consistent picture with a full width about 150 MeV and photocoupling of about 0.09 $GeV^{-1/2}$ with much smaller error bars than previously seen. More complete coupled channels analyses will give the most correct values.

The interpretation of these results is unclear in terms of the microscopic resonance structure of $S_{11}(1535)$. The lines shown in Fig. 2 come from various constituent quark model (CQM) analyses. They don't agree well with the data or with each other, perhaps due to a breakdown in the CQM decay assumptions. In addition, there is uncertainty about resonance character of the strong threshold enhancements seen in these and other data. In any case, these data provide very strong constraints for any model of $S_{11}(1535)$.

References

[Th01] R. Thompson, S. Dytman, K.Y. Kim, J. Mueller et al., Phys. Rev. Lett., Feb., 2001.

[Aj98] J. Ajaka et al., Phys. Rev. Lett. **81**, 1797 (1998).

[Kr95] B. Krusche et al., Phys. Rev. Lett. **74**, 3736 (1995).

[Kn95] G. Knochlein, D. Drechsel and L. Tiator, Z. Phys. **A352**, 327 (1995); L. Tiator, C. Bennhold, and S.S. Kamalov, Nucl. Phys. **A580**, 455 (1994).

[Ar99] C. S. Armstrong et al., Phys. Rev. **D60** 052004 (1999).

2.6 E89-042

Measurement of the Electron Asymmetry in $p(\vec{e}, e'p)\pi^o$ and $p(\vec{e}, e'\pi^+)n$ in the Mass Region of the $\Delta(1232)$ for $Q^2 < 2(GeV/c)^2$

V. Burkert, R. Minehart, L.C. Smith, and the CLAS collaboration

2.6.1 Introduction

The goal of the experiment is to measure the electron spin asymmetry and the so- called 5th response function for the charged and neutral pion channels in the resonance region, especially for the $\Delta(1232)$. This provides new and unique information on the interference between resonant and non-resonant amplitudes in meson production. The polarized differential cross section for single pion production is given by:

$$\frac{d\sigma}{d\Omega} = \sigma_T + \epsilon\sigma_L + \epsilon\sigma_{TT}\cos(2\phi) + \sqrt{2\epsilon(\epsilon+1)}\sigma_{LT}\cos\phi + h_e\sqrt{2\epsilon(1-\epsilon)}\sigma'_{LT}\sin\phi \qquad (1)$$

σ'_{LT} contains the imaginary part of the same combination of amplitudes that σ_{LT} contains the real part of. It thus provides orthogonal and complementary information. In the region of the $\Delta(1232)$ resonance, σ'_{LT} can be expanded in terms of s- and p- waves, and the electromagnetic multipoles S_{0+}, S_{1+}, M_{1+}. In this approximation one has:

$$\sigma'_{LT} \approx \sin\theta[Im(S_{0+}M^*_{1+}) + 6\cos\theta Im(S_{1+}M^*_{1+})] \qquad (2)$$

This term can be determined by analyzing the azimuthal angular distribution. The two contributing terms in (2) can be separated by a fit to the polar angle distribution.

2.6.2 Experiment Status

Data have been taken mostly at 1.5 GeV and 2.5 GeV during the E1c and E1d run periods in spring 1999 and 2000 with a hydrogen target. Data on deuterium were also taken at 2.5

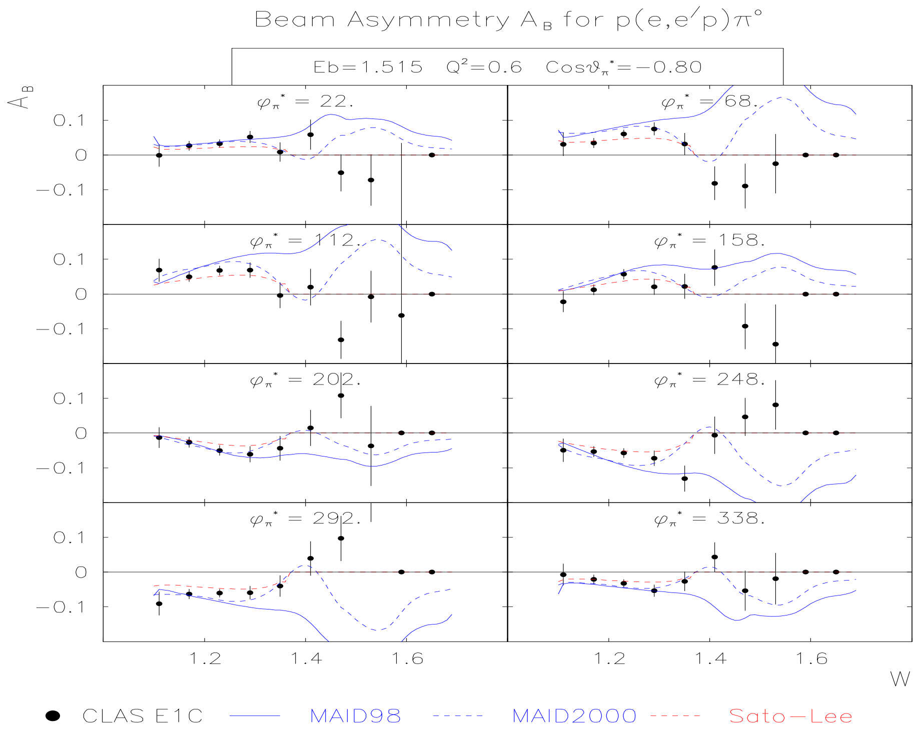

Figure 1: Preliminary beam asymmetries for $p\pi^0$ electroproduction at fixed polar angle $\cos\theta$ off protons for different out-of-plane angles ϕ.

GeV during the E1d run period but have not been analyzed yet. Electron polarization was in the range from 0.6 to 0.7. This report deals only with the data from the E1c run period. To complete data taking for this experiment, additional runs with the hydrogen target at higher energies and with the deuterium target at 1.5 GeV will be needed.

2.6.3 Results - or Expected Results

Analysis of the 1.5 GeV data has begun and preliminary results have been obtained for the beam asymmetry in the $p\pi^0$ and $n\pi^+$ channels. The data show clear evidence for sizeable beam asymmetries throughout the resonance region. The σ'_{LT} term can be determined by properly accounting for the normalization of numerator and denominator in the asymmetry. At this stage in the analysis the acceptance corrections have not been applied. However, in the Delta region the MAID description gives a sufficiently accurate description of the cross

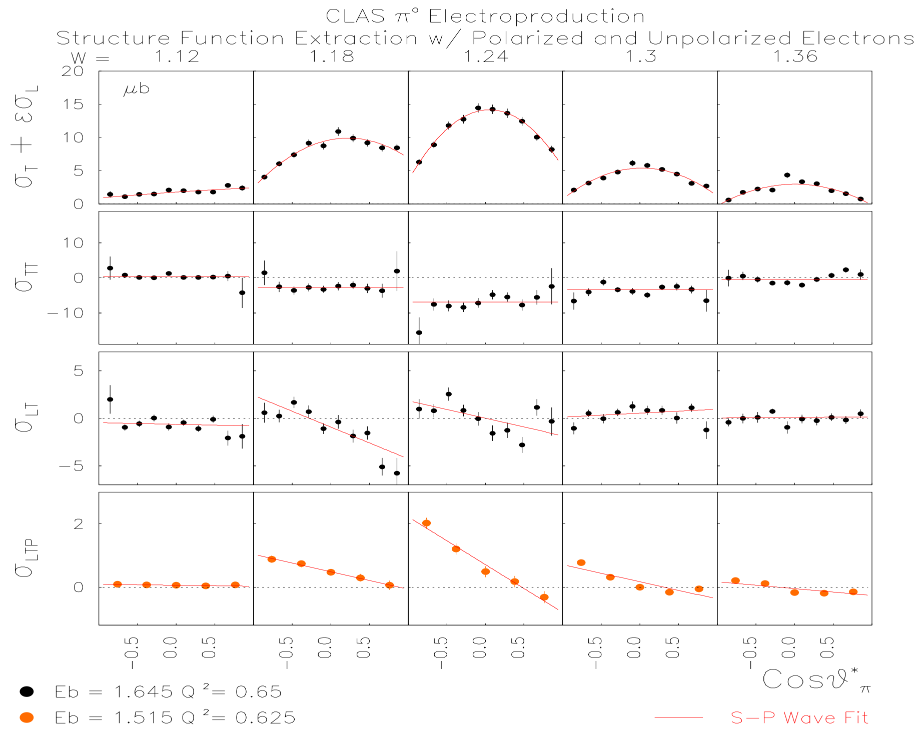

Figure 2: Response functions for unpolarized π^0 production (top 3 panels) and for π^0 production with polarized electron beam (bottom panel).

section, and deviations are much smaller than the statistical accuracy of the asymmetry data. Using this procedure, we can extract approximate values for σ'_{LT}. The results are shown in Figure 2 together with the unpolarized response functions. The σ'_{LT} response function gives a significant contribution in the Delta region. The large slope suggests that the S_{1+} multipole has a significant non-resonant component near the $\Delta(1232)$ mass.

Further analysis of the polar angle distribution will allow precise determination of $Re(S_{1+})$, and $Re(S_{0+})$ in the region where M_{1+} is the dominating multipole.

We are currently in the process of finalizing the data analysis and aim at completing the physics analysis of the 1.5 GeV data by the summer of 2001.

2.7 E89-043

Measurements of the electroproduction of the $\Lambda(1116)$, $\Lambda(1520)$, and $f_\circ(980)$ via the K^+K^-p and $K^+\pi^-p$ reactions

L. Dennis, H. Funsten, and the CLAS collaboration

2.7.1 Introduction

This experiment is providing an extensive data set for the production and decay of the $\Lambda(1116)$ and $\Lambda(1520)$. Preliminary results for the $\Lambda(1116)$ polarization, $\Lambda(1520)$ production as a function of Q^2 and its decay (observed in the helicity frame) are briefly summarized in this report. These data are expected to advance our understanding of the hyperon production mechanism and the intermediate $s\bar{s}$ pair.

During the 1970s there were three published measurements of $\Lambda(1520)$ photo- and electroproduction [1]-[3]. To date there are few hadron production and photoproduction $\Lambda(1116)$ polarization measurements [4]. The single, recent, electroproduction measurement [4] for the $\Lambda(1116)$ determined a polarization between -0.21 and +0.89 at $Q^2 = 1.5 GeV^2$ and $\Theta_{K\gamma}^{CM} = 14°$ from 40 events.

The most recent photoproduction measurement [1] for beam energies from 2.8 to 4.8 GeV (W from 2.5 to 3.1 GeV), concludes that $\Lambda(1520)$ photoproduction has an exponential t-dependence, and is dominated by t-channel exchange of the $K^*(892)$ meson, and not the lighter K(494) meson. There are several models of $\Lambda(1116)$ electroproduction [5], [6] that predict large contributions from the longitudinal spin projection of the virtual photon. Similar behavior in $\Lambda(1520)$ electroproduction could possibly result in an enhanced K(494) t-channel contribution to the total cross section. If such behavior were observed, it would be interesting to examine the relationship between Q^2 and the K(494) exchange, since it would be a direct measurement of the Q^2 dependence of the reaction mechanism.

2.7.2 Experiment Status

The data for this experiment were taken as part of the CLAS E1 run period. Eleven different combinations of beam energies, from 2.5 to 4.4 GeV, relevant for this analysis have been completed. Presently, analysis is ongoing for eight of the data sets, and the other three settings are in the calibration phase. The results discussed here require the detection of at least three of the particles in the final state. To accurately determine the acceptance of the detector in this case, a large number of simulations must be performed for each energy and magnet configuration. The simulations are complete for the $\Lambda(1520)$ and for approximately one-half of the $\Lambda(1116)$ (we have produced over 200 million simulated events for the two reactions reported here). A draft publication summarizing the results for $\Lambda(1520)$ is presently undergoing review by the CLAS collaboration. Further details of the analysis can be found in Ref. [7]. A thesis is being prepared based on the analysis of the $\Lambda(1116)$ polarization measurements.

2.7.3 Results for the $\Lambda(1520)$

The $\Lambda(1520)$ is a $\mathrm{J}^{\pi} = \frac{3}{2}^{-}$ baryon. For its decay into the p-K$^-$ mass partition, an $m_z = \pm\frac{3}{2}$ parentage is characterized by a $\sin^2\theta_{K^-}$ distribution, while an $m_z = \pm\frac{1}{2}$ parentage is characterized by a $\frac{1}{3}+\cos^2\theta_{K^-}$ distribution. The t-channel helicity frame $\cos\theta_{K^-}$ decay angular distributions for four regions of Q^2 are shown in Fig. 1, along with fits to the two $\Lambda(1520)$ decay distributions. A $\cos\theta_{K^-}$ term was added to the fits shown in Fig. 1 to incorporate the interference between the $\Lambda(1520)$ and other hyperons. The dashed lines are the results of those fits, while the solid lines are the contributions to the fits of the two $\Lambda(1520)$ decay angular distribution terms. These results suggest K*(892) exchange is not the dominant production process for $\Lambda(1520)$ electroproduction; a significant departure from the photoproduction result [1].

The Q^2 dependence of the cross section for $W < 2.43$ GeV, and $\cos\theta_{K^+} > 0.2$, is shown in Fig. 2. The fitted mass shown in Fig. 2 is the same (within errors) as the mass term derived from the Q^2 dependence of the $\Lambda(1116)$ cross section [3], [8] - [10] from $Q^2 = 0$ to 4.0 GeV^2. This new result for the $\Lambda(1520)$ Q^2 dependence is consistent with a model [11]

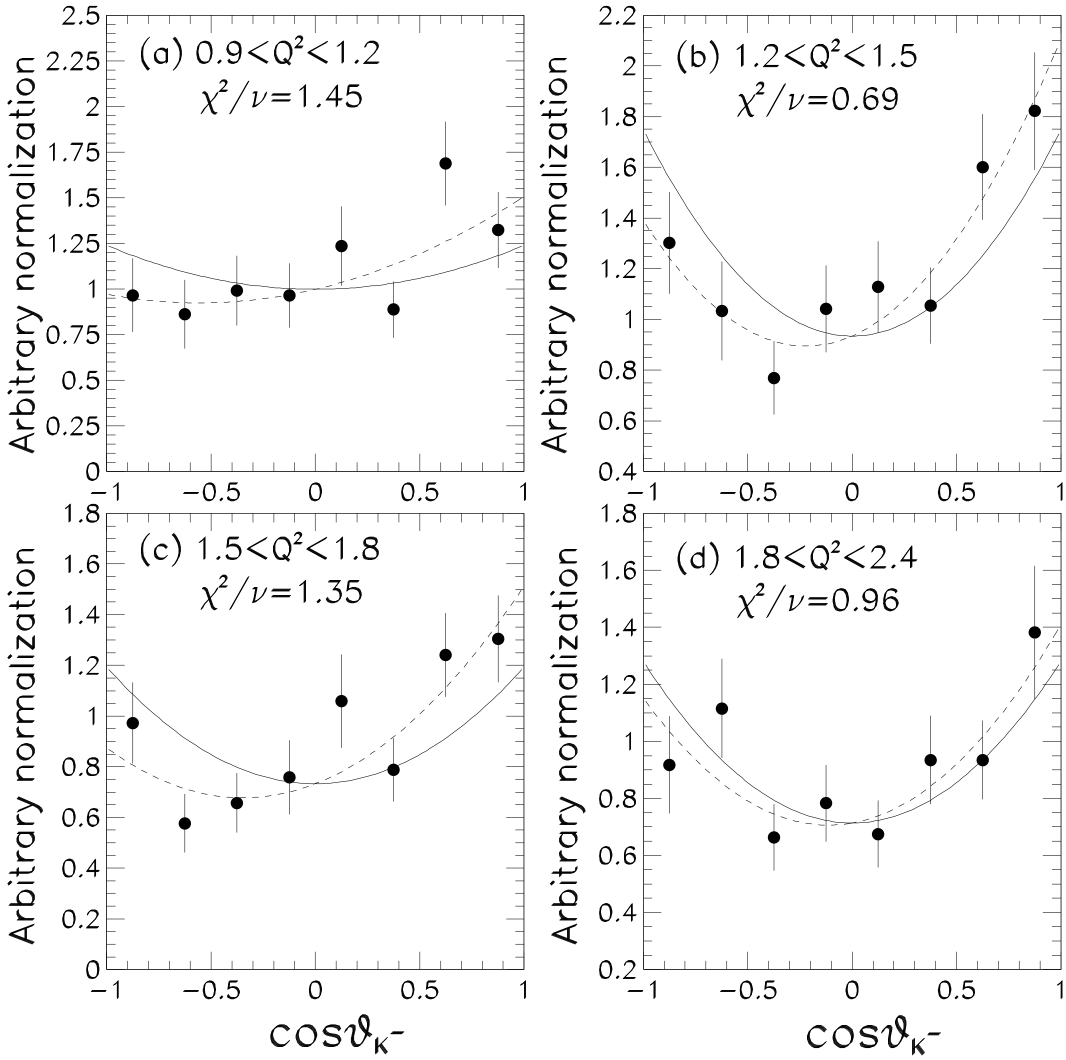

Figure 1: Preliminary results for the $\Lambda(1520)$ $\cos\theta_{K^-}$ decay angular distribution for four regions of Q^2. These distributions are averaged over the region of W from threshold to 2.43 GeV. The error bars are statistical errors only.

that suggests isospin is an important quantity in determining the Q^2 dependence of hyperon production.

2.7.4 Results for the $\Lambda(1116)$ polarization.

Through the use of the missing mass technique to identify a missing $\Lambda(1116)$ and a missing π^- from the decay of the Λ, 38,630 kinematically complete events containing an electron, kaon, and proton were selected. This data covers a Q^2 range of 0.5 GeV^2 to 2.4 GeV^2, a W range of 1.61 GeV to 2.65 GeV, and provides full angular coverage in the center of mass frame.

The $\Lambda(1116)$ polarization is deduced from the detection of the proton in the $\Lambda(1116) \to p\pi^-$ decay channel. The distribution of these protons in the rest frame of the Λ follows the equation:

$$\frac{dN}{d\Omega_p^{RF}} \propto 1 + \alpha P_\Lambda \cos\Theta_p^{RF}, \tag{1}$$

where α is the weak-decay asymmetry parameter, P_Λ is the $\Lambda(1116)$ polarization, and Θ_p^{RF} is the proton polar decay angle in the Λ rest frame relative to the axis normal to the hyperon production plane.

Preliminary results show large polarizations. Figure 3 suggests the $\cos\Theta_{K^+}^{CM}$ dependence of the $\Lambda(1116)$ polarization is qualitatively the same for electroproduction and photoproduction over the same range of W. [12]

References

[1] D. Barber *et al.*, Z. Physik C, **7**, 17, 1980.

[2] A. Boyarski *et al.*, Phys. Lett. B **34**, 547, 1971.

[3] T. Azemoon *et al.*, Nuclear Physics **95**, 77, 1975.

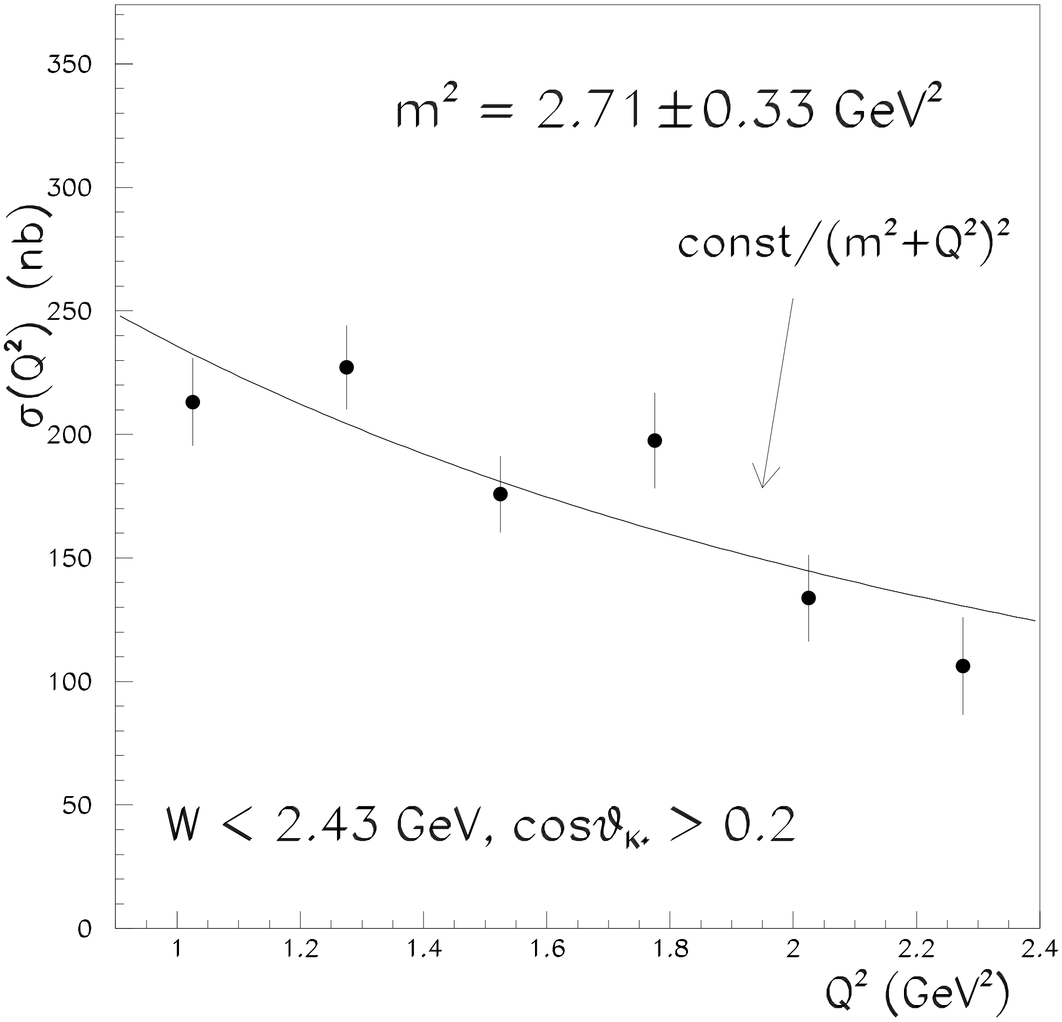

Figure 2: Preliminary results for the Q^2 dependence of the cross section for $W < 2.43$ GeV, and $\cos\theta_{K^+} > 0.2$. The error bars are statistical errors only. Also shown in this figure is a fit to the data which assumes a $(m^2 + Q^2)^{-2}$ dependence to the cross section.

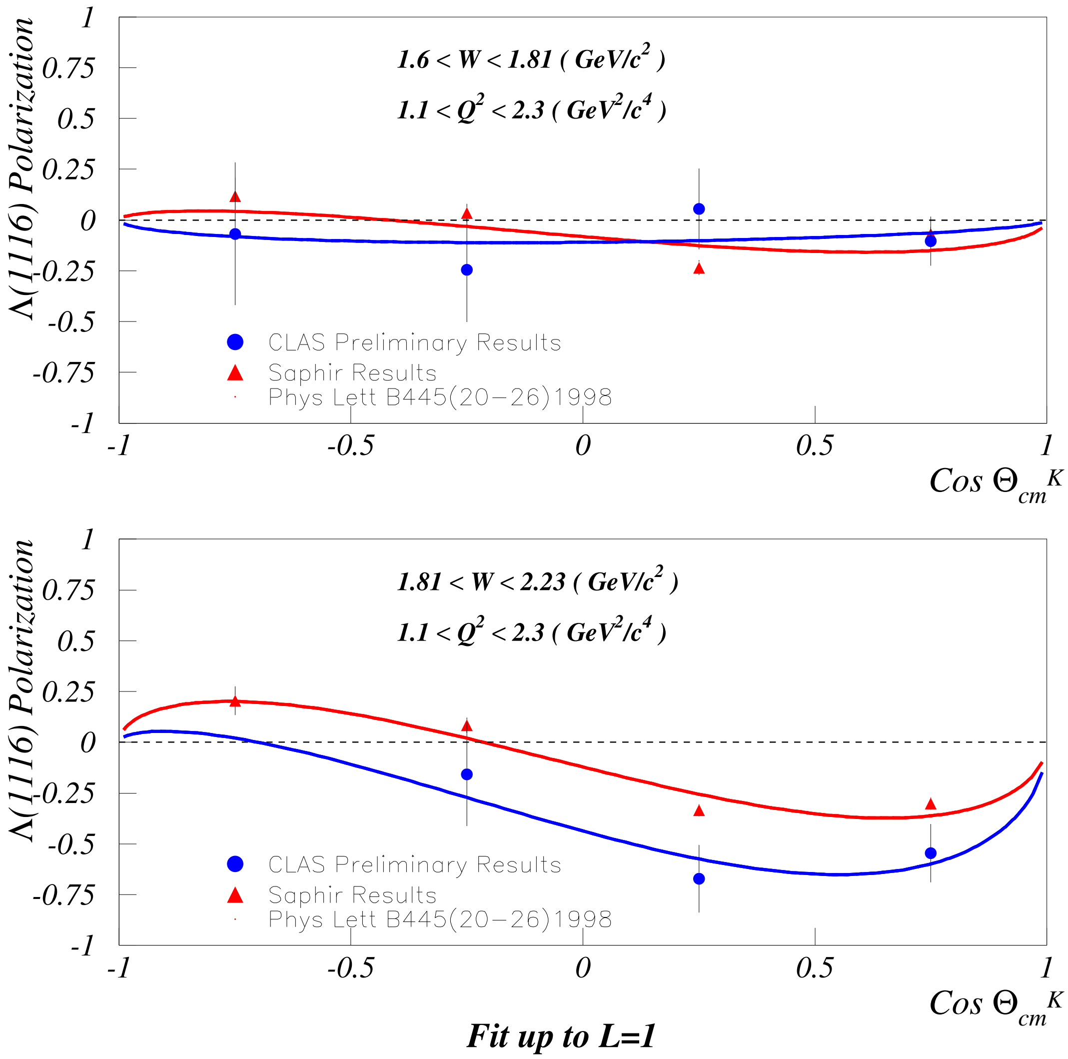

Figure 3: Preliminary results for the $\Lambda(1116)$ recoil polarization versus $\cos\Theta^{CM}_{K+}$ for two different Q^2 and W bins. The blue circles show preliminary CLAS data. The red triangles are data from SAPHIR. [12] The lines correspond to a fit up to L=1 for each corresponding data set. Error bars are statistical only.

[4] L. Teodorescu, *et al.*, Nuc. Phys. **A658** 362 (1999)

[5] R. Williams, C. Ji, and S. Cotanch, Phys. Rev. C **46** 1617, 1992.

[6] J. David *et al.*, Phys. Rev. C **53** 2613, 1996.

[7] S. Barrow, CLAS-ANALYSIS 2000-002, June, 2000.

[8] C. J. Bebek *et al.*, Phys. Rev. D **15** 594, 1977.

[9] C. Brown *et al.*, Phys. Rev. Lett. **28** 1086, 1972.

[10] G. Niculescu *et al.*, Phys. Rev. C **81** 1805, 1998.

[11] J. Cleymans and F. Close, Nucl. Phys. B **85** 429, 1975.

[12] M. Q. Tran, *et al.*, Phys. Lett. **B445** 20 (1998)

2.8 E91-024

Search for "Missing" Resonances in the Electroproduction of omega Mesons

V.Burkert, H.Funsten, F.Klein, A.Larabee, B.Mecking, for the CLAS Collaboration

2.8.1 Introduction

The purpose of the experiment is to search for "missing" N^*, $2\hbar\omega$ positive parity resonances predicted to lie in the mass region from 1.7 to $\approx$ 2.2 GeV [1]. The search is performed analyzing $(e, e'p\pi^+)$ events from omega meson electroproduction from a proton target in the CLAS detector.

2.8.2 Experiment Status

Omega meson electroproduction data for approximately 10^9 events from five separate run series comprising the spring 1998 e1b and spring 1999 e1c CLAS run periods are being analyzed. The five run series are:

1) e1b spring 1998, 4.0 GeV, high torus field, 100 million events
2) e1c spring 1999, 4.0 GeV, reduced torus field, 200 million events
3) e1c spring 1999, 4.0 GeV, high torus field, 200 million events
4) e1c spring 1999, 4.2 GeV, reduced torus field, 400 million events
5) e1c spring 1999, 4.4 GeV, reduced torus field, 200 million events.

2.8.3 Results

The analyses examined outgoing electron tracks in coincidence with those of the recoiling proton and a π^+ from the ω decay. Events having at least e' p π^+ outgoing tracks were analyzed. Missing mass techniques were applied to identify the outgoing ω in the $mm_{e'p}$ missing mass distribution. To reduce contributions from $\rho(770)$ and 2π final states a $m >$

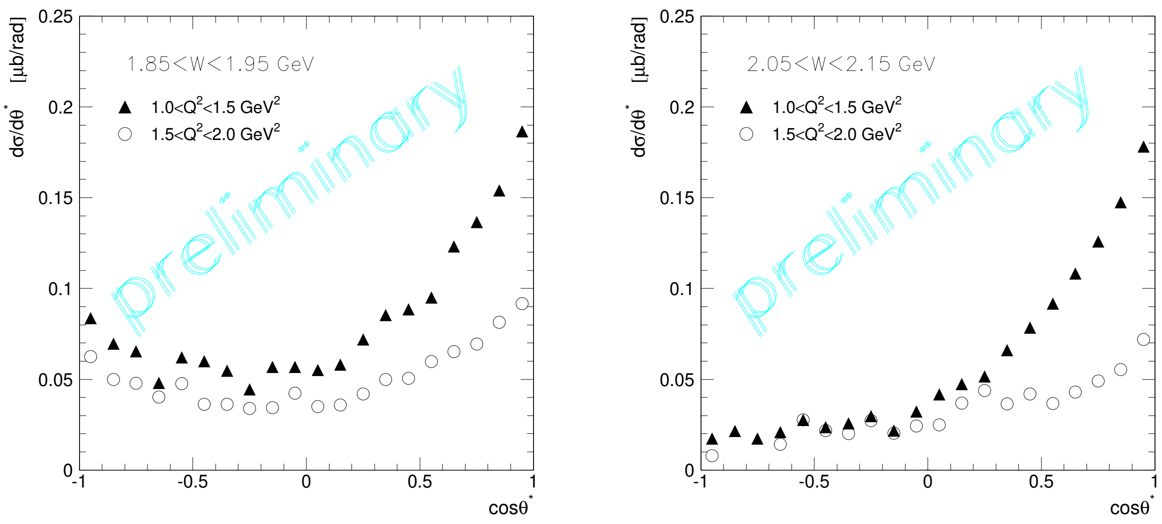

Figure 1: Preliminary results from CLAS for omega electroproduction at $E_{beam} = 4.2$ GeV: differential cross section for selected W ranges.

$2m_\pi$ cut was made on the $mm_{e'p\pi^+}$ missing mass distribution. For each event these missing masses were obtained together with $W = \sqrt{s}, Q^2$ from the outgoing e' track and t from the outgoing p track. CLAS detection efficiency was obtained using the GEANT procedure and an omega event generator. (Analysis #3 used efficiencies extrapolated from those of Analysis #1).

The resulting $mm_{e'p}$ missing mass distributions clearly show an ω mass peak superimposed on a predominantly 3-pion phase space background. The ω mass peak was sufficiently narrow ($\approx$ 30 MeV FWHM) to permit fits in the immediate omega mass neighborhood using a 2^{nd} order polynomial to represent the underlying 3π phase space background.

The angular distributions in each of the five above analyses were characterized by a monotonic fall-off with increasing production angle for $W > 2.0$ GeV. This is characteristic of diffractive/π exchange process(es). However, in the W region from threshold to $\approx$ 2.0 GeV, the cross section shows additional strength in intermediate and backward direction, an indication for a strong nucleon pole (u-channel) and possible N^* resonance (s-channel) contributions.

Tentative conclusions:

1) The forward production is dominated by t-channel processes showing a steep Q^2 dependence.

2) For $W < 2$ GeV, the data show considerable strength in backward angles for the lower Q^2 range, consistent with contributions from the nucleon pole term.

3) The remaining strength at production angles between 45° and 135° has to be analyzed with respect to possible s-channel resonance contributions. Investigations on ϕ^* dependence and angular momenta are in progress.

Existing N* Resonances and Quark Model predictions

Three established ($\geq$ two star) N^* resonances exist in the 1.8 $\rightarrow$ 2.0 GeV region. Their masses and widths are inconsistant with the data:

$\mathbf{J}^P$	**M (MeV)**	**Status**	**Γ(MeV)**	$\Gamma_{\pi N}/\Gamma_{Tot}$
$3/2^+$	1900	**	500	26 %
$7/2^+$	1990	**	200-500	6 %
$5/2^+$	2000	**	100-500	8 %

The data, however, agrees with Capstick and Roberts' [2] [3] calculations for a group of seven N^*, $2\hbar\omega$ positive parity states.

An estimation of relative ω electromagnetic production rates for these states using their $A_{\gamma N}$ and $A_{\omega N}$ couplings displays an intesting result. One state, a 1910 MeV $\frac{3}{2}^+$ state carries > 80 % of the *full* ω electromagnetic production strength of the group.

References

[1] Nathan Isgur *Proc. CEBAF/SURA 1984 Summer Workshop* (1984).

[2] Simon Capstick, *Phys. Rev.* **D46**, 2864 (1992).

[3] Simon Capstick and Winston Roberts, *Phys. Rev.* **D49**, 4570 (1993).

2.9 E93-006

TWO PION DECAY OF ELECTROPRODUCED
LIGHT QUARK BARYON RESONANCES

M. Ripani, V. Burkert and the CLAS collaboration

2.9.1 Introduction

The excitation of baryon resonances is genuinely a non-perturbative phenomenon. Measurements of the transition amplitudes from the nucleon to its excited states are sensitive to the spatial and spin structure of the transition. Many of the nucleon excited states in the mass region around and above 1.7 GeV tend to decouple from the single-pion and eta channels, while πN scattering experiments have shown that many of them decay predominantly in multipion channels, such as $\Delta\pi$ or $N\rho$, leading to $N\pi\pi$ final states[1]. A measurement of the transition form factors of these states is very important for testing symmetry properties of the quark model. Moreover, SU(6) symmetric quark models[2, 3] predict more states than have been found in experiments. QCD mixing effects could decouple many of these states from the pion-nucleon channel[2], with consequent lack of evidence in elastic πN scattering, while strongly coupling them to two-pion channels such as $\Delta\pi$[2, 4, 5, 6]. However, other models such as the Quark Cluster Model[7] predict a fewer number of states than the symmetric model, more in accordance with experimental observation. Search for the states still missing from the experimental evidence is therefore crucial in understanding the basic degrees of freedom in baryon structure. The present experiment is devoted to a precise measurement of the cross sections for reaction $ep \to e'p\pi^+\pi^-$, to extract information on poorly known baryon states and to investigate the existence of new, unobserved states.

2.9.2 Experiment Status

Data taking on hydrogen has been successfully completed during the year 2000, and for a large fraction of the data the detector reconstruction required for the physics analysis has been performed. Physics analysis has been started for a subset of the data taken at beam energies of 2.567 and 4.247 GeV, with the goal of extracting cross sections for a

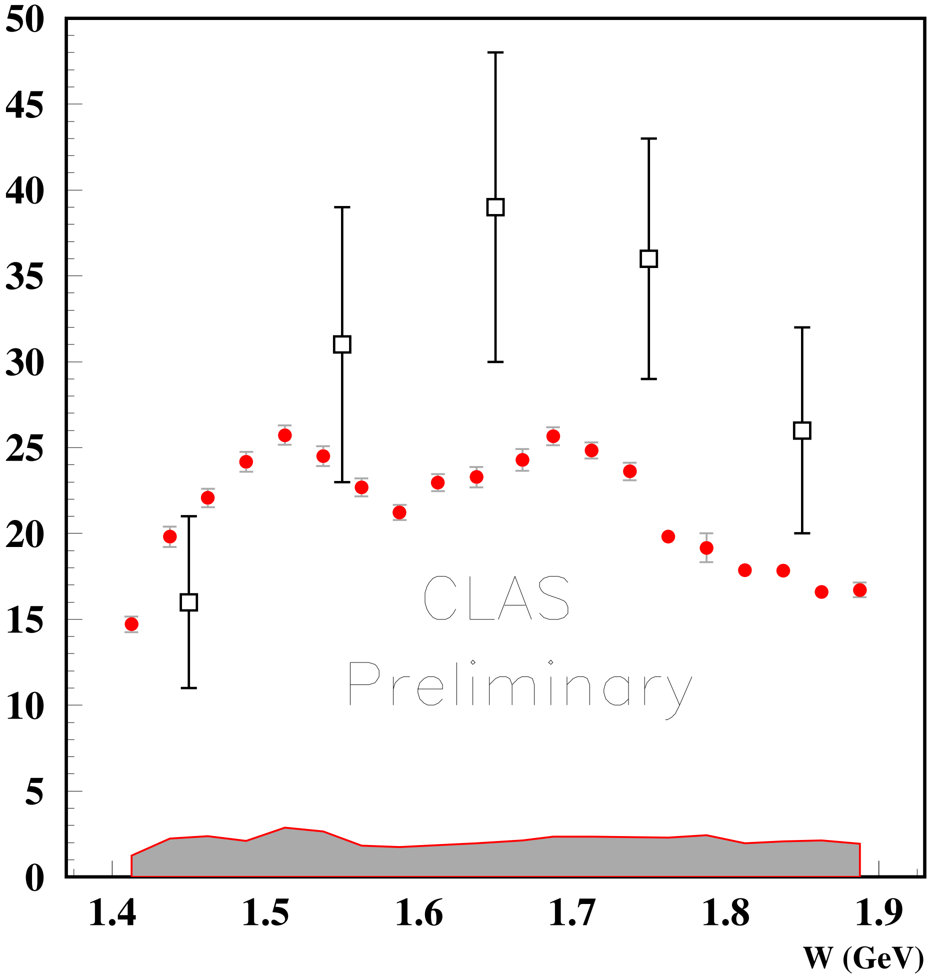

Figure 1: Total virtual photon cross section as a function of the CMS energy W for $ep \to ep\pi^+\pi^-$ from CLAS at Q^2 between 0.5 and 0.8 GeV^2 (E_{beam}=2.567 GeV, red points) and from a previous experiment at DESY (open black squares)[8]. Error bars for CLAS are statistical only, while the grey band is showing the corresponding systematic error.

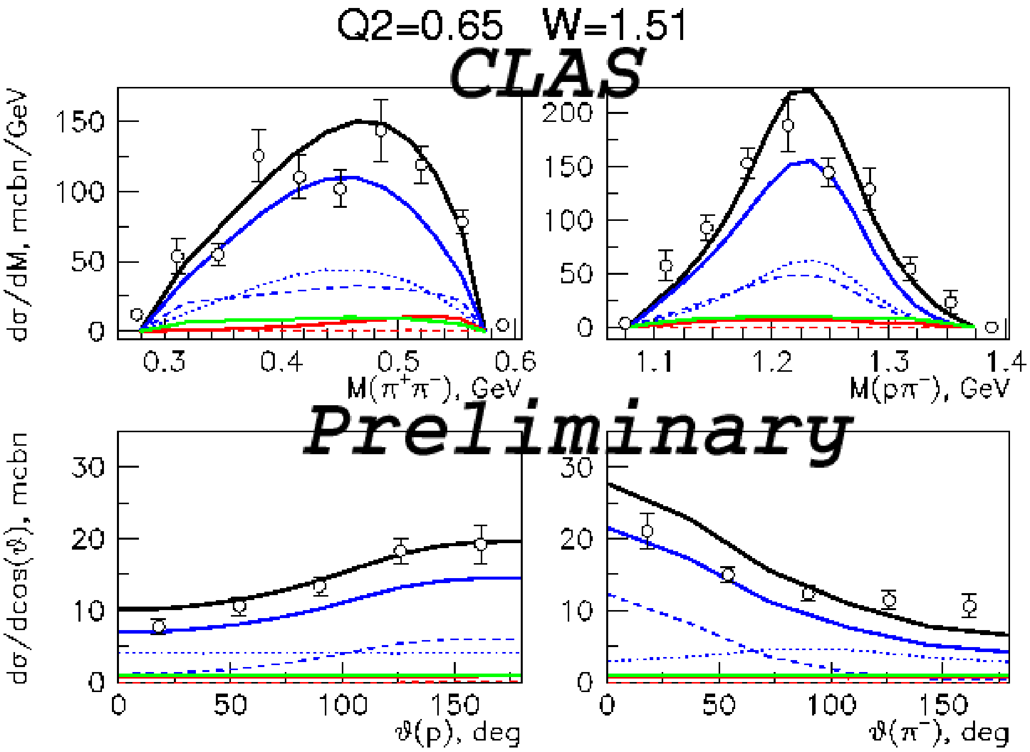

Figure 2: Virtual photon cross section for $ep \to ep\pi^+$ (missing π^-) at Q^2 between 0.5 and 0.8 GeV^2, for W between 1.5 and 1.525 GeV, differential in (left to right and top to bottom): π^+-π^- invariant mass; proton-π^+ invariant mass; proton angle θ; π^- angle θ. Data from CLAS; lines represent "nominal" model calculation (after fixing the phase space contributions) as follows; blue dashed line: $\Delta\pi$ non-resonant contribution; blue dotted line: $\Delta\pi$ resonant contribution; blue full line: $\Delta\pi$ total contribution; red dashed line: ρ non-resonant contribution; red dotted line: ρ resonant contribution; red full line: ρ total contribution; green full line: phase space contribution; black full line: total of all contributions.

few momentum transfers and in a broad range of CMS energy W, where we expect to see significant contributions from excited baryons production.

2.9.3 Results - or Expected Results

Among several detailed results obtained up to now, in Figure 1 we report the total cross sections measured with CLAS at three different Q^2 intervals and for W in the resonance region. The comparison with the previous data from DESY show the enormous improvement in statistics and accuracy that allows us to see clearly the structures in the cross sections produced by the baryon resonance excitation. To perform a first physical analysis of the data, we started from a phenomenological calculation[9], which provides a reasonable description of the two important intermediate isobar production mechanisms, $\gamma p \to \Delta\pi \to p\pi^+\pi^-$ and $\gamma p \to \rho^0 p \to p\pi^+\pi^-$; a third mechanism, the direct $\gamma p \to p\pi^+\pi^-$, often called “phase space”, was included as a pure phase space amplitude and fitted from the data. In our ”nominal” calculation, we described resonance excitation and decay using a Single Quark Transition Model fit[10] for the electromagnetic part and partial decay widths from a previous analysis of hadronic data[11], renormalised in order for the total width to be consistent with PDG. A typical comparison between a data sample and our calculation is reported in Figure 2: in this case, the good agreement with the data tells that we are controlling a well known baryon state, the $D_{13}(1520)$; this gives confidence in the model and will allow us to explore further resonance features.

References

[1] Particle Data Group, 1998.

[2] R. Koniuk and N. Isgur, Phys. Rev. Lett. **44**, 845 (1980); Phys. Rev. **D21**, 1868(1980).

[3] M.M. Giannini, Rep. Prog. Phys., **54**, 453 (1990).

[4] R. Koniuk, Nucl. Phys. , **B195**, 452 (1982).

[5] S. Capstick, W. Roberts, Phys. Rev. **D49**, 4570 (1994).

[6] F. Stancu and P Stassart, Phys. Rev. **D47**, 2140 (1993).

[7] K.F. Liu and C.W. Wong, Phys. Rev. **D28**, 170 (1983).

[8] V. Eckart et al. , Nucl. Phys. **B55**, 45 (1973); P. Joos et al., Phys. Lett., **B52**, 481 (1974); K Wacker et al., Nucl. Phys., **B144**, 269 (1978).

[9] M. Ripani et al., Phys. of At. Nucl., **62**, 1437 (1999); M. Ripani et al., Nucl. Phys. **A 672**, 220 (2000); M. Ripani et al., Phys. of At. Nucl., **63**, 76 (2000); M. Ripani et al., Phys. of At. Nucl., **63**, 1943 (2000).

[10] V. D. Burkert, Czech. Journ. of Phys., **46**, 627 (1996).

[11] D.M.Manley, E.M.Salesky, Phys. Rev. **D45**, 4002 (1992).

2.10 E93-022

Measurement of the Polarization of the $\phi(1020)$ in Electroproduction

H. Funsten, P. Rubin and E.S. Smith, spokespersons

and the CLAS Collaboration

2.10.1 Introduction

The hadronic structure of the photon arises from fluctuations of the virtual photon into short-lived quark-antiquark ($q\bar{q}$) states of mass M_V during a formation time [Ba78]

$$\Delta\tau = \frac{2\nu}{(Q^2 + M_V^2)}, \tag{1}$$

where -Q^2 is the squared mass and ν is the laboratory-frame energy of the virtual photon (See Fig. 1a). To date, no clear dependence on the formation time has been observed in ϕ meson production by virtual photons [Ca81, Di77, Di79]. We present measurements of exclusive ϕ meson electroproduction off a proton target for $2.0 \leq W \leq 2.6$ GeV and $0.7 \leq Q^2 \leq 2.2$ GeV^2 where there is extremely limited data. In this kinematic regime, the short formation distance of the virtual $q\bar{q}$ state ($0.35 \leq c\Delta\tau \leq 0.75$ fm) limits the time for interaction and probes the ϕ production mechanism at small formation times.

2.10.2 Experiment Status

Experiment E93-022 is part of the Hall B e1 run group, which took data with an electron beam incident on a liquid hydrogen target. The data were taken with an inclusive electron trigger and with the CLAS torus magnet current set to 2250 A, bending negatively charged particles toward the beam axis. The data at 4.2 GeV were analyzed and correspond to an integrated luminosity $L_{int} = 1.5 \cdot 10^{39}$ cm^{-2}. Additional data were collected under similar conditions at a beam energy of 4.0 GeV and correspond to an integrated luminosity of $L_{int} = 1.2 \cdot 10^{39}$ cm^{-2}, which have been processed but not yet analyzed. Together, these two samples correspond to approximately 22% of the PAC approved beam time for this experiment. After all selection cuts, a sample of 197 events was identified which corresponds

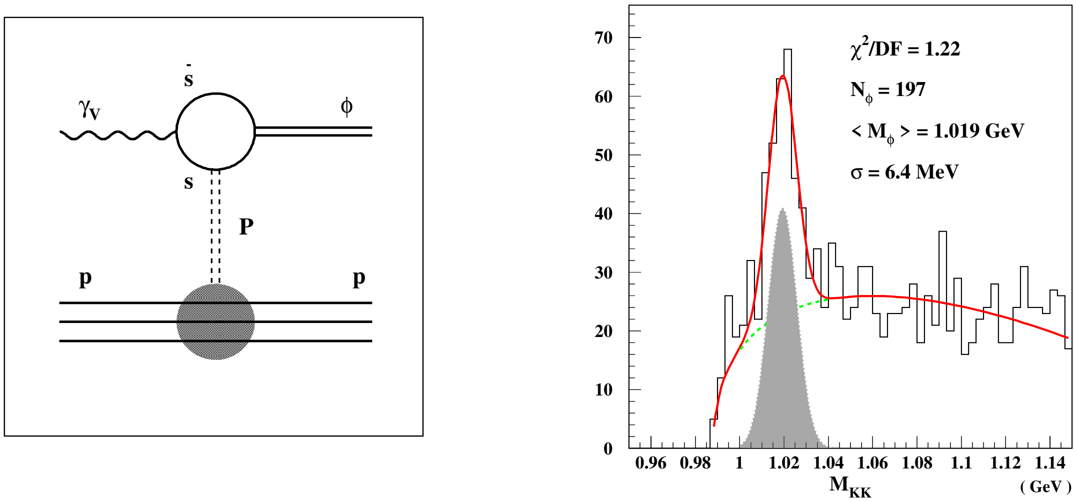

Figure 1: a) Pomeron exchange diagram and b) ϕ mass peak.

to the exclusive reaction $ep \to ep\phi$ with the ϕ meson decaying into K^+K^-. The identification of this signal is very clean as shown in Fig. 1b. This analysis is summarized in a thesis [Lu00] and a paper which has been submitted for publication [Lu01].

2.10.3 Results

The cross section, $d\sigma/dt'$, is generally parameterized at small $-t'$ by

$$\frac{d\sigma}{dt'} = A_\phi \, e^{b_\phi t'} . \tag{2}$$

The slope parameter b_ϕ was determined by fitting the data for $-t'$ less than 1.2 GeV^2 to compare to previous measurements (see Fig. 2a). At $\langle c\Delta\tau\rangle = 0.6$ fm, we measure $b_\phi = 2.27$ ± 0.42 GeV^{-2}. In a geometrical model of elastic ϕ p scattering, the slope b_ϕ is proportional to the square of the radius of interaction. The dependence of the t-slope, b_ϕ, on formation distance, $c\Delta\tau$, for ϕ meson production is shown in Fig. 2b together with previous data. Both of our data points (solid stars) lie in the region of $c\Delta\tau$ below 1 fm, and show a decrease of b_ϕ with decreasing formation time when combined with other data. This is consistent with the well-measured dependence for ρ meson production [Ca81].

The world data on elastic virtual photon production of ϕ mesons are shown as a function

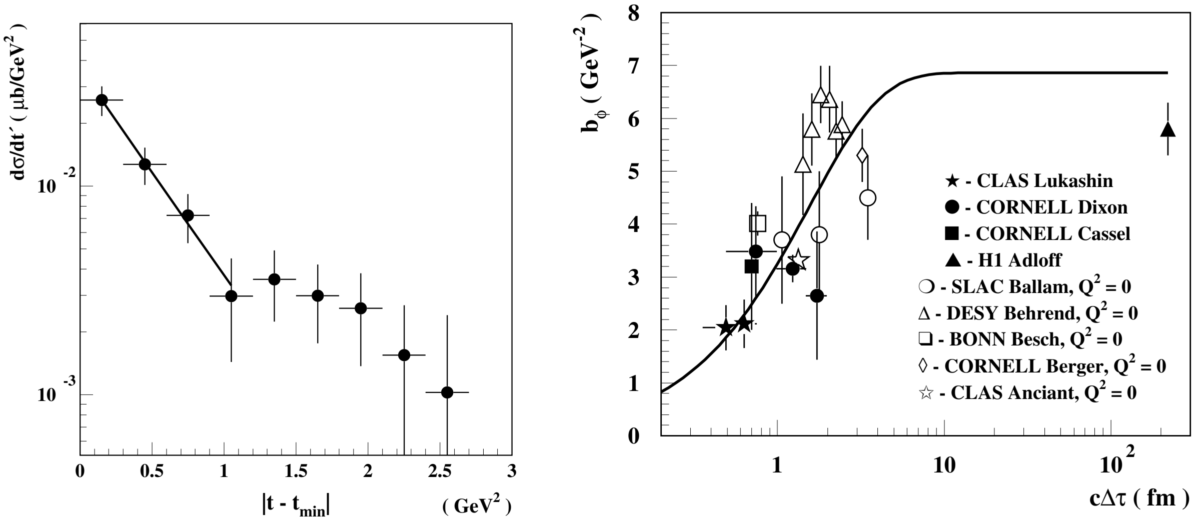

Figure 2: a) Differential cross section $d\sigma/dt'$ and b) dependence of the exponential slope b_ϕ on formation distance $c\Delta\tau$.

of Q^2 in Fig. 3a, and as a function of W in Fig. 3b. Selected photoproduction data are also plotted for completeness. All HERA data [Ad00, De96a, De96b] correspond to W ranging from 40 to 130 GeV, where the gluonic density in the proton at low $x = Q^2/2M_p\nu$ plays a significant role. Only the Cornell measurement [Ca81] exists at low W in the valence region. For the high-energy data, the Q^2 behavior of the cross section is well described by the vector meson propagator squared. The data are not yet in the asymptotic perturbative QCD regime where the longitudinal cross section for vector meson production is dominant, and should scale as Q^{-6}.

The photoproduction cross section increases slowly with W, reflecting the pomeron trajectory. At higher Q^2, a stronger dependence on W has been observed in preliminary analysis of HERA data [Na00]. If the cross section is parameterized as W^δ, δ varies from about 0.2 for photoproduction to $\delta \sim 0.7$ at a Q^2 of 8 GeV^2. This increased dependence of the cross section on W has been interpreted as being due to the rise of the gluon momentum density in the proton at small x [Br94]. We obtain a cross section dependence on W as $W^{0.2\pm0.1}$ at $Q^2 = 1.3$ GeV^2 after correcting for threshold effects. This is the same dependence as observed in photoproduction.

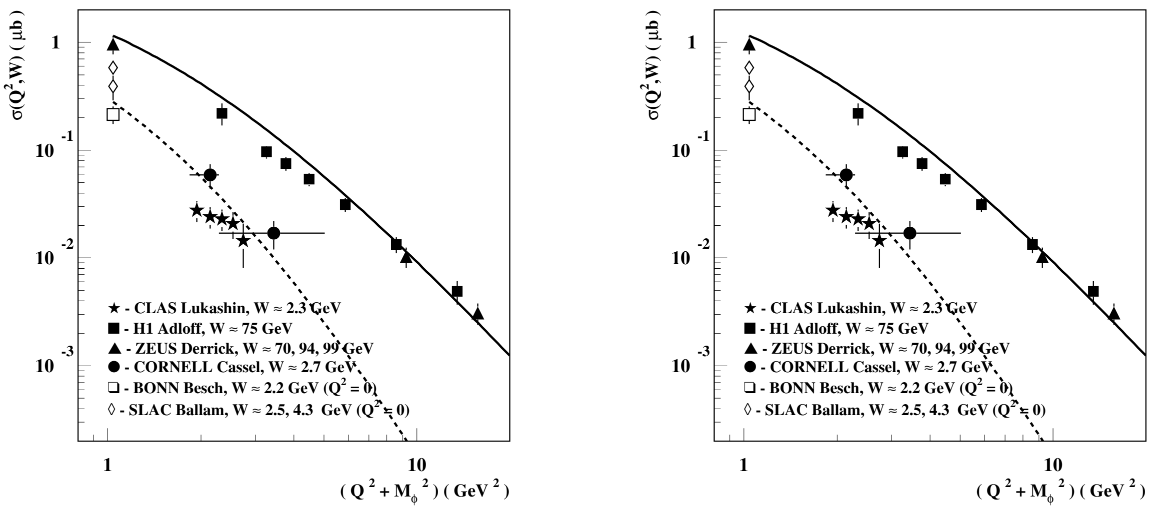

Figure 3: The ϕ meson cross section dependence on a) Q^2 and b) W.

References

[Ba78] T.H. Bauer *et al.,* Rev. Mod. Phys. **50**, 261 (1978).

[Ca81] D.G. Cassel *et al.,* Phys. Rev. D **24**, 2787 (1981).

[Di77] R. Dixon *et al.,* Phys. Rev. Lett. **39**, 516 (1977).

[Di79] R. Dixon *et al.,* Phys. Rev. D **19**, 3185 (1979).

[Lu00] K. Loukachine, "Electroproduction of the $\phi(1020)$ Vector Meson at 4 GeV," Ph.D. thesis, Virginia Polytechnic Institute and State University, February 2000.

[Lu01] CLAS Collaboration, K. Lukashin *et al.,* hep-ex/0101030, submitted to Phys Rev C.

[Ad00] H1 Collaboration, C. Adloff *et al.,* Phys. Lett. B **483**, 360 (2000).

[De96a] ZEUS Collaboration, M. Derrick *et al.,* Phys. Lett. B **380**, 220 (1996).

[De96b] ZEUS Collaboration, M. Derrick *et al.,* Phys. Lett. B **377**, 259 (1996).

[Na00] B. Naroska, hep-ex/0006010 (2000).

[Br94] S.J. Brodsky *et al.,* Phys. Rev. D **50**, 3134 (1994).

2.11 E93-030

Measurement of the Structure Functions for Kaon Electroproduction

R. Feuerbach, Carnegie Mellon University
K. H. Hicks, Ohio University
M. D. Mestayer, Jefferson Lab.
G. Niculescu, Ohio University

2.11.1 Introduction

The goal of the experiment is to measure all four structure functions which describe kaon hyperon electroproduction over a large range in Q^2 (0.5 to 2.5 GeV^2) and W (threshold to 2.2 GeV) with an almost complete angular coverage. By separately measuring the $e + p \to e' + K^+ + \Lambda$ and $e + p \to e' + K^+ + \Sigma^0$ channels the isospin dependence of the interference terms, of the L/T ratio, etc. are investigated.

2.11.2 Experiment Status

The data were acquired using a liquid hydrogen target. To date, an estimated 75 % of the experiment's data were acquired and analyzed. These data will be enough for an initial publication. For the more sensitive parts of the analysis (Rosenbluth separation) the whole data set will be needed.

2.11.3 Results

To date, the analysis has produced results for σ_{LT}, σ_{TT}, and the unseparated $\sigma_T + \varepsilon\sigma_L$, for two different beam energies[1] (2.5 and 4 GeV). The results were subjected to a series of systematic and consistency tests, including comparisons between the two independent analyses performed for this experiment. The results were found to be very stable and in

[1] Additional data at 3. GeV was acquired but not yet analyzed.

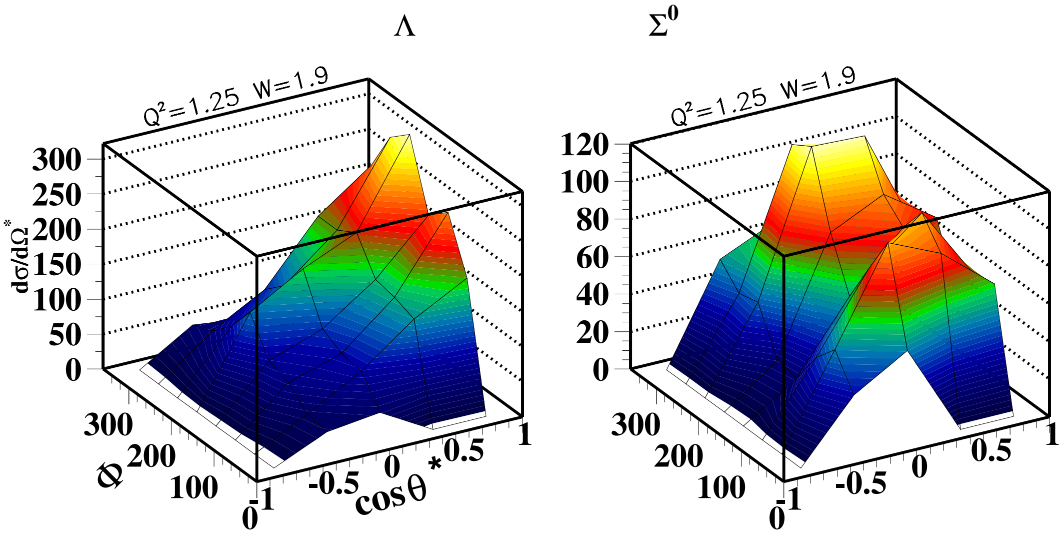

Figure 1: Preliminary $\cos\theta^*$ and Φ dependence of the differential cross–section $d\sigma/d\Omega^*$ for the $e + p \to e' + K^+ + \Lambda$ (left panel) and the $e + p \to e' + K^+ + \Sigma^0$ (right panel) reactions at fixed Q^2 ($1.25\ GeV^2$) and W ($1.90\ GeV$).

reasonable agreement with theoretical predictions (e.g. [Ma95]) in the forward direction[2]. Figures 1 and 2 show a small sample of our preliminary results: Figure 1 shows the differential crosssection $d\sigma/d\Omega^*$ as a function of Φ (x axis) and $\cos\theta^*$ (y axis) for a given Q^2 and W bin. Here θ^* is the polar angle of the K+ as measured from the direction of the virtual photon's momentum vector in the virtual photon–proton center of mass system while Φ is the azimuthal angle.

Fitting the differential crosssections to a functional form $a + b * \cos\phi + c * \cos 2\phi$ the coefficients b and c are proportional to the strengths of the interference terms, σ_{LT} and σ_{TT}, respectively. Figure 2 shows the angular dependence of interference terms σ_{LT} (top left panel) and σ_{TT} (top right panel) at fixed Q^2 and W (same bins as in Fig. 1) for the $e+p \to e' + K^+ + \Lambda$ reaction. The same dependences are shown for the $e+p \to e' + K^+ + \Sigma^0$ reaction in the bottom two panels. The results shown in Fig. 2 were obtained for the 4.2 GeV beam energy. For consistency they were compared (after taking into account the explicit ε

[2]Where most models were constrained by older measurements.

dependences) with the results obtained for the 2.5 GeV energy[3] and found to be in excellent agreement.

The uncertainties obtained in this experiment for the interference terms σ_{LT} and σ_{TT} are at least a factor of two smaller than those obtained in older measurements [Az74] [Be77] [Br79], with a greatly increased angular coverage. The projected uncertainties for the L/T separation will be comparable with those reported in [Ni98], while spanning a much larger $\cos\theta^*$ range. No current theoretical model can explain the angular dependence of both structure functions for either the Λ or Σ^0. The results should inspire new theoretical models of kaon electroproduction reactions.

References

[Be77] C. J. Bebek *et al.*, Phys. Rev. D **15**, 3082 (1977).

[Br79] P. Brauel *et al.*, Z. Phys. C **3**, 101 (1979).

[Az74] T. Azemoon *et al.*, DESY–report 74/75 (1974).

[Ma95] T. Mart, C. Bennhold, and C. E. Hyde-Wright, Phys. Rev. C **51**, R1074 (1995).

[Ni98] G. Niculescu, *et al.*, Phys. Rev. Let. **81**, 1805 (1998).

[3] Independently analyzed at Carnegie Mellon.

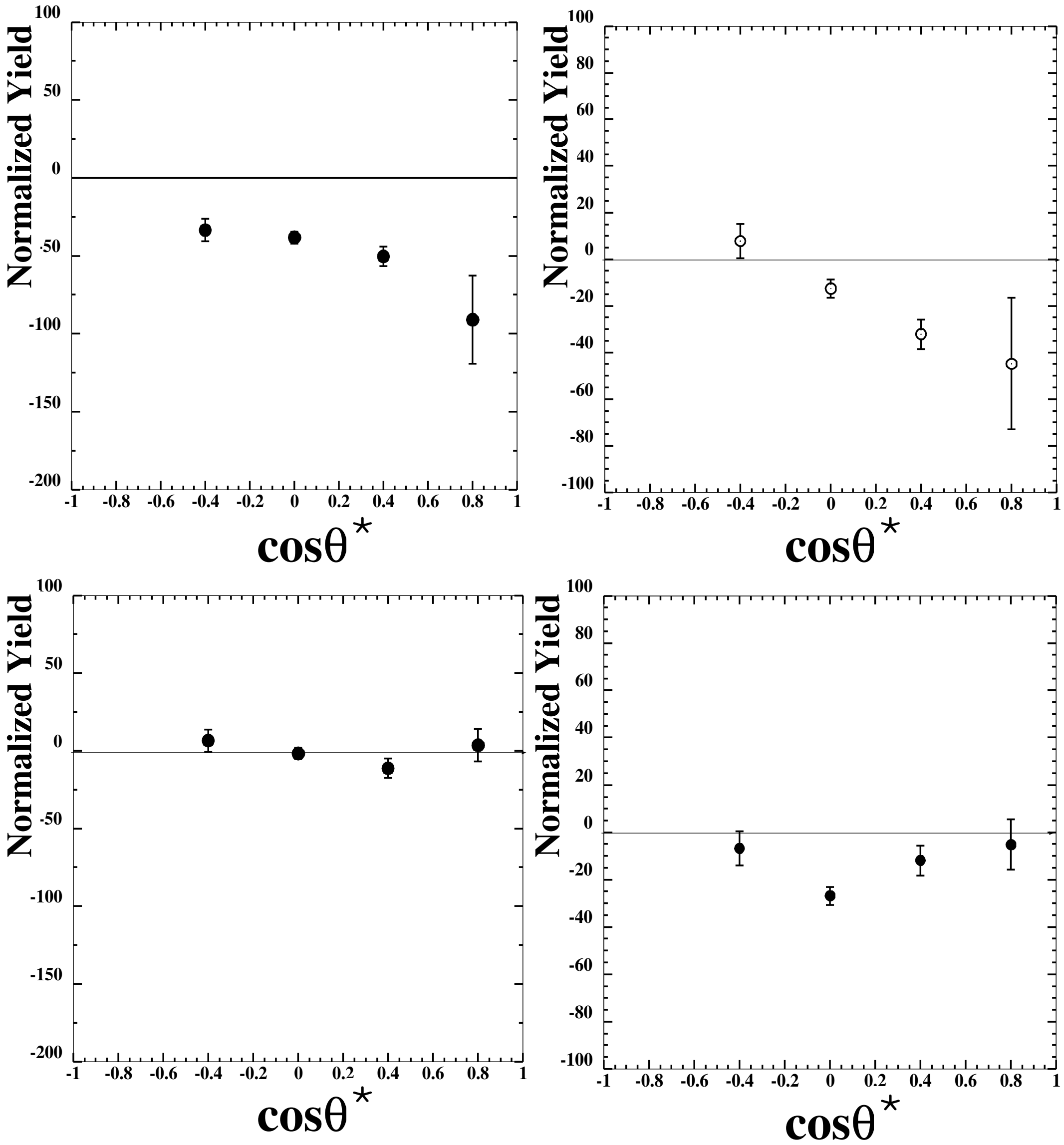

Figure 2: Preliminary $\cos\theta^*$ dependence of the LT (left) and TT (right) interference terms, shown here as "normalized yields" for the $e + p \to e' + K^+ + \Lambda$ reaction (top two panels) at fixed Q^2 and W (same values as in Fig. 1). The bottom two panels show the same dependence for the $e + p \to e' + K^+ + \Sigma^0$ reaction.

2.12 E93-043

Measurement of the $\Delta\Delta$ Component of the Deuteron
by Exclusive Quasi-elastic Electron Scattering
B. Quinn (Spokesperson) and the CLAS collaboration

2.12.1 Introduction

Experiment 93-043 is intended to make measurements of a small component of the deuteron wavefunction in which the constituent baryons are virtual Δ isobars. The signature sought is evidence of a pre-existing Δ^{++} observed in coincidence with scattering of an electron from the Δ^{-} constituent. This signature may be observable as an excess of events with a Δ^{++} emitted at back angles, where final-state interaction background is expected to be minimal. A small $\Delta\Delta$ component of the deuteron's wavefunction is required to explain observed results on electron-scattering from the deuteron [Fa79][Dy90] and is predicted at a similar (fraction of a percent) level by a number of calculations [Je74][Ar75][Dy90] including a recent calculation [Iv00].

Because the experiment depends on observation of the decay products of the backwards-going Δ^{++}, the acceptance depends critically on running with the CLAS torus field reversed. At lower beam energies, it is expected that sufficient statistics can be obtained, even with normal torus polarity, if the field is run at only a fraction of full field. The dedicated beam time for the experiment is 16 days of running with reversed field at 4 GeV. The intention is that lower-energy (2-3 GeV) data on deuterium for the E1 running period will be used in studying the Q-dependence of both the signal and background reactions.

2.12.2 Experiment Status

The dedicated running time has not yet been scheduled for this experiment. In part this is because the requirement of reversed torus field makes the experiment incompatible with simultaneous running of other experiments, so optimization of total data-collection argued against scheduling the experiment as part of the early CLAS running. Also, because final-state interaction backgrounds are very difficult to accurately estimate, it is prudent to try to study the back-angle backgrounds parasitically before dedicating beam time to the measurements.

The E1D running period took data on a deuterium target, including several days ($\approx 640\mu$C of accumulated charge) of running at 2.475 GeV with the toroid current set slightly below half-field. Furthermore, the E5 running period which took data on a combination hydrogen-deuterium target, included a few days of running ($\approx 190\mu$C) at 2.558 GeV with the torus field reversed (at -2/3 full field).

Analysis of these data sets should give a good calibration of the rate and angular distribution of background production through final-state interactions. Calibration constants are being determined for these sets in preparation for "cooking" of the data. Meanwhile, a first look at a small fraction of the data from the E1D running period has qualitatively confirmed the expected shape of the background, with production of Δ^{++} being strongly peaked along the momentum-transfer direction. While the background was seen to fall off rapidly with increasing angle, no quantitative conclusions can yet be reached, since statistics at back-angles were very low both because of the expected fall-off in cross-section and because of the decrease in acceptance. Once "cooking" of the E5 data begins, it should be possible to apply acceptance corrections and obtain a first glimpse of the background production at back angles for this 2.558 GeV beam energy. This should make it possible to determine whether it is advisable to go ahead with the presently planned 4.0 GeV running.

References

[Fa79] W. Fabian and H. Arenhovel, Nucl. Phys. **A314**, 253 (1979).

[Dy90] R. Dymarz, *et al.*, Nucl. Phys. **A507**, 531 (1990).

[Je74] S. Jena and L.S. Kisslinger, Annals of Physics **85**, 251 (1974).

[Ar75] H. Arenhovel, Z. Phys. **275**, 189 (1975).

[Iv00] A.N. Ivanov, *et al.*, European Physical Journal **A8**, 125 (2000).

2.13 E94-005

Determination of the $N\Delta$ Axial VectorTransition
Form Factor $G_A^{N\Delta}$ from the $ep- > e'\Delta^{++}\pi^-$ Reaction

L. Elouadrhiri, D. Heddle, R. Hicks (spokespersons)

D. Lawrence and S. Stepanyan

and the CLAS Collaboration

2.13.1 Introduction

Chiral Perturbation Theory (CPT) is one attempt to apply QCD to low-energy phenomena. For example, providing resonance contributions can be controlled, CPT provides largely model-independent predictions for the near-threshold cross sections for the $\gamma N \rightarrow N'\pi$ and $\gamma N \rightarrow \Delta\pi$ reactions. Closely related to CPT, but historically developed much earlier, are Low Energy Theorems (LET) which are also expected to give exact predictions under certain kinematic conditions.

Since the leptonic vertex is well understood, leptons can be used to probe hadronic structure in a much more meaningful way than is possible in purely hadronic interactions. The leptonic interaction is represented by the electromagnetic and axial vector current operators, operators sensitive to different aspects of the hadronic current. Whereas the electromagnetic coupling is usually dominant in photo- and electro-production reactions, the axial vector current is unfortunately only isolated in neutrino scattering experiments. Due to the minuscule cross sections, neutrino experiments have yet to yield acceptable results for either the axial vector form factor of the nucleon, or the axial vector form factors of the $N\Delta$ transition.

As a result, more sensitive methods have long been sought for investigating the axial vector currents of nucleons. For example, Nambu and Schrauner[1] developed a theoretical framework for connecting $\nu N \rightarrow eN\pi$ to $eN \rightarrow e'N\pi$ near threshold, and showed that the latter reaction is directly related to the axial vector form factor of the nucleon. This work was later extended by Adler and Weisberger[2] to the $ep \rightarrow e'\Delta^{++}\pi^-$ process near threshold,

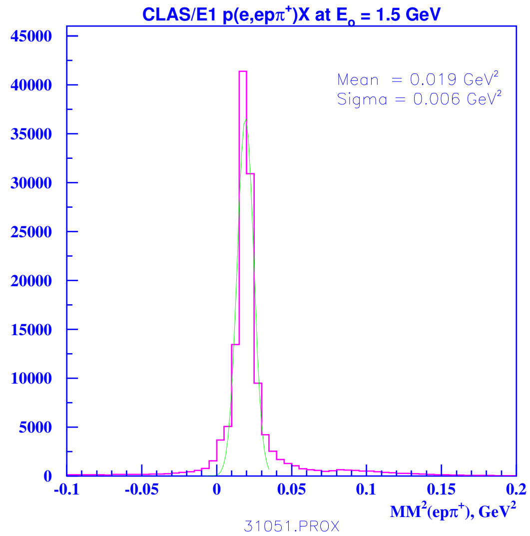

Figure 1: Missing mass for $ep \to ep\pi^+X$ The peak corresponds to the π^- mass

where the π^- is constrained to near-zero momentum in the hadronic center-of-mass system.

2.13.2 Experiment Status

Data from CLAS/E1c run period are used to extract $N\Delta$ axial vector transition form factor from the $e + p \to e' + \Delta^{++} + \pi^-$ reaction. First pass analyses of data were finished at the beginning of May 2000. Parallel to that, DST N-tuples were produced for 1.5 GeV. This is the main part of the data to be analyzed for the form factor extraction; about 1.6×10^8 electron events are stored in the 600 N-tuple files. For storage, a 200GB raid area was bought and configured with a stand-alone Linux box which serves as a file server for different physics analyses.

The reaction $e + p \to e' + \Delta^{++} + \pi^-$ is identified by the $e'p\pi^-\pi^+$ final state. CLAS acceptance at nominal torus field direction - negatives bend in - is favorable to the $e'p\pi^+X$ final state. The soft π^- is then unambiguously identified by missing mass due to the high resolution of CLAS as shown in Figure 1.

To check the quality of the data, studies of other possible combinations: $(e, e'p\pi^-)\pi^+$,

$(e, e'\pi^+\pi^-)p$, $(e, e'p\pi^+\pi^-)$ were completed.

There have been some issues related to target stability during the measurements. In order to get proper normalization, calculation of the elastic scattering cross section is integrated in the newly developed analyses code. Systematic checks and corrections of the integrated luminosity for each run were done in parallel with data analyses.

The cross section of the $e + p \to e' + \Delta^{++} + \pi^-$ must be determined as a function of W, Q^2 and t. The important components in the cross section calculations are acceptances and efficiencies of detected final state particles.

The analyses began with refining the particle ID, defining fiducial regions of CLAS acceptance, and determining of detection efficiencies for selected final states.

- PID - separate studies have been done using data from E1 and E2 runs. Based on those studies a scientific paper is prepared for publication.

- Acceptance and fiducial cuts - detailed studies of fiducial regions for final state particles and acceptances are completed. Bad channels and dead regions of the detector are identified. Work has been started towards the calculation of acceptances using GSIM and a realistic event generator which includes $ep \to e'p\pi^+\pi^-$ events generated through the Δ^{++} and Δ^o resonances as well as the phase space channel.

- Detection efficiencies. Efficiency functions are completely determined. They were obtained from analyses of the reactions $e + p \to e' + p$ in the elastic kinematics and $e + p \to e' + p + \pi^+ + \pi^-$.

We expect to have the first cross sections of the $e + p \to e' + \Delta^{++} + \pi^-$ in one month. After the first results are obtained, work will be done to finish final analyses and do the theoretical part of the work - extraction of the transition form factors (within the next six months). Final results on the Axial Transition form factor will be prepared for publication by the end of the year.

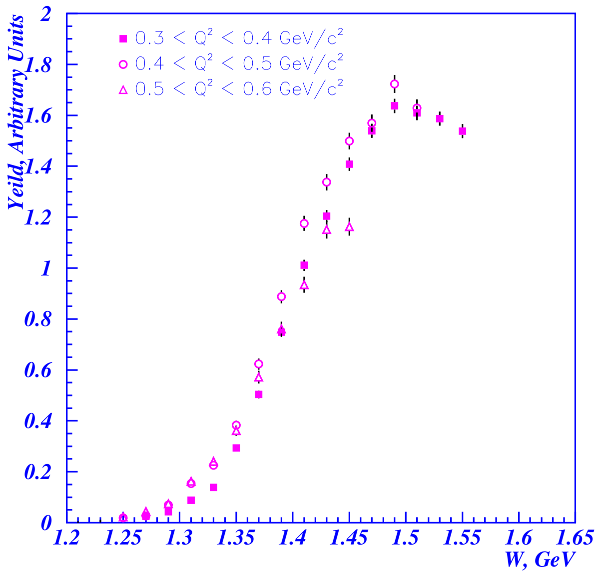

Figure 2: Yield of the cross section of of $ep \to e'p\pi^+\pi^-$ as measured with the CLAS detector for 3 different values of Q^2.

2.13.3 Results - or Expected Results

Figure 2 shows the yield of the measured cross section of $ep \to e'p\pi^+\pi^-$ as measured with the CLAS detector for 3 different values of Q^2. In this case, full detection of the scattered electron, proton and π^+ was required in each of the three drift chamber regions. Time-of-flight information was also required, as was detection of the electron in the Cerenkov counter and electromagnetic calorimeter.

The kinematic region of interest in this experiment, $W < 1.5$ GeV, lies below the $W \approx 1.6$ GeV threshold for ρ-meson production. There then remain two main background processes to the $ep \to \pi^-\Delta^{++}$ reaction we seek to study; these lead to the $\Delta^0\pi^+$ and non-resonant 3-body $p\pi^+\pi^-$ final states. According to theoretical predictions Δ^{++} production should dominate at low W, an expectation confirmed by the experimental results[7] from DESY. At $Q^2 = 0.5$ (GeV/c)^2 we assume production in the ratio of

$$p\pi^+\pi^- \ : \ \Delta^{++}\pi^- \ : \ \Delta^0\pi^+ \quad = \quad 1.8 \ : \ 9 \ : 1 \ ,$$

values that are consistent with the DESY results. This is also clearly seen in the CLAS data

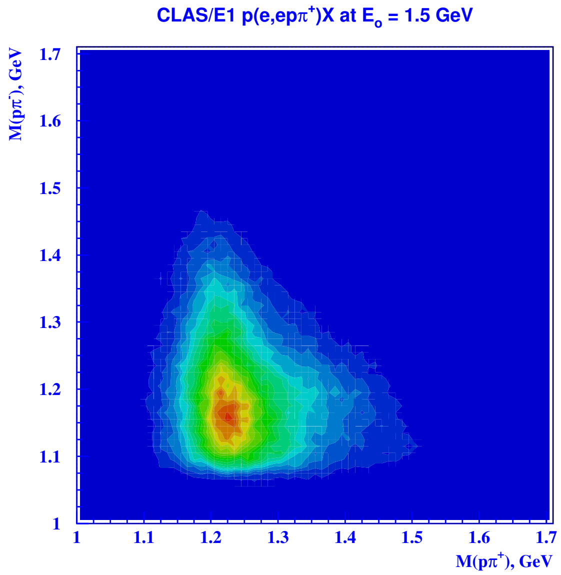

Figure 3: Data from CLAS show clearly the dominance of the Δ^{++} at low W.

(see Figure 3).

These projections show that in both precision and Q^2 range, the quality of the CLAS results will far surpass that of the only previous measurement of Δ^{++} electroproduction.

References

[1] Y. Nambu and E. Schrauner, Phys. Rev. **128**, 862 (1962).

[2] S. L. Adler and W. I. Weisberger, Phys. Rev. **169**, 1392 (1968).

[3] N. M. Kroll and M. A. Ruderman, Phys. Rev. **93**, 233 (1954).

[4] Aachen–Berlin–Bonn–Hamburg–Heidelberg–München collaboration, Phys. Rev. **175**, 1669 (1968).

[5] P. Joos *et al.*, Phys. Lett. **52B**, 481 (1974).

[6] P. Joos *et al.*, Phys. Lett. **62B**, 230 (1976).

[7] K. Wacker *et al.*, Nucl. Phys. **B144**, 269 (1978).

2.14 E94-103

The Photoproduction of Pions
W.J. Briscoe, J. Ficenec and D. Jenkins (co-spokespersons)
P. Heimberg and S. Philips
The George Washington University and Virginia Tech
and the CLAS Collaboration

2.14.1 Introduction

In this experiment, we have measured single-pion photoproduction using CLAS and the Tagged-Photon Facility in Hall B. Electron beams of energies from 1.8 to 3.2 GeV have been used to produce incident tagged photons with energies between 0.36 and 3.1 GeV. Cryogenic liquid hydrogen (g1) and deuterium (g2) targets were used for protons and neutrons, respectively. Once all of our systematics are understood, differential cross sections for the reactions $\gamma p \rightarrow \pi^0 p$, $\gamma p \rightarrow \pi^+ n$, $\gamma n \rightarrow \pi^- p$, and $\gamma n \rightarrow \pi^0 n$ will be determined with an absolute accuracy better than 4% for the first two of these reactions and 6% for the latter two reactions. The relative precision of the measurements will reach the 1-2% level. Angular increments of $\approx 5°$ for angles between 20° and 140° in the center of mass (CM) are obtainable for energy increments of $\approx$ 10 MeV. The larger uncertainty in the g2 measurements that use deuterium to provide a neutron target is a reflection of the uncertainties involved in correcting for the motion of the bound neutron. Comparison with the inverse photoproduction measurements (via detailed balance) currently being performed at BNL with the Crystal Ball can provide a test of the validity of these corrections. These measurements will provide unique and self-consistent results from tagged photons over a broad range of angles and energies, and with few exceptions, will represent the only pion-photoproduction data above 1.8 GeV.

The cross sections extracted from these data will be analyzed to determine the partial-wave amplitudes and the photocouplings for the baryon resonances in the energy range of this experiment. The photocouplings of baryon resonances are crucial in testing models which are based on our understanding of nonperturbative quantum chromodynamics. Couplings extracted from precision measurements can be used to test not only quark models of baryon structure and lattice-gauge calculations, but also models of the electromagnetic operator responsible for these couplings. Photoproduction provides a straightforward means of approaching these operators - a real-photon induced photoproduction experiment isolates the transverse degrees of freedom of the photon and fixes the $Q^2 = 0$ point for the complementary pion-electroproduction analysis.

2.14.2 Experiment Status

The data being analyzed come from the *g1a* run in Spring 1998, the *g1b* run in July 98, the *g1c* run period in November 1999 and the *g2a* run of 1999. We are presently analyzing runs from the *g1a* (D. Jenkins) and the *g1b* (P. Heimburg) periods for π^0 production from the proton. In this analysis, we are particularly looking at photon beam normalization and acceptance effects. Analysis is just under way on π^+ production from the proton for *g1b* and the π^- from the neutron for the *g2a* data. An all neutral trigger was also used during the *g2a* run that may allow us to look at π^0 production from the neutron. It is anticipated that the data obtained in run period *g1c* will provide the bulk of the information for this experiment. These data are about to undergo the "cooking" process.

2.14.3 Results

Since the GW group is also responsible for double-neutral-pion production, analysis on the neutral channel is being carried out first. The analysis can be done for three different event topologies: zero, one, and two photons (from the π^0 decay) detected along with the final state proton. Although detecting photons limits the angular coverage to the forward hemisphere (or less), extracting cross sections for all three topologies provides a powerful consistency check of our Monte-Carlo simulation of the CLAS, which is used to determine the detection volume for this channel. In all three cases, the detected proton, identified by its velocity-momentum correlation, is used to determine the invariant mass of the system not including the proton. When no photons are required, the g1a run period (0.5-2.3 GeV) will yield approximately 7 million events, while g1b (0.36-1.7 GeV) will yield a similar number. Even with 40 energy bins and 20 angular bins, the average statistical accuracy is better than 1 %

in each bin. While problems with beam normalization are evident in $g1a$, they are believed to be well understood in $g1b$ and $g1c$.

The differential cross section values obtained using the three different event topologies as described above agree well with each other. This is encouraging, since the acceptance varies dramatically as more photons are required and no fiducial cuts on the detector volume have yet been applied. These also agree fairly well with SAID [GW00] phase shift analysis solutions. An important systematic check is the constancy of the yield from run to run. In our initial survey, we find that after corrections for deadtime, the normalized yield for events requiring two photons is constant within statistics.

In the near term, the analysis will focus on obtaining the photon flux. Requiring agreement between fluxes deduced from two independent downstream devices, we hope to achieve an accuracy within 2% for the normalization. This is aided in part by our analysis efforts of the g5 (photofission) experiment, which was the first measurement using the Tagged Photon Facility. Completion of the analysis for the first two production runs will also provide a framework in which to extend the analysis to the higher-energy, higher-statistics g1c production run, which completed data-taking in the Fall of 1999.

The George Washington University group is supported by the U. S. Department of Energy.

[GW00] R.A. Arndt, R.L. Workman, and I.I. Strakovsky, Phys. Rev. C 56, 577 (1997)

2.15 E99-006

Polarization Observables in the ^{1}H($\vec{e}$,e$'$K$^+$)$\vec{\Lambda}$ Reaction

D.S. Carman, K. Joo, L.H. Kramer, B.A. Raue

2.15.1 Introduction

E99-006 was designed to provide the first ever beam-recoil double-polarization measurements in the reaction $p(\vec{e}, e'K^+)\vec{\Lambda}, \vec{\Sigma}^0$. The electroproduction reaction provides insight into the basic reaction mechanism for the open-strangeness production process, as well as information regarding fundamental hadronic structure. Both of these aspects are expected to provide insight into the nature of QCD in the confinement domain.

This experiment will provide data at beam energies of 2.5 and 4.2 GeV using the Hall B CLAS spectrometer. The large acceptance of CLAS enables us to detect the final-state electron and kaon, as well as the proton from the mesonic decay of the Λ hyperon over a range of Q^2 from 0.4 to 2.7 (GeV/c)^2 and W from 1.6 to 2.4 GeV. Using CLAS provides a unique opportunity to probe the interaction well beyond the usual parallel or in-plane kinematics of typical dual spectrometer experiments, through study over a broad range of momentum transfers and kaon azimuthal angles. This allows for simultaneous study of the reaction over varying kinematical regions where the different reaction channel processes have varying strengths. Thus we can effectively limit the intermediate baryonic or mesonic resonances involved in the reaction. An important aspect of our analysis is the search for the so-called "missing" N^* resonances predicted by constituent quark models but not seen through $N\pi$ or $N\gamma$ channels. Many of these states are predicted to have sizeable branching fractions to hyperons [1].

In hadrodynamic models, polarization observables are sensitive to the details of the reaction mechanism, that is, the specific intermediate resonances involved in the reaction, as well as their coupling constants. From the point of view of quark models, double-polarization observables will shed light on descriptions of strong decays through $q\bar{q}$ pair production and address the ambiguity in the quantum numbers of the $s\bar{s}$ pair created in the intermediate state. As well, our kinematics span the transition regime where it is expected that the hadrodynamic formalism will begin to give way to a description in terms of quarks and gluons. Newly developed gauge invariant models based on Regge exchanges may provide a convenient formalism over these kinematics, as well as above the resonance region.

2.15.2 Data Analysis

During the 1999 run period, the beam was longitudinally polarized to an average value of nearly 70%. Data for this experiment were acquired at beam energies of 2.567 GeV and 4.247 GeV. Event readout was triggered by a scattered electron candidate whose signal was a coincidence between a forward calorimeter and a Cerenkov counter hit in the same CLAS sector. Further substantial improvement in the electron sample was performed during the analysis.

Once the electron sample was isolated, the coincident charged-hadron spectrum was reconstructed. The primary technique for selecting charged hadrons is a cut on the reconstructed hadron mass spectrum, which is derived from the reconstructed track momentum divided by the particle velocity measured by the time-of-flight system. Fig. 1 highlights the positive hadron mass distribution as reconstructed from our data set filtered with loose requirements on particle identification of the $e'K^+$ final state. Cuts on this distribution are used to identify the detected charged particles in the final state.

The main analysis technique for identifying the final-state hyperons relies on missing-mass reconstructions of the $e'K^+$ final state. This is highlighted in Fig. 2 from analysis of the 4.247 GeV data. The main source of background beneath the hyperon missing-mass peaks comes from pions misidentified as kaons from the reaction $ep \to e'\pi^+ n$. The majority of these background pions can be eliminated with cut on the π^- mass from the reconstructed $p(e, e'K^+p)X$ distribution. This results in a very clean spectrum with essentially only the Λ and Σ^0 peaks remaining. The hyperons of interest are then selected with a cut on this last distribution. The width of the hyperon peaks in this spectrum, summed over all Q^2 and W, is about 14 MeV.

Summing over all Q^2 and W, we have roughly 20k (15k) Λ (Σ^0) hyperons at 4.2 GeV and roughly 35k (20k) Λ (Σ^0) hyperons at 2.5 GeV whose polarization we can measure. With

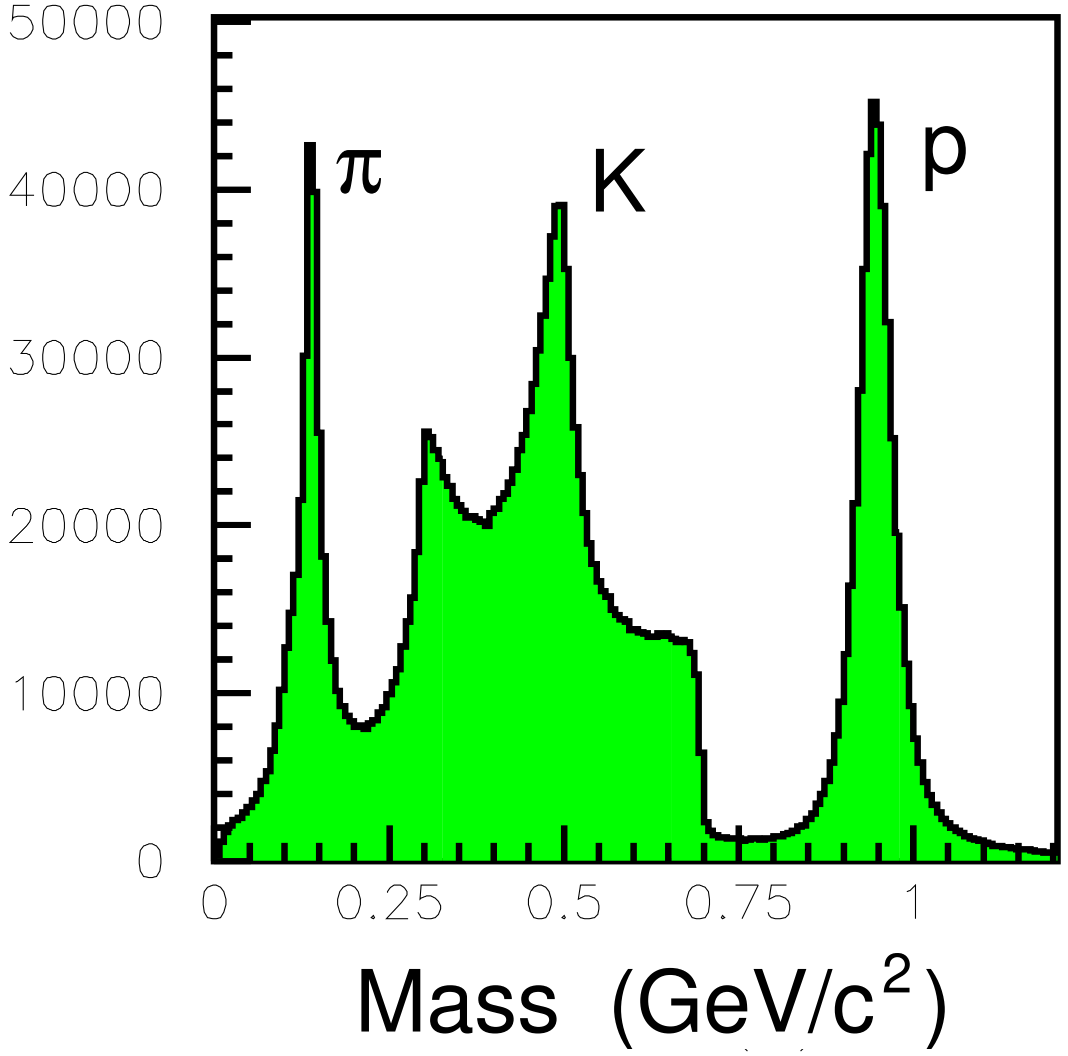

Figure 1: Reconstructed positive-hadron mass distribution from the kaon filtered data files.

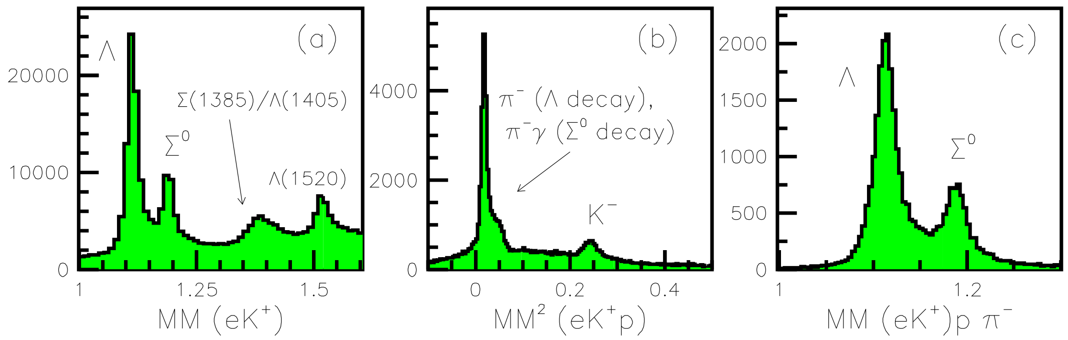

Figure 2: Hyperon missing-mass reconstructions from 4.247 GeV CLAS data. (a) Missing-mass spectrum for $p(e, e'K^+)X$, (b) missing-mass for the $p(e, e'K^+p)X$ reaction, and (c) hyperon distribution after cutting on the missing π^- (Λ decay) or $\pi^-\gamma$ (Σ^0 decay) peak.

our detected three-body final state, CLAS has an average acceptance of ≈6% for typical Q^2 and W values.

2.15.3 Polarization Extraction

The Λ hyperon decays mesonically via $\Lambda \to p\pi^-$ (B.R.=64%). The measured angular correlation of the decay proton with respect to a given spin quantization axis in a given bin of Q^2, W, and $d\Omega_K^*$, allows for the determination of the average hyperon polarization in that bin. In the hyperon CM frame, the decay-proton angular distribution is of the form:

$$\frac{dN}{d\theta_p^{RF}} \propto 1 + \alpha P_\Lambda \cos\theta_p^{RF}, \qquad P_\Lambda = P^0 + hP'. \tag{1}$$

Here, P_Λ is the Λ polarization, α is the weak-decay asymmetry parameter (measured to be 0.642±0.013 [2]), and θ_p^{RF} is the decay-proton polar angle in the hyperon rest frame relative to the spin-quantization axis. A standard choice is the so-called ℓ,n,t system, defined with $\hat{\ell}$ along the Λ direction and $\hat{n}$ normal to the hadronic plane. The Λ polarization is given by the sum of two terms, the induced and transferred polarizations. P^0 represents the induced Λ polarization when the electron beam is unpolarized, and P' represents the spin-transfer polarization to the Λ.

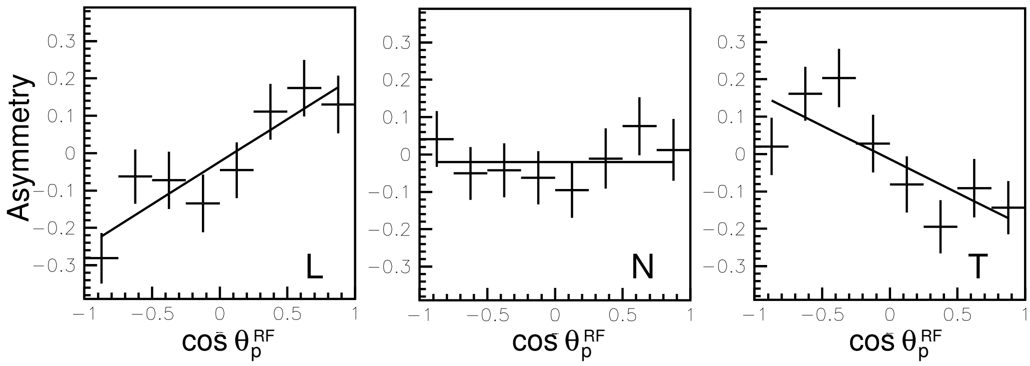

Figure 3: Polarization yield asymmetries for Λ production at 4.247 GeV integrated over all Φ for the bin defined by Q^2:[1.3-1.8 (GeV/c)^2], W:[1.6-1.9 GeV], and $\cos\theta_K^*$:[0.75-1.0]).

The analysis of the transferred polarization employs the technique of extracting the yield asymmetries for the two different electron beam helicity states (h=$\pm$1) of the form:

$$A_i = \frac{N^+ - N^-}{N^+ + N^-} = \frac{\alpha \cos\theta_p^{RF} P_i'}{1 + \alpha\cos\theta_p^{RF} P_i^0}, \qquad\qquad i = \ell, n, t. \tag{2}$$

This asymmetry is formed separately for each of the three spin-quantization axes of the decaying hyperon. In forming these asymmetries and integrating over all Φ, the angle between the electron and hadron planes, the form of the cross section dictates that $P_t^0 = P_\ell^0 = P_n'$ $= 0$. Thus A_n must be zero, but A_ℓ and A_t can be non-zero and provide a direct measure of the transferred polarization, as $A_i = \alpha\cos\theta_p^{RF} P_i'$. Fig. 3 shows results of our asymmetry fits at 4.247 GeV to indicate the quality of our data in a representative bin of Q^2, W, and $\cos\theta_K^*$, integrated over Φ.

The advantage of studying spin asymmetries is that they are relatively insensitive to the detector acceptance and efficiency, where the common factors associated with the two beam helicity states appear in both the numerator and denominator. Due to limited statistics in the present analysis, we have decided to study integrated quantities, in which the numerator and denominator are integrated over the angle Φ. This requires that the helicity-gated yields then be corrected for the acceptance of CLAS.

In this analysis, geometric fiducial cuts are employed for the electrons and hadrons. These define a precise region of the detector where events are accepted. The acceptance within the fiducial region can be calculated and used to apply an acceptance correction (including bad detector components, kaon in-flight decays, etc.) on an event-by-event basis. This approach has been shown to agree well with Monte Carlo simulations.

At the present time, the analysis is reaching an advanced stage, where detailed estimates of the contributing systematics are being evaluated. These studies include: effects of the pion background on our hyperon polarization signal, beam charge asymmetry effects, studies of our analytic acceptance corrections, etc. Results of the analysis have been presented at several conferences and work is progressing towards first publication of the results. Inherent in this work is performing detailed comparisons between the analysis results and the predictions of the existing theoretical models.

References

[1] S. Capstick and W. Roberts, Phys. Rev. D **58**, 74011 (1998).

[2] C. Caso *et al.*, Rev. of Particle Physics, Eur. Phys. J **C3**, 1 (1998).

2.16 e1-DVCS

Deep Virtual Compton Scattering at 4 GeV to 5 GeV with CLAS

V. Burkert, L. Elouadrhiri and S. Stepanyan
CLAS/DVCS collaboration

2.16.1 Introduction

Studies with leptonic beams in the deep inelastic scattering region (DIS) led to discovery of the quark-gluon structure of the nucleon. Although much was learned on the structure of the nucleon from DIS reactions, more information is needed for its description through interacting quarks and gluons. Recent developments in the theory showed that more reach information can be obtained in hard exclusive leptoproduction experiments. A formalism for the QCD description of hard exclusive reactions, developed by Ji [1], Radyushkin [2] and others, introduces new Generalized Parton Distributions, GPDs (or Skewed Parton Distributions) that contain information on the correlations between different quark configurations, on transverse and angular momentum distributions, and provide a unified description of a wide range of inclusive and exclusive reactions.

One of the key experiments for studying GPDs is Deep Virtual Compton Scattering (DVCS). There is evidence that in the case of DVCS the scaling regime may be reached at $Q^2 \sim 2$ $(\mathrm{GeV/c})^2$. This can be tested with data already available from CLAS.

2.16.2 Experiment Status

In the framework of this study, electroproduction data from CLAS, obtained with 4.247 GeV, 4.462 GeV and 4.872 GeV polarized electron beams (E1c and E1d run periods), are being analyzed. The data from the E1c run period (February-April of 1999) are calibrated and processed, and the calibration of the data from the E1d run period (February-April of 2000) is in progress.

First pass analyses of two data sets from the E1c run period have been completed, corresponding to total integrated luminosity $\sim 1.5\text{fb}^{-1}$ for each set. One of the important parts of the analysis is the identification of the $ep \rightarrow ep\gamma$ final state. CLAS resolution does not allow a complete separation of γ and π^0 final states at the kinematics of these studies ($W \geq 2$ GeV and $Q^2 \geq 1$ (GeV/c)^2.

To estimate contribution of pions in the selected sample, events with two photons in the final states are used. In Figure 1(a) missing mass of $ep \rightarrow epX$ vs invariant mass of two photons is plotted. Cuts on the invariant mass are applied to select $ep \rightarrow ep\pi^0$ events. Missing mass distribution of $ep \rightarrow ep\pi^0$ is fitted with Gaussian and a second order polynomial functions, Figure 1(b). The fit parameters of the Gaussian are used to fit the missing mass distribution for selected $ep \rightarrow epX$ events. In Figure 2 the results of the fit of $ep \rightarrow epX$ missing mass to two Gaussian and a second order polynomial functions is shown. Parameters P1 and P7 corresponds to the number of events from each Gaussian in the distribution. The estimated ratio of the π^0 events to photon events is $< 5\%$.

2.16.3 Preliminary Results

At these beam energies, the main contribution to the cross section of the reaction $ep \rightarrow ep\gamma$ is from the Bethe-Heitler (BH) process. While DVCS information cannot be accessed by measuring cross section, it can be obtained via measuring the Beam Spin Asymmetry (BSA) in the reaction $\vec{e}p \rightarrow ep\gamma$. This asymmetry arises as a result of an interference between real and imaginary parts of longitudinal and transverse amplitudes. The difference of the cross sections at different beam helicities is proportional to the imaginary part of the DVCS amplitude [3].

At this stage of the analysis only count rate asymmetries will be studied.

References

[1] X. Ji, Phys. Rev. Lett. **78**, 610 (1997); Phys. Rev. D **55**, 7114 (1997).

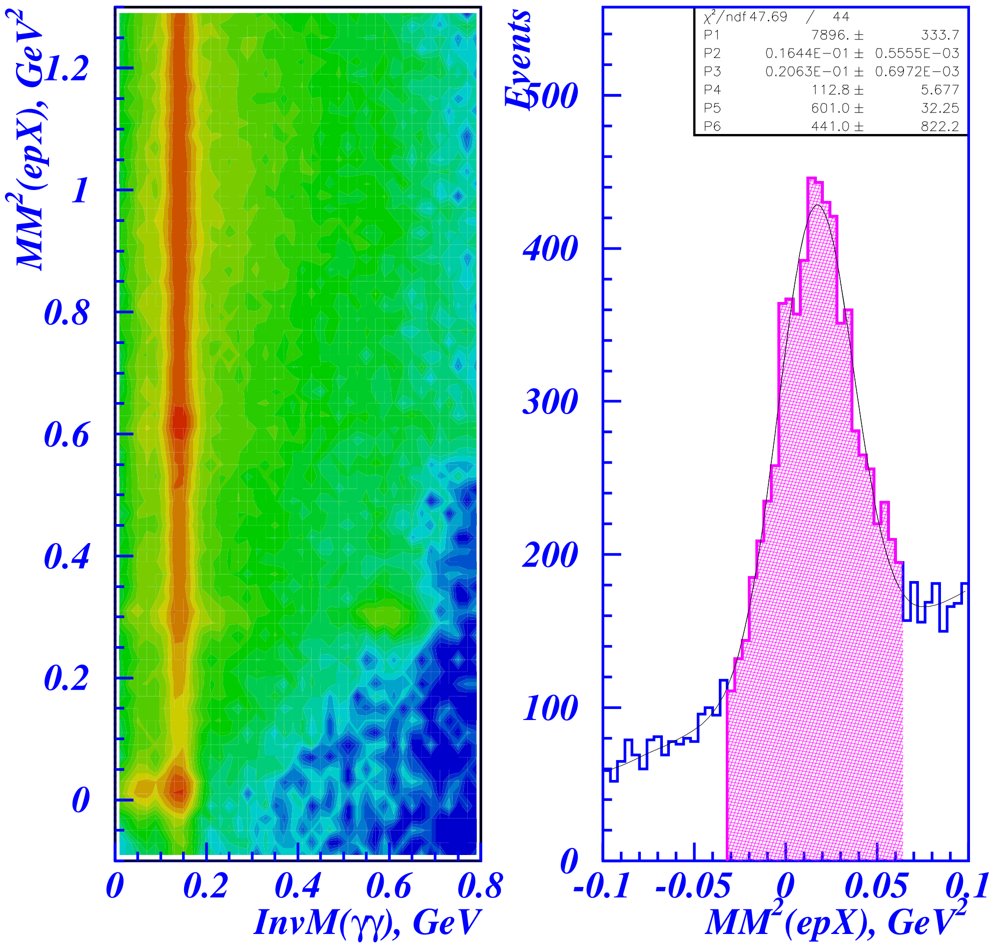

Figure 1: a) Missing mass of $ep \rightarrow epX$ vs invariant mass of two photons for selected $ep \rightarrow ep\gamma\gamma$ events. b) Missing mass distribution after cut on invariant mass to select π^0s. Fit to the distribution is with Gaussian (parameters 1 to 3) and second order polynomial (parameters 4 to 6) functions.

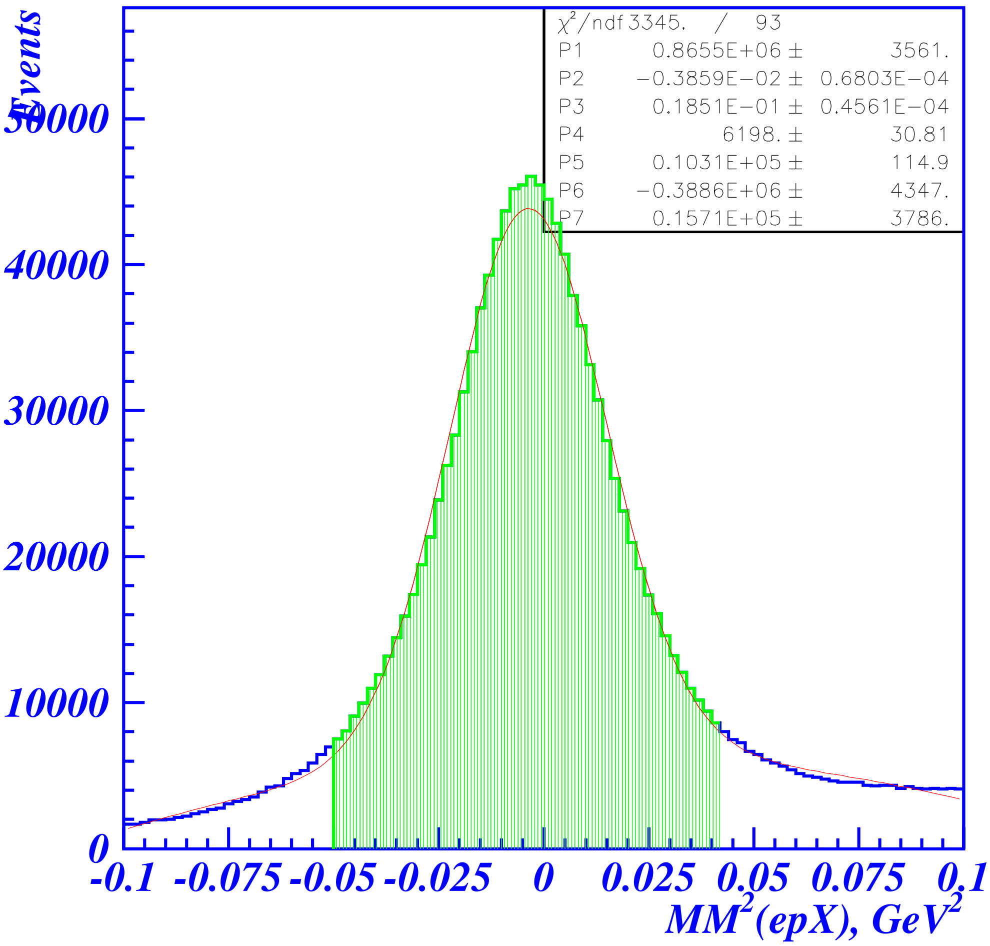

Figure 2: Missing mass distribution of $ep \rightarrow epX$. Fit to the distribution is with two Gaussian and second order polynomial functions. Fitted parameters of the first Gaussian function are P1 to P3, fitted parameters for the polynomial are P4 to P6. Centroid and sigma of the second Gaussian were fixed from the fit to π^0 peak in the two photon events. Only the constant of the second Gaussian is fitted, parameter P7.

[2] A.V. Radyushkin, Phys. Lett. B **380**, 417 (1996); Phys. Rev. D **56**, 5524 (1997).

[3] M. Diehl *et al.*, Phys. Lett. B **411**, 193 (1997).

2.17 e2 Run Group Overview

S. Stepanyan, E2 Run Coordinator
for the CLAS/E2 Run Group

2.17.1 Introduction

The CLAS/E2 run period includes seven experiments of the Multihadron Physics Working Group of the CLAS collaboration: PR-89-15, PR-89-17, PR-89-27, PR-89-31, PR-89-32, PR-89-36 and E-98-104. All seven experiments require nuclear targets and electron beam (polarized for E-98-104) and have similar requirements for detector setup. The main focus of these experiments is the study of nuclear structure in multinucleon knockout reactions at moderate to high momentum transfer.

2.17.2 Experiment Status

The first part of the CLAS/E2 run was from April 15 to May 27, 1999 (34 calendar days). The CLAS detector was used in its nominal configuration. CLAS also was equipped, for the first time, with four nuclear targets, two liquid targets, ^{3}He and ^{4}He, and two solid targets, ^{12}C and ^{56}Fe. Polarized electron beams with energies 1.1 GeV, 2.2 GeV and 4.4 GeV have been used. Overall data taking time was 17 days. Data were acquired with the CLAS "single electron trigger". A total of 2300M physics triggers from $\vec{e}A$ interactions were recorded on tape. The average (nucleon) luminosity during the run was $\mathcal{L} = 7 \times 10^{33}$ sec^{-1}cm^{-2}. At low energies the luminosity was limited by the CLAS DAQ, at high energies the limitation was the high occupancy of CLAS region 1 drift chambers. The table below summarizes the collected triggers by beam energy and target.

Collaborative efforts were organized for data calibration and for the first pass analyses. Work load was distributed among the several graduate students involved in the CLAS/E2 experiment. Data were calibrated and processed between June 1999 and May 2000 using the standard CLAS software release with few modifications. A web based package was developed for real-time monitoring of analysis processes. Also a new DST format in form of ROOT

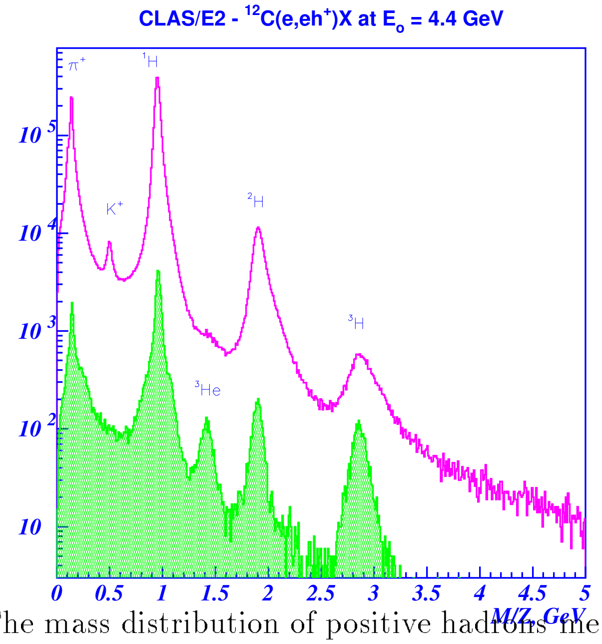

Figure 1: The mass distribution of positive hadrons measured in the reaction ^{12}C(e,e'h$^+$)X. The open histogram corresponds to the mass distribution of all positive particles. The dashed histogram is the mass distribution after the $\frac{dE}{dX}$ cut, to enhance the contribution of ^3He.

trees [1] has been implemented for the processed data set. More than 4000 data files were processed and DSTs in the form of PAW N-tuples [1] and ROOT Trees have been saved on the JLAB tape silo.

Beam Energies Targets	1.1 GeV	2.2 GeV	4.4 GeV	Total Triggers
^3He	134M	255M	188M	577M
^4He		310M	442M	752M
^{12}C	87M	323M	346M	756M
^{56}Fe		23M	63M	86M
CH_2	10M	34M	22M	66M
Empty	8M	25M	33M	66M
Total Triggers	239M	970M	1094M	2303M

The quality of the calibration and data processing were continuously monitored during the first pass. Since most of the physics reactions studied require multi particle final states, special attention was paid to the calibration of the CLAS time-of-flight system and the quality of the particle identification. In Figure 1 the mass spectra of positively charged particles, measured by the TOF system and the reconstructed momentum, is presented. It shows that not only pions, kaons and protons, but also light fragments ^{2}H and ^{3}H are

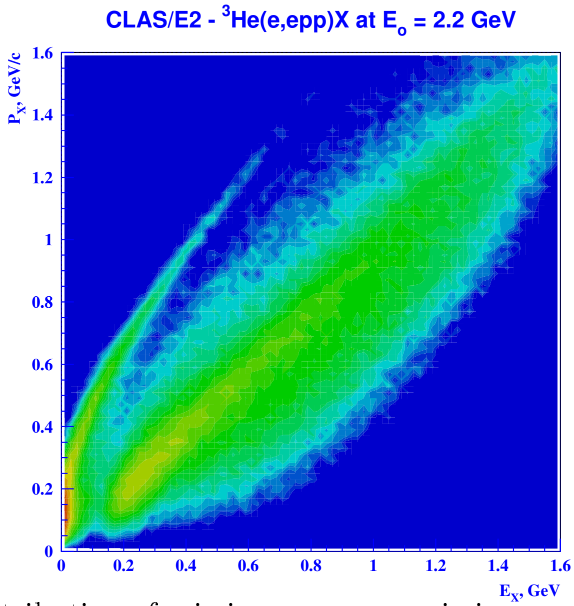

Figure 2: Distribution of missing energy vs missing momentum in the reaction ^{3}H(e,e'pp)X. There is clean separation of the ^{3}H three body break-up channel.

cleanly separated. Moreover, using energy losses in the scintillator, the mass peak of the ^{3}He fragments becomes visible as well.

2.17.3 Organization of Physics Analyses

Physics analyses were organized similar to the calibration and processing of raw data. Individual groups took responsibility to develop correction functions and fiducial acceptances for different detector settings. There is one CLAS-NOTE [2] published on fiducial acceptances and a few others are in progress.

There is a common analysis framework, E2ANATool [3] based on ROOT. This is a code for general use, that is developed by many users of the CLAS/E2 collaboration, and allows analyses of various different final states.

The first steps in the physics analyses show the high quality of obtained data. In Figure 2 the distribution of missing kinetic energy vs missing momentum for the reaction ^{3}H(e,e'pp)X is shown. The left band in the plot indicates the three body break-up of ^{3}He. This is the most promising channel for studying short range NN-correlations.

References

[1] CERN Program Library.

[2] D. Protopopescu et al., Fiducial cuts for electrons in the CLAS/E2 data at 4 GeV. CLAS-NOTE-2000-07.

[3] http://improv.unh.edu/Maurik/E2Root/E2AnaTool.html

2.18 E89-017

DELTA EXCITATION IN NUCLEI

D. Branford (Edinburgh)

S. McLauchlan, W. Ingram, D. Ireland, J. Kellie, and K. Livingston (Glasgow)

2.18.1 Introduction

Inclusive electron scattering experiments carried out in the late 1980s [Se89a] appeared to show that the centroid position of the $\Delta(1232)$ peak (in medium) had some dependence upon the Q^2 of the exchanged virtual photon (most prominently at low Q^2).

The results of these experiments were questionable, however, as in the region of interest there are background processes (2N knockout, non-resonant π production and higher resonances) and these need to be subtracted from the inclusive spectrum. This led to a significantly model dependent result.

With this in mind Richard Sealock et al. proposed [Se89b] utilising the large acceptance of JLab's CLAS detector array to detect the decay products of the $\Delta(1232)$ exclusively and measure the Q^2 dependence of the invariant mass, removing the neccessity for the above background subtraction.

2.18.2 Experiment Status

Preliminary analysis has been carried out, mainly concentrating on the (e,e'pπ) channels. As yet none of the Q^2 dependence of the original work has been observed. It should be noted, however, that this work lacks corrections, including radiative tail and detector acceptence.

2.18.3 Analysis Goals

Once the above mentioned corrections are finalised it is hoped that the Q^2 dependence of the Δ mass will become clear. If the Δ mass varies with Q^2, then the $\Delta - N$ potential must be

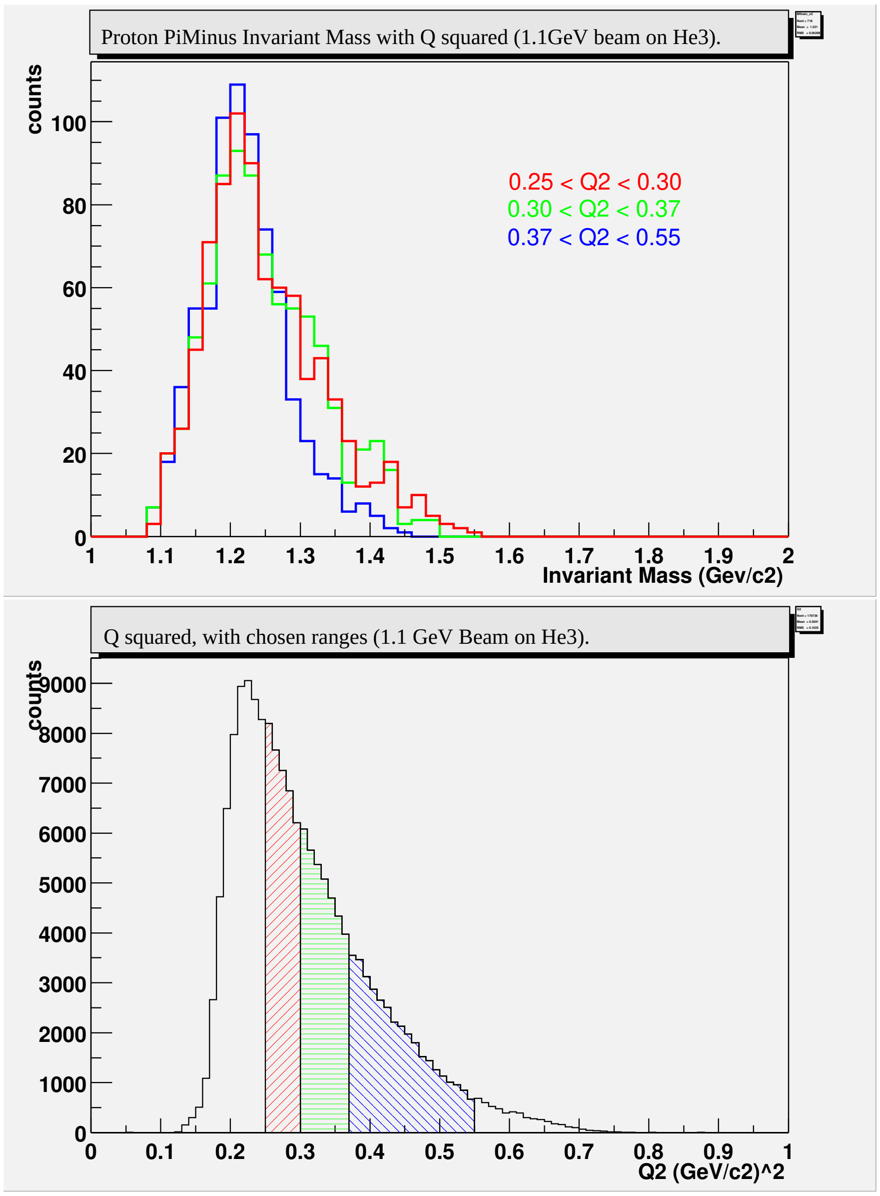

Figure 1: Proton pi-minus Invariant mass (top) with varying Q^2 bins (bottom)

momentum dependent and the nature of this potential may be found from the e2 data. In the event that the Δ mass is independent of Q^2, then the inclusive W spectrum must have its exclusively measured channels subtracted, exposing the source of the observed effect.

References

[Se89a] Phys Rev Lett **62**, 12 (1989).

[Se89b] proposal to the CLAS PAC(1989): PR-89-017.

2.19 E89-027

Correlations in ^{3}He(e,e'pp)n

Rustam Niyazov and Lawrence Weinstein, Old Dominion University

2.19.1 Introduction

The single nucleon energy and momentum distributions in nuclei have been thoroughly measured by nucleon knockout, pickup and stripping reactions. The shapes of these distributions, although not their magnitudes, are well described by mean-field impulse-approximation calculations. The discrepancies between the measured and calculated magnitudes indicate that nucleon-nucleon correlations are an important part of the nuclear wavefunction. To date, there have been almost no measurements of correlated NN momentum distributions in nuclei.

This experiment was part of the CLAS e2 run group. The status of data acquisition and analysis is described in the e2 overview.

2.19.2 Preliminary Results

We see strong evidence for NN correlations in the 2.2 GeV ^{3}He$(e, e'pp)$n data. Figure 1a) shows a modified Dalitz plot with the kinetic energy of proton 1 vs the kinetic energy of proton 2 (where the kinetic energies are scaled by the energy transfer). The detection threshold for protons is about 250 MeV/c and the software cut for neutrons is $p_n > 250$ MeV/c. We see peaks where one nucleon has most of the kinetic energy and the other two nucleons have momenta significantly greater than the fermi momentum. We select these events by choosing two nucleons each with $p_N \geq 250$ MeV/c, but kinetic energy less than 20% of the energy transfer, $T_N \leq 0.20\omega$ (the boxes in the corners of figure 1a). For these events, those two nucleons are emitted preferentially back to back in the lab frame (figure 1b). When we require that the third (struck) nucleon be within 20° of $\vec{q}$ (in order to emphasize quasifree knockout and decrease final state interactions), then the NN pair is more back-to-back and has zero average momentum parallel to $\vec{q}$ (figure 1c). In addition, the relative momentum of the NN pair, $\vec{p}_{rel} = (\vec{p}_{N1} - \vec{p}_{N2})/2$, is isotropic with respect to the total momentum, $\vec{p}_{tot} = \vec{p}_{N1} + \vec{p}_{N2}$. We see this for both pn and pp pairs.

Thus, because the two nucleon pair is

- high momentum,
- back to back,
- carries none of the virtual photon's momentum, and
- is isotropic

we conclude that we are seeing events where the virtual photon is absorbed by one nucleon and the other two correlated nucleons are not involved in the reaction. This means that we are directly observing undisturbed correlated nucleon-nucleon pairs. This sample of the relative momentum distribution is shown in Figure 1d. The spectrum is cut off at high momentum by the kinetic energy cuts on the paired nucleons ($T_N < 0.2 * \omega$).

Further analysis will concentrate on the 4 GeV data set and on comparison to various models and theories. This analysis will form the Ph.D. thesis of R. Niyazov. He is expected to graduate in 2001.

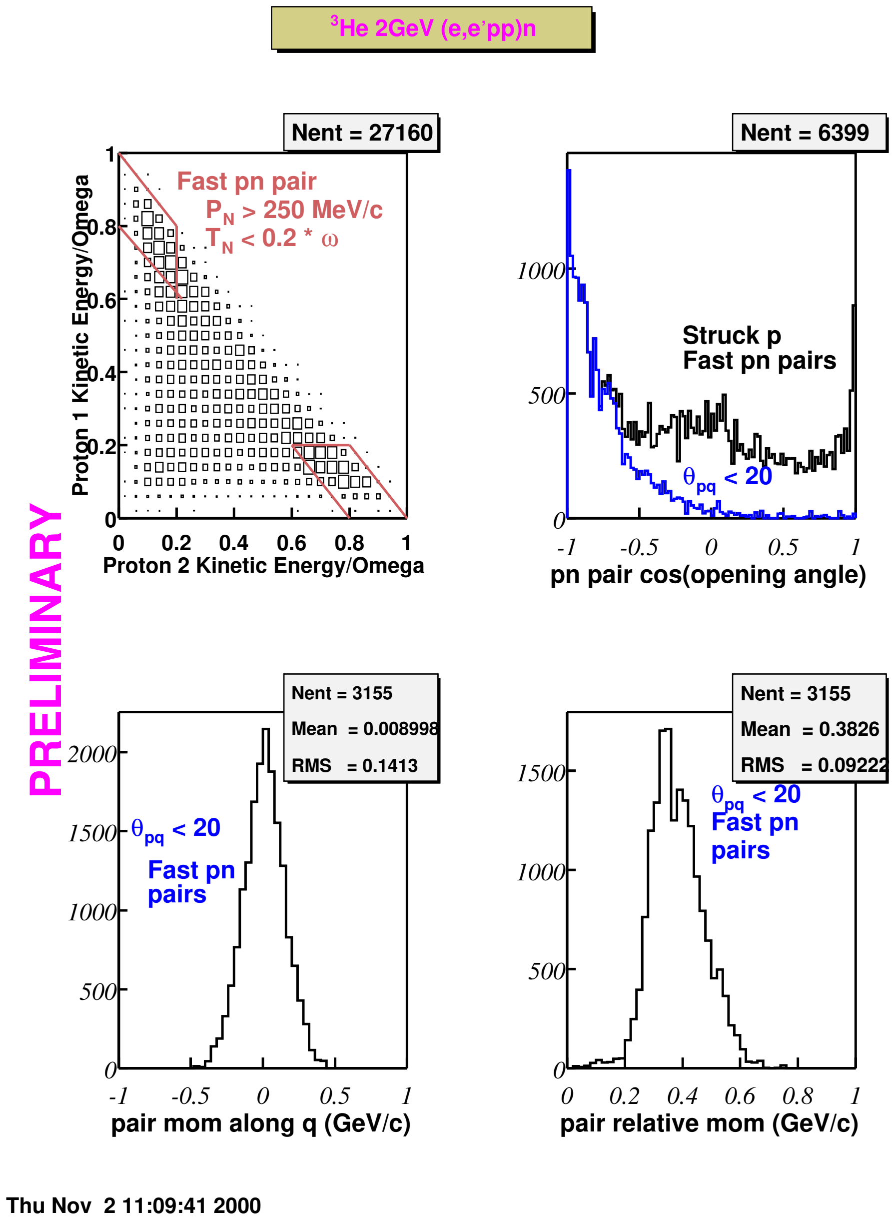

Figure 1: $^3\mathrm{He}(e,e'pp)n$ data from CLAS Multihadron experiment. a) Kinetic energy distribution of events, the boxes indicate the data selected for the other figures; b) opening angle of pn pairs where the two nucleons each have $p > 250$ MeV/c and $T < 0.2\omega$ (upper curve) and where the third nucleon is within 20° of $\vec{q}$ (lower curve); c) the total momentum along $\vec{q}$ of the pn pair where the third nucleon is within 20° of $\vec{q}$; and d) the relative momentum of the pn pair where the third nucleon is within 20° of $\vec{q}$.

2.20 E89-027a

Search for NN Correlations in Nuclei with the Signature of Fast Backward Protons

Bin Zhang, MIT

2.20.1 Introduction

This analysis is focused on the search for high momentum NN pairs in ^{3}He, ^{4}He, and C. The result shown below is from ^{3}He. Nucleons with high momentum, higher than the Fermi momentum, are a signature of short range correlation (SRC). SRC is the probe of the nucleons when they are very close to each other.

2.20.2 Preliminary Results

In ^{3}He we searched for pp and np pairs with high momenta. The relative abundance of these two pairs is another important physics observable to look at. The kinematical coverage of these selected events is shown in Figure 1-a. The beam energy was 2.2 GeV. We took data with 3 different beam energies: 1.2, 2.2, and 4.4 GeV. A cut was chosen to select the missing particle to be the third nucleon. Then events where a proton emerged backward to the 3-momentum transfer q are selected by requiring the angle $cos\theta_{p1q}$ to be greater than 100° (see Figure 1-b).

The momentum distribution of the pp pairs is shown in Figure 1-c and for pn pairs in Figure 1-d. The momenta distributions extend to large momenta, showing the signature of SRC. The real signal comes if the mean field theory fails to describe the enhanced high momenta contributions shown by these data which means the nucleons can get closer to each other than the existing models have assumed.

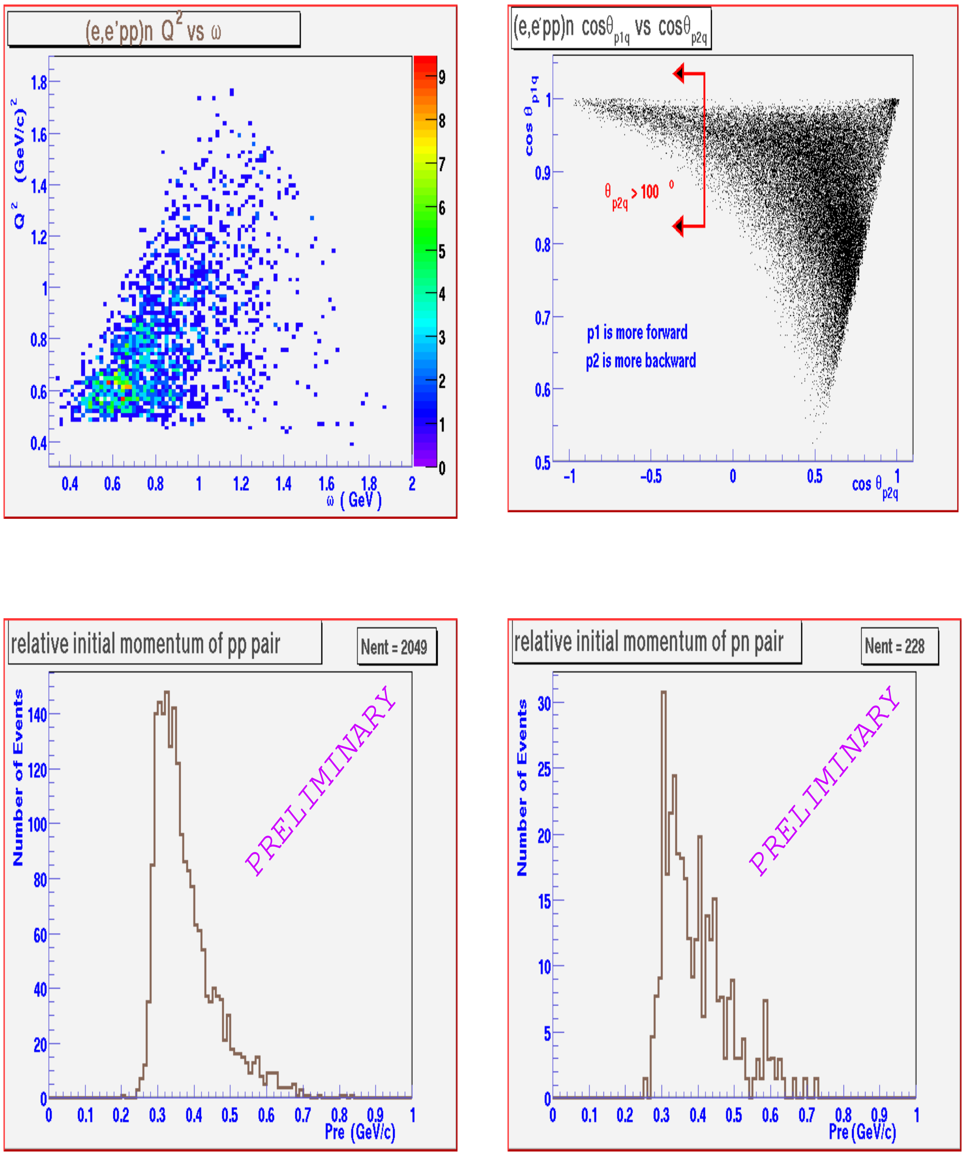

Figure 1: a) The kinematical coverage of the pp pair at 2.2 GeV beam energy. Q^2 is the four-momentum trasfered-squared and ω is the energy transfer to the pair; b) the angular distribution of the pp pair relative to q. Backward protons were selected to study SRC. c) the momentum distribution of the pp pairs in ^{3}He. The distribution extends to large momenta, showing the signature of SRC; and d) the momentum distribution of the np pairs in ^{3}He. The distribution extends to large momenta, showing the signature of SRC.

2.21 E89-036

Study of Short-Range Properties of Nuclear Matter in Electron-Nucleus and Photon-Nucleus Interactions with Backward Particle Production using the CLAS Detector

K. EGIYAN

2.21.1 Introduction

Studies of Short Range Properties (SRP) of nucleons in nuclei are planned. The SRP of nucleons should be manifested first of all in Short Range Correlations, as well as in high momentum transfer electron scattering from nuclei. Consequently, SRP in nuclei will be studied for two classes of struck nucleons: i) those involved in a Short Range Correlation, and therefore strongly off-shell, and ii) those in a single particle (quasiparticle) state and therefore almost on shell. The short distance properties of nucleons in the second case is connected to quantum fluctuations, which can be seen only at relatively high momentum transfers. It was shown that the best method for both studies, at moderate (CEBAF) momentum transfer, is two nucleon emission in electron-nucleus scattering. Therefore, we will study $A(e,e'pp)A-2$ reactions for different nuclei over a broad range of momentum transfer. The simplest of these reactions is $^3He(e,e'pp)$.

2.21.2 Experiment Status

This experiment is a part of the CLAS E2 run. We analyzed only the 2.26 GeV set of data with approximately 450,000 $^3He(e,e'pp)$ events.

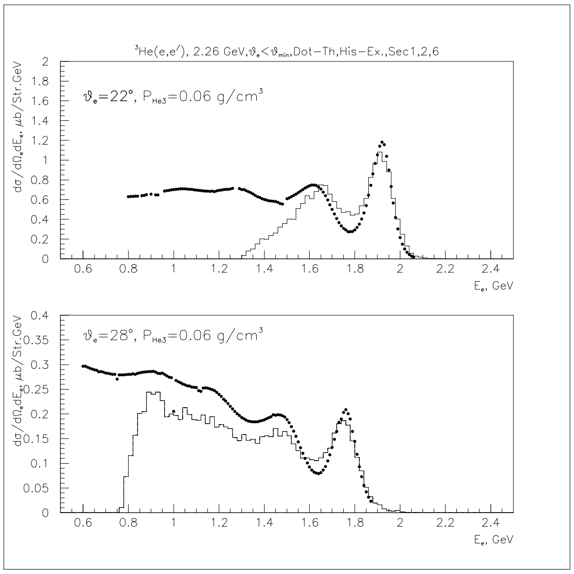

Figure 1: The energy spectra of scattered electrons measured (histogram) and calculated in virtual particle approach (dots).

2.21.3 Some Preliminary Results

1. Absolute cross section. To obtain absolute cross sections, complicated (and expensive) CLAS acceptance calculations are needed. These calculations require accurate and realistic event generators for processes under investigation. In the framework of our proposal, we have started to develop a theoretical approach for different targets and processes. For ^3He a code was developed to calculate inclusive (e,e') and $(e,e'NN)$ cross sections using a realistic ^3He wave function. This calculations agrees with existing SLAC inclusive (e,e') data. For this experiment we compare theoretical and experimental results at 3 beam energies: 1.16 GeV, 2.26 GeV and 4.46 GeV. Satisfactory agreement is obtained, at least in the quasielastic and the first resonance regions. In Fig.1 some of these results (at 2.26 GeV) are presented.

2. Measurements of Final State Interaction (FSI) in the $(e,e'pp)$ reaction on ^{3}He. The SRP of quasifree protons in nuclei can be studied using the nuclear transparency of the fast protons. In quasielastic electron scattering from a (modified) proton, the formation length (the distance from the interaction point to the point where the proton turns in to the normal state) is linearly proportional to the momentum of the knocked-out

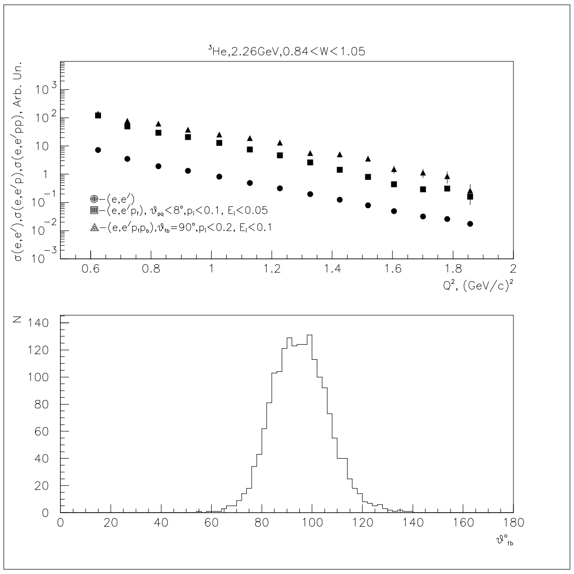

Figure 2: The Q^2 dependencies of (e, e'), $(e, e'p_f)$ and $(e, e'p_bp_f)$ cross sections (upper box) and forward-backward opening angle distribution for selected $(e, e'p_bp_f)$ events.

proton. At 2 GeV/c, e.g., this length is ≈ 1 fm. Therefore, to observe any modification of the FSI, the other nucleons have to be within 1 fm. This requirement fits the ^3He nucleus. By measuring the Q^2 dependence of the proton double scattering cross section in ^3He we hope to learn about any possible proton modification effects.

Fig. 2 shows the Q^2 dependencies of inclusive (e, e'), quasielastic $(e, e'p_f)$ and double scattering $(e, e'p_bp_f)$ cross sections. (p_f is a forward proton (with respect to $\vec{q}$) and p_b is a backward proton.) The two nucleon opening angle distribution peaks around 90^o, indicating the dominance of FSI in the $(e, e'p_bp_f)$ reaction.

The theoretical calculations, to obtain the transparencies, now are in progress.

2.22 pp INTERFEROMETRY AT eA INTERACTIONS (e2-run).

K. Mikhailov[1], *A. Stavinskiy*[1], A. Vlassov[1]

We report preliminary results on correlations between protons in the region of small relative momentum(velocities) produced in the $eA \to e'ppX$ reaction at 4.46 GeV for $A = 3, 4, 12$ and 56.

The effect of interference correlation of identical particles at small relative momenta produced in inclusive processes is based on the general principles of quantum mechanics. Correlations between two protons in the region of small relative velocities arise due to strong and Coulomb final state interaction and quantum statistics, i.e. antisymmetrization of the wave function of identical fermions.

The study of correlations between identical particles at small relative momenta is widely used for the analysis of heavy ion, hadron and lepton collisions starting from low energies up to the greatest accessible ones.

This interest is justified as the interferometry method permits us to link the correlations of particles with the space-time parameters of their emission. Such information is not accessible to direct measurements and cannot be easily obtained with other methods.

Measurements of the size of the emission regions in lepton-lepton and lepton-nucleon interactions gave sizes of slightly less than in hadron-hadron collisions. This difference may arise from the relatively simpler situation in ll and lh interactions then in hh interactions: in the first two cases correlations arise from hadronization of relatively simple parton configurations, while this is not the case in hh interactions, which also need not be limited to single primordial quark interactions.

Deep-inelastic lepton-nucleus interactions is one of the most favorable processes for a quantitative study of particle correlations at small relative momentum. It is now widely

[1]Permanent address: ITEP, B. Cheremushkinskaya 25, 117259 Moscow, Russia

realized that investigation of this process has enormously increased the understanding of short-range nuclear structure. The study of $A(e, e'ppX)$ reactions provides the fixed energy and momentum transfered in the process. At large relative momentum between protons asymptotic properties of particles leaving the reaction zone are monitored. Besides that, the study of this process at the region of small relative momentum between protons provides unique information on the proton-proton interaction just after the collision which is sensitive to source size.

Despite this favorable property, the results on particle interferometry in lepton-nucleus collisions are very scarce. Two factors preclude such measurements. Pairs of particles with small relative momentum are rare. Additional suppression of the experimental counting rate arises from lepton vertex. The unique properties of the CEBAF electron beam and the CEBAF Large Acceptance Spectrometer (CLAS) provide the possibilities of new generation experiments for particle interferometry in lh and lA collisions.

Experimental data were obtained by the CLAS detector at CEBAF. By measuring the scattered electron we restrict the transfered energy range to $\langle\nu\rangle \sim 2GeV$ and transfered momentum $\langle Q^2\rangle \sim 1GeV^2$ and study the dependence of the correlation function of two protons on the momentum difference in the pair reference frame. The mean value of the proton momentum and emission angle (with respect to γ) are $\langle p\rangle \sim 0.47GeV/c$ and $\langle\theta\rangle \sim 44^o$ respectively.

The correlation function was calculated as the ratio

$$R(\vec{q}, \vec{p}) = \frac{N_r(\vec{q}, \vec{p})}{N_b(\vec{q}, \vec{p})}, \tag{1}$$

where $\vec{q} = (\vec{p_1} - \vec{p_2})$, and N_r and N_b are the numbers of proton pairs combined from protons taken from the same and different events("mixing" procedure), respectively. Both distributions were normalized to the same numbers of pairs in the region outside the correlation effect $(0.15 < q < 0.30GeV/c)$. The pairs of protons from different events were submitted to the same selection procedure as those from the same events. Mixed pair distributions were corrected to take into account kinematical constraints for real pairs; experimental distributions were corrected to take into account inefficiency for close tracks. We estimated close track efficiency by two methods: it was studied for simulated events within the standard vertion of GEANT for the CLAS detector (GSIM) and also was extracted from experimental data by the study of the experimental correlation function for particles with different masses. Both methods are in good agreement within errors.

Experimental data on correlation functions are shown in Fig. 1. One can clearly see the enhancement of the correlation function at small q. Its width and position correspond to theory which takes into account final state interaction, Fermi statistic and Coulomb repulsion (curves corresponding to theory for the best values of the source size parameter r, are shown in Fig. 1 with χ^2/DF). Source size parameters extracted for low and high momentum protons are shown in Fig. 2.

Our preliminary data leads us to the conclusions:

- In eA interactions at 4.46 GeV, enhanced production of pairs of protons with small relative momentum has been observed. For nuclei lighter then C ($^3He,^4He$) data on pp correlations have been obtained for the first time.

- Assuming that the observed enhancement is due to strong and Coulomb final state interaction and Fermi-statistics we apply the standard theoretical approach to extract source size parameters. Within our statistical and systematic errors, data are consistent with a spherical Gaussian distribution of proton source.

- Measured values and A-dependence of the source size (see Fig. 2) corresponds to the size of the nucleus for low momentum protons ($p < 0.9GeV/c$). No significant A-dependence has been measured for high momentum protons ($p > 1.3GeV/c$).

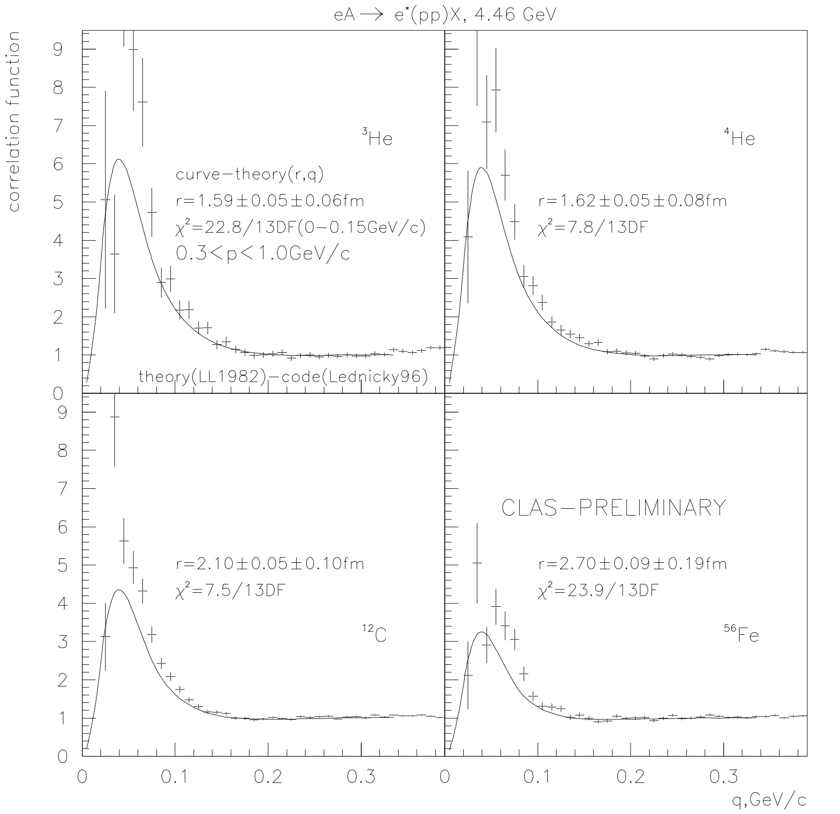

Figure 1: Correlation function for total momentum range.

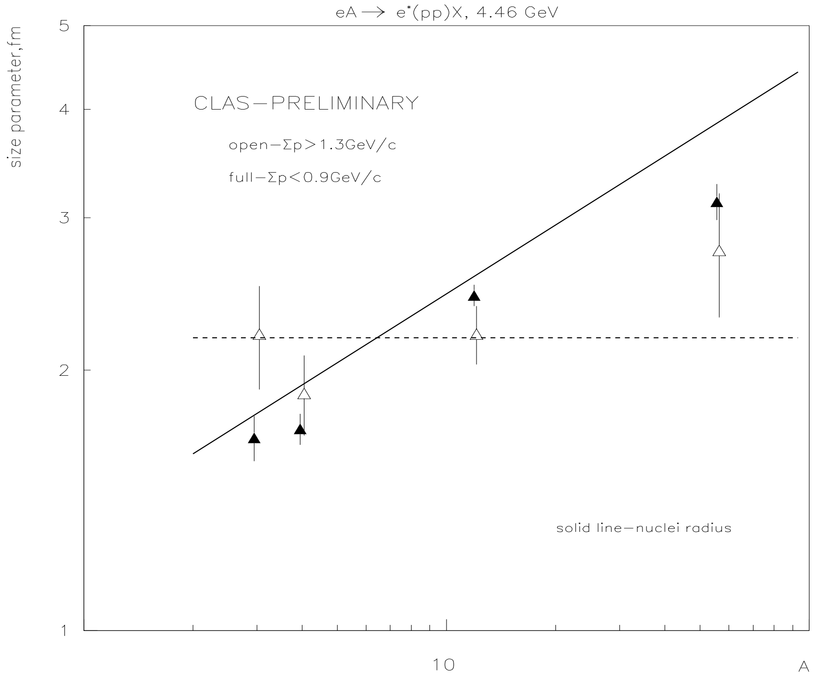

Figure 2: A-dependence for measured size parameter (fast and slow).

2.23 $A_{LT'}$ Preliminary results 02/2001

D. Protopopescu, F. W. Hersman, M. Holtrop
University of New Hampshire, Durham, NH 03824

Abstract

CLAS E2 data at 1.1, 2.2 and 4.4 GeV is used to search for the azimuthal asymmetry function in ^{12}C(e,e'p), and ^{3,4}He(e,e'p) reactions. Preliminary results showing a clear physics signal are presented.

Introduction

The high polarization of the beam during the data taking allows for a precise measurement of the beam asymmetry, $A_{LT'}$ and the associated response function $R_{LT'}$ also called the fifth response function. This quantity is calculated as the imaginary part of the interference between two amplitudes, longitudinal and transverse, and is odd under time reversal. Consequently it vanishes for all direct reactions. It can be non-zero for reactions involving multiple steps, such as final state interactions, meson exchange currents and overlapping resonances. As such, it provides information that is uniquely different from that available with the response functions accessible without polarization observables.

A central question of the multi-hadron reactions program is to determine the extent to which the virtual photon absorbtion mechanism that leads to multinuclear emission arises from a pre-existing configuration or via final-state rescattering. Measurement of this asymmetry can provide a powerful method for identifying and characterizing the multi-step final-state processes, thereby disentangling the relevant degrees of freedom in exclusive electron scattering on complex nuclei.

In what follows, we show that a physics signal can be seen in the E2a data. What remains to be done is to refine our analysis.

Preliminary Results

We measured the electron beam asymmetry ($A_{LT'}$) on various targets (^{3}He, ^{4}He, ^{12}C and ^{56}Fe) at various beam energies (1.1, 2.2 and 4.4 GeV). Here we shall present preliminary analysis of approximately 40% of the 1.1 GeV ^{12}C(e,e'p) data. Parallel analyses are being done on ^{3}He and ^{4}He and are documented in [1].

The first steps of the data analysis consist of a number of cuts on the data to eliminate background and to select the kinematical region of interest. First we make target vertex cuts to eliminate some background from events that do not come from the target region. We then cut on $W < 1.05$ GeV and $E_{miss} = \nu - T_{prot} - p^2_{recoil}/(2M_{A-1}) < 0.1$ GeV to select quasielastic events. Here W is calculated with $W^2 = m^2_{prot} + 2\nu m_{prot} - Q^2$ where m_{prot} is the mass of the proton. We cut on $Q^2 < 0.23$ GeV^2 to limit the kinematic area we integrate over. This selects the peak of the distribution in Q^2. Fiducial cuts and momentum corrections have not yet been applied. We binned the data in 3 degree bins in θ_{pq} and plotted the total number of counts vs ϕ_{pq}, the angle between the electron and hadron reaction planes, for positive and negative beam helicity (the absolute sign of the helicity is not yet known). Figure 1 shows the data for $8^o < \theta_{pq} < 11^o$, region where we expect a strong signal. Figures 1.1, 1.2 and 1.3 show the number of counts vs ϕ_{pq} for positive helicity, negative helicity and their sum, respectively. The sum gives us a good image of the acceptance function. Figure 1.4 shows the vertex position data and 1.5 shows the E_{miss} spectrum. Figure 1.6 shows the asymmetry:

$$A\text{asym} = \frac{h^+ - h^-}{h^+ + h^-} \tag{1}$$

We fit this quantity with the function:

$$f(\phi_{pq}) = b + A \sin \phi_{pq} \tag{2}$$

In ideal conditions, we expect the offset b to be equal to zero since the target is unpolarized. A non-zero b parameter indicates an asymmetry in the amount of charge for positive and negative helicity states. Such an asymmetry can be corrected for in a separate step. The A parameter of the function is directly proportional to the beam asymmetry $A_{LT'}$.

Now, if we vary θ_{pq} we obtain the dependency shown in Fig.2. The amplitude on the

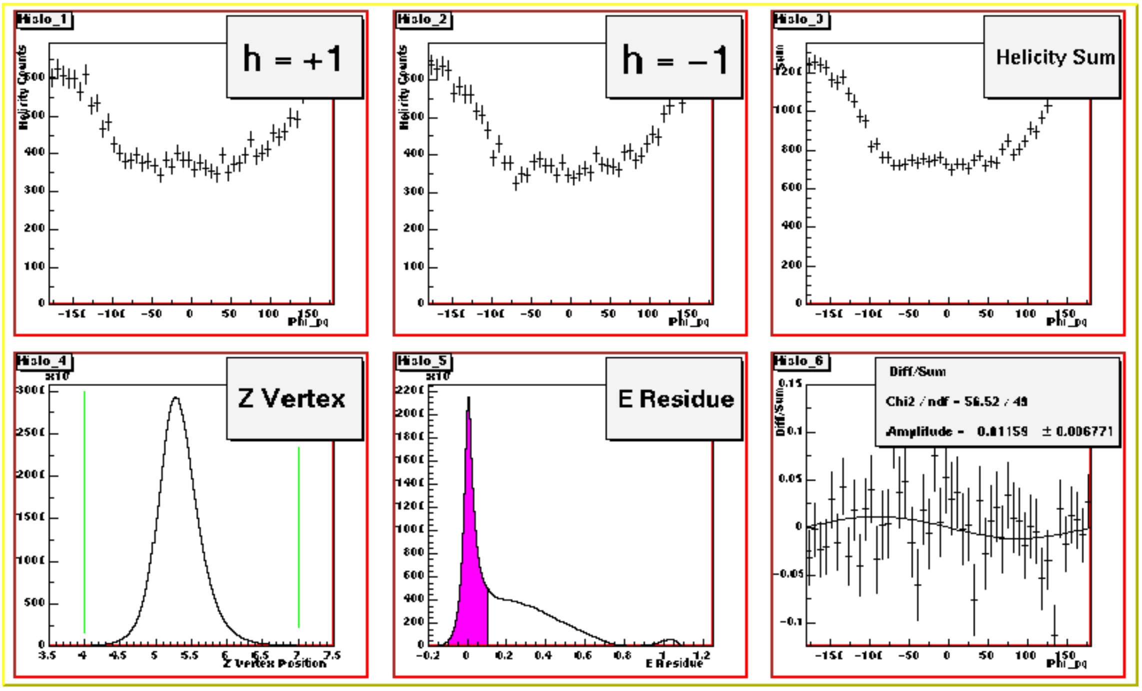

Figure 1: Typical asymmetry plot for ^{12}C data. The complete set is available in [2]

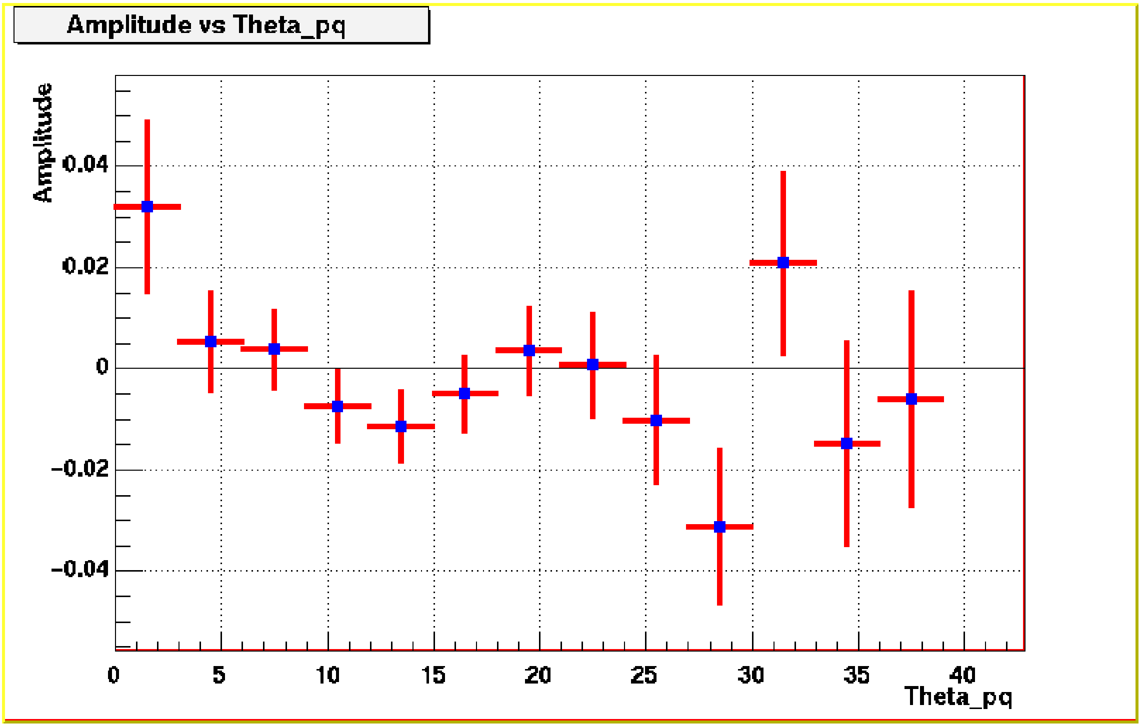

Figure 2: Plot of the amplitude of the azimuthal asymmetry versus θ_{pq} angle.

vertical axis is the fit parameter A from formula (2). The cuts employed to obtain this result filter 12M events out of approximately 30M triggers. The individual plots used to obtain this dependence are available in [2].

The results presented here are not influenced by the acceptance effects and therefore we can say that we are close to the final stages of our analysis. For improved results we will need to analyze more statistics and to understand the sources of error. We also need to determine the absolute normalization of the asymmetry, and study the dependence of these results to our choice of cuts. We have 87M triggers available for ^{12}C at 1.1 GeV, but 323M for 2.2 GeV and 346M for 4.4 GeV. The analysis of the higher energy data will enable us to make useful comparisons.

References

[1] E2 Analysis Updates, M. Holtrop, documentation in html format, *http://einstein.unh.edu/Maurik/Analysis/E2Analysis.shtml*

[2] ^{12}C Analysis Webpage, D.Protopopescu, January 2001, documentation in html format, *http://einstein.unh.edu/protopop/c12details.html*

2.24 e5 Run (E94-017)

The Neutron Magnetic Form Factor from Precision Measurements of the Ratio of Quasielastic Electron-Neutron to Electron-Proton Scattering in Deuterium

W. K. Brooks (Jefferson Lab), M. F. Vineyard (University of Richmond)
and the CLAS Collaboration

2.24.1 Introduction

The E5 run period consists of a single experiment, E94-017. The goal of this experiment is to determine the neutron magnetic form factor over a Q^2 range from 0.2 to $4.8(GeV/c)^2$ from precision measurements of the ratio of quasielastic electron-neutron to electron-proton scattering in deuterium.

Nucleon structure is one of the most fundamental issues in hadronic physics. Elastic electron scattering provides detailed information about the electromagnetic structure of the nucleon. The differential cross section for elastic electron- nucleon scattering in the one-photon-exchange approximation is given by the Rosenbluth formula [Ro50] in which the nucleon structure information is contained in the Sachs electric and magnetic form factors. These form factors are used for comparison between experiment and theoretical models of nucleon structure. In addition to being of fundamental importance in understanding nucleon structure, the form factors are a necessary input for calculations of nuclear response functions.

The proton electromagnetic form factors have been rather well determined at low Q^2 values using a Rosenbluth separation [Bo95], and more recently at higher Q^2 using a polarization transfer technique [11]. However, the neutron form factors have been determined with much less precision than those of the proton [Bo95]. Until the last decade most of the neutron form factor data came from analyses of inclusive quasielastic electron scattering from deuterium that introduce a number of significant systematic errors. More recently progress has been made in measurements [Ma93, Br95, 12, An98] of the neutron magnetic form factor, G_M^n, at low Q^2 values by measuring the ratio of quasielastic electron-neutron to electron-proton scattering in deuterium, a method in which many of the systematic uncertainties cancel. However, there are discrepancies among these measurements. Recently, measurements [Ga95] of inclusive quasielastic scattering of polarized electrons off a polarized ^3He target were performed in Hall A at Jefferson Lab that will yield another precise measurement of G_M^n at low Q^2.

In this experiment, precise measurements of the ratio of quasielastic electron- neutron to electron-proton scattering in deuterium have been made over a Q^2 range from 0.2 to $4.8(GeV/c)^2$ with the CLAS. The neutron magnetic form factor will be extracted from this ratio with the use of the more accurately known proton form factors. Data are taken simultaneously on separated hydrogen and deuterium targets. The $e+p \rightarrow e'+n+\pi^+$ reaction on the hydrogen target will be used to measure the neutron detection efficiency. The data from electron-proton and electron-neutron scattering in deuterium will be treated in an identical way insofar as possible. The use of this ratio technique, with the simultaneous calibration of the neutron detection efficiency, significantly reduces or eliminates many of the systematic errors associated with inclusive quasielastic scattering from deuterium. The results of this experiment will provide a significant improvement in our knowledge of the neutron magnetic form factor over the Q^2 coverage of existing measurements, and will extend the range to $4.8(GeV/c)^2$. In addition to providing accurate information on the magnetic structure of the neutron, these data will be important for the extraction of the electric form factor of the neutron from measurements of polarization observables which determine a linear combination of the electric and magnetic form factors (see for example Refs. [Da93, Ma93]) and will allow a more accurate extraction of the strange quark form factor [An99].

An extension of this experiment was approved by PAC9 to make measurements with a 6-GeV beam and increase the Q^2 coverage to 7.5 $(GeV/c)^2$. The measurements at high momentum transfer will have special significance in relationship to QCD. It has been observed that the proton magnetic form factor falls off with Q^{-4} behavior beginning at about 5-10 $(GeV/c)^2$. A functional dependence of this type is predicted by quark dimensional scaling, but this level of interaction was expected to occur only at much higher momentum transfer. On the other hand, estimates of nonperturbative soft contributions indicate that the soft terms are comparable to the data in magnitude [Ra99]. This has fueled a great deal of controversy over the validity of perturbative QCD at such low momentum transfer. The approved extension of this experiment will address this issue by providing the first reliable measurements of the neutron magnetic form factor in the momentum transfer range where the proton magnetic form factor exhibits the Q^{-4} behavior.

2.24.2 Experiment Status

Data for E94-017 were collected during the E5 run in April and May of 2000 with the CLAS detector in Hall B at Jefferson Lab and are currently being analyzed. Approximately 2.3 billion triggers were acquired, about half at an electron beam energy of 2.6 GeV and half at 4.2 GeV. The low beam energy data were divided into two-thirds normal torus polarity and one-third reversed torus polarity. The reversed torus polarity data were taken to reach the lowest possible limit in Q^2. There is considerable overlap in Q^2 between the data taken at the two beam energies that will provide important systematic cross- checks.

There were several distinctive features of this run period. A dual-cell target containing liquid hydrogen and liquid deuterium was used. The full detector design luminosity of $10^{34} cm^{-2} s^{-1}$ hydrogen-equivalent was achieved. A new online monitor was used that displays parallel-processed reconstructed data online using a Root-based gui. The gain monitoring systems for the forward and large angle calorimeter was used for the first time during a production run. Finally, while monitoring the second target cell by means of a PC, the monitored quantities were transferred from the LabVIEW interface to the EPICS control system, a capability that has not been used in Hall B before, which will be useful in many future applications.

The dual-cell target system was developed for this experiment to enable the use of the $e + p \to e' + n + \pi^+$ reaction to calibrate the neutron response of the calorimeters simultaneously with the measurements of quasielastic scattering from deuterium. This assures that the calorimeters are calibrated with the same thresholds and background conditions at which the primary measurements of interest are made. Two 4-cm long cells were aligned along the beam axis such that the beam passed through one and then the other. One cell contained liquid deuterium, the other liquid hydrogen. With the two target cells separated by 4 cm, vertex reconstruction can be used to determine from which cell an event originated.

Shown in Figure 1 are spectra taken with a 4.2-GeV electron beam during the E5 run. The top-left panel is a two-dimensional spectrum of azimuthal angle, ϕ, versus the z vertex, Vz, for electrons scattered from the empty dual target system. The top-right panel is the ϕ spectrum and the bottom-left panel shows the z vertex distribution for electrons scattered from the empty target. These spectra show the excellent alignment of the target along the beam axis and demonstrate the ability of the vertex reconstruction to determine from which target the electron was scattered. The sharp peaks at Vz = 4 cm and 6 cm in the z vertex distribution from the empty target (lower-left panel) are due to insulation around the target. The lower-right panel of Figure 1 shows the Vz spectrum for electrons scattered from the full target system. This spectrum shows that the insulation makes a very small contribution to the scattering from the full target system and can easily be eliminated with cuts on the Vz distribution.

2.24.3 Expected Results

The data from the E5 run will provide the magnetic form factor of the neutron over the Q^2 range from 0.2 to 4.8 $(GeV/c)^2$, with uncertainties of a few percent over most of the range, with many systematic cross-checks. These measurements should eclipse and extend the entire world's data for this fundamental quantity. In addition, there are a number of other interesting physics quantities which will be extracted from this data set.

References

[Ro50] M. N. Rosenbluth, Phys. Rev. **79**, 615 (1950).

[Bo95] P. E. Bosted, Phys. Rev. **C51**, 409 (1995); and references therein.

[Jo00] M. K. Jones *et al.*, Phys. Rev. Lett. **84**, 1398 (2000).

[Ma93] P. Markowitz *et al.*, Phys. Rev. **C48**, R5 (1993).

[Br95] E. E. W. Bruins *et al.*, Phys. Rev. Lett. **75**, 21 (1995).

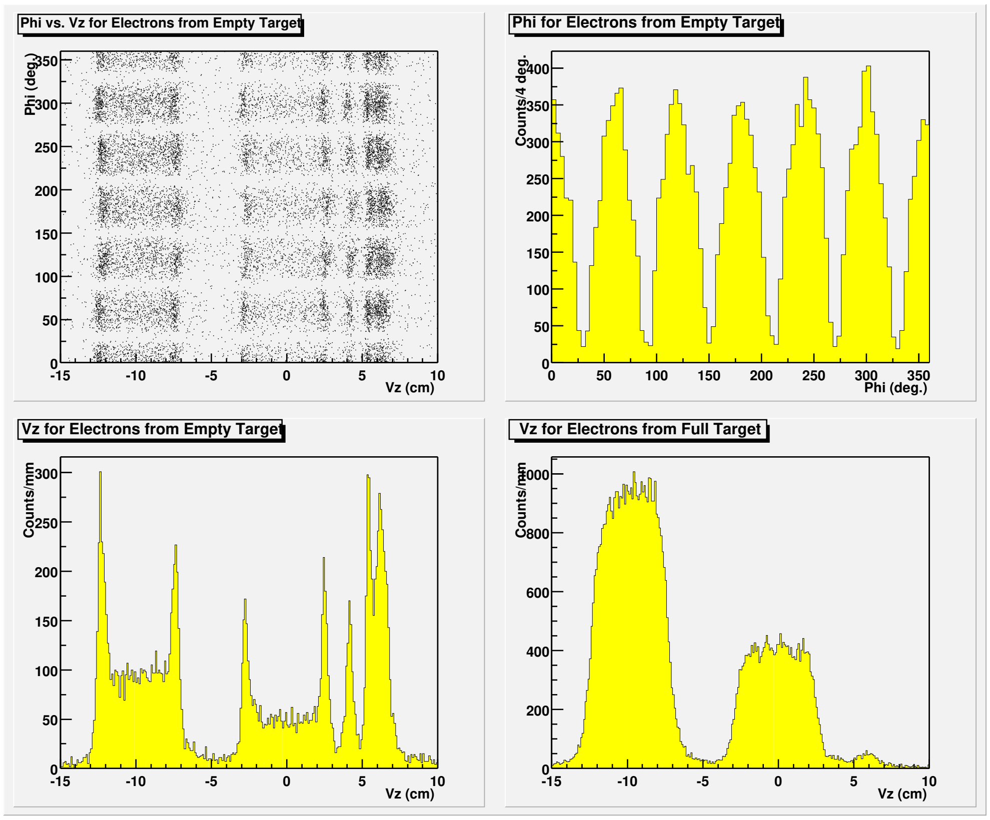

Figure 1: Spectra taken with a 4.2-GeV electron beam during the E5 run. The upper-left panel shows the azimuthal angle, ϕ, as a function of the z vertex, Vz, for electrons scattered from the empty dual target system. The upper-right panel is the ϕ distribution and the lower-left panel is the z vertex distribution for electrons scattered from the empty target. The lower-right panel shows the Vz spectrum for electrons scattered from the full target system.

[An94] H. Anklin *et al.*, Phys. Lett. **B336**, 313 (1994).

[An98] H. Anklin *et al.*, Phys. Lett. **B428**, 248 (1998).

[Ga95] H. Gao and O. Hansen, Jefferson Lab Experiment Proposal E- 95-001.

[Da93] D. Day (spokesperson), CEBAF Experiment Proposal E-93-026 (1993).

[Ma93] R. Madey (spokesperson), CEBAF Experiment Proposal E-93-038 (1993).

[An99] K. A. Aniol *et al.*, Phys. Rev. Lett. **82**, 1096 (1999).

[Ra99] A. V. Radyushkin, Few Body Syst. Suppl. **11**, 57 (1999).

2.25 eg1 Run Group Overview

Sebastian Kuhn for the CLAS Collaboration

2.25.1 Introduction

One of the most fundamental goals in Nuclear Physics is to understand the structure of nuclear building blocks, protons and neutrons, in terms of their elementary constituents, the quarks. We want to understand better how quarks are bound together inside protons, how this binding gives rise to the excited states of the proton (called resonances), and how the quarks become "asymptotically" free at high momenta. One of the outstanding puzzles in this quest is the origin of the intrinsic angular momentum, the spin, of the proton. Spin structure measurements at very high energy accelerators (SLAC, CERN, HERA) have revealed that the quark spins themselves contribute very little, at least in this region of "asymptotic freedom". However, many more data at lower momenta (where the quark binding becomes strong) are needed to get a consistent picture describing both the complicated structure of protons and their resonances at low energies and the deep inelastic regime of high energies and momenta.

The EG1 run group comprises a large program of spin structure measurements on the proton and the deuteron, using polarized electron scattering at low to moderate Q^2 and circularly polarized photon absorption in Hall B. The run group is composed of experiments 91-015 (Helicity Structure of Pion Photoproduction; D. Sober, spokesperson), 91-023 (Measurement of Polarized Structure Functions in Inelastic Electron Proton Scattering; V. Burkert, D. Crabb, R. Minehart, spokespersons), 93-009 (The Polarized Structure Function G_{1n} and the Q^2 Dependence of the Gerasimov-Drell-Hearn Sum Rule for the Neutron; S. Kuhn, M. Taiuti, G. Dodge; spokespersons) and 93-036 (Measurement of Single Pion Electroproduction from the Proton with Polarized Beam and Polarized Target; R. Minehart, M. Anghinolfi, H. Weller, spokespersons). The total allocated beam time for these experiments is 100 days. In addition, a conditionally approved experiment (94-003 - Study of the $\Delta(1232)$ Using Double Polarization Asymmetries; V. Burkert, R. Minehart, P. Stoler, spokespersons) will also receive data from EG1 running.

During the time span covered by this report, the EG1 run group took first data for the 3 electron beam experiments (91-023, 93-009 and 93-036), in Fall of 1998 (September through December). We scattered polarized electrons from longitudinally polarized NH_3 and ND_3 targets in the CEBAF Large Acceptance Spectrometer (CLAS) to study inclusive and exclusive polarization observables. These data will yield new information on transition amplitudes for the excitation of proton and neutron resonances, as well as on non-resonant contributions to the inclusive cross section. The large kinematic coverage of CLAS, from pion production threshold well into the deep inelastic regime, allows us to study resonance amplitudes close to the photon point ($Q^2 \approx 0.2$ GeV^2) as well as to improve dramatically on the existing data set [9] at higher W and moderate momentum transfer (Q^2 up to 2 GeV^2). Among the topics studied are the transition from the non-perturbative regime at low Q^2 to the deep inelastic limit, including the applicability of local duality. Studying spin asymmetries of the deuteron (93-009) in addition to those of the proton (91-023) allows us to disentangle isoscalar (p+n) and isovector (p-n) contributions. Of particular interest is the Q^2-dependence of the first moments of the structure functions $g_1^p(x,Q^2)$ and $g_1^d(x,Q^2)$, which are constrained by the Gerasimov-Drell-Hearn (GDH) sum rule [1] at the photon point $Q^2 = 0$ and by DIS data and the Bjorken sum rule [2] at high Q^2. In addition, the large acceptance of CLAS allows us to measure multi-particle final states. For example, we are measuring double polarization asymmetries for single pion production in the resonance region (93-026), which will greatly increase our understanding of the spin structure of nucleon resonances.

2.25.2 Experimental Details and Rungroup Status

The EG1 run group uses the standard detector configuration of CLAS. A dedicated polarized solid state cryogenic target was built and commissioned by a collaboration of Oxford Instruments, the University of Virginia, the University of Genova and the Jefferson Lab target group. The movable target stick contains samples of frozen ammonia beads immersed in a 1 K liquid helium bath and dynamically polarized through microwave irradiation. Polarization values as high as 90% for NH_3 and 35% for ND_3 were measured using NMR. In addition,

^{12}C and empty target cups were used for background studies. Installation of the polarized target, at a position roughly 55 cm upstream of the usual CLAS target location, required removal of the mini-torus and other substantial beam line modifications.

During the first run of EG1 in fall of 1998, about 3 billion triggers (2 billion electron events) were recorded, constituting about one third of the approved data set. Data were taken at beam energies of 2.5 GeV and 4.2 GeV, with the CLAS superconducting torus running at both inbending and outbending polarity. We finished calibrations and the first pass analysis of the data in 1999 and worked on radiative corrections, systematic studies and physics interpretation in 2000. More details on the analysis status and first results can be found in the following subsections on the individual experiments in EG1.

In September, 2000, we began the second EG1 run which will complete the electron data set on both targets with beam energies of 1.6, 2.5, 4.2 and 5.7 GeV. Due to the much larger data sample and improved target polarization expected from this run, we will reduce the statistical errors dramatically and cover a much larger kinematic region ($0.1 \leq Q^2 \leq 5.0$ and W up to 3.0 GeV).

References

[1] E143, K. Abe *et al.*, *Phys. Rev. D* **58**, 112003 (1998).

[2] S. Gerasimov, Sov. J. Nucl. Phys. **2**, 430 (1966); S.D. Drell and A.C. Hearn, *Phys. Rev. Lett.* **16**, 908 (1966).

[3] J.D. Bjorken, Phys. Rev. **148**, 1467 (1966).

2.26 E93-009

THE POLARIZED STRUCTURE FUNCTION G_1^n AND THE Q^2 DEPENDENCE OF THE GERASIMOV-DRELL-HEARN SUM RULE FOR THE NEUTRON

SEBASTIAN KUHN, GAIL DODGE AND MAURO TAIUTI
(SPOKESPERSONS) and THE CLAS COLLABORATION

2.26.1 Introduction

Experiment 93-009 is part of a large program of spin structure measurements at low to moderate Q^2 in Hall B (known as the "EG1" run group). We scatter polarized electrons from longitudinally polarized NH_3 and ND_3 targets in the CEBAF Large Acceptance Spectrometer (CLAS) to study inclusive and exclusive polarization observables. These data will yield new information on resonant and non-resonant transition amplitudes and on the transition from the non-perturbative regime at low Q^2 to the deep inelastic limit. Studying spin asymmetries of the deuteron (93-009) in addition to those of the proton (91-023) allows us to disentangle isoscalar (p+n) and isovector (p-n) contributions. Of particular interest is the Q^2-dependence of the first moments of the structure functions $g_1^p(x, Q^2)$ and $g_1^d(x, Q^2)$, which are constrained by the Gerasimov-Drell-Hearn (GDH) sum rule [1] at the photon point $Q^2 = 0$ and by DIS data and the Bjorken sum rule [2] at high Q^2. In addition, the large acceptance of CLAS allows us to measure multi-particle final states. For example, we are measuring double polarization asymmetries for single pion production in the resonance region, which will greatly increase our understanding of the spin structure of nucleon resonances.

2.26.2 Experiment Status

During the first run of EG1 in the fall of 1998, about 10% of the approved data set for 93-009 was taken with a beam energy of 2.5 GeV and a $\approx 20\%$ polarized $^{15}ND_3$ target (the polarization was limited by insufficient microwave power). The large acceptance of CLAS allowed us to take data simultaneously over a large range of Q^2 (from $Q^2 = 0.13$ to $Q^2 = 1.2$) and W (up to a maximum of $W \approx 2$). About 350 million electron events, were recorded on tape. We finished calibrations and the first pass analysis of the data in the winter of 1999 and worked on radiative corrections, systematic error analysis and physics interpretation in 2000. The analysis of the inclusive data set is the thesis of Junho Yun (ODU, expected completion February 2001). Mehmet Bektasoglu (ODU) is analyzing π^- production from the deuteron, which is primarily sensitive to the polarized neutrons in the target (Ph.D. thesis expected by the end of 2001). First results from these analyses have been presented in several invited and contributed talks (GDH2000, DNP2000). In September, 2000, we began the second EG1 run which will complete the data set on ND_3 with beam energies of 1.6, 2.5, 4.2 and 5.7 GeV.

2.26.3 Results

Figure 1 shows our preliminary results on the first moment of the structure function $g_1^d(x, Q^2)$, integrated over the resonance region $W \leq 2$. In spite of their statistical limitations, the new data improve our knowledge of spin structure functions for the deuteron considerably, indicating for the first time a transition from positive to negative values for the first moment, as required by the GDH sum rule. Due to the much larger data sample and improved target polarization expected from the second EG1 run now underway, we will reduce the statistical errors dramatically and cover a much larger kinematic region ($0.1 \leq Q^2 \leq 5.0$ and W up to 3.0 GeV) once the complete data set is in hand.

References

[1] S. Gerasimov, Sov. J. Nucl. Phys. **2**, 430 (1966); S.D. Drell and A.C. Hearn, *Phys. Rev. Lett.* **16**, 908 (1966).

[2] J.D. Bjorken, Phys. Rev. **148**, 1467 (1966).

[3] V.D. Burkert and B.L. Ioffe, *Phys. Lett. B* **296**, 223 (1992).

J. Soffer and O.V. Teryaev, *Phys. Rev. D* **51**, 25 (1995).

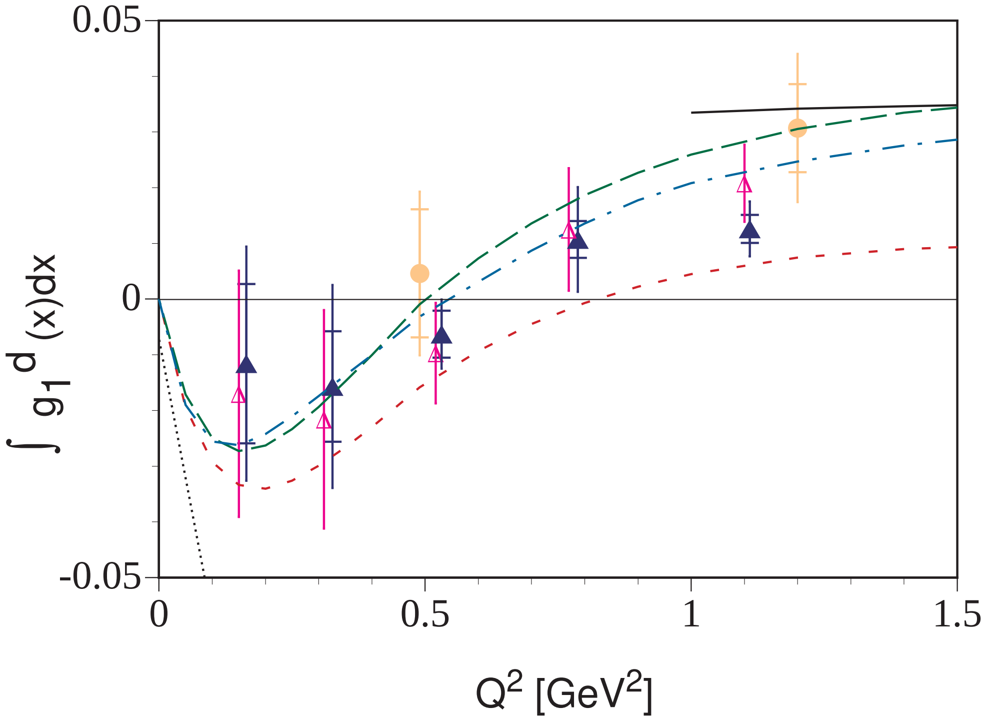

Figure 1: Preliminary data (solid triangles) from 93-009 on the integral $\int g_1^d(x, Q^2)dx$ for the deuteron as a function of Q^2. The inner error bars (caps) are statistical only, while the outer error bars include systematic errors (dominated by model uncertainties). The data are integrated over the resonance region $W \leq 2.0$ GeV. A fit to all existing DIS data was used to estimate the contribution to the integral above the measured region, which would move the data points as indicated by the open triangles. Previous data on the integral over the full x range from E143 [9] at SLAC are shown as circles, and a pQCD-fit to all existing DIS data is shown as the solid line. The expected contribution of resonances alone is indicated by the short-dashed line (based on the code AO). The two parametrizations [3] by Burkert and Ioffe (long-dashed line) and by Soffer and Teryaev (dash-dotted line) are adjusted to converge to the deep inelastic limit at high Q^2 and their slope at $Q^2 = 0$ is constrained by the GDH sum rule [1] (dotted line).

[4] E143, K. Abe *et al.*, *Phys. Rev. D* **58**, 112003 (1998).

2.27 E93-036

Spin Asymmetries in Pion Electro-production

Marco Anghinolfi, Ralph Minehart, and Henry Weller (Spokespersons)
and the CLAS Collaboration

2.27.1 Introduction

Experiment E93-036 was proposed to measure spin asymmetries in the nucleon resonance region for electro-production of single π^+ and π^0 using polarized electrons on polarized protons. Both single and double spin asymmetries in the electroproduction can be measured. These asymmetries, which result from interference terms, are sensitive to details of the hadronic structure not accessible in unpolarized electroproduction. Data for this experiment are collected as part of the "EG1" run group in Hall B.

2.27.2 Experiment Status

A first period of data taking was completed in the Fall of 1998, during which two beam energies, 2.5 and 4.2 GeV, and several magnetic field settings were used. The processing of the 1998 data was completed in 1999 and the analysis of the pion production channel has been focussed on data taken at the lower beam energy. The analysis of the π^+ channel formed the basis for the Ph.D. thesis of Raffaella DeVita (Genova), who passed her oral examination in December, 2000. First results from these analyses have been presented in several invited and contributed talks (NSTAR2000, GDH2000, DNP2000, DNP Town Meeting, CIPANP 2000).

The second EG1 run, which began in September, 2000, will complete the data set on NH_3, providing data at beam energies of 1.6, 2.5, 4.2 and 5.7 GeV.

2.27.3 Results

The double spin asymmetry extracted in the $ep \to e\pi^+n$ channel is the first measurement of this observable for an exclusive inelastic electroproduction. The electron was identified by a coincidence of the Cerenkov Counter and the Electromagnetic Calorimeter that also defines the hardware trigger used for data taking. The scattered pion was detected in coincidence using the combined information of drift chambers and time-of-flight scintillators, and a cut on the reconstructed missing mass of 0.85 GeV $< M_x <$ 1.05 GeV was used to select the exclusive π^+n final state. Geometrical cuts were used to select the events within the fiducial regions of the detector that exclude the low efficiency edges of the Cerenkov Counter, large multiple scattering from the magnet coils, dead wires and TOF scintillators. A correction for the acceptance of these fiducial regions was evaluated using an analytical approach and was applied on an event-by-event basis.

Data with different orientations of the electron and proton polarization were used to isolate the double spin term of the cross section,

$$\sigma = \sigma_0 + P_e\sigma_e + P_p\sigma_p + P_eP_p\sigma_{ep}, \tag{1}$$

The double spin asymmetry is defined as $A_{ep} = -\sigma_{ep}/\sigma_0$. The π^+n events were directly accumulated in bins of Q^2, W, and $\cos\theta^*$ while an integral over the azimuthal angle ϕ^* was performed because of the limited statistics. The double spin asymmetry was then obtained as

$$A_{ep} = \frac{1}{f}\frac{1}{P_eP_p}\frac{N(+-) + N(-+) - N(++) - N(--)}{N(+-) + N(-+) + N(++) + N(--)}, \tag{2}$$

where the signs in parenthesis refer to the electron and proton helicity and f denotes the dilution factor for the NH_3 target. This quantity represents the percentage of events from polarized nucleons and accounts for the contribution of the unpolarized nuclei that are part of the target assembly (liquid helium, ^{15}N, and vacuum windows). The contribution from the unpolarized nitrogen and He in the target was estimated from measurements using ^{12}C and liquid-helium targets.

The analysis is being extended to the 4.2 GeV data recorded in 1998. The analysis of the target asymmetry for the two beam energies is also in progress.

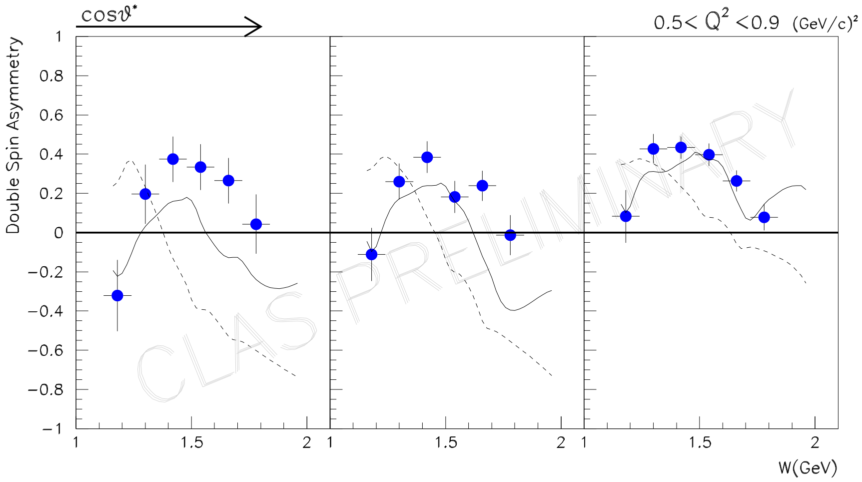

Figure 1: Angular dependence of the double spin asymmetry. The plots show the asymmetry as a function of W for different $\cos\theta^*$ intervals (0.25-0.5, 0.5-0.75, 0.75-1.0 from left to right) for Q^2 between 0.5 and 0.9 GeV^2/c^2. The solid line is the prediction of the MAID model for the double spin asymmetry including all dominant resonances and the background. The dashed line is the MAID prediction for the background only.

The product of beam and target polarization, routinely monitored during data taking with a Moller polarimeter and a NMR system respectively, was also extracted from elastic events that were measured simultaneously with the $\pi^+ n$ reaction thanks to the loose trigger condition of the experiment. The elastic asymmetry can be predicted from the known values of the proton form factors. Elastic events were selected both by detecting the final electron alone and using a W cut, and by detecting in coincidence the electron and the proton in the final state. The measured asymmetry, corrected for the corresponding dilution factor, was compared with the expected value and the polarization product was obtained as the ratio of the two quantities. The systematic error due to uncertainties in the elastic form factors was estimated to be of the order of 1%. When combined with the statistical error, the uncertainty in $P_e P_t$ is $2-3\%$.

Radiative corrections were calculated using a Monte Carlo integration of the Mo and Tsai formula. Two different models (AO and MAID) were used to generate the Born cross section and the discrepancy in the final results was used to estimate the model dependence of the correction. A detailed study of systematic errors was completed including the effect of the pion decay, the false asymmetry related to helicity dependent beam intensity, the particle detection and the acceptance correction, and finally the ^{15}N polarization.

The double spin asymmetry for three different cosθ^* bins for an interval of $0.5 < Q^2 < 0.9$ GeV^2 is plotted as a function of the invariant hadronic mass W in Figure 1 and compared with predictions of the isobar model, MAID 2000, developed by the Mainz group. The model is based on the fit of the world data of electro- and photo-production. The effect of the resonances is illustrated by the MAID calculation with only the background terms turned on.

2.28 g1 Run Group Overview

The CLAS g1 running period consists of several experiments that use a liquid hydrogen target and the Photon Tagging Facility. These experiments have similar running requirements which are outlined below.

E89-004, *Electromagnetic Production of Hyperons*, is exploring the photoproduction of the ground state hyperons Λ, Σ^o and Σ^+, and is well on the road to provide polarization data for the first time. This makes it possible to extract several hadronic couplings and definitively describe the resonance structure of these reactions.

E89-024, *Radiative Decays of the Low-Lying Hyperons*, uses CLAS as a source of excited hyperons, such as the $\Lambda(1405)$, and is attempting to extract the small radiative decay branching ratios by reconstruction of the hadronic decay products. These provide particularly sensitive tests of quark model structure of the hyperons.

91-008, *Photoproduction of η and η' Mesons*, is measuring the differential cross sections for η and η' photoproduction using detection of the recoil protons in CLAS. These measurements are viewed as providing a foundation for related eta production measurements on nuclei being done in the g2 and g3 running periods, and provide the first data above threshold for studying baryon resonances that couple to etas.

93-033, *Search for Missing Baryons Formed in $\gamma p \rightarrow p\pi^+\pi^-$*, is searching for firmly predicted, yet undiscovered baryon states that decay to $\Delta\pi$ instead of the better-studied Nπ. This experiment undertakes the analysis of $p\pi^+\pi^-$ final states and is currently studying and evaluating various partial wave analysis solutions.

94-015, *Study of the Axial Anomaly Using the $\gamma\pi^+ \rightarrow \pi^+\pi^o$ Reaction Near Threshold*, seeks to measure the anomalous amplitude $\gamma \rightarrow 3\pi$ which arises through the QCD axial anomaly. This experiment plans to use the $\gamma p \rightarrow \pi^+\pi^o n$ reaction to extract the t-channel pole term that corresponds to the anomalous reaction.

94-103, *The Photoproduction of Pions*, is a survey of the single pion photoproduction reaction on hydrogen and deuterium, and seeks to minimize systematic errors and to provide highly accurate data for a full amplitude analysis of the nucleon resonance region.

The running conditions for the first three allocations of beam time (g1a, g1b, and g1c) were determined by a consensus of the spokespersons and pre-supposed that the trigger for the CLAS of up to a 1,500/sec single-particle recorded event rate with acceptably small deadtime. The trigger provided a "minimum bias," with no on-line selection of rare types of events necessary. The early runs had a lower than expected event rate of about 400 events/sec in g1a (375 million events total) to from 450 to 800 events/sec in g1b (420 million events). The latest run, g1c, obtained an event rate of almost twice our original expectation. Because the tagged photon spectrum goes as 1/E, data taking was prescaled at the trigger level to roughly equalize the recorded rate as a function of energy. The break points for pre-scaling are set first below the eta threshold, and also at a higher energy away from known thresholds. This prescaling scenario caused major normalization difficulties and was modified in g1b and dropped altogether in g1c. The magnetic field in CLAS was mostly run at 3/4 of the full field. This represented a compromise between resolution and acceptance. Some lower field setting runs were taken to increase acceptance and test systematics.

The beam time allocated to these experiments has been approximately half used and has acquired data with electron energies, E_0, of about 1.8, 2.4 and 3.2 GeV and tagged photon energies ranging from 20% to 95% of E_0. A good estimate of how the remaining time (about 60 days) will best be used can only be made after the data (4,550 million events) for g1c is cooked and evaluated. We expect this will be accomplished soon.

2.29 E89-004

ELECTROMAGNETIC PRODUCTION OF HYPERONS

Reinhard Schumacher, *Carnegie Mellon University*
for the CLAS Collaboration

2.29.1 Introduction

The CEBAF Large Acceptance Spectrometer (CLAS) [Br99] at Jefferson Lab has been used to measure the elementary photoproduction of kaons and hyperons at center-of-mass energies from threshold up through the the nucleon resonances. Data have been obtained for the charged kaon reactions

$$\gamma + p \to K^+ + \{\Lambda,\ \Sigma^\circ, \Lambda(1405)/\Sigma(1385),\ \Lambda(1520)\}\,. \tag{1}$$

These reactions can be analyzed in terms of chiral-perturbation theory near threshold, in terms of hadrodynamic models in the nucleon resonance region, and with Regge models at higher energies. Since the reactions are related by SU(6), they are complimentary to each other in theory, while experimentally it is good to measure them all simultaneously, as we have done at CLAS. The results of these measurements should be: (1) improved understanding of the electromagnetic associated-strangeness production mechanism, and (2) an investigation of the higher-mass region of the nucleon resonance spectrum using these reaction channels.

As an example of the recent interest in this area, recently-published data from the SAPHIR experiment at Bonn [Tr98] has provided some evidence [17] for a resonance structure at a total c.m. energy of $W = 1900$ MeV. If confirmed by our data from CLAS, it would be very interesting, since there are few well-established nucleon resonances in that mass range, and none that are known to couple strongly to strange particle final states. It would be an example of the kind of "missing resonance" discussed in quark models [Ca98]. The interpretation of those data are, however, controversial [Sa99], and await new and better data from CLAS.

Our goal is to produce differential cross sections for the ground-state hyperons suitable for partial wave analysis, as well as several polarization observables: the hyperon recoil polarizations P_Λ and P_{Σ°, and the beam-recoil double-polarization observables $C_{x'}$ and $C_{z'}$. For the excited hyperons we aim to measure the differential cross sections.

2.29.2 Experiment Status

In this report we concentrate on the data for Λ and Σ° production. Data under analysis now come from the *g1a* run in mid-1998, discussed in a previous contribution. Kaon skim files were created during the cooking process which resulted in 210,000 strangeness-containing reconstructed events out of 100M "good" single-hadron CLAS triggers. Analysis of these data form the thesis work of CMU graduate student John McNabb. In November 1999 we obtained another data set in the *g1c* run which is about 50 times more voluminous than what we have analyzed so far. Analysis of that data set awaits completion of the first-pass cooking. The excited state cross-sections are being extracted by Henry Juengst (U. Minnesota), while the complimentary K° channel analysis is underway at Catholic University by Brian Carnahan.

2.29.3 Results

Kaons with momenta up to 2 GeV/c were identified using momentum and time-of-flight measurements, with an average signal-to-noise ratio with respect to pions of about 4:1. Sideband subtraction of the pion background resulted in a hyperon missing mass spectrum shown in Figure 1, which shows cleanly separated Λ and Σ° samples, as well is several well-known excited hyperons.

Kaon events were normalized using the integrated photon flux, and corrected using Monte Carlo techniques for acceptance and in-flight kaon decay. The systematic uncertainties associated with both the normalization and the acceptance are under study. At the present time we believe that both the point-to-point and the overall normalization uncertainty is $\pm 20\%$. Final uncertainties will be under $\pm 10\%$. Sample differential cross sections are shown in Figure 2 for both Λ and Σ° photoproduction. The forward peaking of the Λ cross section

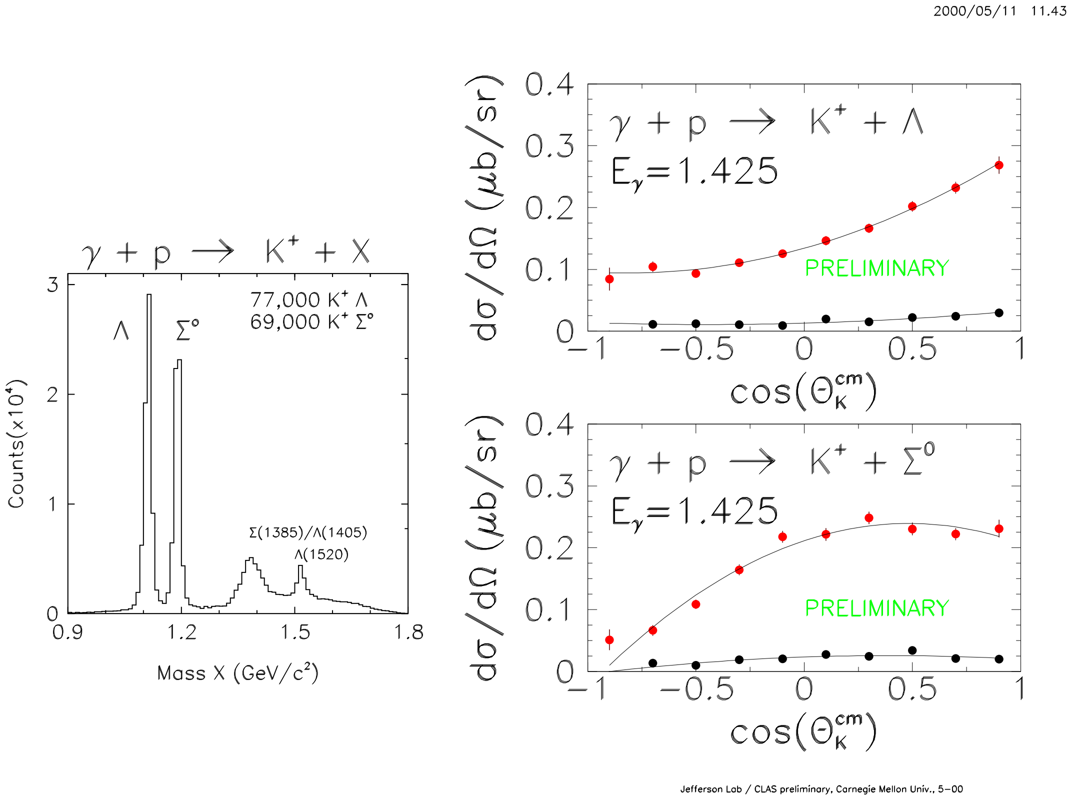

Figure 1: (left) Missing mass spectrum for $\gamma + p \to K^+ + X$ for $W > 1.6$ GeV. The events span all of CLAS in angle and momentum. Background pions misidentified as kaons were subtracted using a sideband technique.

Figure 2: (right) Preliminary differential cross sections for photoproduction of the ground state hyperons at one photon energy (50 MeV bin width). In each case, the upper (red) data points are the cross sections, the lower (black) data points are the subtracted background, showing the signal-to-noise ratio. The curves are second-order Legendre fits.

is due, in a current hadrodynamic model [17], to both the interference of S and P wave isobar resonances, and the strong contribution of t-channel processes. The Σ° cross section is of comparable size at $Q^2 = 0$, in contrast to our results for electroproduction, but it is not forward peaked, which may be explained by a much less dominant role of the t-channel relative to resonance excitation.

Total cross sections were obtained from Legendre polynomial fits to the angular distributions at each photon energy. Figure 3 shows σ_{tot} compared to several previous calculations [Ma99]. There is considerable disagreement among the calculations and the data; some calculations [Wi92, Ad89] were primarily designed to fit the near-threshold energies below 1.5 GeV, not the higher energy region, and do not preserve unitarity. The calculations of Ref [Ma99] were fitted to the data of Ref [Tr98] by the inclusion of hadronic form factors [Ha98]. The calculations of Ref [Sa99] invoke only "known" resonances and provide the most satisfactory fit. The calculation in Ref [La99] is a Regge model applied outside its range of (higher energy) applicability, for qualitative comparison.

More detailed comparison of these reaction models with our results is in progress, and we will soon show preliminary hyperon polarization data as well.

References

[Ad89] 6. R. A. Adelseck and L. E. Wright, Phys. Rev. **C38**, 1965 (1988); C. Bennhold, Phys. Rev. **C39**, 1944 (1989).

[Br99] W. Brooks, Nucl, Phys. **A663**, 1077c (2000).

[Be99] C. Bennhold, H. Haberzettl, and T. Mart, nucl-th/9909022, Proceedings of "Trieste 99" World Scientific; T. Mart and C. Bennhold, $nucl - th/9906096, 30Jun1999$

[Ca98] S. Capstick and W. Roberts, Phys. Rev. **D58**, 1 (1998).

[Ha98] H. Haberzettl, C. Bennhold, T. Mart, and T. Feuster,Phys. Rev. **C58**, R40 (1998).

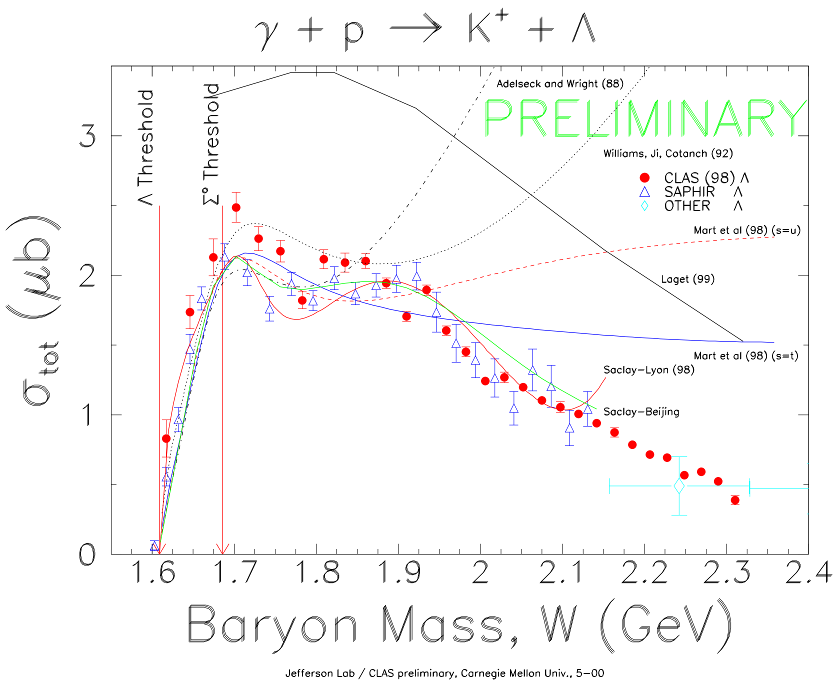

Figure 3: Preliminary total cross sections for $\gamma + p \to K^+ + \Lambda$. The data were acceptance corrected; uncertainties are statistical only, and do not reflect a $\pm 20\%$ systematic uncertainty. CLAS data are the solid (red) points. The curves are cited in the text.

[La99] J.-M. Laget, private communication, based on M. Guidal, J.-M. Laget, and M. Vanderhaegen, Nucl. Phys. **A627**,645 (1997); M. Vanderhaegen, M. Guidal, and J.-M. Laget, Phys. Rev. **C57**,1454 (1998).

[Ma99] T. Mart provided code for several published models, private communication.

[Sa99] Bijan Saghai, Hampton Workshop, 12/99, and private communication.

[Tr98] M. Q. Tran *et al*, Phys. Lett. **B445**,20 (1998).

[Wi92] R. Williams, C. R. Ji, and S. R. Cotanch Phys. Rev. **C46**, 1617 (1992).

2.30 E-89-024

Radiative Decays of the Low-lying Hyperons
G. S. Mutchler for the CLAS Collaboration
Rice University

2.30.1 Introduction

This experiment probes the quark wavefunctions of the *uds* baryons by measuring the branching ratios of the electromagnetic decays of the lower-lying excited state hyperons $\Sigma(1385)$, $\Lambda(1405)$, and $\Lambda(1520)$. The excited hyperons, Y^*, are produced via the reaction:

$$\gamma p \longrightarrow K^+ Y^* \longrightarrow K^+ \gamma \Lambda \longrightarrow K^+ \gamma p \pi^-. \tag{1}$$

As shown in Figure 1, the decay structure for excited states is quite complicated; moreover, the radiative widths for transitions between excited states are predicted to be small. The dominant decay modes $Y^* \to \Sigma\pi, \Lambda\pi$ are not shown. Unfortunately, photo-production experiments do not distinguish between the I=0 $\Lambda(1405)$ state and the I=1 $\Sigma(1385)$ state in the production channel because the electromagnetic interaction does not conserve isospin.

The K, p and π^- are detected in the CLAS with large solid angle and good momentum resolution. The 4-momentum of the Y^* can be reconstructed from the beam E_γ and P_K. That of the Λ can be reconstructed from the measured P_p and P_π^-. The hyperon mass is reconstructed to better than 5 MeV and the Λ mass to better than 1.5 MeV. The data have a momentum dependent cut on the K^+ mass and a tight cut on the Λ mass. See ref[Ta00] for further details.

The available calculations and measurements of the radiative widths are tabulated in Table 1. Darewych, Horbatsch, and Koniuk [Da83] and Kaxiras *et al.*[Ka85] used the Isgur-Karl non-relativistic quark model (NRQM) [Is78]. Warns, Pfeil, and Rollnik [Wa91] used a relativized constituent quark model (CQM), with the Isgur-Karl wave-functions. They obtained a smaller $\Lambda(1405) \to \Sigma^0\gamma/\Lambda(1405) \to \Lambda\gamma$ ratio than seen in the data [Bu91, Wh89]. These observations lead them to conclude that a non-three quark model for the $\Lambda(1405)$ may be more appropriate. Kaxiras*et al.*[Ka85] used the MIT bag model [De75]. In the

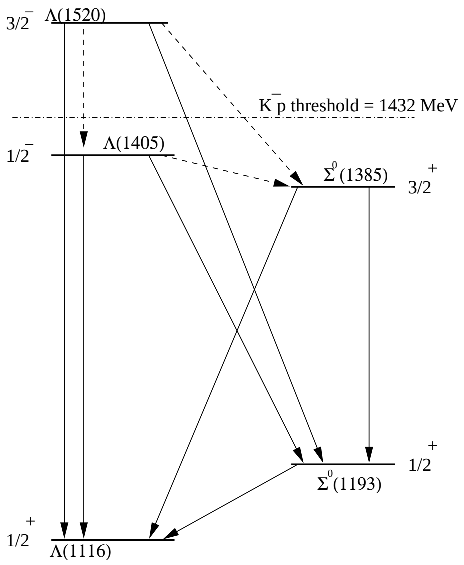

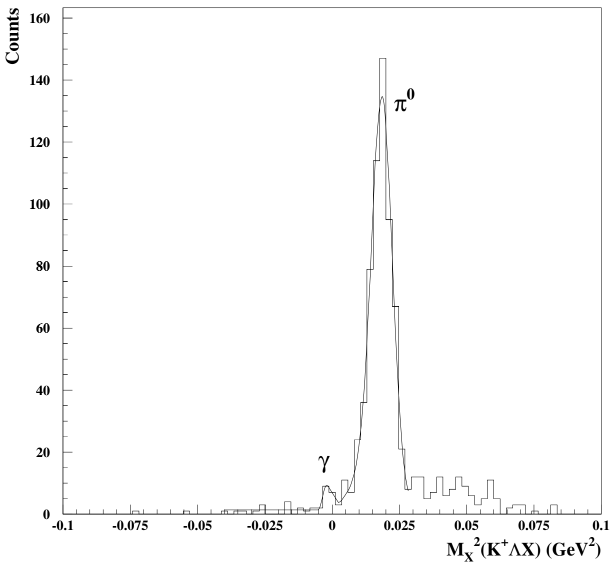

Figure 1: (left) Radiative decays of the lower-lying excited state hyperons. The dashed lines indicate transitions that are forbidden or very small in most models. The J^P assignments are on the outer boundaries of the diagram.

Figure 2: (right) Missing mass squared from $Y^* \to \Lambda X$ for hyperon masses in the range 1.34< M_X <1.43 GeV.

chiral bag model of Umino and Myhrer[Um93], the bag is dressed by a mesonic cloud. The widths predicted by bag models are generally lower than those predicted by constituent quark models. The predictions of the models vary from a factor of two up to an order of magnitude. Hence, measuring the radiative decays of these hyperons provides a means of discriminating between the various models.

Transition	NRQM	MIT Bag	Chiral Bag	RELQM	Experiment
$Y^* \to \Lambda\gamma$	[Ka85, Da83]	[Ka85]	[Um93]	[Wa91]	K^-p
$\Lambda(1520)$	156	46	32	215	134±23 [Ma68]
					30±11 [Be87]
$\Lambda(1405)$	200	60†, 17‡	75	118	27±8 [Wh89, Bu91]
$\Sigma(1385)$	273	152		267	
$\Sigma(1193)$	8.5	4.6		4.1	8.6±1.4 [Pe86]
$Y^* \to \Sigma\gamma$					
$\Lambda(1520)$	55	17	51	293	47±17 [Be87]
$\Lambda(1405)$	72	18†, 2.7‡	1.9	46	10±4 [Wh89, Bu91]
					23±7 [Wh89, Bu91]
$\Sigma(1385)$	22	15		23	

Table 1: Comparison of theoretical predictions for the radiative widths (in keV) for the transitions $Y^* \to \Lambda\gamma$ and $Y^* \to \Sigma\gamma$ to experimental results. In the case of the predictions of the MIT bag model for the $\Lambda(1405)$, † marks the value corresponding to the $\left|\Lambda\left(\frac{1}{2}^-\right)\right\rangle_1$ state and ‡ marks the value corresponding to the $\left|\Lambda\left(\frac{1}{2}^-\right)\right\rangle_2$ state ([Ka85]). The result of Mast*et al.*[Ma68] has been recomputed using a full width of 15.6 ± 1.0 MeV[Ca98].

Despite this sensitivity, few measurements of neutral hyperon radiative decays are available. All have been measurements of the $K^-p \to Y^*$ system, which can only access the high mass tails of the $\Lambda(1405)$ and the $\Sigma(1385)$ since these states are below the $\overline{K}N$ threshold. Whitehouse *et al.*[Wh89] studied the $\Lambda(1405)$ system obtaining a branching ratio of $(0.86 \pm 0.12) \times 10^{-3}$ for the $\Lambda\gamma$ channel, (499 events), and $(1.44 \pm 0.23) \times 10^{-3}$ for the $\Sigma^0\gamma$

channel, (850 events). They measured the photon spectrum, using a NaI(Tl) detector, from a K^- beam stopping in a liquid hydrogen target. Burkhardt and Lowe [Bu91] extracted the widths using an isobar-model calculation. Mast *et al.*[Ma68] measured the $\Lambda(1520) \rightarrow \Lambda\gamma$ decay. They observed 258 $K^- p \rightarrow \Lambda\gamma$ events in a hydrogen bubble chamber and obtained a branching ratio of 0.0086 ± 0.0014. A later unpublished CERN experiment reported a width of 33 ± 11 keV for the $\gamma\Lambda$ channel and 47 ± 17 keV for the $\gamma\Sigma^0$ channel [Be87]. The decay $\Sigma^0(1385) \rightarrow \gamma\Lambda(1116)$ has never been observed even though its radiative branching ratio is expected to be $\sim$1%.

2.30.2 Experiment Status

The data were taken during the g1a run in mid-1998 with an electron beam energy of 2.487 MeV. The preliminary results presented below are from the Ph.D. thesis of Rice student Simon Taylor [Ta00]. He analyzed Kaon skimmed files with a total of about 125 million triggers. A 50 times larger data set was taken during the November 1999 g1c run. The analysis of this data set should complete 89-024 and will begin once the first pass cooking is completed.

2.30.3 Results

Figure 2 shows the $M_X^2(K^+\Lambda X)$ distribution for hyperon masses in the range $1.34 < M_X < 1.43$ GeV. There is a small excess of counts at zero missing mass squared sitting on top of the tail of the π^0 peak from the decay $\Sigma^0(1385) \rightarrow \Lambda\pi^0$ and a roughly flat background. The counts above the π^0 peak come from the decay $\Lambda(1405) \rightarrow \Sigma^0\pi^0$. Based on the experimental result for the decay $\Lambda(1405) \rightarrow \gamma\Lambda$ we estimate the $\Lambda(1405)$'s contribution to the gamma peak is negligible. The number of π^0 and γ counts are $N_\pi^0 = 538.2 \pm 36.8^{+22.1}_{-13.1}$, and $N_\gamma = 11.87 \pm 4.7^{+2.2}_{-3.9}$. Further details are given in Ref [Ta00] . The preliminary result for the branching ratio is

$$R_{\Lambda\pi}^{\Lambda\gamma} \equiv \frac{\Gamma(\Sigma^0(1385) \rightarrow \gamma\Lambda)}{\Gamma(\Sigma^0(1385) \rightarrow \pi^0\Lambda)} = 0.0206 \pm 0.0084^{+0.0043}_{-0.0073}. \qquad (2)$$

corresponding to a partial width:

$$\Gamma(\Lambda\gamma) = 640 \pm 270^{+130}_{-220} \text{ keV}. \tag{3}$$

This radiative width is roughly twice as large as the largest theoretical prediction. The MIT bag model calculation[Ha78] and the NRQM calculation[Ko80] for the partial width for the process $\Delta^+(\frac{3}{2}^+) \to p\gamma$ are 338 keV and 361 keV, respectively – both $\approx$ 50% of the experimental result of 686 ± 37 keV[Ca98]. The MIT bag model also under-predicts the Σ^0 width by ≈50% [Ka85]. Clearly, there is an indication of something wrong or missing in the models.

When the g1c data has been analyzed we should have a statistically significant measurement of the $\Sigma^0(1385) \to \gamma\Lambda$ branching ratio. In addition the 2.9 and 3.2 GeV beam energy data should allow a measurement of the $\Lambda(1520) \to \gamma\Lambda$ branching ratio.

References

[Be87] R. Bertini, *Nuclear Physics* **B279** 49 (1987).

[Bu91] H. Burkhardt and J. Lowe, *Physical Review* **C44.2** 607 (1991).

[Ca98] C. Caso *et al.*,(Particle Data Group), *European Physical Journal* **C3** 1 (1998).

[Da83] J. W. Darewych *et al.*, *Physical Review* **D28.5** 1125 (1983).

[De75] T. DeGrand *et al.*, *Physical Review* **D12.7** 2060 (1975).

[Ha78] R. H. Hackman *et al.*, *Physical Reviews* **D18** 2537 (1978).

[Is78] N. Isgur and G. Karl, *Physical Review* **D18.11** 4187 (1978).

[Ka85] E. Kaxiras *et al.*, *Physical Review* **D32.3** 695 (1985).

[Ko80] R. Koniuk and N. Isgur, *Physical Review* **D21** 1868 (1980).

[Ma68] T. S. Mast *et al.*, *Physical Review Letters* **21.25** 1715 (1968).

[Pe86] P. C. Petersen *et al.*, *Physical Review Letters* **57** 949 (1986).

[Ta00] S. Taylor, "Radiative Decays of Low-Lying Excited-State Hyperons," Ph. D. thesis Rice University, May 2000.

[Um93] Y. Umino and F. Myhrer, *Nuclear Physics* **A529** 713 (1991); *Nuclear Physics* **A554** 593 (1993).

[Wa91] M. Warns *et al.*, *Physics Letters* **B258.3,4** 431 (1991).

[Wh89] D. A. Whitehouse *et al.*, *Physical Review Letters* **63.13** 1352 (1989).

2.31 E91-008

PHOTOPRODUCTION OF η AND η' MESONS FROM THE PROTON

M. Dugger, J. Ball, E. Pasyuk, and B. Ritchie (spokesman)
Arizona State University
for the CLAS Collaboration

2.31.1 Introduction

We have used the CEBAF Large Acceptance Spectrometer (CLAS) [Br99] to measure the photoproduction of η and η' mesons on the proton at center-of-mass energies from threshold up to 2.4 GeV. Data have been obtained for the reactions

$$\gamma + p \to p + \{\eta, \eta'\}. \tag{1}$$

These measurements are targeted at supplying an 'isospin filter' to the nucleon resonance spectrum, due to the isoscalar nature of the eta mesons. The $S_{11}(1535)$ resonance lying at the η production threshold has a large coupling to the ηN channel ($\sim$50%), and that resonance has continued to be a natural focus of both experimental and theoretical investigations of nucleon resonances. Many new experiments are deepening the knowledge (and mysteries) associated with the $S_{11}(1535)$ resonance. But other isospin $\frac{1}{2}$ resonances may also be selectively studied with these probes. For instance, while angular momentum arguments can explain part of the reason for the smaller coupling of the $P_{11}(1710)$ and $D_{13}(1655)$ resonances to the ηN channel, a deeper understanding of these states will require much more extensive information than we have available. The small ηN coupling of the $S_{11}(1650)$ is problematic in many quark models, and the data available are simply not sufficient to be overly helpful. Indeed, above $W = 1.6$ GeV or so, the cross section database for electromagnetic production of η mesons from the nucleon is starkly limited.

In addition to these questions, another frontier being opened for deeper exploration involves electromagnetic production of η' mesons. Here the existing experimental situation is even more rarefied. With so little information available, even formulating questions is hard. Which resonances couple to this meson? Do any couple to a great extent?

Our goal, then, is to produce differential cross sections for the photoproduction of η and η' mesons suitable for partial wave analysis to further clarify the nucleon resonance spectrum. Additional studies of the data set may also better determine several of the branching ratios for decays of η' mesons.

2.31.2 Experiment Status

Data under analysis now come from the $g1a$ run in mid-1998 and the $g1c$ run period in November 1999. A subset of runs from the $g1a$ period with exceptionally stable operation was selected for detailed analyses. From this subset, 9.6 M proton reconstructed events were found out of 44 M "good" single-hadron CLAS triggers. Analysis of these data form the thesis work of ASU graduate student Michael Dugger. Additional data obtained in the $g1c$ running period possess about 50 times more voluminous data than what we have analyzed so far from $g1a$. Analysis of the $g1c$ data set awaits completion of the first-pass cooking. The $g1c$ analysis forms the thesis work of ASU graduate student James Ball.

2.31.3 Results

The data collected in the $g1a$ data set will yield cross sections for η and η' photoproduction from threshold to 2.4 GeV incident photon energy, with total cross sections and angular distributions throughout that range.

The cross sections are being obtained by detecting the recoil proton in the CLAS and using the recoil proton information along with the tagged photon energy to generate a missing mass. Particle identification for CLAS in this running environment is quite good. As illustrated in Figure 1, using this particle identification information, the missing mass resolution was far more than adequate to see the η and η' peaks above the multi-pion background.

The ability to use the recoil proton missing mass reconstruction means that finding the yield in the analysis for the experiment essentially requires only knowledge of the acceptance

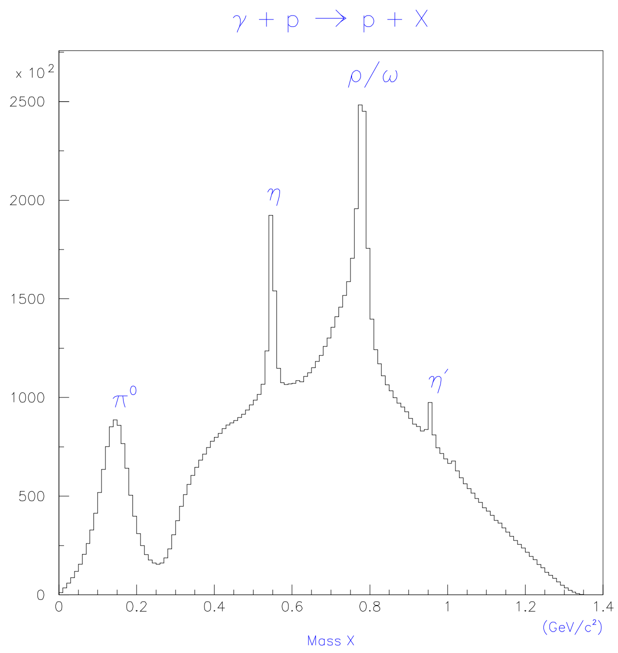

Figure 1: Missing mass spectrum for $\gamma + p \rightarrow p + X$ using the subset of $g1a$ data described in the text. The events shown span all photon energies used in $g1a$.

for a single, heavy, stable, positively-charged particle, the proton. This acceptance has been simulated using the standard CLAS software. As a check of the simulated acceptance, an empirical acceptence measurement also was determined from the $g1a$ dataset. This measured detection efficiency was realized by requiring a π^+ and a π^- to be detected by the CLAS in the final state, with the additional requirement that the missing mass X in the reaction $\gamma+p \to p+X$ be consistent with that of the proton. The measured detection efficiency is then the number of times the proton was detected divided by the number of times the proton was expected within the bin of interest. Systematic errors associated with the simulated efficiency calculation are then estimated by comparing the measured proton acceptence to the simulated proton acceptence for the reaction $\gamma + p \to p + \pi^+ + \pi^-$.

Obtaining angular distributions from the $g1a$ data set involved subtracting the multi-pion background from beneath the η yield peak for each particular angle bin. This subtraction was nearly always unambiguous. Samples of the resulting angular distributions are shown in Figure 2.

Current work on the $g1a$ data set is directed at the incident photon flux measurement. With this obtained, the η and η' differential and total cross sections will be published. The $g1c$ analysis is in the midst of the first 'cooking' pass of the entire data set. Subsequent analyses of both data sets to look at branching ratios awaits publication of the differential cross sections.

The work of the Arizona State University group is supported by the U. S. National Science Foundation.

References

[Br99] W. Brooks, Nucl, Phys. **A663**, 1077c (2000).

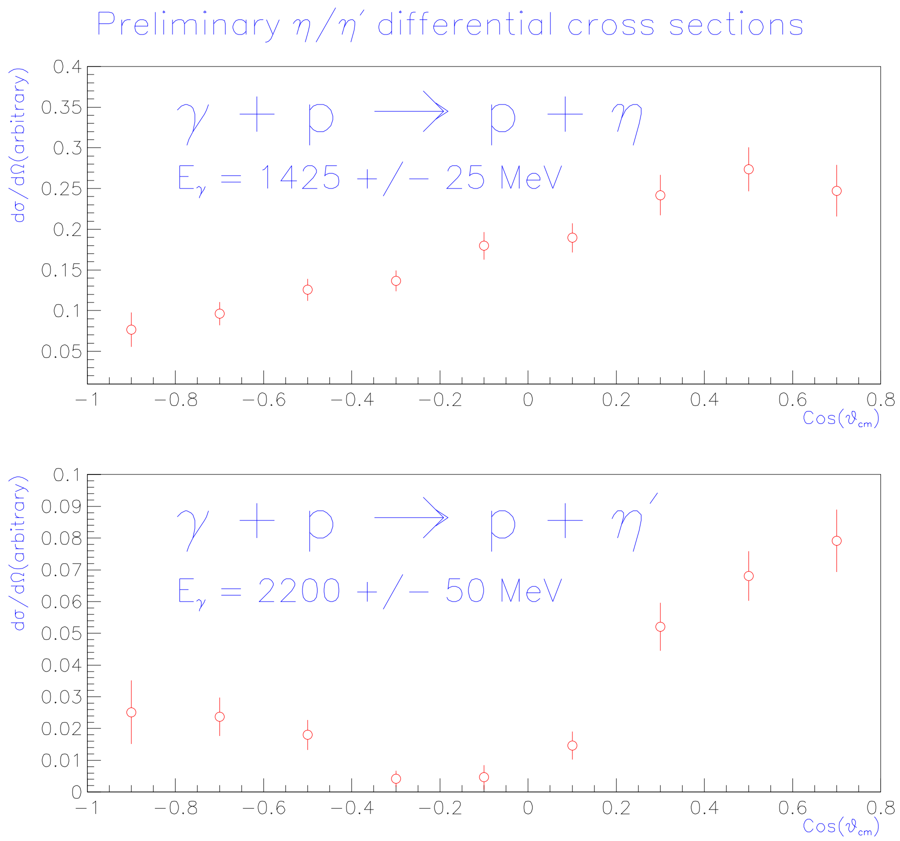

Figure 2: Preliminary differential cross sections for photoproduction of η and η' mesons at 1400 and 2200 MeV.

2.32 E93-033

A SEARCH FOR MISSING BARYONS
FORMED IN $\gamma p \to p\pi^+\pi^-$
USING THE CLAS AT JEFFERSON LABORATORY

M. Bellis, J. Cummings, M. Klusman,
J. Napolitano (Spokesperson) and D. Weygand (Spokesperson)
Rensselaer Polytechnic Institute
THE CLAS COLLABORATION

Introduction

The spectrum of observed baryons is incomplete. Although predicted by the quark model, a large number of non-strange positive parity states with masses near 2 GeV/c^2 are "missing". This has been known since the early days of baryon spectroscopy [Cl79].

The quark model firmly predicts these states exist [Ca86]. It also provides a possible explanation for why these states are missing; the decay widths to $N\pi$ are smaller for the missing states [Ca93]. Experiments, however, have concentrated on measurements with $N\pi$ in the incident or exit channel, or both. Thus, one would expect weak evidence at best for the "missing" states.

This problem is of more than academic interest. The pattern of missing states is not entirely random and may suggest an unexpected underlying symmetry. In the "diquark" model [Li69, Cu77], qq pairs cluster strongly, reducing the number of available degrees of freedom in such a way that the observed baryon spectrum is predicted. Dynamical evidence for diquarks has been further suggested [An93].

This experiment aims to identify new baryon states, with quantum numbers of at least some of the "missing" states, using reactions that *do not* rely on $N\pi$ couplings. In particular, we are searching for baryon excitations $B \equiv \{N^\star, \Delta^\star\}$ in the reactions

$$\gamma p \rightarrow B \rightarrow \left\{ \begin{array}{c} \Delta^{++}\pi^- \\ \Delta^0\pi^+ \\ p\sigma \\ p\rho^0 \\ N^{\star 0}\pi^+ \end{array} \right\} \rightarrow p\pi^+\pi^- \tag{1}$$

Data is acquired with real photons in the CLAS. We are developing a model- and mass-independent partial wave analysis (PWA) to extract baryon resonance parameters in as unambiguous a manner as possible.

Experiment Status

Our data is in hand. Low energy ($E_\gamma \leq 1$ GeV) events from the $g1a$ run are being used to prove the PWA technique and to extract new information about the $P11(1440)$ "Roper" resonance. Data from the $g1c$ run will be used to search for new states at higher energies, with $M_B \approx 2$ GeV$/c^2$. We select events with two positively charged particles and identify the π^- by missing mass. A large body of data results, and no severe acceptance corrections need to be applied.

Progress, Results, and Plans

Our effort concentrates on the PWA technique. Baryon states are broad and numerous, leading to many overlapping partial waves. This is compounded by the many quasi-twobody decays represented in Reaction 1. Furthermore, for known states, existing information on photoproduction and multipion decay amplitudes from experiment [6, Ma92] and from theory [Ca92, Ca94] leads to large uncertainties in the predicted cross sections. This all implies to us that a model independent analysis is necessary to unambiguously identify new states.

Our approach is based on the "isobar model" [He75, Ma84] with an expanded density matrix to account for the spin-1 photon. We form decay amplitudes for an assumed set of intermediate states B and decay isobars from Reaction 1. We then build the density matrix

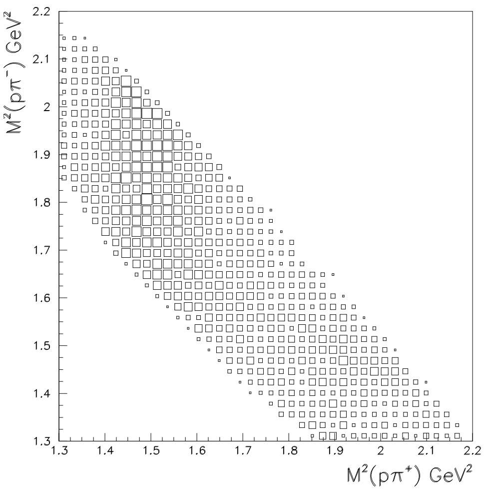

Figure 1: Dalitz plot of the $p\pi^+\pi^-$ system produced in the reaction $\gamma p \to p\pi^+\pi^-$ for $E_\gamma \approx 964$ MeV ($1635 \le M_{p\pi^+\pi^-} \le 1640$ MeV/c^2). The projection on the $M^2(p\pi^+)$ axis shows clear evidence for Δ^{++}, i.e. the reaction $\gamma p \to \Delta^{++}\pi^-$. There is also evidence for Δ^0 production. These and other contributions need to be unraveled in the Partial Wave Analysis.

from complex "production amplitudes" which are fit to the data, independently for each photon energy bin, or $\sqrt{s} = M_{p\pi^+\pi^-}$. We fit using an extended maximum likelihood technique to incorporate detector acceptance on a wave-by-wave basis. This technique has been used by members of this collaboration for meson spectroscopy in the $\pi^-\pi^+\pi^-$ system [Ad98].

Figure 1 shows Dalitz plots for the $p\pi^+\pi^-$ system for photon energies near 1 GeV. There is clear Δ^{++} isobar production, and other structure as well. The PWA is to find the set of partial waves which best describes this Dalitz plot, independently at each energy, and then to examine these partial waves to see if they resonate[1] as a function of mass.

We are testing the procedure now by including $\Delta\pi$ decay amplitudes. Figure 2 shows angular distributions for events with $E_\gamma \approx 635$ MeV ($1440 \le M_{p\pi^+\pi^-} \le 1445$ MeV/c^2) and compares the data (black points) to the prediction based on a phase space Monte Carlo weighted according to the fitted amplitude. Including isospin-1/2 s and p amplitudes (i.e. $D13$ and $P11$) gives a reasonable fit. A better fit includes some d wave (also $D13$). A preliminary result for the lower photon energies of the $g1a$ data set is shown in Fig. 3. The large s-wave intensity likely corresponds to the "contact" term expected in photoproduction reactions.

At higher energies in the $g1c$ run, we will examine the $M_{p\pi^+\pi^-} \approx 2$ GeV/c^2 region for

[1]A "resonance" should exhibit an amplitude whose imaginary part peaks at the "mass" of the state it represents, and whose real part passes through zero at this point. For example, see [Ma92].

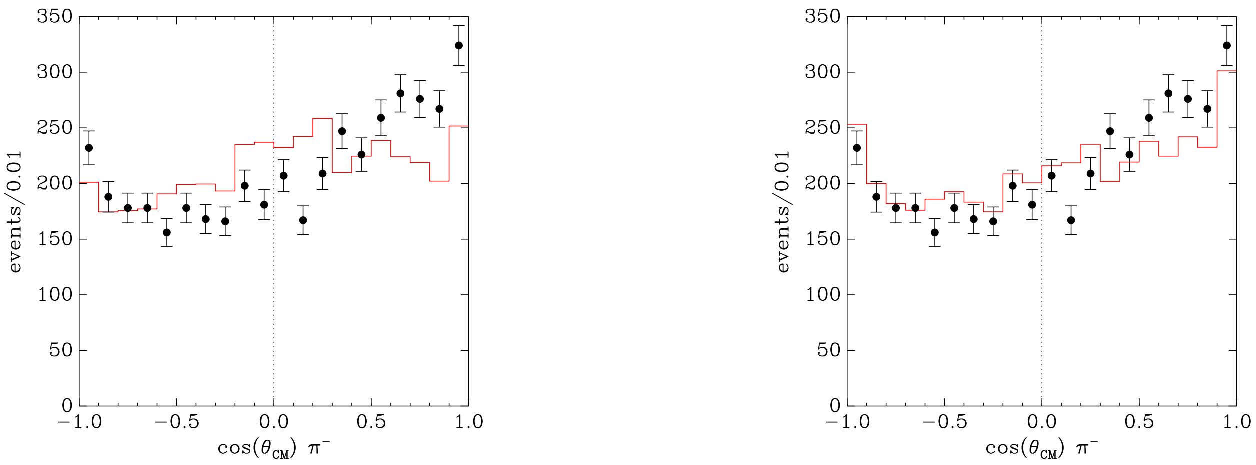

Figure 2: Experimental and "fitted" angular distributions for $\gamma B \to \Delta\pi$, using the π^- angle in the center-of-mass frame. The black points are the experimental data. The red histogram shows the "predicted" distribution, based on the best fit partial waves. The plot on the left includes only isospin-1/2 $\Delta\pi$ s- and p-waves. The right includes a small amount of d-wave.

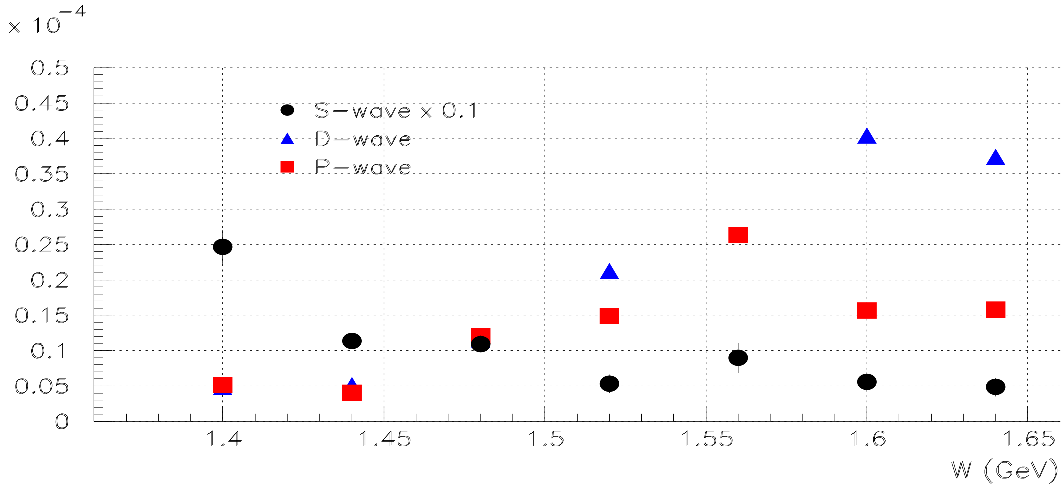

Figure 3: A preliminary result of the mass-independent and model-independent partial wave analysis. A large s-wave $\Delta\pi$ component is attributed to the "contact" term in photoproduction reactions.

missing baryon resonances. This will of course be difficult. However, it should be possible to test for the need to include some particular cases. For example, consider the $\frac{5}{2}^+$ states predicted by the quark model, dominated by the $N = 2$ harmonic oscillator band. The quark model predicts five states, but only two are clearly identified. What's more, the diquark model predicts exactly two states. A specific object of this experiment would be to clearly identify at least one of the three "missing" states. Some large signals are suggested based on the quark model [Ca92, Ca94], and these will guide us as we begin our investigation.

References

[Ad98] G.S. Adams, *et al.*, Physical Review Letters, **81**, 5760 (1998).

[An93] M. Anselmino, *et al.*, Reviews of Modern Physics, **65**, 1199 (1993).

[Ar96] R.A. Arndt, I.I. Strakovsky, and R.L. Workman, Physical Review C **53**, 430 (1996).

[Ca86] S. Capstick and N. Isgur, Physical Review D **34**, 2809 (1986).

[Ca92] S. Capstick, Physical Review D **46**, 2864 (1992).

[Ca93] S. Capstick and W. Roberts, Physical Review D **47**, 1994 (1993).

[Ca94] S. Capstick and W. Roberts, Physical Review D **49**, 4570 (1994).

[Cl79] F. Close, "An Introduction to Quarks and Partons", Academic Press (1979)

[Cu77] R.E. Cutkosky and R.E. Hendrick, Physical Review D **16**, 2902 (1977).

[He75] D.J. Herndon, *et al.*, Physical Review D **11**, 3183 (1975)

[Li69] D.B. Lichtenberg, Physical Review **178**, 2197 (1969).

[Ma84] D.M. Manley, *et al.*, Physical Review D **30**, 904 (1984).

[Ma92] D.M. Manley and E.M. Saleski, Physical Review D **45**, 4002 (1992).

2.33 g2 Run Group Overview

The G2 run group is composed by 5 experiments, running concurrently, which use the high energy tagged photon beam on a liquid deuterium target.

The 5 experiments are:

- E89-045 *Studies of Kaon Photoproduction on Deuterium*

  Spokesperson: B. Mecking

- E93-008 *Inclusive η Photoproduction in Nuclei*

  Spokesperson: M. Vineyard

- E93-017 *Study of $\gamma d \to pn$ and $\gamma d \to p\Delta^0$ Reactions for Small Momentum Tranfers*

  Spokespersons : E. De Sanctis, P. Rossi

- E94-008 *Photoproduction of η and η' Mesons from Deuterium*

  Spokesperson: B. Ritchie

- E94-103 *The Photoproduction of Pions*

  Spokespersons: W. Briscoe, J. Ficenec, D. Jenkins

The running period of the g2 experiments (called "g2a") was performed during the months August (13-31) and September (15-28) 1999. Approximately 75% of the approved run time has been completed; the final run period will probably be scheduled by the end of 2002.

During that period we had the following running conditions:

- **energy Energy** of the incident **electron beam** (incident upon a gold radiator of 10^{-4} radiation lengths): $\mathbf{E_0}$**=2.5 GeV** (August) and $\mathbf{E_0}$**=3.1 GeV** (September);
- **Current** intensity: **10-13 nA**;
- Torus **magnetic field**: **3375 A** (88% full field) with positive particles out-bending;
- **Target**: mylar cylinder 4 cm in diameter and 10 cm long, filled with **liquid deuterium**;
- **Photon energy** : **0.5-2.4 GeV** (August) and **0.6-2.9 GeV** (September);

- **Photon intensity** : about $\mathbf{7 \times 10^7}$ tagged γ/s (production runs) and about $\mathbf{10^5}$ tagged γ/s (normalisation runs);

- **Tagger**: full focal plane **(0.2-0.95)$\mathbf{E_0}$ GeV** for about 70% of the running time **(0.35-0.95)$\mathbf{E_0}$ GeV** for the remaining time;

- **1st Level Trigger**: coincidence between a signal in the tagger [Master OR] and either 1 charged track in CLAS (80%) or 2 neutral hits (20%) in calorimeter;

- **2nd Level Trigger**: used for the first time both in "late failed" mode and "real rejection" mode (though only a few runs in the latter configuration) , to reject events in which a reconstructed track does not correspond to a time-of-flight counter hit in that sector;

- **DAQ** Rate: about **2.7 kHz**

- **Overall Efficiency**:beam availability=**85** %; experiment ready=**78** %.

Under these conditions, we collected about **2.4 billion** valid events and an additional **22 million** empty target events. Also, a number of normalization runs were taken at low intensity to allow both determination of the photon tagger characteristics and a measurement of the photon flux. A total of **178 million** normalization events were collected.

Analysis of the data began soon after data collection, using a multi-step process. The first step involved calibration of the CLAS detector, a step which took almost 6 months. Following this calibration, we were able to proceed with the so-called pass-0 cooking at the end of April 2000.

During the pass-0 cooking each event was reconstructed by the program *a1c* (using prod-2-0-g2a), which finds particles tracks and computes momenta from the raw data. This first pass data reconstruction took almost 2 months, and at the beginning of June 2000 pass-1 cooking began.

In pass-1 cooking, events reconstructed by a1c, were sent not only to the standard data monitoring utilities but also to a filter program. This program controls several specific physics filters and outputs several files, one for each physics filter. These files were then analyzed separately, allowing individuals interested in one specific reaction channel to work with smaller files, rather than using the whole data set. Pass-1 cooking ended at the beginning of August 2000.

Subsequent to the completion of pass-1 cooking, B-field studies showed an increase in the particle detection efficiency using a magnetic field map in the tracking algorithm different from that used in the pass-1 cooking. Consequently, the g2 pass-1 cooking will be repeated with this new field map, beginning about the middle of February 2001.

2.34 E93-008

Inclusive η Photoproduction in Nuclei

M. F. Vineyard (University of Richmond)
and the CLAS Collaboration

2.34.1 Introduction

Jefferson Lab Experiment 93-008 uses the CEBAF Large Acceptance Spectrometer (CLAS) and the photon tagging system in Hall B to measure inclusive η photoproduction in nuclei. The primary motivation of this experiment is to investigate nuclear medium modifications of nucleon resonances and the η-nucleon interaction. According to the run plan developed by the CLAS collaboration to maximize the scientific output of Hall B by exploiting the capability of the CLAS to simultaneously obtain data for experiments with similar running conditions, this experiment is being performed during the g2 and g3 running periods.

Through the study of the excitation, propagation, and decay of nucleon resonances in the nuclear environment one ultimately expects to understand how the strong interaction is affected by baryon structure. A wealth of information on the $\Delta(1232)$ and its dynamics within the nuclear medium has been obtained through pion studies. However, very little is known about medium properties of the higher energy excited states of the nucleon. This is primarily due to the fact that the dominance of the Δ and the overlapping of higher resonances prevents studying one specific state by π-production experiments. The η meson, on the other hand, couples only with isospin-1/2 N^* resonances since it is an isoscalar particle, and therefore provides a way to isolate these resonances. In this experiment, inclusive measurements of the photoproduction of η mesons in nuclei are performed to investigate medium modifications of the $S_{11}(1535)$ and $P_{11}(1710)$ resonances which are the only nucleon resonances of mass less than 2 GeV with significant η decay branches.

These measurements will also provide information on the η-nucleon interaction. Due to the lack of η beams, very little is known about the interaction of η mesons with nucleons. In this experiment, final- state interactions of the η meson propagating through the nucleus will be used to investigate the ηN interaction. The study of η interactions with nucleons and nuclei can provide significant tests of our understanding of meson interactions which has been developed through pion studies. Also a comparative study of the response of η and η' mesons in the nuclear medium may provide insight into the mixing in these two mesons and the structure of the η'.

Data were obtained several years ago at Mainz for the inclusive reaction on ^{12}C, ^{40}Ca, ^{93}Nb, and ^{nat}Pb nuclei for photon energies $\leq$790 MeV [Ro96]. However, though these data are of high quality, the energy range covered is from threshold to just below the peak of the $S_{11}(1535)$ resonance. From the analysis of these data, it was concluded that the total cross section scales as $A^{2/3}$ and a Glauber model analysis indicated an ηN cross section of about 30 mb. No evidence of a shift in mass or a depletion of strength of the $S_{11}(1535)$ was observed from a comparison with the effective Lagrangian model of Carrasco [Ca93]. However, it should be stressed that this conclusion was drawn from a comparison of the slopes of the data and calculations on the low-energy side of the $S_{11}(1535)$ rather than over the entire line shape of the resonance.

There have been a number of theoretical results on η photoproduction from nuclei in the last decade. In the effective Lagrangian approach of Carrasco *et al.* [Ca93], the ηN final state interactions are taken into account by a Monte Carlo code using calculated reaction probabilities. In the work of Lee *et al.* [Le96], the quasifree production is calculated in the distorted-wave impulse approximation and the final state interactions are treated with an ηA optical potential. Effenberger *et al.* [Ef97] use the production cross sections on the free nucleon as input and take into account the final state interactions with a coupled- channel Boltzmann-Uehling-Uhlenbeck model. All three models provide reasonable descriptions of the Mainz total cross sections. However, detailed agreement with the differential cross sections is not obtained with any of the models.

The Jefferson Lab experiment discussed here will extend the Mainz measurements to higher energies and more targets. The extended energy range will completely cover the region of the $S_{11}(1535)$ resonance and allow for a more thorough investigation of possible nuclear medium modifications. It will also allow for the measurement of contributions to the cross section from the $P_{11}(1710)$ resonance and non-resonant production. The measurements are being made on ^{2}H, ^{3}He, ^{4}He, and ^{12}C targets enabling the study of the evolution of medium effects with target mass and the investigation of the ηN interaction.

2.34.2 Experiment Status

During the g2a cooking process, filtered data files were created that contained events with at least two neutral particles. These filtered data files are being further analyzed to produce data summary files that are used in the physics analysis for E93-008. Shown in Figure 1 is a preliminary invariant mass spectrum for $\gamma\gamma$ events recorded during the g2a run. The spectrum has been fitted with a function consisting of a quadratic piece to describe the background in the mass region 0-0.23 GeV, an exponential part to fit the background in the mass range 0.23-0.9 GeV, and two gaussians to fit the π^0 (mass = 0.135 GeV) and η (mass = 0.547 GeV) peaks.

The g3 run group received about 23 days of beam in December of 1999. Approximately 2 billion photon-induced events were recorded from liquid ^3He and ^4He targets. Data were taken at an electron beam energy of 1.6 GeV corresponding to the tagged photon energy range of 0.4-1.5 GeV. The calibration of the detectors for this run is currently being completed and the cooking of the data will begin soon.

References

[Ro96] M. Roebig-Landau, *et al.*, Phys. Lett. **B373**, 45 (1996).

[Ca93] R. C. Carrasco, Phys. Rev. **C48**, 2333 (1993).

[Le96] F. X. Lee, L. E. Wright, C. Bennhold, and L. Tiator, Nucl. Phys. **A603**, 345 (1996).

[Ef97] M. Effenberger *et al.*, Nucl. Phys. **A614**, 501 (1997).

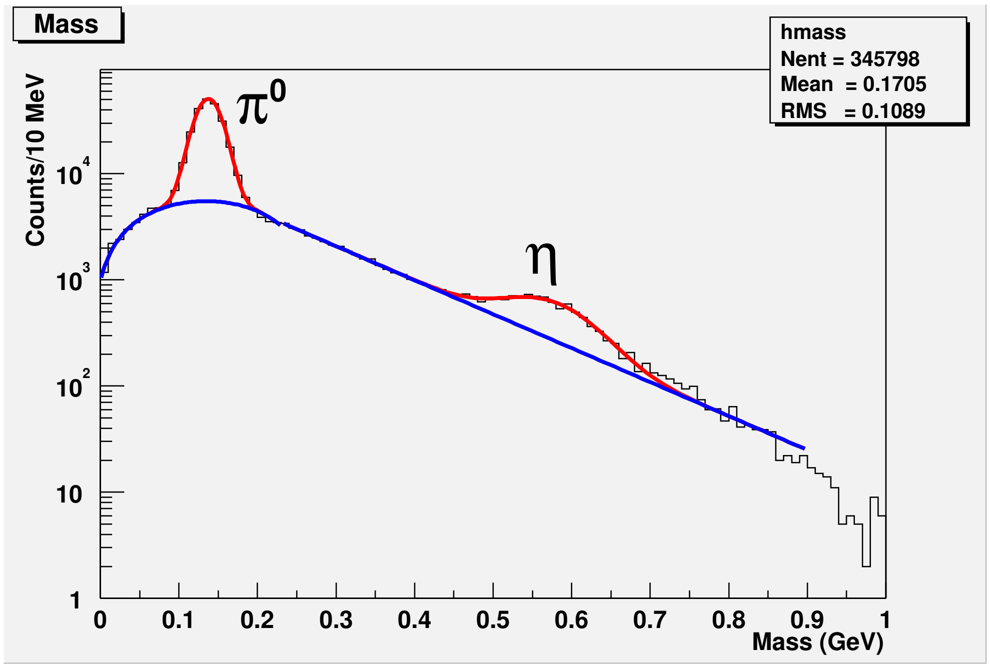

Figure 1: Invariant mass spectrum for $\gamma\gamma$ events recorded during the g2a run period of the CLAS Collaboration. The spectrum is fitted with a background function and two gaussian functions. The background function has a quadratic form over the range 0-0.23 GeV and an exponential form over the range 0.23-0.9 GeV. The π^0 (mass = 0.135 GeV) and η (mass = 0.547 GeV) peaks are fitted above the background with the gaussian functions.

2.35 E93-017

STUDY OF $\gamma d \rightarrow pn$ AND $\gamma d \rightarrow p\Delta^0$ REACTIONS FOR SMALL MOMENTUM TRANSFERS

E. De Sanctis, P. Rossi (spokespersons)-*Laboratori Nazionali di Frascati (INFN)*
for the CLAS Collaboration

2.35.1 Introduction

The experiment intends to measure the differential cross section for the processes $\gamma d \rightarrow pn$ and $\gamma d \rightarrow p\Delta^0$ in the region of small momentum transfers and over the energy range from 0.5 to 3.2 GeV, in order to check the predictions of the Regge phenomenology and the Quark Gluon String (QGS) model [1], [2].

The study of high-energy two-body photodisintegration of the deuteron has renewed interest in recent years with attempts to illuminate the quark structure of the nucleus. The physics interest deals with how and at what energy the transition takes place from the hadronic picture of the deuteron, which is established in the reactions at low energies (below 1 GeV), to the quark-gluon picture, which is expected to be a correct theory at the energy much higher than 1 GeV, where small distances of the order of 0.2 fm play a role.

A possible signature for the emergence of quark-gluon degrees of freedom would be the observation of the onset of scaling of the cross section. Recent measurements [3] of $\gamma d \rightarrow pn$ at high energy have shown an energy dependence of the cross section which is consistent with constituent-counting rules at angles of 69° and 89° up to 4 GeV photon energy. However, at 36° and 52°, the data disagree with the counting rule behaviour.

Recently an expression for the cross section for the reaction $\gamma d \rightarrow pn$ at small momentum transfers t and u has been derived in the framework of the quark-gluon-string model and Regge phenomenology [4]. In this approach the cross section is a rapidly decreasing function of the photon energy and t. At fixed angle and in a limited energy region, the energy dependence of the cross section can be parameterized as a simple power law with different powers at different angles in distinction from the quark counting rule which predicts a constant power at all angles.

2.35.2 Experiment Status

We started the preliminary data analysis using the filtered data files of the August g2a period. We explored our reaction channels in the photon energies range between 0.5 and 2.4 GeV. Using the particle identification contained in the PART bank to select our events and the photon energy from the TAGR bank using the events with status 7 and 15 (this last ones suitably selected), we were able to determine the missing mass of the neutron in $\gamma \mathrm{d} \rightarrow \mathrm{pn}$ and of the proton and pion in $\gamma \mathrm{d} \rightarrow \mathrm{p}\Delta^0$.

An extensive analysis of the normalization for this data set has been performed. The standard procedure, which makes use of the total absorption counter and the pair spectrometer, has been used, but a new approach, based on the tagger T-scalers, also was developed and utilized for the first time for the "g2 runs". To accomplish the normalization, all data collected at low intensity (the so-called "normalization runs") throughout the g2a period were analyzed using both approaches. The efficiency of the tagger and pair spectrometer calculated, and the stability of the beam monitoring systems was verified.

To perform the Monte Carlo simulation of the experiment we used the a1c re-construction program of the GSIM banks with an input of GENBOS event generator. This generator, describing photoreactions on free nucleons from pion production threshold up to 10 GeV, was incorporated and updated to include reactions on deuterons as well.

Finally, from the theoretical point of view, we have continued to investigate the deuteron two-body photodisintegration within the framework of the Quark-Gluon String Model with nonlinear baryon Regge trajectories. Special attention has been paid to the use of QCD motivated Regge trajectories with the logarithmic and square root form. We found that the recent experimental data [3] in the few GeV region can reasonably be described by the model [2].

2.35.3 Results - or Expected Results

The preliminary data thus far obtained for the $\gamma \mathrm{d} \rightarrow \mathrm{pn}$ reaction are based on only 17 million events of the 2.4 billion collected in g2a. We used production runs 20220 and 20221 and normalization run 20228 (10 million events). To identify the photodisintegration events, the following cuts have been used:

- only one proton as a charged particle in the final state,

- z proton vertex inside the the target,

- missing mass between 0.88 and 1 GeV to identify the neutron.

The preliminary results of the $d\sigma/dt$ [Fig.1] show good agreement with previous measurements [3], [5], [6] in the overlapping regions. A particular striking and unique feature of this differential cross section data are the measurements at very small angles obtained with the CLAS detector.

References

[1] N. Bianchi *et al.*, CEBAF proposal E-93-017.

[2] V. Yu. Grishina, L. A. Kondratyuk, W. Cassing, A. B. Kaidalov, E. De Sanctis, P. Rossi , hep-ph/0101129.

[3] C. Bochna *et al.*, Phys. Rev. C **41** (1998) 4576.

[4] L.A. Kondratyuk *et al.*, Phys. Rev. C **48** (1993) 2491.

[5] S. J. Freedman *et al.*, Phys. Rev. C **48** (1993) 1864.

[6] J. E. Beltz *et al.*, Phys. Rev. Lett. **74** (1995) 646.

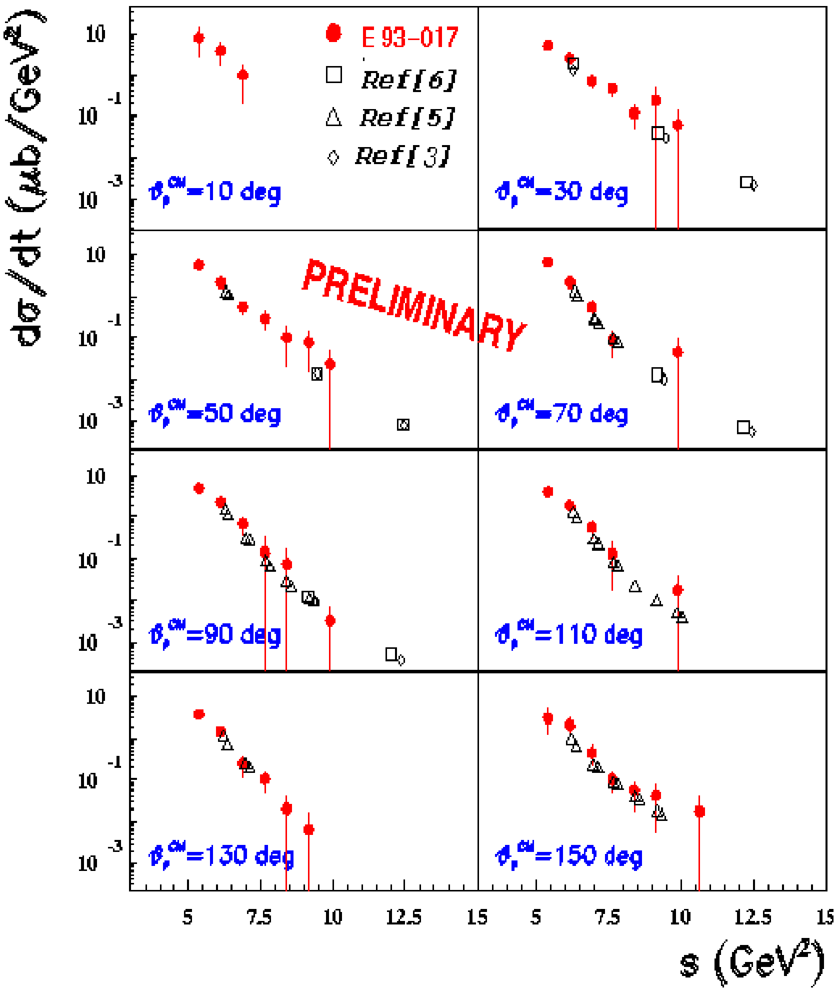

Figure 1: Differential cross section, $d\sigma/dt$, for the γd $\rightarrow$ pn reaction based on a few percent of the total data accumulated in the g2a running period.

2.36 g3 Run Group Overview

The g3 run group is comprised of the following approved Hall-B proposals:

- **E91-014** *Quasi-free Strangeness Production in Nuclei*,
  Spokesman: C. Hyde-Wright (ODU)
- **E93-008** *Inclusive η Photoproduction in Nuclei*,
  Spokesman: M. Vineyard (U. of Richmond)
- **E93-044** *Photoreactions on ^3He and ^4He*,
  Spokesmen: B.L. Berman (GWU), G. Audit (Saclay), P. Corvisiero (Genoa)

The g3 experiments collected data for about three weeks in December, 1999. We obtained data over the full range of the Photon Tagger – 0.33 to 1.56 GeV with an incident electron-beam energy of 1.645 GeV. Tagged, circularly polarized photons, produced by the 70% longitudinally polarized electrons, were incident on liquid-helium targets positioned at the center of the CLAS. This was the first experiment to use a second-level trigger, and we were able to collect data at rates exceeding 3 kHz, twice the design rate of the CLAS. We succeeded in collecting approximately 1.2 billion events for ^{3}He and 0.8 billion for ^{4}He. [The ^{12}C part of g3 was not run at this time – in fact, it was only because we were able to obtain data at such a high rate that we were able to perform the ^{4}He part in the allotted time.]

2.37 E93-044

PHOTOREACTIONS ON ^{3}He AND ^{4}He

Spokesmen: B.L. Berman (GWU), G. Audit (Saclay), P. Corvisiero (Genoa)

A small part of the data from the 1999 run (a few million events) were analyzed with existing calibrations; they show (see below) that the main goals of the experiment have been reached. That is, we do indeed have sufficient data for the principal reaction channels of interest.

Progress since then has been concentrated in four areas:

- Normalization procedures for the tagged-photon flux have been studied at length. The two main techniques were shown to give results generally within 5% of each other.
- Calibration studies have revealed certain problems with the time-of-flight counters for sectors 3 and 4, which are now under intensive scrutiny.
- Data transfer to the new GW mass-storage facility (our "minisilo"), for eventual cooking and analysis by the new GW computer cluster (our "minifarm") has been slow, because of difficulties encountered in the transfer of a data set of this magnitude (about 5 TB), but is now approximately 70% complete.
- Pass-zero cooking (the first file of each data run, comprising between 5 and 10% of the total) is complete, and shows generally very good stability throughout the running period.

Figures 1 - 3 illustrate the data on the three-body breakup channel of ^{3}He. Figure 1 shows the striking peak in the missing-mass spectrum of two protons just at the mass of the neutron. Figure 2 shows the distribution of three-body-breakup events on a triangular Dalitz plot, showing a large number of "star" events, candidates for three-body-force effects because all three nucleons have approximately the same energy and relative momentum. Figure 3 shows a cut along the neutron-energy axis in the Dalitz plot, showing that a valley exists between the regions dominated by two-body and three-body events, and that the three-body events peak near the symmetric "star" kinematics.

Figures 4 and 5 illustrate the data on the quasifree delta production on a nucleon in ^{4}He, focusing on Δ^0 production on a neutron in the nucleus and its subsequent decay into the $p\pi^-$ channel. Figure 4 shows the remarkable peak in the $p\pi^-$ missing-mass spectrum just at the mass of the (spectator) ^{3}He. Figure 5 shows the invariant mass of the events in this peak, showing that most of them occur near (but possibly peaking just below) the mass of the Δ^0. This is the first example of the use of ^{4}He as a neutron target.

Further analysis of these data await pass-one cooking of all of the (properly calibrated) data, but prospects for excellent progress during the next year are bright.

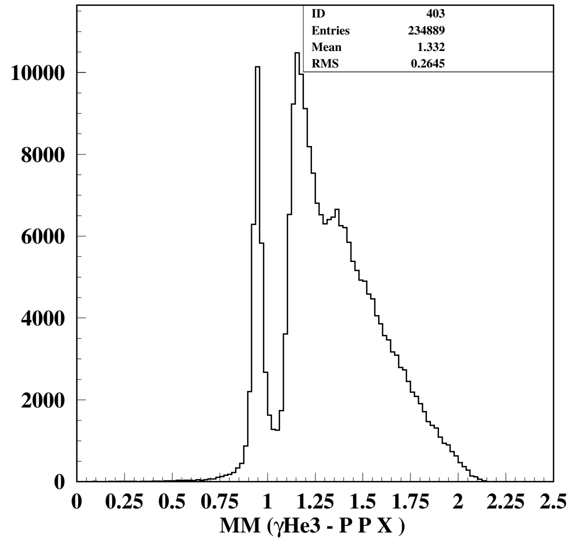

Figure 1: Missing-mass distribution when two protons were detected in CLAS. The target is ^{3}He. The narrow peak at the neutron mass signals the three-body- breakup reaction.

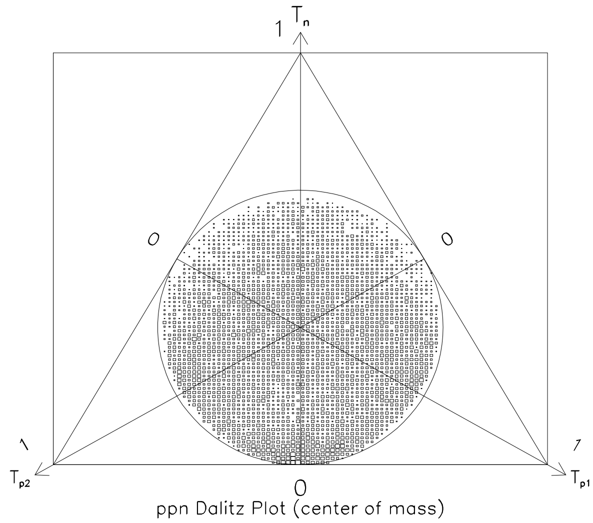

Figure 2: Distribution of three-body-breakup events on a triangular Dalitz plot. “Star” events fall near the center.

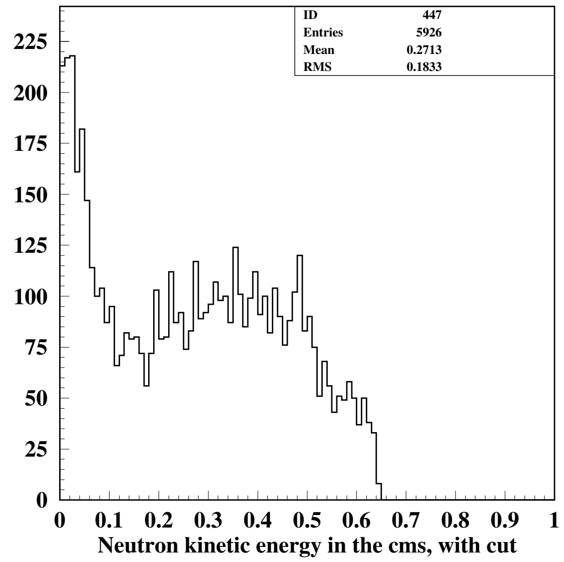

Figure 3: Distribution of neutron energies for those three-body events in which the two detected protons had nearly equal energies.

2.38 g5 Run (E93-019)

PHOTOFISSION OF HEAVY NUCLEI

Spokesman: B. L. Berman (GWU)

The g5 experiment ran for about four days in April, 1998. This was the commissioning experiment for the Photon Tagger, and we obtained data over its full energy range for three different incident electron energies – 0.9, 1.7, and 4.0 GeV, thus yielding data from 0.2 to 3.9 GeV. The tagged photons were incident on thin fission-foil targets positioned, each with its own parallel-plate avalanche detector for the fission fragments, in a common reaction chamber filled with isobutane at a pressure of 15 torr. In spite of the adverse running conditions at this early date and the short running time made available to us, we were able to obtain data of high quality. These data are the substance of the GW Ph.D. thesis of Catalina Cetina; part of them have been published as Phys. Rev. Lett. **84**, 5740 (2000), the first physics results from Hall B to be published. A longer article, for Phys. Rev. C, is

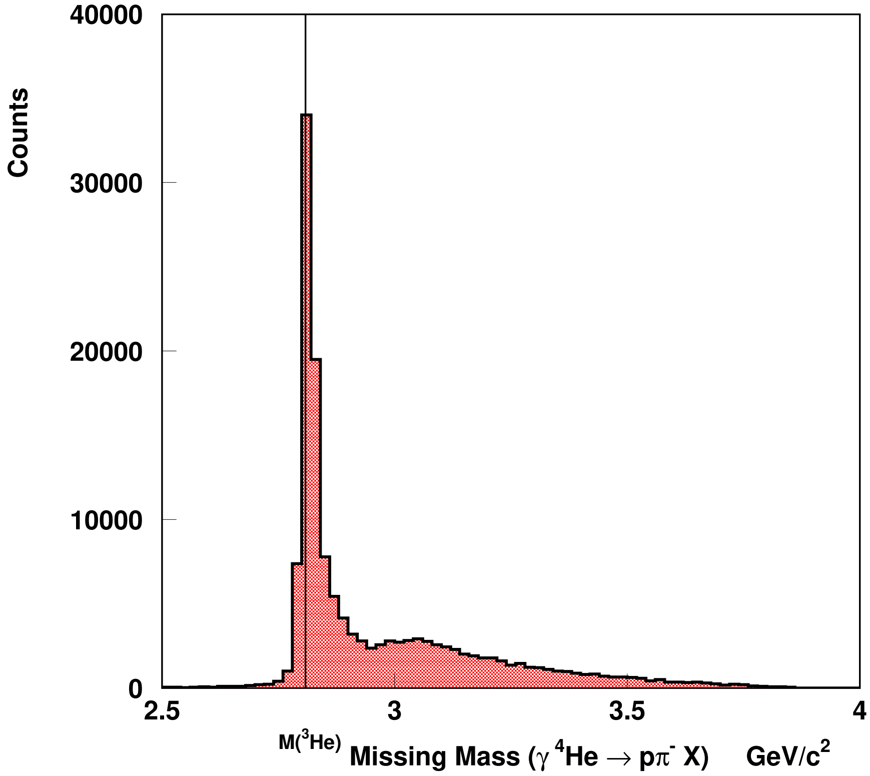

Figure 4: Missing-mass distribution when a proton and π^- were detected in CLAS. The target is ^{4}He. The peak at the ^{3}He mass indicates the importance of the quasifree pion-production reaction.

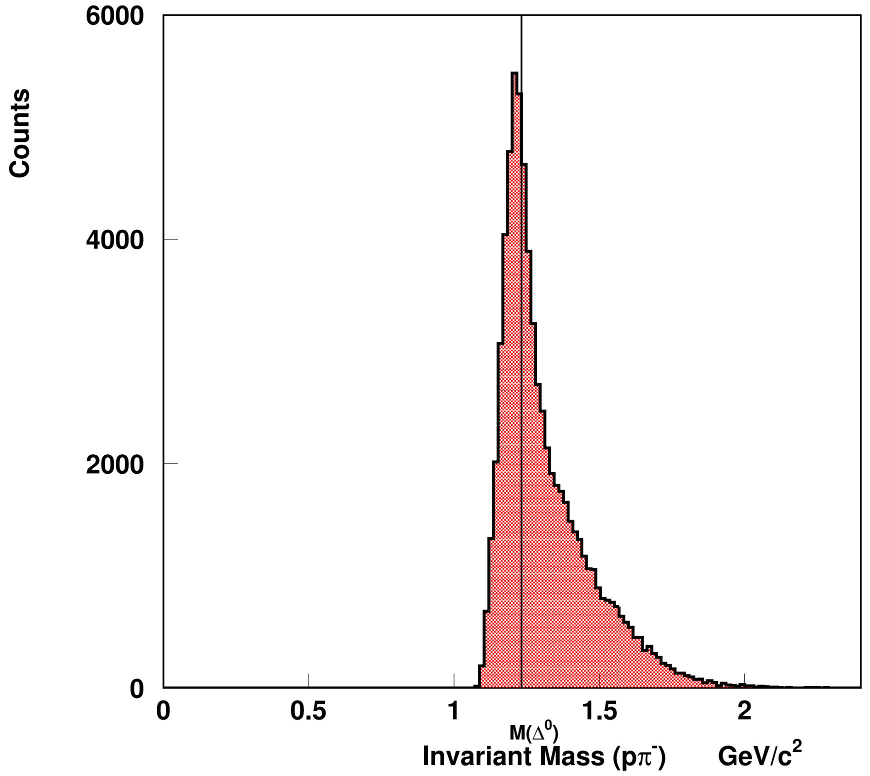

Figure 5: Invariant mass disribution for the quasifree events in Fig. 4. The line marks the mass of the Δ^0.

in the course of preparation.

Some of the results are shown in Figs. 1 and 2. Figure 1 shows the photofission cross sections per nucleon for ^{237}Np, ^{238}U, and ^{232}Th (those for ^{235}U, ^{233}U, and $^{\mathrm{Nat}}$Pb are not shown here), compared with previous data. Clearly, the cross section for ^{237}Np is substantially larger than that for ^{238}U, showing that the fission probability of the latter could not be 100%, as had been commonly believed prior to this experiment. However, the near-equality of the photofission cross section per nucleon for ^{237}Np and the photon absorption cross section per nucleon for lead, together with the asymptotic behavior of the ^{237}Np cross section as a function of fissionability Z^2/A, leads one to the conclusion that the fission probability for ^{237}Np is indeed nearly 100%. This in turn enables us to accurately determine the degree of shadowing of photons by nuclei in the GeV energy region. This effect is shown in Fig. 2, where the onset of the shadowing effect on ^{237}Np is seen to occur below 1 GeV, and its magnitude is approximately 20% by 4 GeV. Finally, although the magnitude of the photofission cross sections for ^{238}U and ^{232}Th is smaller than that for ^{237}Np, they have roughly the same shape, as is also shown in Fig. 2, so that one can conclude that the shadowing effect for these nuclei is at least as large as that for ^{237}Np.

The success of this experiment shows that interesting and important measurements on heavy, as well as light, nuclei can and should be done in the GeV energy region. Heavy nuclei approximate nuclear matter in a sense, and thus such measurements can provide important insights into its nature.

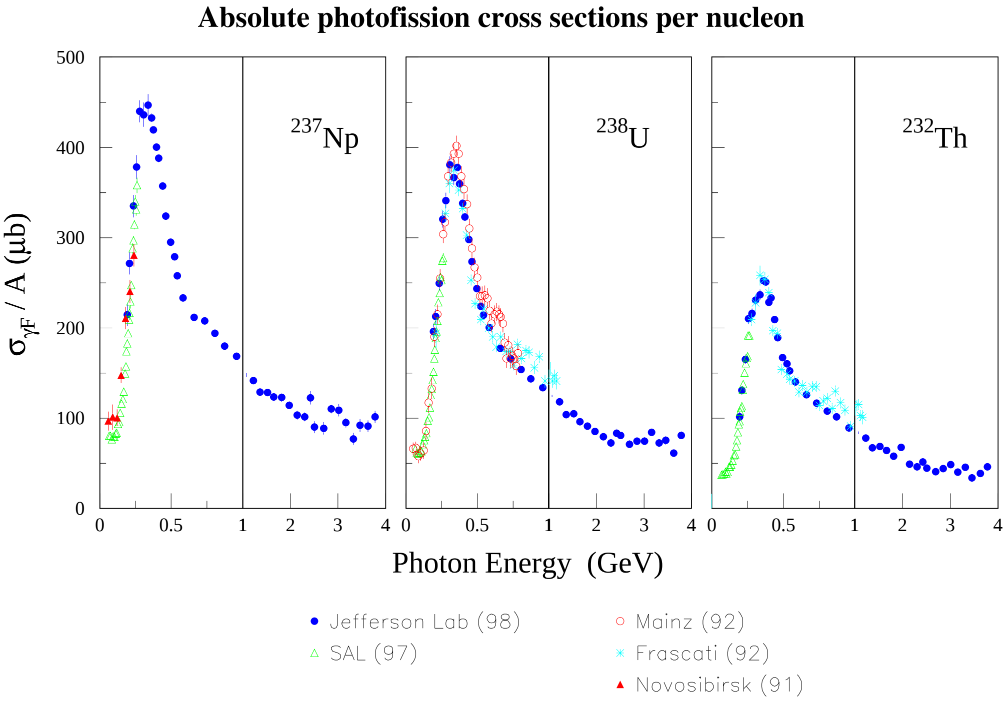

Figure 1: Photofission cross sections per nucleon for ^{237}Np, ^{238}U, and ^{232}Th.

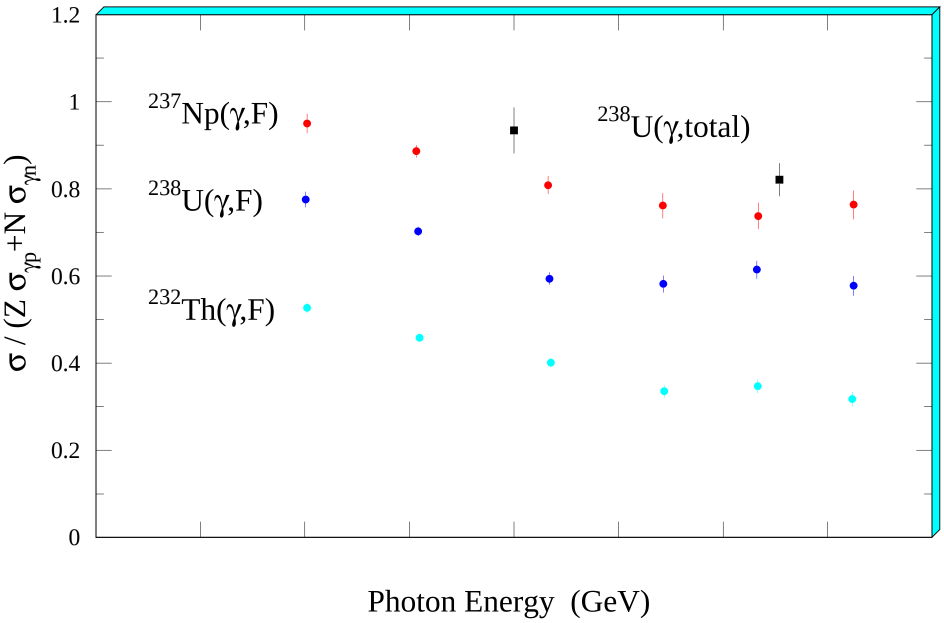

Figure 2: Fission cross section divided by the effective scaled free-nucleon cross section $(Z\sigma_{\gamma p} + N\sigma_{\gamma n})$. The decrease with energy indicates the onset of nuclear shadowing.

2.39 g8 Run Group Overview

2.39.1 Experiments

The physics with linearly-polarized photons in Hall B encompasses four experiments, which together have been awarded a total of 43 days of dedicated beamtime to form the g8 running period:

1. "*Photoproduction of ρ Mesons from the Proton with Linearly Polarized Photons*," E94-109, P.L. Cole* (Univ. of Texas at El Paso), J.P. Connelly (Cisco Corp.), and K. Livingston (Univ. of Glasgow, UK), cospokespersons.
2. "*Photoproduction of ϕ Mesons with Linearly Polarized Photons*," E98-109, D.J. Tedeschi* (Univ. of South Carolina), P.L. Cole, and J.A. Mueller (Univ. of Pittsburgh), cospokespersons.
3. "*Photoproduction of ω Mesons off Protons with Linearly Polarized Photons*," E99-013, F.J. Klein* (Florida Intl. Univ.) and P.L. Cole, cospokespersons.
4. "*Photoproduction of Associated Strangeness using a Linearly Polarized Beam of Photons*," CLAS Approved Analysis, F.J. Klein*, J. Kellie (Univ. of Glasgow, UK), and J.C. Sanabria (Univ. de los Andes, Colombia), cospokespersons.

The focus of the g8 running period is to extract polarization observables in the photoproduction of vector mesons and associated strangeness. We will make use of the technique of coherent bremsstrahlung to produce a linearly-polarized beam of photons from a thin diamond radiator (20 μm). The coherent bremsstrahlung facility (CBF) consists of an orientable diamond radiator, photon collimator, and electron tagging system. The status of these systems is described on our web page.

The g8 collaboration passed the Technical/Readiness Review on Feb. 5, 2001; Phase I of g8 is scheduled to run June 1 to July 26, 2001. For further information on the physics, instrumentation, and members of the g8 collaboration, we refer the reader to http://www.physics.gla.ac.uk/~cgordon/.

2.39.2 Goniometer Tests

In May 2000 and October 2000, Hall-B Facility Development Time was dedicated to calibrate the goniometer, a device possessing six degrees of freedom – three rotational and three translational axes. Accurately positioning the [002] lattice vector of the thin diamond crystal (50 μm) with respect to the direction of the electron beam allows one to produce highly linearly polarized coherent bremsstrahlung within well-defined ranges of energy.

The beam tests were quite successful. We were able to demonstrate that the goniometer operates at sufficient accuracy and that the peak of the coherent bremsstrahlung can be kept fixed at a specific photon energy while rotating the diamond crystal. The result of an energy scan is shown in Fig. 2.39.2, where the darkened region indicates that the energy of the coherent peak varies as function of the crystal orientation.

2.39.3 Polarimeter Tests

The photon polarization will be determined by fitting the tagger intensity spectra after taking into account the effects of collimation. We are continuing our testing of a pair polarimeter, which will measure the photon polarization directly. This pair polarimeter consists of 4 layers of 384 Si-μstrips that detect the e^+e^--pairs produced in a thin scintillator target. The asymmetry of the produced pairs is 0.26 and the plane of the polarization is in the direction where the distribution is maximized. Fig. 2.39.3 shows data from a prototype tested with 300 MeV photons at the LEGS facility of Brookhaven National Laboratory. Here, the histogram is from a GEANT simulation and we fit the data with a smooth $\cos 2\phi$ function. The polarimeter will be calibrated using 2 GeV photons at SPring8 (Osaka, Japan) in March of 2001.

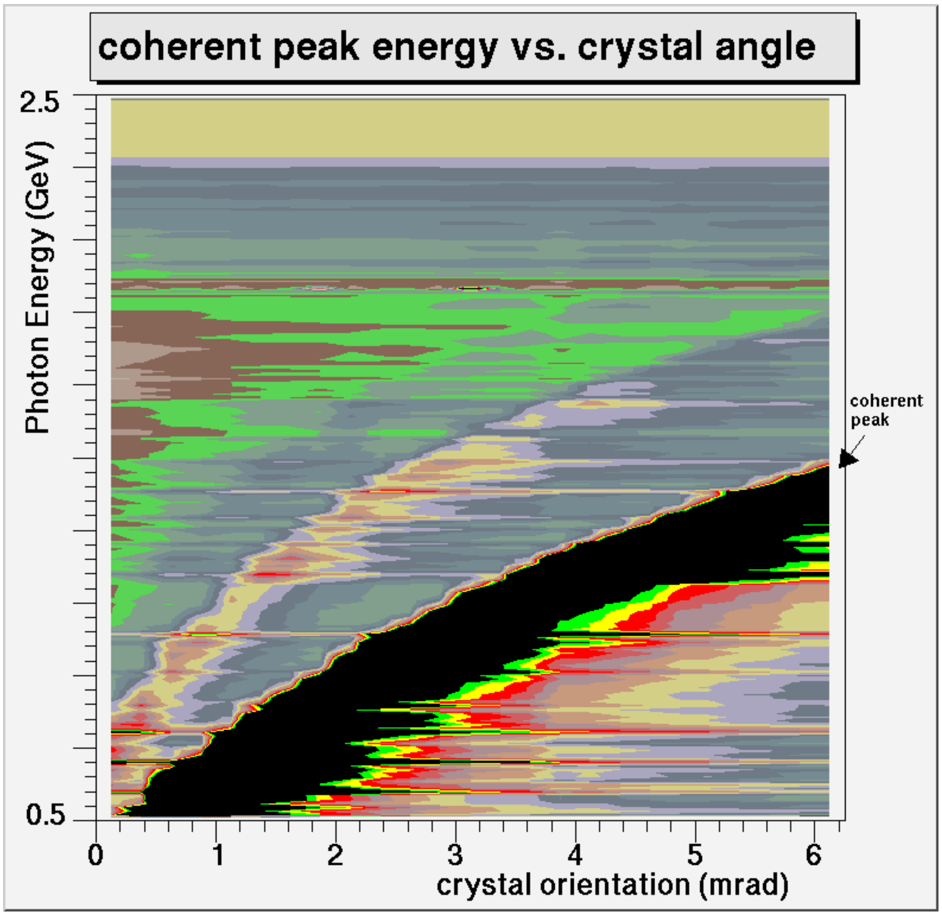
coherent peak energy vs. crystal angle
2.5
0.5
Photon Energy (GeV)
0
1
2
3
4
5
6
crystal orientation (mrad)
coherent
peak

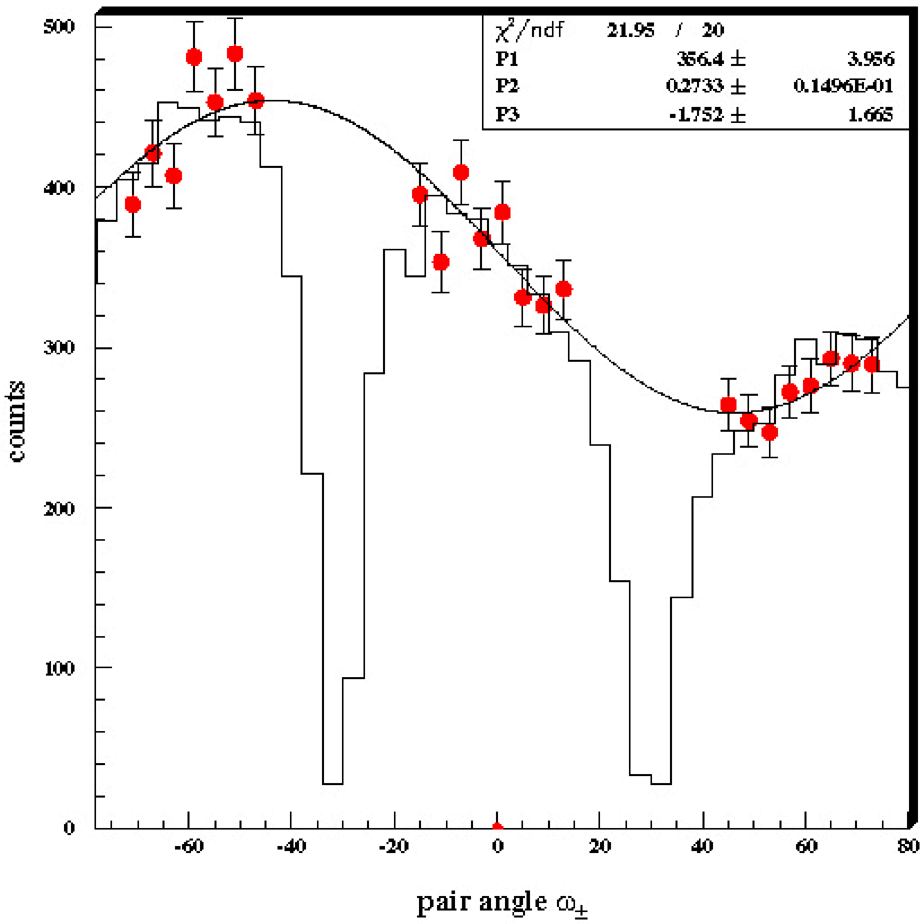

χ^2/ndf 21.95 / 20
P1 356.4 ± 3.956
P2 0.2733 ± 0.1496E-01
P3 -1.752 ± 1.665
500
400
300
200
100
0
-60
-40
-20
0
20
40
60
80
counts
pair angle $\omega_{\pm}$

2.40 E99-014

A Precision Measurement of the Neutral Pion Lifetime via the Primakoff Effect

The PrimEx (Primakoff Experiment) Collaboration is preparing to perform a high precision (one percent level) measurement of the two photon decay width of the neutral pion, $\pi^o \to \gamma\gamma$. This measurement will provide a stringent test of the predictions of quantum chromodynamics in the confinement scale regime. Photons from the Hall B photon tagging system will be used to produce neutral pions in the Coulomb field of a nucleus. The two photons from the pion decay will be detected in a hybrid calorimeter (HYCAL) which will utilize lead tungstate ($PbWO_4$) scintillating crystals as well as lead glass Cherenkov shower counters. In addition to the development of this state-of-the-art calorimeter detector technology, a major experimental challenge in this measurement involves control of the luminosity. As such, extensive studies of the photoproduction targets are underway, and a pair production luminosity monitor, which will become a part of the standard beamline in Hall B, is presently under construction.

Major milestones and activities of the PrimEx Collaboration include:

- A $960k award from the Major Research Instrumentation program of the National Science Foundation for development of experimental apparatus for this experiment.
- Refurbishment of the pair production luminosity monitor dipole and its installation in Hall B.
- Design, construction, and delivery to JLab of the dipole vacuum box for the pair production luminosity monitor and procurement of its power supply.
- Construction of prototype lead glass and lead tungstate detectors, and beam tests performed in Hall B to evaluate the relative performance of different modules.
- Construction and successful test of a temperature control system for the hybrid calorimeter. Control at the $\pm 0.2°$C was attained.

- Contract for fabrication and procurement of 1000 lead tungstate ($PbWO_4$) modules established with a company in China.

- Target thickness measurements are being performed using an X-ray absorption technique.

- Field mapping system for the PrimEx dipole designed and constructed. Preliminary field map complete.

- Development of the fast trigger electronics for π^o detection and purchase of 1000 channels of high voltage for the hybrid calorimeter.

In anticipation of the proposed CEBAF 12 GeV energy upgrade, the PrimEx Collaboration has also been pursuing the development of a program to measure the electromagnetic properties of other pseudoscalar mesons (the η and η') utilizing instrumentation under development for E99-014.

3 Hall C

3.1 Hall C Overview

A total of 18 experiments has been executed in Hall C covering a broad spectrum of topics in nuclear physics since the fall of 1995. Forty six graduate students have conducted their Ph.D. research using the Hall C facility. The research program has produced 16 experimental publications.

The initial complement of equipment in Hall C includes two general purpose magnetic spectrometers: the High Momentum Spectrometer (HMS), which has a large solid angle, moderate resolution (δp/p=10^{-3}), and a maximum momentum of 7.3 GeV/c; and the Short Orbit Spectrometer (SOS), which has a large momentum acceptance and a very short (7.4 meter) optical path length to facilitate the detection of particles having short lifetimes, such as low momentum πs and Ks. This base set of equipment has been used to conduct experiments measuring: The Energy Dependence of N Propagation in Nuclei in (e,e$'$p), Photodisintegration of the Deuteron, Inclusive Scattering from Nuclei at x $>$ 1 and High Q^2, Electroproduction of Kaons and Light Hypernuclei, L/T Separation in p(e,e$'K^+$), Δ (1232) Form Factor at High Momentum Transfer, Charged Pion Form Factor, Pion Electroproduction in ^{2}D, ^{3}He, and ^{4}He, Color Transparency, Measurement of R = σ_L/σ_T in the Resonance Region, Correlated Spectral Function & (e,e$'$p) Reaction Mechanism, and Electroproduction of Kaons and Light Hypernuclei.

Hall C also supports the installation of specialized detectors designed to investigate specific problems. Examples include: the T_{20} experiment (E94-018), which separated the elastic form factors of the deuteron to high momentum transfer; and the HNSS experiment (E89-009), an investigation of the feasibility of performing hypernuclear physics experiments in which a nucleon in the nucleus is replaced by its strange counterpart, the Λ hyperon. The HNSS experiment has been successfully completed and the next phase of the program has been approved. It will consist of the Enge split-pole spectrometer used in the first hypernuclear experiment plus a new high resolution kaon spectrometer system (HKS) constructed and funded (4M$) by the Japanese collaborators. The system will have ~350keV resolution and a 50 fold increase in data collection rate with respect to the first generation experiment. Additional "major installation" experiments in Hall C include: Two complementary measurements of the electric form factor of the neutron; one using a neutron detector in conjunction with a polarized target and low-current polarized beam (E93-026), and the other employing a neutron polarimeter together with an unpolarized deuterium target and high current polarized beam (E93-038), and precision measurements of parity violation in the scattering of polarized electrons from protons to investigate their weak neutral current structure and possible contributions from strange quarks (E91-017), to be carried out using a major new specialized apparatus now under construction - the G^0 spectrometer. The superconducting magnet that is at the heart of the spectrometer is funded by the NSF. In addition, a new collaboration is being formed to conduct a search for physics beyond the standard electroweak model via a precision measurement of the weak charge of the proton. Pending future PAC and JLab approval this collaboration plans to use the G0 magnet upon completion of the G^0 program.

3.2 Duality

Experimental Verification of Parton-Hadron Duality

C. E. Keppel and R. Ent,
and
Argonne/Caltech/Colorado/Hampton/Illinois/JLab/Maryland/Northwestern
Pennsylvania/Rensselaer/Virgina/William & Mary Collaboration

3.2.1 Introduction

Three decades ago, Bloom and Gilman observed a fascinating correspondence between the resonance electroproduction and deep inelastic kinematic regimes of inclusive electron-nucleon scattering [2]. Specifically, it was observed that the resonance strength could be related to the deep inelastic strength via a scaling variable which allowed for a comparison of the lower W^2 and Q^2 resonance region data to the higher W^2 and Q^2 deep inelastic data. Furthermore, this behavior was observed over a range in Q^2 and W^2, and it was found that, with changing Q^2, the resonances move along, but always average to, the smooth scaling curve typically associated with deep inelastic scattering (DIS). This behavior clearly hinted at a common origin for resonance (hadron) electroproduction and deep inelastic (partonic) scattering, termed parton-hadron, or Bloom-Gilman, duality.

A global kind of parton-hadron duality is well established: low-energy resonance production can be shown to be related to the high-energy behavior of hadron-hadron scattering; the familiar ratio of $e^+e^- \rightarrow$ hadrons over $e^+e^- \rightarrow$ muons uses duality to relate the hadron production to the sum of the squared charges of the quarks. Here duality is guaranteed by unitarity; in Perturbative QCD (PQCD) the high-momentum transfer behavior of nucleon resonances can be related to the high-energy transfer behavior of DIS. Poggio, Quinn, and Weinberg [2] suggested that inclusive hadronic cross sections at high energies, averaged over an appropriate energy range, had to approximately coincide with a quark-gluon perturbation theory. However, it is not clear why duality should also work in a localized region, and even at relatively low momentum transfers, and to what precision it works.

Inclusive deep inelastic scattering on nucleons is a firmly-established tool for the investigation of the quark-parton model. At large enough values of W^2 and Q^2, with $W^2 >> Q^2$, a precise description of the Q^2 behavior of the nucleon structure function $F_2 = \nu W_2$ can be given in terms of a perturbative series in $\alpha_S(Q^2)$, up to next to leading order [4]. Such Q^2 behavior becomes especially transparent in comparing the high Q^2 (> 10 (GeV/c)^2) moments of F_2 with PQCD predictions.

An analysis of the resonance region at smaller W^2 and Q^2 in terms of QCD was presented in [3], where Bloom and Gilman's duality was re-interpreted, and the integrals of the average scaling curves were equated to the $n = 2$ moment of the F_2 structure function. The Q^2 dependence of these moments can be described by ordering the contributing matrix elements according to their twist (= dimension - spin) in powers of $1/Q^2$. The fall of the resonances along a smooth scaling curve with increasing Q^2 was attributed [3] to the fact that there exist only small changes in these lower moments of the F_2 structure function due to higher twist effects. Such effects are inversely proportional to Q^2, and can therefore be large at small Q^2. If not, averages of the F_2 structure function over a sufficient range in x at moderate and high Q^2 are approximately the same.

A sample of high-precision data in the nucleon resonance region, in combination with substantial progress made over the last twenty years in determining the scaling behavior of deep inelastic structure functions with electron, muon, and neutrino probes, enables us to revisit local duality in detail.

3.2.2 Experiment Status

We accumulated data, as part of various experiments in 1996 in Hall C, in the nucleon resonance region, $1 < W^2 < 4$ GeV^2, for both hydrogen and deuterium targets. Measurements in the elastic region were included in the data to verify our absolute normalizations to better than 2%. The Q^2 range covered by our data set is between 0.3 and 5 (GeV/c)^2. The data were obtained using electron beam energies between 2.4 and 4 GeV. Incident beam currents between 20 and 100 μA were used on 4 and 15 cm long targets. Scattered electrons were detected in both the HMS and the SOS, each utilized in a single arm mode to measure the inclusive cross sections. At all beam energy-scattering angle combinations, the central momentum of the spectrometers was varied to cover the full resonance region. The change in central momentum was kept smaller than the momentum acceptance of each spectrometer, to ensure that overlapping data were accumulated. We accumulated of order 10^5 counts for every beam energy-scattering angle combination (9 in total for hydrogen, 8 for deuterium). The overall systematic uncertainty in the measured cross sections due to target density, beam charge, beam energy, spectrometer acceptance, radiative corrections, and detection efficiency is 3.5% and larger than the statistical uncertainties. The data analysis was completed in 1998 [5].

3.2.3 Results

The obtained high precision data on the F_2 structure function [6] have quantified the earlier observations by [2, 3], and demonstrated that duality works to better than 10% for both the total nucleon resonance region and each of the separate low-lying nucleon resonance regions, for $Q^2 \geq 0.5$ (GeV/c)^2. This is illustrated in Fig. 1, where the nucleon resonance data for various Q^2 is compared to parameterizations of deep inelastic scattering data at constant $Q^2 = 5$ and 10 (GeV/c)^2. Such behavior shows that the distinction between the nucleon resonance region and the deep inelastic region is spurious; if properly averaged, the nucleon resonance regions closely mimic the deep inelastic region. It was in addition shown that duality works remarkably well for each of the low-lying resonance regions, including the ground state [7], and also works for the F_2 structure function results determined from the D(e,e$'$) data [8]. The theoretical conditions for the averaging region in the nucleon resonance spectra required for duality to work have only recently been under investigation [9]. In addition, the origin of duality has recently been studied in the context of a large N_c-based relativistic quark model [10].

Our data showed, additionally, that the nucleon resonance region data *at all* Q^2 tend to average to a single smooth curve even down to $Q^2 \approx 0.2$ (GeV/c)^2 [6, 8]. This curve coincides with the deep inelastic scaling curve at $Q^2 > 0.5$ (GeV/c)^2, consistent with Bloom-Gilman

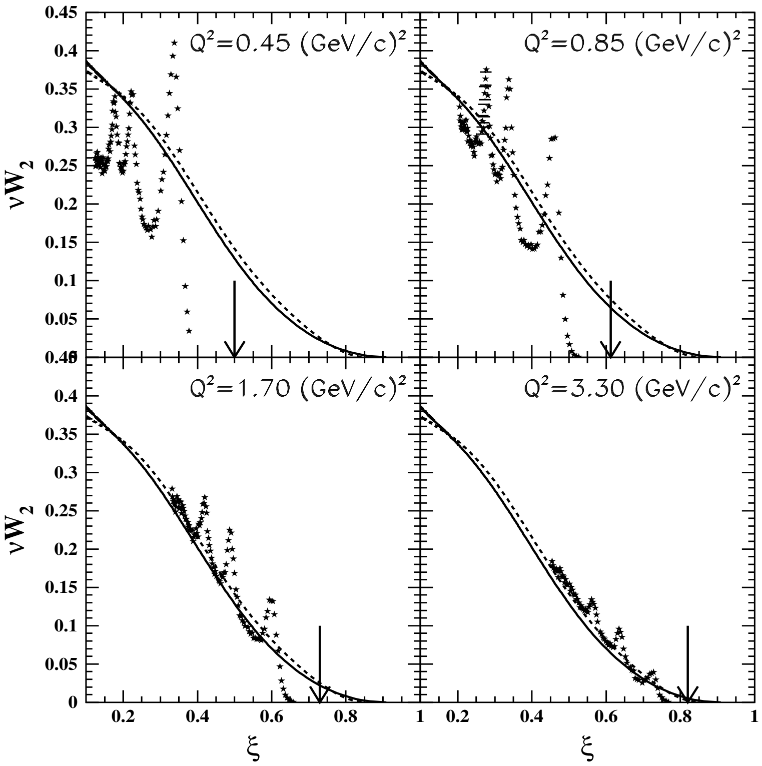

Figure 1: Sample hydrogen νW_2 structure function spectra obtained at Q^2 = 0.45, 0.85, 1.70, and 3.30 $(\mathrm{GeV/c})^2$ and plotted as a function of the Nachtmann scaling variable ξ [11]. Arrows indicate elastic kinematics. The solid (dashed) line represents the NMC fit of deep inelastic structure function data at Q^2 = 10 $(\mathrm{GeV/c})^2$ (Q^2 = 5 $(\mathrm{GeV/c})^2$).

duality, and resembles neutrino/anti-neutrino xF_3 data or a valence-like sensitivity only [8] below $Q^2 \approx 0.5$ (GeV/c)^2. This is perhaps not too surprising in the quark model where the nucleon resonances act as valence quark transitions, while at low Q^2 not many sea quarks can be "seen" yet. However, it is surprising that all the strongly-interacting nucleon resonances seem to exchange their strength as function of Q^2 to closely follow a single scaling curve.

These data, in combination with older, less precise, very low Q^2 data from SLAC, enabled us to construct moments of F_2 down to $Q^2 \approx 0.1$ (GeV/c)^2, with a precision of 5% [4]. The second moment is only slowly varying with Q^2 down to $Q^2 = 1$ (GeV/c)^2, which is a reflection of duality. Similarly, the world's data on F_2, down to this Q^2, are reasonably well described within PQCD, if one averages over each low-lying resonance region. Below $Q^2 = 1$ (GeV/c)^2, the Q^2 dependence of the lower moments is predominantly governed by the elastic contribution at large x. The contribution of the nucleon resonances to the lower moments of F_2 (n = 2, 4, 6, 8) dies out at very small Q^2, as they have moved to smaller Bjorken x, and on average mimic a valence-like behavior. Their averaged F_2 strength, even down to $Q^2 \approx 0.1$ (GeV/c)^2, does not disappear linearly yet with Q^2 [8, 4], as expected by gauge invariance for $Q^2 \rightarrow 0$.

References

[1] E.D. Bloom and F.J. Gilman, Phys. Rev. D **4** (1971) 2901; Phys. Rev. Lett. **25** (1970) 1140.

[2] E.C. Poggio, H.R. Quinn, and S. Weinberg, Phys. Rev. D **13**, 1958 (1976).

[3] A. DeRujula, H. Georgi, and H.D. Politzer, Annals of Phys. **103** (1977) 315.

[4] A.J. Buras, Rev. Mod. Phys. **52** (1980) 199.

[5] I. Niculescu, Ph.D. Thesis, Hampton University (1999).

[6] I. Niculescu *et al.*, Phys. Rev. Lett. **85**, 1186 (2000).

[7] R. Ent, C.E. Keppel, and I. Niculescu, Phys. Rev. D **62**, 73008 (2000).

[8] I. Niculescu *et al.*, Phys. Rev. Lett. **85**, 1182 (2000).

[9] F.E. Close and N. Isgur, "The Origins of quark-hadron duality: How does the square of the sum become the sum of the squares?", JLAB-THY-01-01 (in preparation).

[10] S. Jeschonnek, N. Isgur, W. Melnitchouk, and J.W. Van Orden, "Quark-Hadron Duality in Structure Functions", JLAB-THY-01-12 (in preparation).

[11] O. Nachtmann, Nucl. Phys. **B63** (1975) 237.

[12] C.S. Armstrong *et al.*, Accepted for publication in Phys. Rev. D (2001).

3.3 E89-008

Inclusive Scattering from Nuclei at $x > 1$ and High Q^2

B. Filippone and D. Day, Spokespersons, and the E89-008 collaboration

3.3.1 Introduction

Inclusive lepton scattering is one of the most powerful tools available for probing parton distributions in nucleons and nuclei. Experiment E89-008 measured inclusive electron scattering from nuclei in the domain of large x and Q^2. In the region where $x > 1$ (corresponding to low energy transfer), the cross section is dominated by quasielastic scattering from nucleons, even at the highest values of Q^2 measured ($\simeq 7$ $(\mathrm{GeV/c})^2$). At large values of x, the measured structure function is sensitive to the high momentum tail of the nucleon momentum distribution. Examining data corresponding to large initial nucleon momenta for several different nuclei allows insight into the nature of the high momentum tail and the short range correlations that dominate this region. Data in this region may also be sensitive to non-nucleonic components of the wavefunction.

Previous measurements of the structure function in this region [1] showed signs of scaling in the Nachtmann variable, $\xi = 2x/(1+\sqrt{1+4M^2x^2/Q^2})$. This scaling is a modified version of Bjorken scaling ($\xi \to x$ as $Q^2 \to \infty$) that reduces target-mass related scaling violations at finite Q^2 . As with traditional Bjorken scaling, this behavior is only expected in the deep inelastic limit, where one is sensitive to the quark structure; nevertheless, the previous data hinted at scaling for all values of ξ, even where the cross section was dominantly quasielastic. This indicates at a connection between the quark structure in the limit of asymptotic freedom and the nucleon/resonance structure in the confinement region, reminiscent of Bloom Gilman duality in the proton [2].

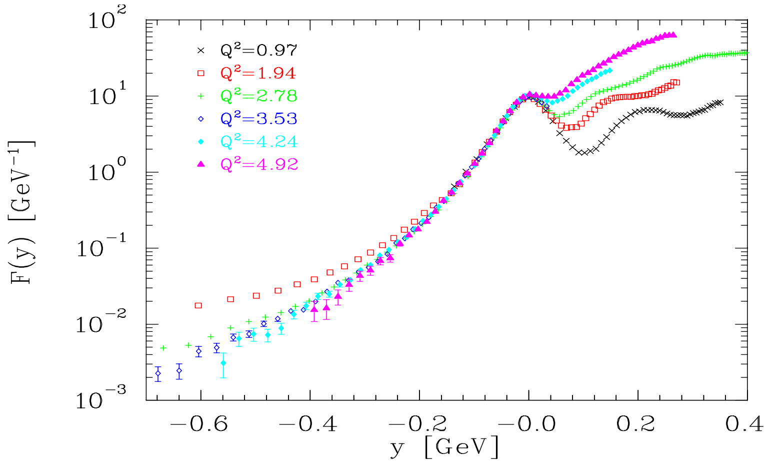

Figure 1: Scaling function $F(y)$ for deuterium. The Q^2 values are given for Bjorken $x = 1$. Errors shown are statistical only. Typical systematic uncertainties are 3-5%.

3.3.2 Experiment Status

E89-008 ran in the summer of 1996, and measured inclusive scattering from deuterium, carbon, iron and gold. Data were taken in both the HMS and SOS spectrometers, for Q^2 values up to $\simeq 7$ (GeV/c)^2. Particle identification cuts were used to remove large backgrounds from negative pions, and contributions from charge-symmetric electron-positron production were measured and subtracted using measurements of positron production at identical kinematics. The final systematic uncertainty on the extracted cross section was typically 3-5%, with somewhat larger uncertainties at the highest values of x. A y-scaling analysis has been published [3], and an analysis of the nuclear structure functions has been submitted [4]. At present, we are concentrating on extraction of the nucleon momentum distributions. Of particular interest are the high momentum components, where the A-dependence can help shed light on the nature of the short range correlations that generate the high momentum tail of the distribution.

3.3.3 Results

A y-scaling analysis [5] of the data was made to study the nuclear wave function at high x in terms of nucleon momentum distributions. The scaling function, $F(y)$, is determined by removing the electron-nucleon cross section from the measured data. In the PWIA limit $F(y)$ can be related to the integral of the nucleon momentum distribution up to nucleon momentum $|y|$. As seen in Figure 1, the data show scaling in y, *i.e.* are independent of Q^2, above $Q^2 \simeq 2$ (GeV/c)^2 for negative values of y where quasielastic scattering is the dominant process. For positive values of y, there are inelastic contributions and the PWIA breaks down. The momentum distribution can be extracted from $F(y)$, and agrees well with calculations of the deuteron momentum distribution using modern N-N potentials. Scaling is also observed for negative values of y in the heavier nuclei; however, the high momentum tail in these nuclei have a different y-dependence from deuterium. The y-scaling model assumes that the separation energy for the single nucleon knockout is a constant value. This is inconsistent with the picture of two nucleon correlations as the source of the high-momentum components. The data from the heavy nuclei have also been analyzed using a parameterization of the separation energy that assumes a two nucleon correlation structure in the tail. In this analysis the low momentum components are essentially unchanged but the tail is substantially different. The y-dependence of the high momentum components becomes identical for all nuclei, including deuterium, with a larger magnitude in heavy nuclei due to the greater number of nucleon pairs.

The measured cross sections were also used to extract the structure function, νW_2. The data do not show scaling in x for any of the Q^2 values measured, which is consistent with the cross section being dominated by quasielastic and resonance scattering. The data do show scaling in ξ (Figure 2), as was hinted at in the previous data. Figure 3 shows the structure function per nucleon for iron as a function of Q^2. For all values of ξ, the structure function is nearly constant for $Q^2 > 3$ (GeV/c)^2, with deviations that are roughly consistent with what one would expect from QCD scaling violations (based on measured QCD scaling violations at high Q^2).

The observation of DIS scaling in the resonance and quasielastic region is very similar to the scaling observed by Bloom and Gilman in the proton [2]. This effect can be illustrated in

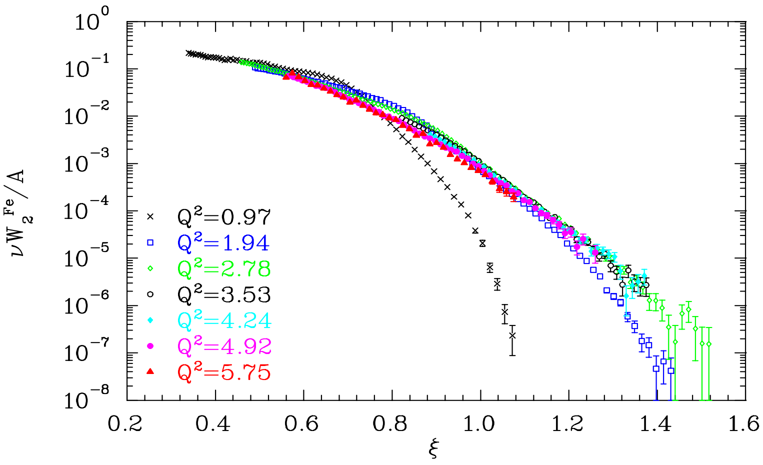

Figure 2: νW_2 for iron. The Q^2 values are given for Bjorken $x = 1$. Data are shown both for $y > 0$ (the inelastic region) and $y < 0$ (where the cross section is dominated by quasielastic scattering). Errors shown are statistical only. Typical systematic uncertainties are 3-5%.

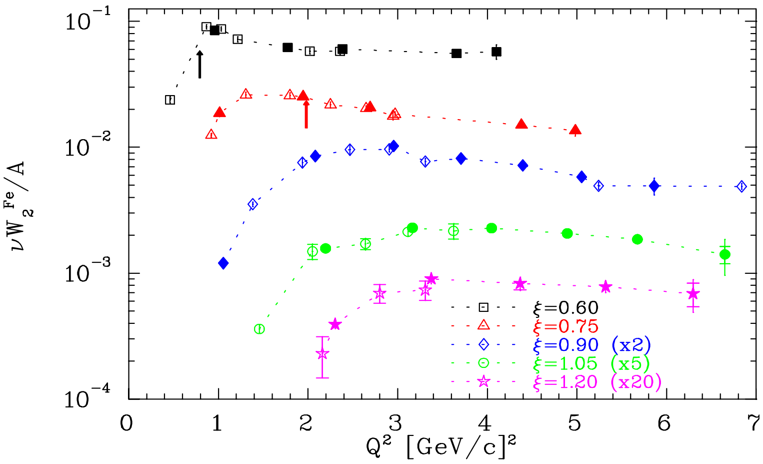

Figure 3: νW_2 for iron as a function of Q^2. The inner errors are statistical, and the outer errors are the total uncertainty. Hollow points are from SLAC measurements [1, 6] The arrows indicate the position of the quasielastic peak.

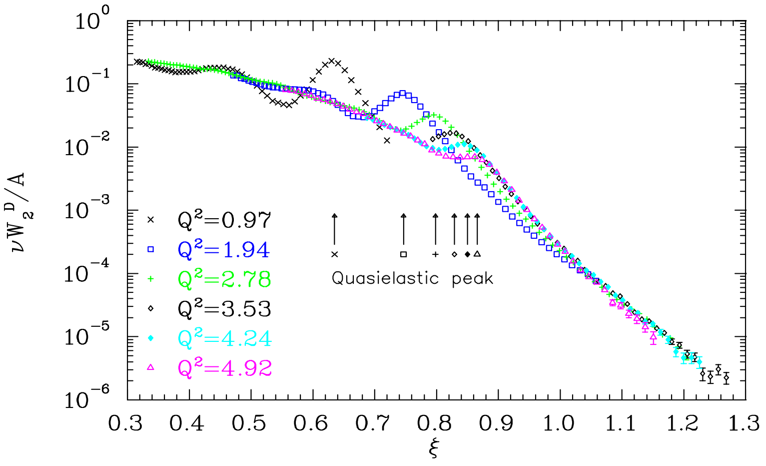

Figure 4: νW_2 for deuterium. The Q^2 values are given for Bjorken $x = 1$. Errors shown are statistical only.

the deuterium data (Figure 4), where the quasielastic peak and the delta resonance (at low Q^2) are visible. While the resonance and QE peaks fall with Q^2 faster than the DIS structure function, they move to higher ξ and maintain a constant strength with respect to the scaling limit curve. This is exactly what was observed for the proton by Bloom and Gilman. In the case of nuclei, however, the Fermi motion broadens the resonances so that for the higher Q^2 values the resonance structure is no longer visible. While the peaks are washed out they still fall along the DIS scaling curve, leading to scaling throughout the resonance region in deuterium, and at extending into the quasielastic region in iron. This extension of scaling into the resonance region for nuclei may allow extraction of quark distributions at high x without requiring the extremely large Q^2 necessary to be in the deep inelastic region.

References

[1] B. W. Filippone *et al.*, Phys. Rev. C **45**, 1582 (1992).

[2] E. Bloom and F. Gilman, Phys. Rev. D **4**, 2901 (1971).

[3] J. Arrington *et al.*, Phys. Rev. Lett. **82**, 2056 (1999).

[4] J. Arrington *et al.*, Submitted to Phys. Rev. C. (2001).

[5] G. B. West, Phys. Rep. **18**, 263 (1975).

[6] J. Arrington *et al.*, Phys. Rev. C **53**, 2248 (1996).

3.4 E89-012

Two-Body Photodisintegration of the Deuteron at Forward Angles and between 1.5 and 4.0 GeV

R. J. Holt, spokesperson, and the E89-012 Collaboration

3.4.1 Introduction

The overall goal of the experiment is to map out the transition region from a nucleon-meson picture of deuteron photodisintegration to the quark-gluon picture. High energy two-body breakup of the deuteron is an excellent means to probe quark effects in nuclear reactions since the energy transfer to the constituents can be large. The objective of the experiment is to extend the cross section measurements for the d(γ,p)n reaction up to a photon energy of 4 GeV. Previous experiments at SLAC were performed only up to 2.7 GeV. The HMS in Hall C was used to detect photoprotons which emerged from a liquid deuterium target that was irradiated by bremsstrahlung photons.

3.4.2 Experiment Status

The experiment was successfully completed, the data were analyzed and a manuscript was published[Bo98].

3.4.3 Results - or Expected Results

Relatively large momentum transfer [Ho90] to the constituents can be obtained in exclusive photonuclear reactions at photon energies of a few GeV, because the absorbed photon delivers all of its energy to the constituents. One obvious signature of a QCD effect in the $d(\gamma, p)n$ reaction is a scaling behavior, for example, the constituent counting rule behavior. For deuteron photo-disintegration $\gamma d \rightarrow pn$ process, the constituent counting rule [Br73, Le73, Ma73] predicts:

$$\frac{d\sigma}{dt} \propto s^{-11}. \tag{1}$$

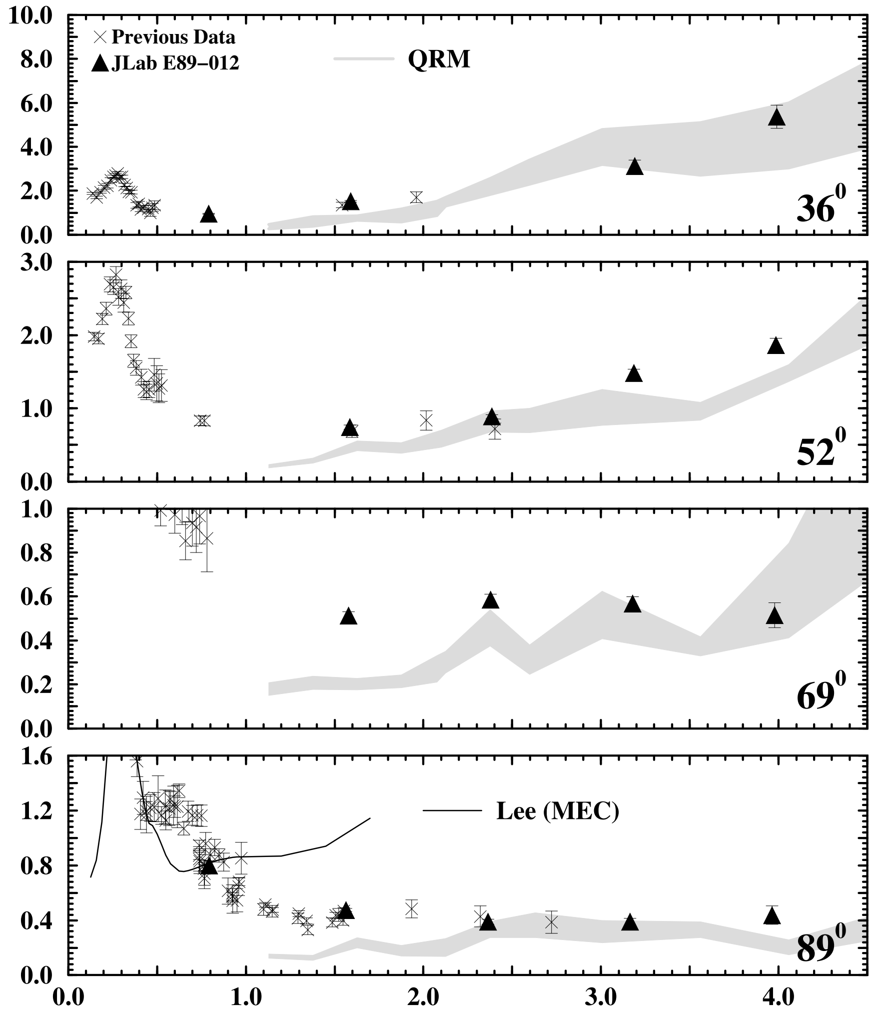

Figure 1: Data for deuteron photodisintegration as a function of the photon energy at four reaction angles. The darkened triangles represent the JLab E89-012 data [Bo98]. The crosses are all the other existing data [Ar84, Be95, Ch66, Cr96, Do76, Fr93, My61, Na88]. The solid line is a traditional meson-exchange calculation [Le88], and the shaded area is the quark rescattering model[Fr00]. These models have an absolute normalization.

This behavior has been observed at large angles, $\theta_{cm} = 70$ and $90°$ as shown in the figure. Here, $s^{11} d\sigma/dt$ is plotted as a function of E_γ. The results [Bo98] shown as the dark circles in the figure are from experiment E89-012 at JLab.

Lee's meson-exchange calculation [Le88], which is a traditional calculation that reproduces the measured NN phase shifts up to 2.0 GeV and is also constrained by photo-meson production data gives a reasonable description of the data below 500 MeV, but above 1.0 GeV the calculation disagrees with the data. Asymptotic meson-exchange calculations also cannot describe the differential cross section data for this reaction[Na92]. Although the results at $\theta_{c.m.} = 90°$ are consistent with the s^{-11} dependence expected from the constituent counting rule, this does not mean that pQCD is valid in this energy region. Polarization data would be necessary to test for the onset of pQCD in this reaction. This is the goal of experiments E89-019, E00-007 and E00-107. However, a new quark rescattering model[Fr00] is in reasonable agreement with the present differential cross section data. This suggests that the GeV region could be a "transition region" between meson-exchange models and pQCD. If we are observing the onset of scaling, then scaling should occur at all angles not just the angles near 90°. Thus, it is essential to measure the cross section at forward angles up to higher photon energies as proposed in experiment E96-003.

References

[Ar84] J. Arends *et al.*,Nucl. Phys. A**412**, 509 (1984).

[Be95] J. E. Belz *et al.*, Phys. Rev. Lett.**74**, 646 (1995).

[Bo98] C. Bochna *et al.*, Phys. Rev. Lett.**81**, 4576 (1998).

[Br73] S. J. Brodsky and G. R. Farrar, Phys. Rev. Lett.**31**,1153 (1973).

[Br83] S. J. Brodsky and J. R. Hiller, Phys. Rev. C**28**, 475 1983.

[Ch66] R. Ching and C. Schaerf, Phys. Rev.**141**, 1320 (1966).

[Cr96] R. Crawford *et al.*, Nucl. Phys. A**603**, 281 (1996).

[Do76] P. Dougan *et al.*, Z. Phys. A**276**, 55 (1976).

[Fr00] L. L. Frankfurt *et al.*, Phys. Rev. Lett.**84**, 3045 (2000).

[Fr93] S. J. Freedman *et al.*, Phys. Rev. C**48**, 1864 (1993).

[Ho90] R. J. Holt, Phys. Rev. C**41**, 2400 (1990).

[Ko93] L. A. Kondratyuk *et al.*, Phys. Rev. C**48**, 2491 (1993).

[Le73] G. P. LePage and S. J. Brodsky, Phys. Rev. Lett.**31**, 1153 (1973).

[Le88] T.-S. H. Lee, Argonne National Laboratory Report No. PHY-5253-TH-88; T.-S.H. Lee, in *Proceedings of the International Conference on Medium and High Energy Nuclear Physics, Taipai, Taiwan, 1988* (World Scientific, Singapore, 1988), p.563.

[Ma73] V. Matveev *et al.*, Nuovo Cimento Lett.**7**, 719 (1973).

[My61] H. Myers *et al.*, Phys. Rev.**121**, 630 (1961).

[Na92] S. I. Nagornyi, YU. A. Kasatkin, and I.K. Kirichenko, Sov. J. Nucl. Phys. **55**, 189 (1992).

[Na88] J. Napolitano *et al.*, Phys. Rev. Lett.**61**, 2530 (1988).

3.5 E91-016

Electroproduction of Kaons and Light Hypernuclei
Ben Zeidman and Jörg Reinhold, Spokespersons
and the E91-016 Collaboration

3.5.1 Introduction

The study of the structure of nuclei containing strange baryons is one of the frontier areas of nuclear research. For reviews see e.g. [Gi95] or the proceedings of the Hypernuclear Physics Conferences ([Mi98] for the most recent). This experiment focuses upon hypernuclear interactions in the lightest nuclei, H_2, D_2, ^{3}He, and ^{4}He, inasmuch as study of two-body and few-body systems limits the complexity of possible interactions and provides information in systems that are amenable to detailed theoretical calculations.

A number of issues are addressed with each of the targets. Comparing quasi-free Σ production from the D_2 target with Σ^0 production from the H_2 target will provide information on charged hyperon production in the $n_{\rm bound}$(e,e'K^+)Σ^- reaction channel. The sensitivity of final-state interactions to Λ-n interactions in photon induced kaon production off deuterium has been discussed by Renard & Renard [Re67]. However, earlier experiments that studied kaon production off deuterium with electromagnetic probes [Bo71, Be77, Qu79] were severely limited in resolution and therefore could not address questions like hyperon-nucleon final-state interaction. More recently, the advent of high intensity electron and photon beams sparked a new theoretical interest in this field [Ad89, Hs86, Co86, Li91, Le98, Ke00, Ya00a, Ya00b].

Bound Λ-hypernuclear states will be produced by the (e,e'K^+) reactions on ^{3}He and ^{4}He targets. Investigation of the bound state angular distributions will provide tests of the wave functions used to describe these states, while the mass spectra will be examined carefully to see if there is evidence for low-lying unbound states. Other features of this study include searches for bound, or nearly bound, Σ-hypernuclei. This initial study will provide a foundation for further investigation of the structure of complex hypernuclei.

Table 1: Central spectrometer settings for the E91-016 angular distributions. Actual average kinematics differ for Λ and Σ final states, repectively.

E_e	$P_{e'}$	$\theta_{e'}$	Q^2	W	ϵ	P_{K^+}	θ_{K^+}	$\theta^{c.m.}_{\gamma K^+}$	target
3.245	1.723	17.19	0.50	1.80	0.80	$\uparrow$	17.67	0	H_2,D_2
						$\mid$	22.00	13	
						1.077	26.45	26	
						&	30.96	38	
						0.929			
2.445	0.918	27.25	0.50	1.80	0.60	$\downarrow$	15.48	3	
3.245	1.593	15.48	0.38	1.90	0.77	1.240	15.45	4	H_2,D_2
							19.92	16	
							25.00	32	
2.445	0.847	24.60	0.38	1.87	0.57	1.150	13.42	4	
3.245	1.576	15.00	0.35	1.91	0.76	1.290	13.30	0	^{3,4}He,H_2,D_2
							19.30	16	^{3,4}He,H_2
							25.30	32	^{3,4}He,H_2

3.5.2 Experiment Status

The experiment involved coincident detection of scattered electrons and kaons, i.e., (e,e'K^+) reactions, on targets of liquid H_2 and D_2 or cooled, pressurized ^{3}He, and ^{4}He. The HMS and SOS spectrometer systems in Hall C were used to detect the emergent electrons and K^+, respectively. During a first run in summer 1996, data were obtained on liquid deuterium and hydrogen targets. At two values for the four momentum transfer ($Q^2 = 0.5$ and 0.38 GeV^2) angular distributions with respect to the direction of the virtual photon were obtained. In forward direction ($\approx$ 0 degree) data were also taken at a lower beam energy, thus, lower virtual photon polarization ϵ. In all settings, additional data have been obtained from a two-layer aluminum target which simulates the background from the target cell walls. These

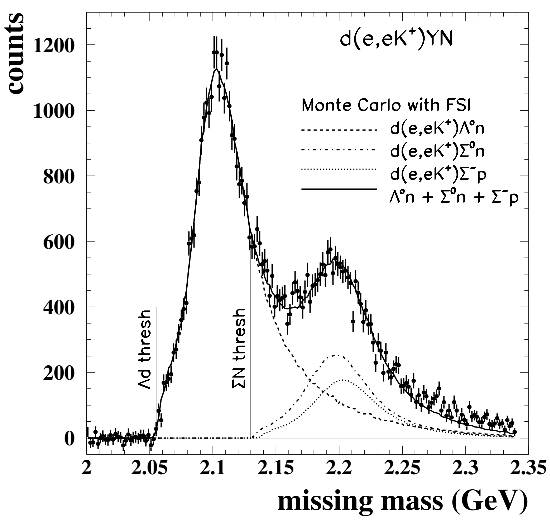

Figure 1: *Reconstructed missing mass for d(e,e′K^+). The lines show Monte Carlo simulations for the different reaction channels.*

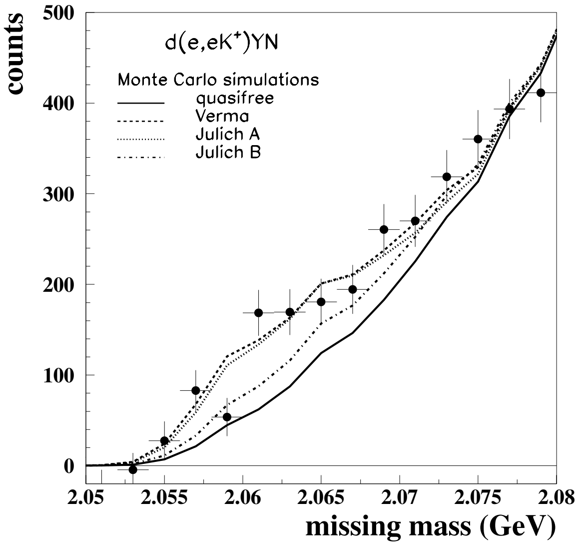

Figure 2: *Reconstructed missing mass for d(e,e′K^+). The lines show Monte Carlo simulations with various Λn potentials.*

aluminum data and a short measurement on ^{12}C extend the measurements to higher mass targets. Further, the large spectrometer acceptance allowed the "parasitic" investigation of ω electroproduction in the H(e,e'p)ω reaction. In the fall of 1999, data on ^{3}He and ^{4}He were obtained at the same beam energy, 3.245 GeV, but slightly lower momentum transfer, $Q^2 = 0.34$ GeV^2. This set completed the data collection phase.

3.5.3 Results

Fig. 1 shows an example of a reconstructed missing mass distribution for d(e,e′K$^+$)YN at E$_{\rm beam}$=3.245 GeV and Q^2=0.38 GeV^2. Background from the target cell walls and accidental coincidences has been subtracted. The two prominent distributions correspond to Λ production (left peak) off the proton and the unresolved Σ^0 and Σ^- production (right peak) off the proton and the neutron, respectively. The width of these peaks is caused by the initial momentum distribution of the nucleons in the deuteron. Due to the relatively low Fermi momentum, the two contributions from Λ and Σ production are well separated. To obtain a quantitative analysis, the data are compared to a Monte Carlo simulation that models the acceptance of both spectrometers and also accounts for radiative effects. Kaon production on the deuterium target is treated as quasi-free production on a nucleon with an initial momentum distribution. A parameterization of the virtual photon-proton cross section that has been obtained from the hydrogen target is used. The cross section for quasi-free Λ production off deuterium is found to be $(99 \pm 3)\%$ of the free production cross section off hydrogen. Assuming the same ratio for Σ^0 production, the Σ^- production cross section can be extracted. An average ratio for Σ^-/Σ^0 of 0.61 ± 0.07 is found.

In the regions of low relative momentum of the residual hyperon-nucleon system, the interaction of the hyperon with the spectator nucleon leads to an increase of the observed yield. This increase has been modeled with three different Λ-nucleon potentials [Ch00]. Fig. 2 shows a comparison of these models to a purely quasi-free simulation near the Λn missing mass threshold. This clearly demonstrates the sensitivity of such a measurement to the Λ-neutron final-state interaction.

Currently, three groups at Argonne National Lab, Florida International University, and Hampton University are analysing the helium data. Preliminary results from different stages of the deuterium and helium data analysis have been presented at several international conferences [Ab98, Hi98, Re00, Ze00]. Three students obtained Ph.D. degrees [Ko99, Ch00, Hi00] and two more will graduate with data from E91-016.

References

[Ab98] D. Abbott *et al.*, Nucl. Phys. A **639**, 197 (1998).

[Ad89] R. A. Adelseck and L. E. Wright, Phys. Rev. **C39**, 580 (1989).

[Be77] C. J. Bebek *et al.*, Phys. Rev. D **15**, 594 (1977).

[Bo71] A. Boyarski *et al.*, Phys. Lett. **B34**, 547 (1971).

[Ch00] J. Cha, "Measurement of the Angular Dependence in H,D(e,e'K^+)", Ph.D. thesis, Hampton University, July 2000.

[Co86] S. R. Cotanch and S. S. Hsiao, Nucl. Phys. **A450**, 419C (1986).

[Gi95] B. F. Gibson and E. V. Hungerford, Phys. Rept. **257**, 349 (1995).

[Hi98] W. L. Hinton, Nucl. Phys. A **639**, 205 (1998).

[Hi00] W. Hinton, "Quasifree Electroproduction of Λ, Σ^0, and Σ^- Hyperons on Carbon and Aluminum", Ph.D. thesis, Hampton University, December 2000.

[Hs86] S. S. Hsiao *et al.*, Czech. J. Phys. **B36**, 426 (1986).

[Ke00] B. Kerbikov, Phys. Atom. Nucl. **63**, 1852 (2000) [hep-ph/9910361].

[Ko99] D. Koltenuk, "Electroproduction of Kaons on Hydrogen and Deuterium", Ph.D thesis, University of Pennsylvania, April 1999.

[Le98] T. S. Lee *et al.*, Nucl. Phys. **A639**, 247 (1998).

[Li91] X. Li and L. E. Wright, J. Phys. G **G17**, 1127 (1991).

[Mi98] D. J. Millener and R. E. Chrien, editors, Nucl. Phys. A639 (1998).

[Qu79] D. J. Quinn *et al.*, Phys. Rev. **D20**, 1553 (1979).

[Re00] J. Reinhold *et al.*, given at 16th International Conference on Few-Body Problems in Physics. March 6-10, 2000 in Taipei, Taiwan. To be published in Nucl. Phys. A.

[Re67] F.M. Renard and Y. Renard, Phys. Lett. **24B**, 159 (1967); Nucl. Phys. **B1**, 389 (1967).

[Ya00a] H. Yamamura *et al.*, Sigma threshold phenomena," Phys. Rev. **C61**, 014001 (2000).

[Ya00b] H. Yamamura *et al.*, Nucl. Phys. **A670**, 293 (2000).

[Ze00] B. Zeidman *et al.*, given at 7th International Conference on Hypernuclear and Strange Particle Physics (HYP 2000), Torino, Italy, 23-27 Oct 2000. To be published in Nucl. Phys. A.

3.6 E93-026

A Measurement of the Electric Form Factor of the Neutron through $\vec{D}(\vec{e}, e'n)p$
D.B. Day and J.H. Mitchell, Spokespersons

3.6.1 Introduction

The magnetic moments measurements by Otto Stern in 1934 were the first evidence that the neutron and the proton were composite particles, ones with internal structure. Without compositeness, one would expect the magnetic moment of the proton to be one nuclear magneton and that of the neutron to be zero.

The source of the nucleon anomalous magnetic moments is the strong interaction which gives rise to complex electromagnetic currents of quarks and antiquarks in the nucleon.The non-zero value of the neutron's magnetic moment implies that the neutron must have a charge distribution. Precise knowledge of this charge distribution will give important information about the strong force that binds quarks together in neutrons and protons and other composite particles. The distribution of the charge is contained in an experimentally determined quantity, G_E^n, the electric form factor, a function of momentum transfer.

In E93-026 it was proposed to extract G_E^n by measuring the spin-dependent part of the elastic electron–neutron cross section. A measurement of the asymmetry in the quasielastic scattering of longitudinally polarized electrons from polarized deuterium nuclei in deuterated ammonia (ND_3) can determine the product $G_E^n \cdot G_M^n$.

In one-photon-exchange the differential coincidence cross section for inelastic polarized electron-polarized deuteron scattering is written as [1]

$$\sigma \approx \sigma_0(1 + hP_1^d A_{ed}^V)$$

where σ_0 is the unpolarized cross section and A_{ed}^V is the electron-deuteron vector asymmetry. respectively. Here P_1^d is the target vector polarization and h is the beam helicity times the electron polarization degree (P_b). A_{ed}^V has been shown to be of special interest [1, 2] when measured in kinematics that emphasize quasi free neutron knockout where it is especially sensitive to G_E^n and relatively insensitive to the nucleon–nucleon (NN) potential describing the ground state of the deuteron, to meson exchange currents (MEC) and to final state interactions (FSI). In $\vec{\mathrm{D}}(\vec{\mathrm{e}},\mathrm{e}'n)p$ A_{ed}^V is responsible for an experimental asymmetry, ϵ, when the helicity of the beam or the target polarization are reversed. The magnitude of the experimental asymmetry, ϵ, depends on the polarization of the beam and target, and through A_{ed}^V on the kinematics and the orientation of the polarization of the target.

The connection between the physics asymmetry and G_E^n can be seen clearly for a (imaginary) vector polarized target of free neutrons with the polarization in the scattering plane and perpendicular to $\vec{q}$. In this case the experimental beam target asymmetry A_{en}^V [3] can be related to G_E^n by

$$A_{en}^V = \frac{-2\sqrt{\tau(\tau+1)}\tan(\theta_e/2)G_E^n G_M^n}{(G_E^n)^2 + \tau[1+2(1+\tau)\tan^2(\theta_e/2)](G_M^n)^2}$$

where $\tau = Q^2/4M_n^2$, and θ_e is the electron scattering angle. A_{en}^V is related to the counts asymmetry $\epsilon = (L-R)/(L+R)$, where L, R are charge normalized counts for opposite beam helicities (or target polarizations) by $A_{en}^V = \epsilon(P_{\mathrm{beam}}P_{\mathrm{neutron}}f)$, where f is the dilution factor due to scattering from materials other than polarized neutrons.

3.6.2 Experiment Status

E93-026 took data in the summer and early fall 1998 in Hall C which provided a measurement of G_E^n at $Q^2 = 0.5(\mathrm{GeV/c})^2$. After a brief discussion of the experimental technique we present the prelimimary results.

The arrangement of the experiment in Hall C is given in Figure 1.

Polarized electrons(with pseudorandom reversal of the helicity at 1 Hz) from the accelerator were delivered to Hall C at 2.725 GeV and a current of $\approx$ 100na. The beam polarization was measured at regular intervals in Møller polarimeter [4] just upstream of the target. The average beam polarization for the data reported here was measured to be 77.6% $\pm$0.21% (stat.) The beam was rastered over the face of the target cylinder in order to prevent localized heating of the target material and to insure uniform irradiation of the

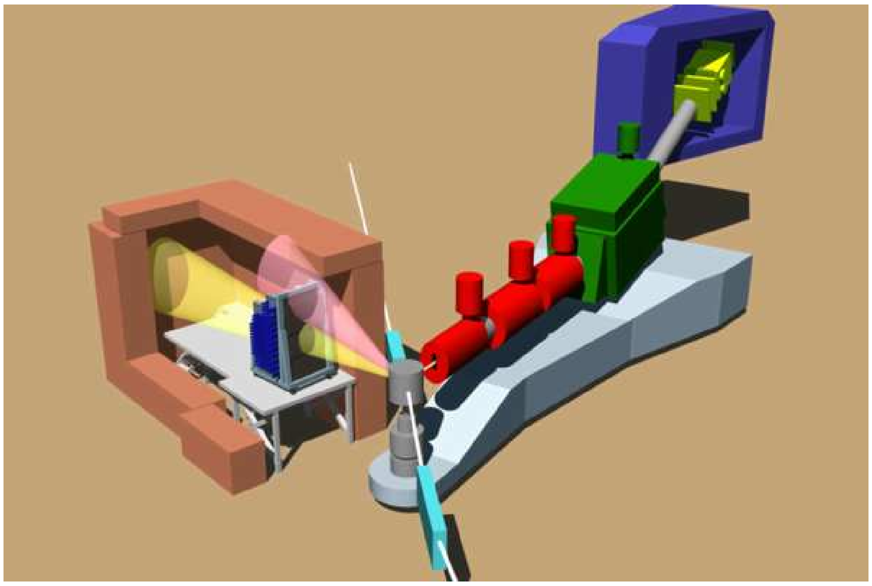

Figure 1: Experimental arrangement in Hall C with cutaway of the neutron detector. The scattered electrons were detected in the HMS (right) and the neutrons and protons were detected in a scintillator array (left). The cones are intended to represent the neutron and protons leaving the target.

target material. The beam position was recorded by a secondary emission monitor (SEM) [5]. A three magnet chicane compensated for the deflection of the electrons by the polarized target magnet.

The beam was scattered from a polarized target[6] of $^{15}ND_3$. The magnetic field was in the horizontal plane with the field oriented at 151.6° with respect to the beam line and perpendicular to the central $\vec{q}$. The material was polarized by driving forbidden transitions in the free electron - deuteron system with 140 GHz microwaves. The polarization was measured continuously via NMR and (P_1^d) averaged $21\% \pm 1\%$.

Electrons were detected at 15.7° in Hall C's High Momentum Spectrometer (HMS). A large solid angle array of plastic scintillators provided for both neutron and proton detection. It consisted of 2 planes of thin (0.5 cm) 1.6 m by 11 cm veto paddles and 5 planes of 10 cm by 10 cm by 1.6 m bars. The detector was housed in a large thick walled concrete hut closed on all sides except that facing the target. Each bar and paddle had a phototube at each end to allow good position and timing resolution. The time resolution was determined from the

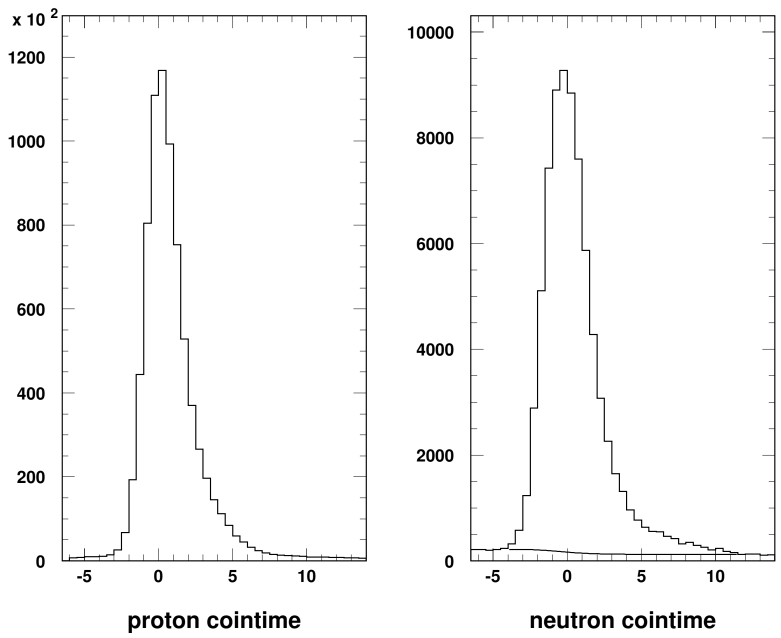

Figure 2: Measured meantime spectra for $(e, e'p)$ (left) and $(e, e'n)$ (right) events. A fit to the accidental background for the neutron events is shown.

time of flight peak of the gammas (from π^0 decay) in the meantime spectrum and was found to be 450 ps (σ). This gave an energy resolution of 16.5 MeV that in combination with the scattered electron energy allowed us to eliminate events associated with pion production. Despite the open geometry of the detector and a luminosity in excess of 10^{35} the system was remarkably free of accidental coincidences – See Fig. (2)

The electron-nucleon trigger was formed by a coincidence between the electron and a hit in any one of the 5 bar planes. Neutrons were identified by inspection of the thin paddles. Those events with no hits in the paddle planes along the track to the target, surviving a narrow timing cut and within a narrow range of invariant mass W around the quasielastic peak were taken to be neutrons.

The experimental asymmetry was diluted by scattering from materials other than polarized deuterium nuclei. This includes the nitrogen in $^{15}ND_3$, the liquid helium in which the target was immersed, the NMR coils, and target entrance and exit windows. A Monte Carlo was developed[7] to aid in the determination of the dilution factor and to perform the

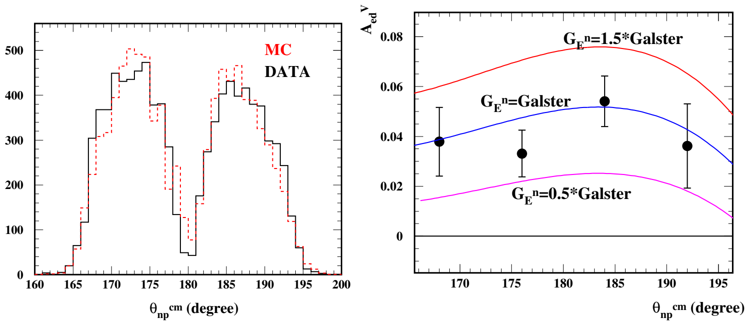

Figure 3: A comparison between the data and the simulation (with identitcal cuts – see text) in θ_{np}^{cm} (the angle between the neutron and proton in the center of mass), for (e,e'n) from the $^{15}ND_3$target. Figure on right is the acceptance averaged A_{ed}^{V}, theory and experiment.

detector averaging of the theoretical asymmetries. It was based on MCEEP[8] and included the neutron detector geometry and approximate efficiencies, the target magnetic field effects on the scattered electrons, the beam raster and radiative effects. The quasielastic scattering from all the target materials was simulated in the Monte Carlo. The good agreement of the distributions indicates that quasielastic scattering is the dominant process for events meeting our selection criteria. See the left hand panel in Fig. 3.

3.6.3 Results

In order to extract G_E^n the corrected experimental asymmetry was compared to the Monte Carlo simulation that folds theoretical calculations of the asymmetry with the event distribution across the acceptances of the electron spectrometer and the neutron detector. The theoretical A_{ed}^{V} values were calculated using the approach of [1, 2]. The calculations are based on a non-relativistic description of the $n-p$ system in the deuteron, using the Bonn R-Space NN potential [9] for both the bound state and the description of final state interactions (FSI). The full calculations include also sub-nuclear degrees of freedom such as meson exchange currents (MEC) and isobar configurations (IC) as well as relativistic corrections. The grid of asymmetries was calculated for 3 values of G_E^n given by the Galster parameterization[10](with $p = 5.6$) (with the magnitude set by an overall scale parameter of 0.5, 1 or 1.5.) and the dipole parametrization for G_M^n.

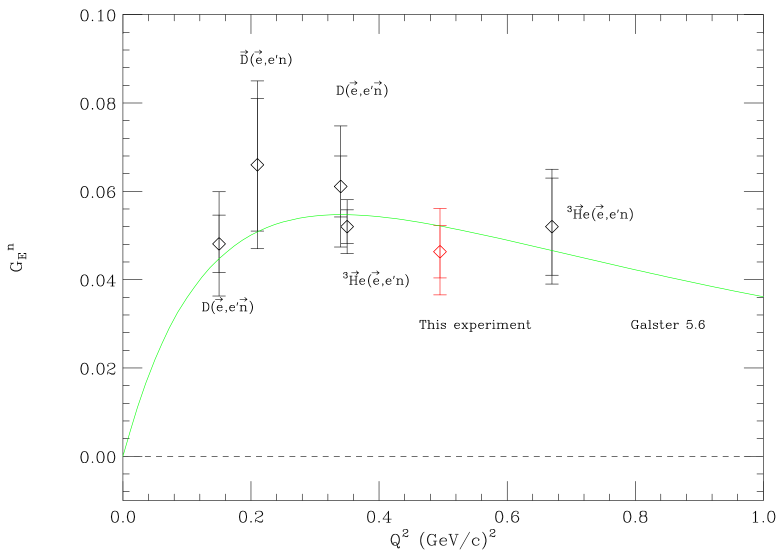

Figure 4: Comparison of present experiment with data from recent polarized scattering measurements, left to right [14, 15, 16, 17, 18]. FSI corrections have been made for for all except [18] for which FSI are thought to be modest. Data from Ref. [17] has been corrected for FSI [19]. The solid line is the parametrization ($p = 5.6$) of Galster [10]

The MC simulation averaged the asymmetry over all kinematic variables except the one under investigation. A comparison is shown in Fig. 3. The detector-averaged theoretical values of A^V_{ed} were obtained for intermediate scale factors by a linear interpolation. The resulting value for G^n_E at $Q^2 = 0.495$ (GeV/c)^2 is $G^n_E = 0.04632 \pm 0.00616 \pm 0.00384$ where the first uncertainty is statistical and the second is the systematic one. Our measurement is compared to G^n_E measurements from other polarized experiments [14, 15, 16, 17, 18] in Fig. 4. A draft to be submitted for publication of these data has been prepared.

The next run of E93-026 is scheduled for the summer and fall of 2001. This run will allow a factor of two improvement in the statistics at $Q^2 = 0.5$ (GeV/c)^2 and an extension of the measurement to $Q^2 = 1.0$ (GeV/c)^2.

References

[1] H. Arenhövel, W. Leidemann and E. L. Tomusiak, Phys. Rev. **C46**, 455 (1992).

[2] H. Arenhövel, W. Leidemann and E. L. Tomusiak, Z. Phys. **A331**, 123 (1988).

[3] T. W. Donnelly and A. S. Raskin, Ann. Phys. (New York) **169**, 247 (1986); **191**, 81 (1989).

[4] M. Hauger *et al;* "A high precision polarimeter", nucl-exp/9910013. To be published in Nucl. Instr. and Meth.

[5] M. Steinacher and I. Sick, Nucl. Instr. and Meth., **A455/3**, 759 (2000).

[6] D. Crabb and D. Day, Nucl. Instr and Meth. **A356** 9, (1995), T.D. Averett *et al.* Nucl. Instr. and Meth. **A427**, 440 (1999).

[7] H. Zhu, Ph.D. Thesis, University of Virginia, August 2000. Details of the analysis can be found therein, available at http://galileo.phys.virginia.edu/ hz5w/thesis.pdf.

[8] P. Ulmer, "Monte Carlo for Electro-Nuclear Coincidence Experiments, MCEEP, version 3.3 March 2000.

[9] R. Machleidt, K. Holinder and Ch. Elster, Phys. Rep. **149**, 1 (1987).

[10] S. Galster *et al.,* Nucl. Phys. **B32**, 221 (1971).

[11] J. Jourdan in Proceedings of the XVIIth European Conference on Few-Body Problems in Physics, Évora 2000.

[12] H. Anklin, *et al;* Phys. Lett B. **336**, 313 (1994), H. Anklin, *et al;* Phys. Lett. B **428**, 248 (1998).

[13] W. Xu, *et al.*, Phys.Rev.Lett. **85**, 2900, (2000).

[14] C. Herberg *et al;* Eur. Phys. J **A5**, 131, (1999).

[15] I. Passchier *et al;* Phys. Rev. Lett. **82**, 4988 (1999).

[16] M. Ostrick *et al.*; Phys. Rev. Lett. **83**, 276 (1999).

[17] J. Becker *et al;* Eur. Phys. J **A6**, 329, (1999).

[18] D. Rohe, *et al;* Phys. Rev. Lett. **83**, 4257 (1999).

[19] J. Golak, *et al.*, arXiv:nucl-th/0008008, 4 Aug 2000.

3.7 E93-038

The Electric Form Factor of the Neutron from the ^{2}H($\vec{e}$,e'$\vec{n}$)p Reaction
R. Madey, Spokesman, and S. Kowalski, Co-Spokesman

3.7.1 Introduction

This experiment is designed to extract G_{En}, the electric form factor of the neutron, from the polarization-transfer reaction ^{2}H($\vec{e}$,e'$\vec{n}$)p. In quasi-elastic scattering from a neutron in deuterium, an incident polarized electron transfers polarization to the neutron. The neutron polarization vector lies in the scattering plane: The longitudinal component is parallel to the direction of the neutron momentum, and the sideways component is perpendicular to the neutron momentum direction. The longitudinal polarization is proportional to the square of the magnetic form factor G_{Mn} divided by the unpolarized cross section; the sideways component is proportional to the product $G_{En}G_{Mn}$ divided by the unpolarized cross section We use a neutron polarimeter to measure the scattering asymmetry from each component. The neutron polarimeter is designed to measure the scattering asymmetry from a transverse polarization; accordingly, to measure the scattering asymmetry from the longitudinal component, it is necessary to use a dipole magnet [Charybdis] to precess this component through 90 degrees. The ratio g [= G_{En}/ G_{Mn}] is proportional to the ratio of the scattering asymmetry $A_{S'}$ from the sideways component to the scattering asymmetry $A_{L'}$ from the longitudinal component. The proportionality factor is a kinematic factor.

A schematic diagram of the neutron polarimeter is shown in Fig. 1. It consists of 20 detectors in the front array and 12 detectors in each of two rear arrays for a total of 44 detectors. A double layer of veto/tagger detectors is located ahead of the front array, and another set of tagger detectors is located behind the front array. This neutron polarimeter was designed specifically for E93-038. To permit high luminosity, the dimensions of each of the 20 detectors in the front array are 10 cm$\times$10 cm$\times$100 cm, and the detectors in each rear array are shielded from the direct path of neutrons from the target. A prototype polarimeter with larger detectors in the front array was tested at Saturne with polarized neutrons of various energies. The analyzing powers and efficiencies extracted from the Saturne measurements

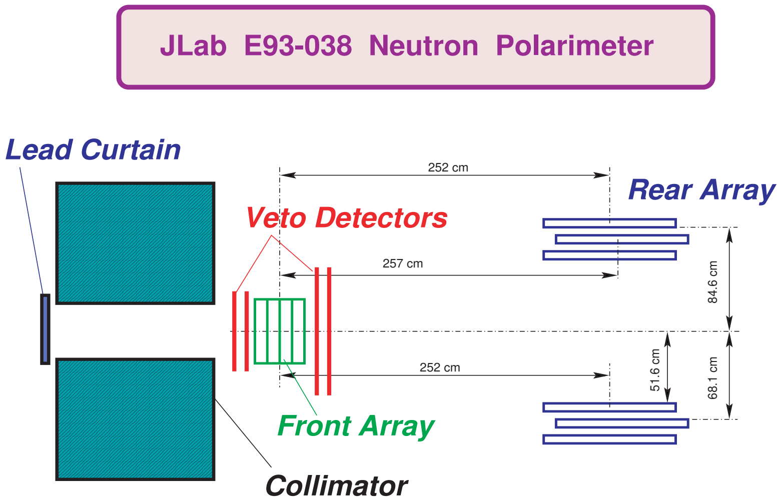

Figure 1: Schematic diagram of the neutron polarimeter.

permitted projections of rates and statistical uncertainties for E93-038.

3.7.2 Experiment Status

Installation of the neutron polarimeter and its shield enclosure took place during the summer of 2000. Commissioning began in September. Running was interrupted for about six weeks to repair the cryotarget. During the period from November 3 to December 21, E93-038 was scheduled for a data acquisition time of 20 days [= 40 days at an overall efficiency of 50 %] at a beam energy of 2.33 GeV. During this running period for G_{En} at $Q^2 = 1.13$ $(\mathrm{GeV/c})^2$, we obtained a total beam charge of 54 Coulombs at a nominal beam polarization of 64.5 %. The product of the beam charge and the square of the beam polarization represents a figure-of merit [FOM] for delivery of usuable beam. The *delivered* FOM of 22.4 Coulombs fell short of the *scheduled* FOM of 34 Coulombs for a beam current of 35 microAmperes at 75 % polarization. For the *delivered* FOM at $Q^2 = 1.13$ $(\mathrm{GeV/c})^2$, our rough projection at this early stage of the preliminary analysis is a relative statistical uncertainty $\Delta G_{En}/G_{EN} \approx 10$

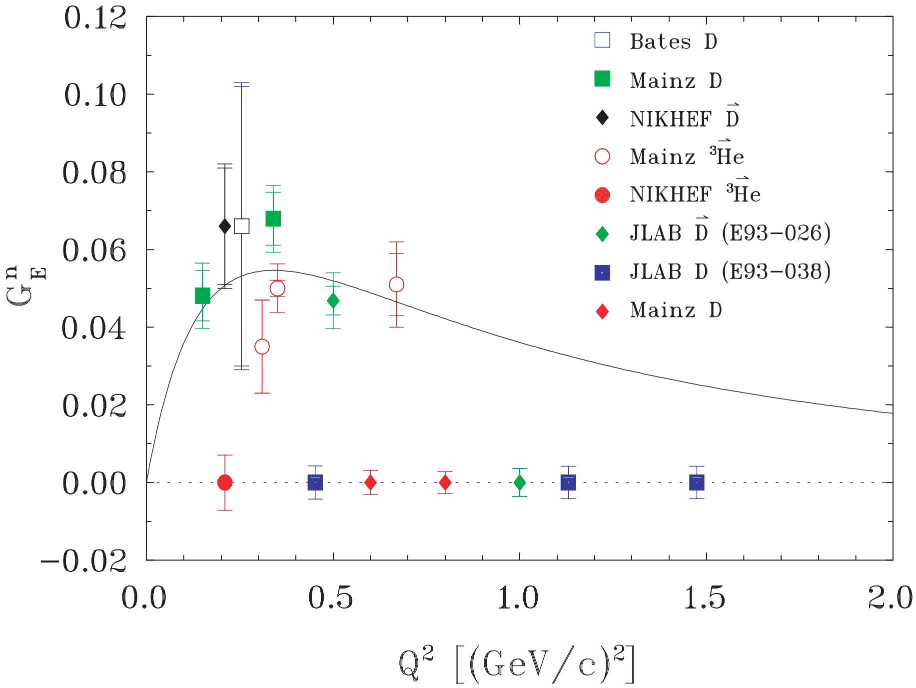

Figure 2: G_{En} vs Q^2 plot.

% for the Galster parameterization of G_{En}. We anticipate that the systematic uncertainty will be substantially less than the statistical uncertainty.

Running resumed on January 5, 2001, at an energy of 3.395 GeV and a beam polarization of 75 %. At $Q^2 = 1.48$ (GeV/c)^2 , the *scheduled* FOM is 40.8 Coulombs for 24 data-acquisition days at 35 microAmperes at 75 % polarization; the *scheduled* FOM for the third Q^2 point at 0.41 (GeV/c)^2 is 36.3 Coulombs for 12 data-acquisition days. Our current projections for the statistical uncertainties in our three Q^2 points are shown in the figure below of G_{En} vs Q^2 .

The preliminary analysis carried out thus far is based on extracting scattering asymmetries from all events incident on the polarimeter without requiring calibration of the timing relationships between detector elements and between the neutron and electron arms. To maximize the signal-to-noise ratio, it is necessary to produce a corrected time-of-flight spectrum that accounts for pathlength variations in both arms and for variations in the delay between event detection and signal generation. Each of the 44 scintillation detectors in the front and rear arrays has a photomultiplier tube on each end of the long axis. The difference between the TDC signals from the two ends of a detector determines the hit position, while the average determines the event time.

The polarimeter functions as a proton polarimeter when we require an event in both tagger planes ahead and behind the front array. We are able to determine the analyzing power of the proton polarimeter from a measurment of the scattering asymmetry from the sideways component of the proton polarization produced in the d($\vec{e}$,e'$\vec{p}$)n reaction. From this measurment, we calculate the ratio g_P [= G_{Ep}/G_{Mp}] as a function of the analyzing power and use the value of g_P measured in Hall A experiment 93-027 to extract the analyzing power. The proton data are a byproduct of E93-038. It is possible to extract g_P without knowing the analyzing power by using Charybdis to precess the proton polarization vector through a small angle in both directions and measuring the ratio of the scattering asymmetries. We require that the protons be deflected through a small angle so that they are incident on the polarimeter at ± 20 cm from the center.

3.7.3 Expected Results

We anticipate having some preliminary results for G_{En} in late 2001.

Many reports were prepared in preparation for E93-038. An index of these reports is appended. Listed below are two publications and one contribution to a conference.

References

[1] Fizika B 8, 35-40 (1999), Richard Madey and Thomas Eden, The Electric Form Factor of the Neutron by Recoil Polarimetry.

[2] R. Madey, A. Lai, and T. Eden, A New Neutron Polarimeter and Measurement of G_{En} from the $^2H(\vec{e}$,e'$\vec{n})^1$H Reaction, Eighth International Symposium on Po-

larization Phenomena in Nuclear Physics, AIP Conference Proceedings 339, 47-54 (1994).

[3] R. Madey and T. Eden, The Electric Form Factor of the Neutron by Recoil Polarimetry, International Conference on Nuclear and Particle Physics with CEBAF at Jefferson Lab, Dubrovnik, Croatia, 3-10 November 1998.

Index of JLAB E93-038 Reports

- 01/29/2001 E. Crouse, R. Madey, J.J. Kelly, and A. Semenov. Cumulative Probabilities as Function of the Energy of Various Particles Incident on the Neutron Polarimeter in E93-038.
- 01/07/2001 C. Howell. Cable Map for Analog Signals.
- 01/07/2001 C. Howell. Cable Map for Timing Signals.
- 01/05/2001 W. Tireman. High Voltage Cabling.
- 12/22/2000 J. Roche, T. Reichelt. Hall C Moeller Measurements and the Contamination Problem.
- 10/26/2000 J.J. Kelly. Time Calibration Procedures for 93-038 Polarimeter.
- 10/13/2000 T. Reichelt. Spin Precession and Field Error in Charybdis.
- Draft: 10/12/2000 R. Madey and A. Semenov. Statistical Uncertainties Projected for Updated JLab E93-038.
- 09/28/2000 J.J. Kelly. Corrected TOF algorithm for 93-038.
- 09/12/2000 A. Ahmidouch. Map of Charybdis. and some comments.
- 09/01/2000 J.J. Kelly. GenGen: Event Generator for G_{En} Using the d($\vec{e}$,e'$\vec{n}$)p Reaction.
- Draft: 08/29/2000 W.M. Zhang, R. Madey, A. Ahmidouch et al. Calibration of a Neutron Polarimeter in the 0.2 to 1.1 GeV Region.
- 08/24/2000 C. Howell. Electronics for E93-038.
- Draft: 08/23/2000 S. Taylor. Some Notes About CHARYBDIS.
- 07/07/2000 T. Reichelt. On the Use of CHARYBDIS.
- Draft: 07/11/2000 S. Taylor. Pion Contamination from Delta (1232) Channels.
- 06/07/2000 Chenyu Yan. Test Results of Cluster Identification Subroutines.
- Draft: 06/07/2000 R. Madey, A. Semenov, and P. Degtiarenko. Beam Current Limitations for Updated JLab E93-038.
- 05/25/2000 S. Tajima. Physics Quantity Reconstruction in E93038 Engine.
- 05/25/2000 S. Tajima and Chenyu Yan Cluster and Neutron Hit Identification.
- 05/02/2000 S. Churchwell. Collimator Design for Pion Photoproduction.
- 04/05/2000 A. Ahmidouch. How To Fix The DAQ Life-Time For The Saturne Data.

- Draft: 03/28/2000 S. Churchwell. Timing Calibration.
- Draft: 02/18/2000 S. Churchwell. E93-038 G_{Mn} Counting Rate Estimation.
- 02/21/2000 S. Tajima. Variable and Subroutine Names for E93038 Analyzer.
- Draft: 02/02/2000 R. Madey and A. Semenov. Statistical Uncertainties Projected at Q^2 = 0.41, 1.13, and 1.51 $(GeV/c)^2$ for Updated JLab E93-038.
- 01/18/2000 S.T. Churchwell. Three Body Kinematics.
- 01/18/2000 S.T. Churchwell. Arenhoevel Coordinates and Conversions for Deuteron Electro-disintegration.
- Draft: 11/19/1999 J.J. Kelly. Model of Scintillator Response.
- Draft: 11/09/1999 C.R. Howell and R. Madey. Neutron Detection Efficiency Measurement for G_{Mn} in JLab E93-038: A Feasibility Study.
- 08/30/1999 D. Barkhuff. A Study of Neutron Spin Transport In the Charybdis Dipole Magnet.
- 08/11/1999 C. Yan. Study of Optical Transmission of HMS in Different Tuning Modes for Experimental Design of G_{En} and G_{Mn} (JLab-TN-99-025).
- 07/13/1999 T. Eden. A Simulation Program for Neutron Polarimetry.
- Draft: 06/23/1999 R. Madey and T. Eden. Beam Current Limitations for JLab E93-038.
- Draft: 06/16/1999 R. Madey and A. Semenov. Statistical Uncertainties Projected for JLab E93-038 with HMS in the Reverse-Quad Mode and in the Intermediate Position.
- Draft: 06/11/1999 R. Madey, T. Eden, and A. Ahmidouch. False Asymmetry from the Two-Step Process: $^2H(\vec{e},e'\vec{p})$ + $Pb(\vec{p},\vec{n})$ and Measurement of the Proton Electric Form Factor.
- Draft: 06/04/1999 R. Madey and T. Eden. Optimization of Kinematic Conditions for JLab Experiments 93-038 and 93-026 to Extract Nucleon Form Factors from Polarized Electrons on Polarized [E93-026] and Unpolarized [E93-038] Deuterium Targets.
- 08/02/1995 R. Madey. JLab E93-038 Abstract.

3.8 E94-014

HIGH Q^2 ELECTROPRODUCTION OF THE $\Delta(1232)$

V. Frolov and P. Stoler for E94014 Collaboration

Electroproduction of the $\Delta(1232)$ resonance was measured via the reaction $p(e,e'p)\pi^0$ in the previously inaccessible momentum transfer range $Q^2 = 2.8$ and 4 GeV^2/c^2, enabling the extraction of electromagnetic multipoles with high statistical precision. Results were reported in [Fr-99]. The electrons were detected by the SOS spectrometer, and protons were detected by the HMS spectrometer in Hall C. Identification of π^0's was accomplished by missing mass reconstruction on an event by event basis, as were the kinematic variables Q^2, W, and the resonance c.m. decay angles θ_{cm} and ϕ_{cm}. Since the protons emerge in a rather narrow cone around $\vec{q}$, cm. coverage was a significant part of 4π. As an example of the overall quality of our data, Fig. 1 shows the $\theta_{c.m.}$ distributions at $Q^2 \sim 2.8$ GeV^2/c^2 for a subset (20%) of intervals of W and ϕ_{cm}. The $Q^2(\approx t)$ dependence of the extracted amplitudes M_{1+}, E_{1+}/M_{1+}, S_{1+}/M_{1+} are shown in Figures 2 3, and 4.

The evolution from low-to-high Q^2 is characterized by different reaction mechanisms. At asymptotically high Q^2 (high t) the transition to pQCD is expected. At low Q^2 the $N \to \Delta$ transition is primarily M_{1+}, with the small E_{1+} and S_{1+} which are extremely sensitive to the reaction mechanism. At $Q^2 = 0$ the most recent data from Mainz [Be-95] and BNL [Bl-92] show that $E_{1+}/M_{1+} \sim -.025$. At very high Q^2, according to valence $pQCD$ only helicity conserving amplitudes should contribute, leading to the prediction $E_{1+}/M_{1+} \to 1$. Figure 3 shows E_{1+}/M_{1+} vs. t, including the measured data from E94-014 as well as the recent low t results. Also, the ratio S_{1+}/M_{1+}, shown in Figure 4, is expected to asymptotically level off. Clearly, the data do not exhibit the increase expected in the eventual evolution to $pQCD$.

Recently, high t form factors have been shown to be related to moments of skewed, or generalized parton distributions (SPDs), which are directly related to the transverse momentum distributions of the partons, especially at high $k_\perp$, where parton correlations are expected to be significant. For the $N \to \Delta$ the relationship is

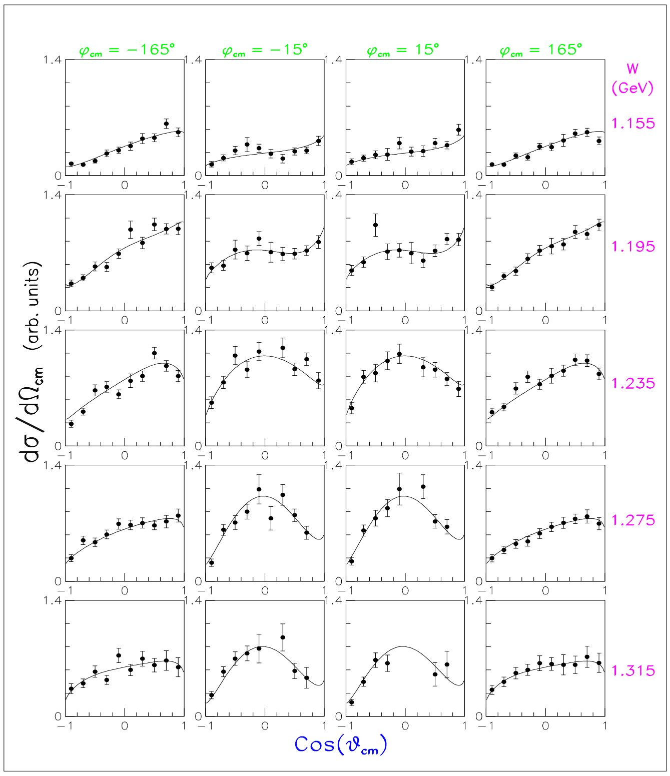

Figure 1: Center of mass angular distribution for π^0 production at the delta resonance, for selected kinematic intervals of W and out of plane angles ϕ_{cm} at Q^2= 2.8 GeV^2/c^2, obtained in experiment 94-014. The curves represent a global fit in terms of multipoles, up to p waves, and assuming M_{1+} dominance.

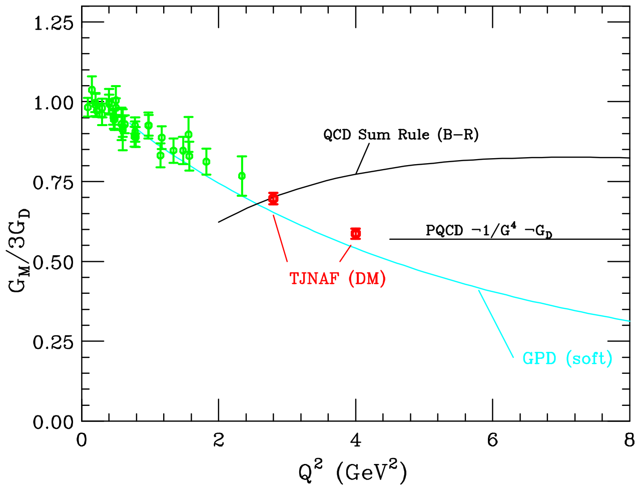

Figure 2: The magnetic form factor G^*_M divided by the dipole $G_D = 3/(1+t/0.71)^2$. The data at Q^2 = 2.8 and 4 GeV^2/c^2 are the results of E94-014. The lower Q^2 data are a compilation of older data by [Ka-99]. The curve labelled GPD is the result using a GPD model discussed in the text. The horizontal curve is what one expects from $pQCD$ scaling.

Figure 3: The result of the $Re E^*_{1+} M_{1+}/|M_{1+}|^2$ measurement of E94-014. The data represent the most recent MAID [MAID-2000] fit to E94-014 plus the the world's lower Q^2 data in a self-consistent way. Also shown are the results of measurements at Q^2=0 from Mainz [Be-95] and LEGS [Bl-92]
.

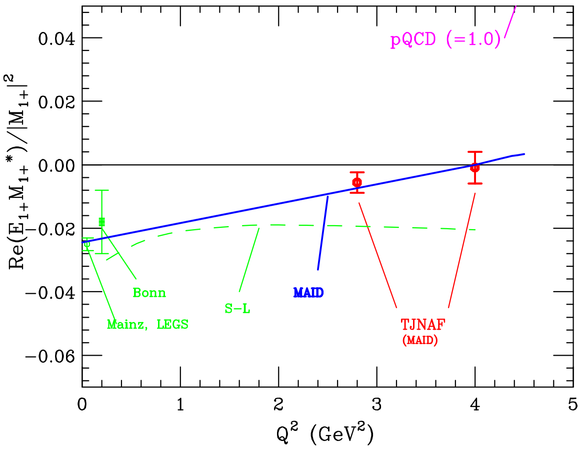

Figure 4: The result of S_{1+}/M_{1+} measurement of E94-014 at Q^2 = 2.8 and 4 GeV^2/c^2. At the lower Q^2 are recent data from Bates and Bonn. All data are the results of MAID [MAID-2000] fits to the compiled recent world data. Fits using *dynamic models* [MAID-2000, Sa-00] yield somewhat different results.

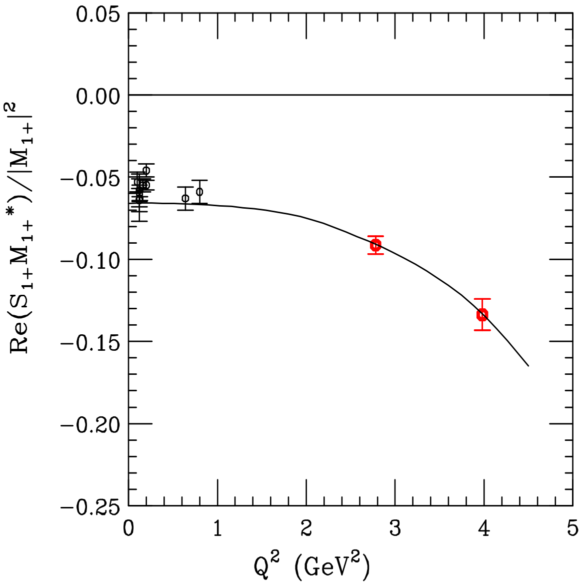

$$G_M^* = \int_{-1}^{1} \sum_q H_M^q(\xi, x, t)dx \quad G_E^* = \int_{-1}^{1} \sum_q H_E^q(\xi, x, t)dx \quad G_C^* = \int_{-1}^{1} \sum_q H_C^q(\xi, x, t)dx$$

where G_M^*, G_E^* and G_C^* are magnetic, electric and Coulomb transition form factors [Jo-79], and H_M^q, H_E^q, and H_C^q are axial (isovector) GPDs. In this region of t the small E_{1+} amplitude is a very sensitive constraint on GPDs since it involves delicate cancellations of larger amplitudes. Significant theoretical work has begun to model them.

The results of experiment 94-014 shows that at least up to a t of 4 GeV^2/c^2 the reaction mechanism is dominated by soft physics. The magnetic form factor G_M^* actually falls faster with Q^2 ($\equiv t$) than the dipole form factor G_D. Figure 2 exhibits the current status of the $N \to \Delta$ magnetic form factor G_M^* divided by the dipole form $3/(1+t/0.71)^2$. For elastic scattering, Ref. [Ra-98] and Ref. [Af-00] utilize the following model for the soft GPD:

$$H^q \sim f^q(x) e^{\bar{x}t/4x\lambda^2}$$

where $f^q(x)$ is the usual longitudinal parton density obtained from inclusive DIS, and λ is a parameter related to $\sqrt{\langle k_\perp^2 \rangle}$.

With this simple model the t dependence of the elastic G_{MP} and G_{EP} can be reasonably and consistently fit up to $t \sim 5$ GeV^2/c^2, with $\langle k_\perp \rangle \sim 250$ MeV/c. For larger t the calculated G_M becomes progressively smaller than the data, presumably due to the onset of higher $k_\perp$ correlations. Figure 2 shows a fit to G_M^* using the GPD model of Refs. [Ra-98, Af-00] with a Gaussian $k_\perp$ distribution. The $\langle k_\perp \rangle \sim 180$ MeV/c implies that either the distribution of the $\Delta(1232)$ is softer than that for the proton, and/or the x dependence of the GPD for G_M^* must be different from that for G_M for elastic scattering. If one parameterizes the hard processes by a power law falloff the model GPD could be expressed as

$$H^q = f^q(x)\{e^{\bar{x}t/4x\lambda^2} + \sum_n c_n \frac{(\alpha_s/\pi)^{2n}}{t^{2n}}\} \equiv H^q_{soft} + H^q_{hard}$$

Since $G^*_{M(soft)}$ for the $\Delta(1232)$ is decreasing with t faster than $G_{MP(soft)}$ for elastic scattering, the contribution of $G^*_{M(hard)}$ may be observable at a lower, more accessible t than for the elastic form factor. This would manifest itself in a leveling off of the G^*_M/G_D vs t.

Current plans are to extend these measurements to $Q^2 = 7.5$ GeV^2/c^2 to see if the transition in all three amplitudes begins to approach that expected from the onset of hard mechanisms and a new regime of physics.

References

[Fr-99] V. V. Frolov, *et al. Phys. Rev. Lett.* **82**,45 (1999).

[Jo-79] H.F. Jones and M.D. Scadron, *Annals of Physics* 81, 1 (1979).

[Ra-98] Radyushkin AV. *Phys. Rev.* D58:114008 (1998)

[MAID-2000] D. Drechsel, O. Hanstein, S.S. Kamalov and L. Tiator, *Nucl. Phys.* A645, 145 (1999); http://www.kph.uni-mainz.de/T/maid/

[Be-95] R. Beck et al., *Phys. Rev. Lett.*, 78, 606 (1995)

[Bl-92] G. S. Blanpied et al., *Phys. Rev. Lett.*, 69, 1880 (1992).

[Ka-99] S.S. Kamalov and S. N. Yang, *Phys. Rev. Lett*83, 4494 (1999).

[Af-00] A. Afanasev, E-print: hep-ph/9910565; it "Proceeding of the JLAB-INT Workshop on Exclusive and Semi-Exclusive Processes at High Momentum Transfer", C.E. Carlson and A. Radyushkin, eds. World Scientific (2000).

[Sa-00] T.Sato and H.T-S. Lee, preprint, nucl-th/0010025, *Phys. Rev.* C ,to be published.

3.9 E94-014a

ELECTROPRODUCTION OF THE $S_{11}(1535)$ AT HIGH Q^2
The JLAB E94014 $S_{11}(1535)$ Collaboration
C.S. Armstrong and P. Stoler for the E94014 Collaboration

The $S_{11}(1535)$ is one of the most strongly excited N^* states over all Q^2, and is easily isolated because it is the only strong resonance that has a large branching fraction to the η. The electroproduction to the $S_{11}(1535)$ resonance was measured in Hall C via the reaction $p(e,e'p)\eta$ in the previously inaccessible momentum transfer range $Q^2 = 2.4$ and 3.6 GeV^2/c^2, enabling the extraction of the helicity conserving $A^p_{1/2}$. The results were reported in [Ar-99]. The electrons were detected by the SOS spectrometer, and protons were detected by the HMS spectrometer. Identification of ηs was accomplished by missing mass reconstruction on an event by event basis, as were the kinematic variables Q^2, W, and the resonance c.m. decay angles θ^* and ϕ^*. Since the protons emerge in a rather narrow cone around $\vec{q}$, cm., coverage was a significant part of 4π.

The five-fold differential cross section for the $e\,p \to e'p\,\eta$ process may be expressed as the product of the virtual photon flux Γ_v and the c.m. cross section for the electroproduction of the $p\eta$ pair: $d\sigma/d\Omega_e dE'_e d\Omega^*_\eta = \Gamma_v d\sigma/d\Omega^*_\eta$. From S-wave fits to the obtained angular distributions, the total cross section $4\pi d\sigma/d\Omega^*_\eta$ was calculated at each Q^2 point as a function of W. This cross section, which consists of resonant and nonresonant parts, was fitted with a relativistic Breit-Wigner shape plus a nonresonant background of form $B_{nr}\sqrt{W - W_{nr}}$. At both values of Q^2 the fitted value of the phenomenological nonresonant term was consistent with zero (with an uncertainty of 1% of the resonant term. Figure 1 shows the obtained resonant cross section as a function of W.

The energy-dependent resonance width $\Gamma(W)$ was parameterized in terms of the branching fractions b_η ($\equiv \Gamma_\eta/\Gamma_R$ at W_R), b_π, and $b_{\pi\pi}$. At present the Particle Data Group [PDG-98] gives an estimated range for the η branching fraction of $0.30 \le b_\eta \le 0.55$. Our results, taken together with previous inclusive [Ke-94] data gives $b_\eta = 0.55$ with $0.45 \le b_\eta \le 0.61$, with a 95% confidence level. Also, we obtain a full width $\Gamma_R = (154 \pm 20)$ MeV which agrees with the PDG estimate (≈ 150 MeV).

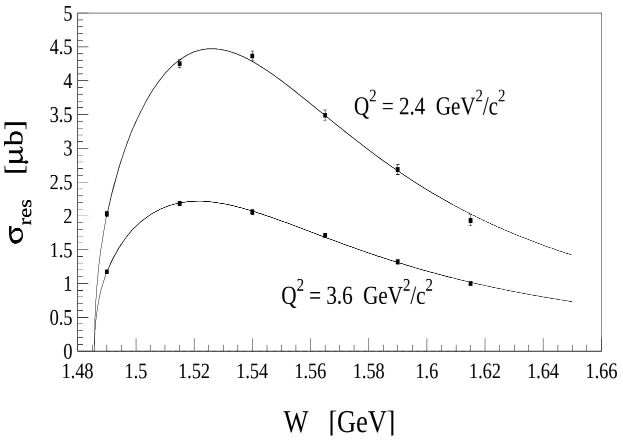

Figure 1: Fit to $\sigma_{\rm res}(W)$ for the two Q^2 points of this work (errors on the data are statistical only). Note the presence of the $p\,\eta$ threshold.

Neglecting resonances other than the $S_{11}(1535)$, we relate the amplitude $A^p_{1/2}$ to $\sigma_{\rm res}$ by

$$A^p_{1/2}(Q^2) = \left[\frac{W_R\,\Gamma_R}{2\,m_p\,b_\eta}\;\frac{\sigma_{\rm res}(Q^2,\,W_R)}{1+\varepsilon\,R} \right]^{1/2} \quad . \tag{1}$$

Here ε is the longitudinal polarization of the virtual photon, and $R = \sigma_L/\sigma_T$. For R we assumed a parameterization based on a quark-model calculation. The expected impact of the longitudinal-to-transverse ratio R on the final physics result is small: a 100% error in the assumed value [$\approx 4\%$ at $Q^2 = 2.4$ (GeV/c)^2] corresponds to an uncertainty of less than 1% in the quoted value of $A^p_{1/2}$.

Table 1 gives our final results. The uncertainties are systematic and statistical added in quadrature; for $A^p_{1/2}$ we included estimates for the uncertainties from Γ_R and b_η. Note that the upper bound on b_η given by [PDG-98].

Figure 2 shows the helicity amplitude results, along with points calculated from previous $e\,p \to e'p\,\eta$ data and some theoretical predictions. All data points in the figure, including previous results, were uniformly normalized using Eq. 1, assuming $\Gamma_R = 154$ MeV and $b_\eta = 0.55$; if either assumption is wrong, *all* data points will scale together. Not included for any of the data points in the figure are the uncertainties in Γ_R and b_η. Note the good agreement between the high-Q^2 point of the present work and the inclusive fit for $b_\eta = 0.55$;

Table 1: Results. The uncertainties are systematic (*including* estimated uncertainties in Γ_R and b_η for $A^p_{1/2}$) and statistical uncertainties are added in quadrature. The top $A^p_{1/2}$ result is for $Q^2 = 2.4$ (GeV/c)^2, the bottom is for $Q^2 = 3.6$ (GeV/c)^2. The 'best value' for b_η assumes S_{11} dominance at $Q^2 = 4$ (GeV/c)^2.

Quantity	Value
W_R (MeV)	1532 ± 5
Γ_R (MeV)	154 ± 20
$A^p_{1/2}$ (10^{-3} GeV$^{-1/2}$) at Q^2=2.4 GeV^2/c^2	50 ± 7
$A^p_{1/2}$ (10^{-3} GeV$^{-1/2}$) at Q^2=3.6 GeV^2/c^2	35 ± 5
$b_\eta = \Gamma_\eta/\Gamma_R$	≈ 0.55 (> 0.45 < 0.61); see text

assumption of a lower branching fraction shifts the data up to a value *g*reater than the inclusive fit, and assumption of a higher branching fraction shifts the data down to a value *l*ess than the inclusive fit.

The present result differs from previous work in both the strength and the slope of the $S_{11}(1535)$ form factor; most notably, we find a cross section 30% lower than that of Ref. [Br-84] [found by interpolating the results of this work to $Q^2 = 3$ (GeV/c)^2]. This difference is reduced in the amplitude by the square root relating $A^p_{1/2}$ to the cross section (Eq. 1). Although the present data were taken at a different value of ε than those of Ref. [Br-84], a longitudinal cross section is not responsible for the difference between the two measurements; value of $R \approx 2.3$ would be necessary to account for the discrepancy.

Of the various CQM curves shown in Figure 2, none exhibit a slope as small as that of the data. Those that indicate an amplitude at $Q^2 \sim 3$ (GeV/c)^2 roughly consistent with experimental data also predict excess amplitude at lower Q^2. Our data also have consequences for a recent coupled-channel model for the $S_{11}(1535)$ [Ka-95]; the proposed quasi-bound $K\Sigma$ (five quark) state is expected to have a form factor that decreases more rapidly than is observed. In summary, the measured magnitude *and* slope in $A^p_{1/2}$ vs. Q^2 is inconsistent with that predicted by any CQM based calculation.

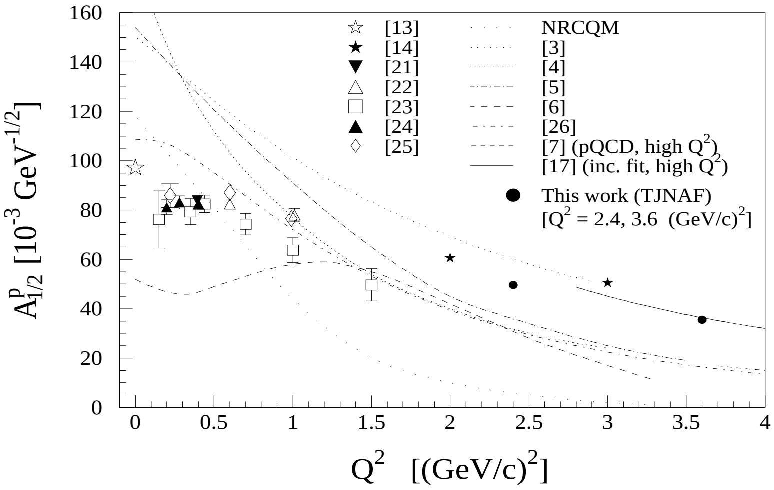

Figure 2: The helicity amplitude $A^p_{1/2}(Q^2)$ of the $S_{11}(1535)$, measured via $e\,p \to e'\,p\,\eta$, together with some theoretical predictions. (see ref. [Ar-99] for references). The curve from ref. 17 above is a fit to inclusive data [Ke-94].

Figure 3 shows the quantity $Q^3 A^p_{1/2}$ for the $S_{11}(1535)$, which is predicted by pQCD to asymptotically approach a constant at high Q^2. As has been pointed out elsewhere [Is-84], such scaling might be due to non-perturbative contributions. While there is no *strong* scaling evident in the figure, our data indicate that $Q^3 A^p_{1/2}$ may be approaching a constant value by $Q^2 \sim 5$ (GeV/c)^2.

While the new data exhibit no strong perturbative signature, they do have a Q^2 dependence that is markedly different than the older high-Q^2 measurement. Even given the new (lower) cross section obtained from this measurement, however, relativized versions of the quark model fail to reproduce the Q^2 dependence seen experimentally. We suggest this may be due to the onset of *hard* processes.

This work was supported in part by the U. S. Department of Energy and the National Science Foundation.

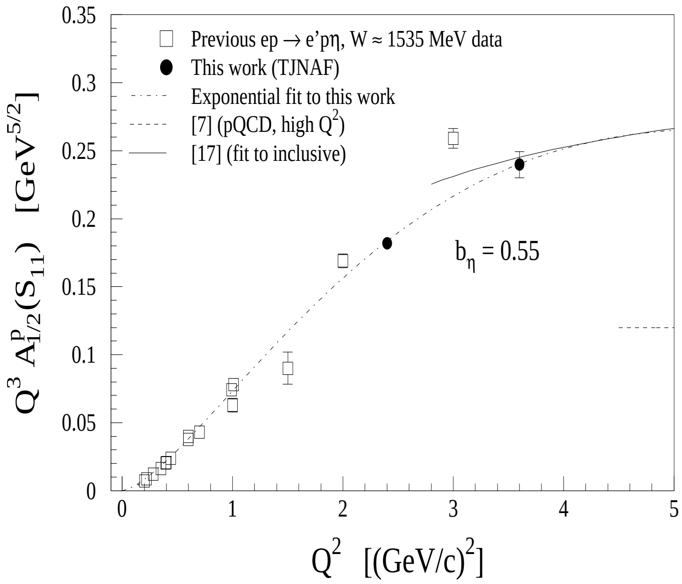

Figure 3: The quantity $Q^3 A^p_{1/2}(Q^2)$ for the $S_{11}(1535)$. See [Ar-99] for explanation.

References

[St-97] G. Sterman and P. Stoler, *Annual Reviews of Nuclear and Particle Science*, 47, 193 (1997); P. Stoler, Physics Reports**226**, 103 (1993).

[Ar-99] C. S. Armstrong,*et al.*, Physical Review **D60**, 52004, (1999).

[Br-84] F. Brasse *et al.*, Z. Phys. **C22**, 33 (1984).

[PDG-98] C. Caso *et al.*, European Physical Journal **C3**, 1 (1998).

[Ke-94] C. Keppel, Workshop on CEBAF at Higher Energies, Newport News, 1994, edited by N. Isgur and P. Stoler; L. M. Stuart, *et al.*, Phys. Rev. **D58**, 032003 (1998);P. Stoler, Phys. Rev. Lett. **66**, 1003 (1991); In the kinematic region of the present work, the Keppel and Stuart fits are in agreement at the 2% level.

[Ka-95] N. Kaiser *et al.*, Phys. Lett. **B362**, 23 (1995); Nuc. Phys. **A612**, 297 (1997).

[Is-84] N. Isgur and C. H. Llewellyn Smith, Phys. Rev. Lett. **52**, 1080 (1984); A. V. Radyushkin, Nucl. Phys. **A527**, 153c (1991).

3.10 E94-018

Measurement of the Deuteron Tensor Polarization at Large Momentum Transfers in $D(e, e'\vec{d})$ Scattering

Serge Kox, Elizabeth. J. Beise, and the t_{20} Collaboration
ISN, IN2P3-UJF, 38026 Grenoble, France
DAPNIA/SPhN, CEA/Saclay, 91191 Gif-sur-Yvette, France
University of Maryland, College Park, MD 20742, USA
TJNAF, Newport News, VA 23606, USA
M.I.T.-Bates Linear Accelerator, Middleton, MA 01949, USA
Rutgers University, Piscataway, NJ 08855, USA
Basel Institut fur Physik, Switzerland
LNS-Saclay, 91191 Gif-sur-Yvette, France
North Carolina A. & T. State University, Greensboro, NC 27411, USA
Florida International University, Miami, FL 33199, USA
IPNO, IN2P3, BP 1, 91406 Orsay, France
Yerevan Physics Institute, 375036 Yerevan, Armenia

3.10.1 Introduction

The deuteron serves as a testing ground for a variety of nuclear models. Because it is a spin one nucleus, the deuteron's electromagnetic structure is described by three form factors: the charge monopole G_C, charge quadrupole G_Q, and magnetic dipole G_M, related non-relativistically to the spatial distributions of charge, quadrupole deformation, and magnetization, respectively. In order to uniquely determine the three individual form factors, polarization measurements are necessary in addition to unpolarized cross section data. The separated form factors provide significant constraints on the different predictions, ranging from non-relativistic NN potential models to extrapolations from perturbative QCD. The experiment described here has determined the behavior of the charge form factor around its node with better accuracy than existing data and extended the determination of the two charge form factors G_C and G_Q to larger momentum transfers, and thus shorter distances, in the deuteron.

3.10.2 Experimental Setup

The E94–018 experiment was the first "Big Experiment" performed at Jefferson Laboratory. It required an overall period of nine months in 1997 for installation, data taking and dismounting in Hall C. This project was proposed by an international collaboration of 60 physicists, with 6 Ph.D. students, all of whom have now graduated.

An unpolarized continuous electron beam with a typical current between 80 and 120 μA was used together with a 12 cm long liquid deuterium target (corresponding to a 500 W power dissipation). This resulted in an average luminosity of about 3×10^{38} cm^{-2}s^{-1}. The scattered electrons were detected in the High Momentum Spectrometer (HMS) of Hall C, in coincidence with the outgoing deuterons. The reconstructed electron trajectories and momenta were used to calculate the vertex position at the primary target, the invariant mass and, with the beam energy, the deuteron kinetic energy.

The scattered deuterons were detected and their tensor polarization measured in a polarimeter using a second nuclear reaction. The deuterons were transported by a specially designed magnetic channel composed of warm magnets, three quadrupoles (including an original large asymmetric aperture one, SARAJEVO, constructed for this experiment) and one dipole. This magnetic channel was optimized to match the HMS acceptance and to maximize the number of elastic deuterons focused on the target of the polarimeter. Since the deuteron magnetic channel was set at a fixed angle, the six different Q^2 values were obtained by changing the beam energy from 1.4 GeV to 4 GeV and by changing the detection angle of the HMS spectrometer.

The elastic scattering events were selected by setting cuts on the primary vertex position, invariant mass, deuteron identification in the hadron arm and time coincidence measurement between the two arms. The tensor polarization observables were deduced from the asymmetries measured in the POLDER polarimeter [1] which was calibrated, prior to its arrival at JLab, with deuteron beams of known polarization at Saturne (Saclay (FR)). With a set of short dedicated runs, the elastic e-d diferential cross sections were also measured in this experiment at Q^2 values corresponding to the polarization measurement. This allowed the determination of the elastic structure function $A(Q^2)$ and required the use of a shorter target and of a small collimator to eliminate any mismatch between the two spectrometers. Finally runs were performed with specific field settings to measure a set of data for the coherent threshold π^0 electroproduction on deuteron. In both cases only the front part of the detection of the polarimeter was used, with no polarization determination for the deuteron.

3.10.3 Results

The final results obtained for the tensor polarization observables t_{ij} [2], for the elastic structure function $A(Q^2)$ [3], and for general parameterizations of the three elastic form factors of the deuteron over a large Q^2 range [4] are now published. In Figure 1 (left), our results for the t_{20} observable are displayed along with the existing world data [5, 6, 7, 8, 9, 10] and several recent theoretical predictions [12, 13, 14, 15, 16]. The error bars include both statistical and systematic errors.

As can be seen in the figure, our new results extend the world data set to much larger momentum transfer. When they overlap with the earlier Bates data [10], our data, even if they agree within the combined uncertainties, appear to be systematically above the Bates results. As a consequence, the electric form factor, G_C, extracted from a combined analysis of the t_{20} data and the elastic structure functions A and B, has its node located around 0.6 (GeV/c)^2, lower than that deduced from the Bates results (see Figure 1 (right)). This brings the node closer to what is expected when compared with that of the three-nucleon system [17].

We also performed, for the first time, a measurement of t_{21} approaching the region of the node of the magnetic form factor of the deuteron. The zero-crossing of this observable, which has been found to be near 2 (GeV/c)^2, corresponds directly to the node of G_M and is thus in good agreement with the location deduced from earlier measurements of $B(Q^2)$ [11].

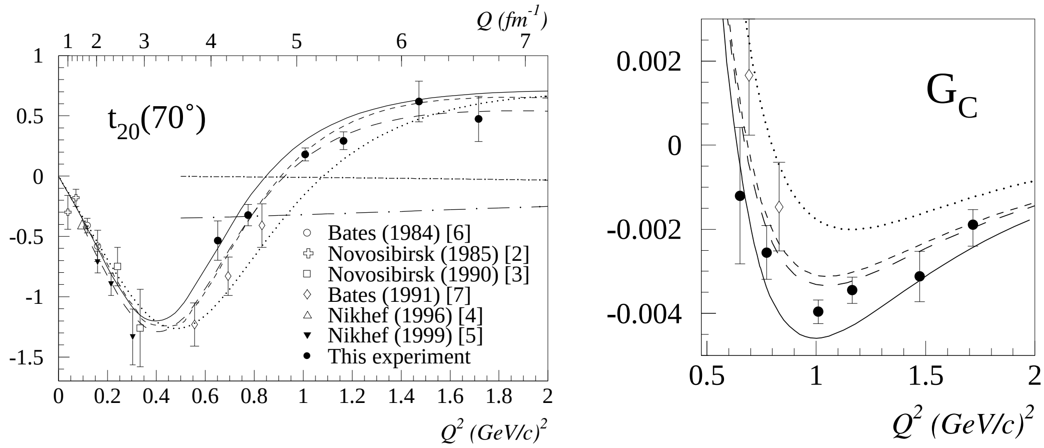

Figure 1: (left) t_{20} compared to theoretical predictions; dotted line (NRIA) and full line (NRIA+MEC+RC)[12]; relativistic models with dashed line[13] and long dashed line[14]; pQCD calculations with dashed-dotted line[15] and long dashed-dotted line[16]. (right) same as left but for the charge form factor G_C.

Several theoretical predictions are available based on different physical hypotheses and/or degrees of freedom (nucleonic and mesonic or quarks). Two pQCD calculations, predicting simple relations between the form factors of the deuteron, are shown by dashed-dotted curves in Figure 1. One [15] uses only the helicity-conserving matrix element of the electromagnetic current while the other [16] also includes the helicity-one-flip matrix element. Comparison with t_{20} measurements (and also t_{21} not shown here) clearly shows that both pQCD predictions fail to reproduce the new data even at our largest Q^2, contrary to the scale in four-momentum transfer given by the authors for the applicability of their calculations. Our data would require double helicity flip amplitudes as large as the non-flip amplitude in pQCD models to be reproduced.

The non-relativistic impulse approximation prediction (NRIA) [12] calculated using the Argonne v_{18} potential for the NN interaction, reproduces our new data quite well once meson exchange currents (MEC) and relativistic effects (RC) (solid curve) are included, which is consistent with expections based on results from the three-body system.

Finally, a lot of progress has been made this last decade in the relativistic and covariant description of the deuteron wave function. Many models are available and two of them are compared to the data. The dashed curve [13] uses the Gross equation, which is a three-dimensional reduction of the Bethe-Salpeter function and includes contribution of $\rho\pi\gamma$ exchange currents. The long dashed curve [14] is the prediction of a model developed in the framework of the explicitly covariant version of light front dynamics (LFD). Both are in good agreement with our data.

References

[1] S. Kox *et al.*, Nucl. Inst. Meth. **A346**, 527 (1994).

[2] D. Abbott *et al.*, Phys. Rev. Lett. **82**, 1379 (1999).

[3] D. Abbott *et al.*, Phys. Rev. Lett. **84**, 5053 (2000).

[4] D. Abbott *et al.*, Eur. Phys. Jour. **A7**, 421 (2000).

[5] V. F. Dmitriev *et al.*, Phys. Lett. **157B**, 143 (1985).

[6] R. Gilman *et al.*, Phys. Rev. Lett. **65**, 1733 (1990).

[7] M. Ferro-Luzzi *et al.*, Phys. Rev. Lett. **77**, 2630 (1996).

[8] M. Bouwhuis *et al.*, Phys. Rev. Lett. **82**, 3755 (1999).

[9] M. E. Schulze *et al.*, Phys. Rev. Lett. **52**, 597 (1984).

[10] M. Garçon *et al.*, Phys. Rev. **C49**, 2516 (1994).

[11] P. Bosted *et al.*, Phys. Rev. **C42**, 38 (1990).

[12] R. B. Wiringa *et al.*, Phys. Rev. **C51**, 38 (1995).

[13] J. W. V. Orden *et al.*, Phys. Rev. Lett. **75**, 4369 (1995).

[14] J. Carbonell and V. A. Karmanov, Eur. Phys. J. **A6**, 9 (1999).

[15] S. J. Brodsky and J. R. Hiller, Phys. Rev. **D46**, 2141 (1992).

[16] A. Kobushkin and A. Syamtomov, Phys. Rev. **D49**, 1637 (1994).

[17] H. Henning *et al.*, Phys. Rev. **C52**, 471–475 (1995).

3.11 E94-139

Measurement of the Nuclear Dependence
and Momentum Transfer Dependence
of Quasielastic (e,e′p) Scattering at Large Momentum Transfer

R.G. Milner and R. Ent, Spokespersons, and the E94-139 Collaboration.

3.11.1 Introduction

The Color Transparency (CT) conjecture by Mueller and Brodsky [1] has stimulated great interest. This QCD effect is predicted to have its most unexpected manifestation in (e,e′p) reactions at very high energy: under the right conditions, three quarks, each of which would have interacted strongly with a nuclear environment, pass right through it. CT was first discussed in terms of perturbative QCD considerations. However, later work [2] indicates that this phenomenon occurs in a wide variety of model calculations with nonperturbative reaction mechanisms. The existence of CT requires that high momentum transfer scattering should take place via selection of amplitudes in the initial and final state hadrons characterized by a small transverse size. Secondly, this small object should be 'color neutral' outside of this small radius in order not to radiate gluons. Finally, this compact size must be maintained for some distance in traversing the nuclear medium. Unambiguous observation of CT would provide a new means to study the strong interaction in nuclei.

In search of CT, measurements of the transparency of the nuclear medium to high energy protons in quasielastic A(p,2p) and A(e,e′p) and to ρ mesons in exclusive incoherent meson production have been carried out. Nuclear transparencies measured in A(p,2p) at BNL [3, 4] have shown a rise consistent with CT but a decrease at higher momentum transfer. The NE-18 A(e,e′p) measurements at SLAC [5] yield distributions in missing energy and momentum completely consistent with conventional nuclear physics predictions and the extracted transparencies exclude sizable CT effects up to $Q^2 = 7$ (GeV/c)^2. At FNAL the nuclear transparencies have been measured [6] in exclusive incoherent ρ^0 meson production from nuclei. Increases in the nuclear transparencies have been observed as the virtuality of the photon increases, as expected from CT. However, combining this data with earlier data from CERN obscures the issue [7]. Recently, FNAL experiment E971 reported a platinum/carbon ratio in high-p_t di-jet production a factor of seven times large than expected if soft physics would dominate, interpreted as evidence for CT effects [8].

3.11.2 Experiment Status

E94-139 measured the nuclear transparency in quasielastic (e,e′p) scattering from hydrogen, deuterium, carbon, and iron nuclei to the highest momentum transfers accessible at JLab in 1999. The experiment used beam currents up to 80 μA, and beam energies up to 5.6 GeV. Data were accumulated at Q^2 = 3.3, 6.1, and 8.1 (GeV/c)^2, the lowest Q^2 value providing a cross normalization with the highest Q^2 value of [9]. The SOS spectrometer was used for electron detection, and the HMS spectrometer for detection of the knocked-out proton. The kinematically overcomplete ^{1}H(e,e′p) reaction was used for energy and angle calibrations, in addition to determining the amount of proton absorption by comparing with simultaneously measured ^{1}H(e,e) elastic scattering events. The use of ^{2}H as a second calibration target proved a valuable check on the radiative correction procedures.

3.11.3 Results

Data analysis of the nuclear transparency results is final and ready for publication. Nuclear transparencies were determined by comparison to Plane-Wave Impulse Approximation (PWIA) calculations. Final results and older nuclear transparency results from Bates [10], SLAC [5], and JLab [9], are shown in Fig. 1. In addition, the results of a Glauber calculation of [11] are shown.

The A- and Q^2-dependence of the nuclear transparency data were investigated in a search for the onset of the CT phenomenon. The A-dependence can be parameterized as nuclear transparency $T(Q^2) = cA^{\alpha(Q^2)}$. Using deuterium, carbon, and iron data we find, within uncertainties, the constant c to be unity as expected, and no Q^2-dependence of α, up

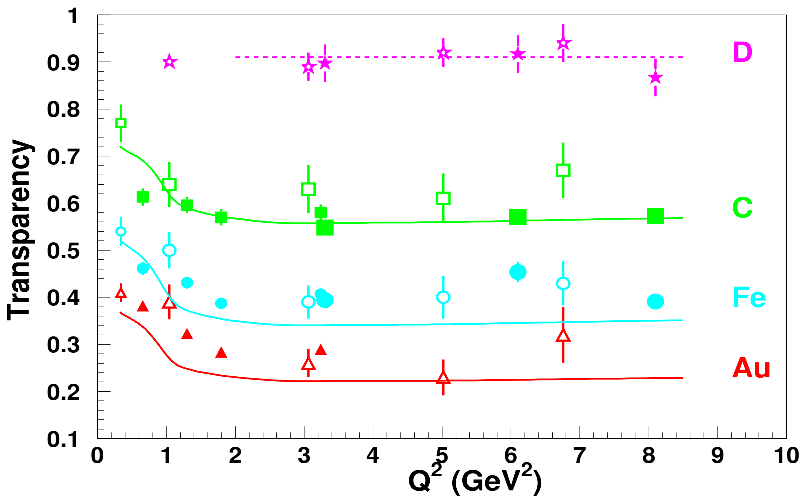

Figure 1: Transparency for (e,e$'$p) quasielastic scattering from D (purple), C (green), Fe (blue), and Au (red). Data from the present work are the large solid stars (D), squares (C), and circles (Fe), respectively. Previous JLab data (small solid squares, circles, and triangles) are from Ref. [9]. Previous SLAC data (large open symbols) are from Ref. [5]. Previous Bates data (small open symbols) at the lowest Q^2 on C, Ni, and Ta targets, respectively, are from Ref. [10]. The errors shown include statistical and systematic ($\pm$ 2.3%) uncertainties, but do not include model-dependent systematic uncertainties on the simulations. The solid curves shown from $0.2 < Q^2 < 8.5$ (GeV/c)^2 are Glauber calculations [11]. The dashed curve shown is a one-parameter fit to the D data for $2 < Q^2 < 8.5$ (GeV/c)^2, with a fit value of 0.91.

to $Q^2 = 8.1$ (GeV/c)^2. Alternatively, one can analyze the nuclear transparency data within a simple geometric Glauber model, using the effective proton-nucleon cross section as a free parameter [12]. We consistently find an effective proton-nucleon cross section of $\approx 70\%$ of the free proton-nucleon cross section, without a noticable Q^2-dependence.

In addition, we have performed a statistical analysis of the Q^2 dependence of the nuclear transparencies determined from the ^{12}C(e,e$'$p) reaction, in comparison with state-of-the-art calculations with and without CT effects [11, 13, 14, 15]. We find no statistical evidence for the onset of CT within our range of Q^2.

Present data analysis concentrates on deradiation of the A(e,e$'$p) spectra to obtain reduced cross sections (within a PWIA model equal to proton momentum distributions in the nucleus). In addition, this would give us an independent verification of the nuclear transparency for protons originating from, e.g., carbon's p- or s-shell, for which CT predictions vary. Alternatively, assuming the Final-State Interaction effects known, this would render spectroscopic factors for valence shells.

References

[1] A.H. Mueller, in *Proceedings of the Seventeenth Recontre de Moriond Conference on Elementary Particel Physics, Les Arcs, France, 1982*, edited by J. Tran Thanh Van (Editions Frontieres, Gif-sur-Yvette, France,1982); S.J.Brodsky, in *Proceedings of the Thirteenth International Symposium on Multiparticle Dynamics, Volendam, The Netherlands, 1982*, edited by W. Kittel *et al.* (World Scientific, Singapore, 1983).

[2] L. Frankfurt, G.A. Miller, and M. Strikman, Comments Nucl. Part. Phys. **21**, 1 (1992).

[3] A.S. Carroll *et al.*, Phys. Rev. Lett. **61**, 1698 (1988).

[4] Y. Mardor *et al.*, Phys. Rev. Lett. **81**, 5085 (1998).

[5] N.C.R. Makins *et al.*, Phys. Rev. Lett. **72**, 1986 (1994); T.G. O'Neill*et al.*, Phys. Lett. **B351**, 87 (1995).

[6] M.R. Adams *et al.*, Phys. Rev. Lett. **74**, 1525 (1995).

[7] M. Arneodo *et al.*, Nucl. Phys. **B429**, 503 (1994).

[8] E.M. Aitala *et al.*, hep-ex/0010044 (2000).

[9] D. Abbott *et al.*, Phys. Rev. Lett. **80**, 5072 (1998).

[10] G. Garino *et al.*, Phys. Rev. C **45**, 780 (1992).

[11] H. Gao, V.R. Pandharipande, and S.C. Pieper, private communications; V.R. Pandharipande and S.C. Pieper, Phys. Rev. C **45**, 791 (1992).

[12] P. Jain and J.P. Ralston, Phys. Rev. D **48**, 1104 (1993).

[13] N.N. Nikolaev *et al.*, Phys. Rev. C **50**, R1296 (1994).

[14] L.I. Frankfurt *et al.*, in Workshop on 'CEBAF at Higher Energies', Eds. N. Isgur and P. Stoler, Conf. Proc. p. 499 (1994).

[15] P. Jain and J.P. Ralston (private communication); B. Kundu, J. Samuelsson, P. Jain, and J.P. Ralston, Phys. Rev. D **62**, 113009 (2000).

3.12 E96-003

Two-Body Photodisintegration of the Deuteron at High Energy
R. J. Holt, spokesperson, and the E96-003 Collaboration

3.12.1 Introduction

The overall goal of the experiment is to map out the transition region from a nucleon-meson picture of deuteron photodisintegration to the quark-gluon picture. High energy two-body breakup of the deuteron is an excellent means to probe quark effects in nuclear reactions since the energy transfer to the constituents can be large. Previous experiments at JLab were limited to 4.0 GeV. However, these experiments found evidence for scaling at reaction angles near 90°. No evidence for scaling was found at forward angles. The objective of the experiment is to extend the cross section measurements for the d(γ,p)n reaction up to a photon energy of 5.5 GeV at forward angles as a test for scaling at the forward angles. The HMS in Hall C was used to detect photoprotons which emerged from a liquid deuterium target that was irradiated by bremsstrahlung photons.

3.12.2 Experiment Status

The experiment was successfully completed, the data were analyzed and a manuscript is being prepared.

3.12.3 Results - or Expected Results

Relatively large momentum transfer [Ho90] to the constituents can be obtained in exclusive photonuclear reactions at photon energies of a few GeV, because the absorbed photon delivers all of its energy to the constituents. One obvious signature of a QCD effect in the $d(\gamma, p)n$ reaction is a scaling behavior, for example, the constituent counting rule behavior. For deuteron photo-disintegration $\gamma d \rightarrow pn$ process, the constituent counting rule [Br73, Le73,

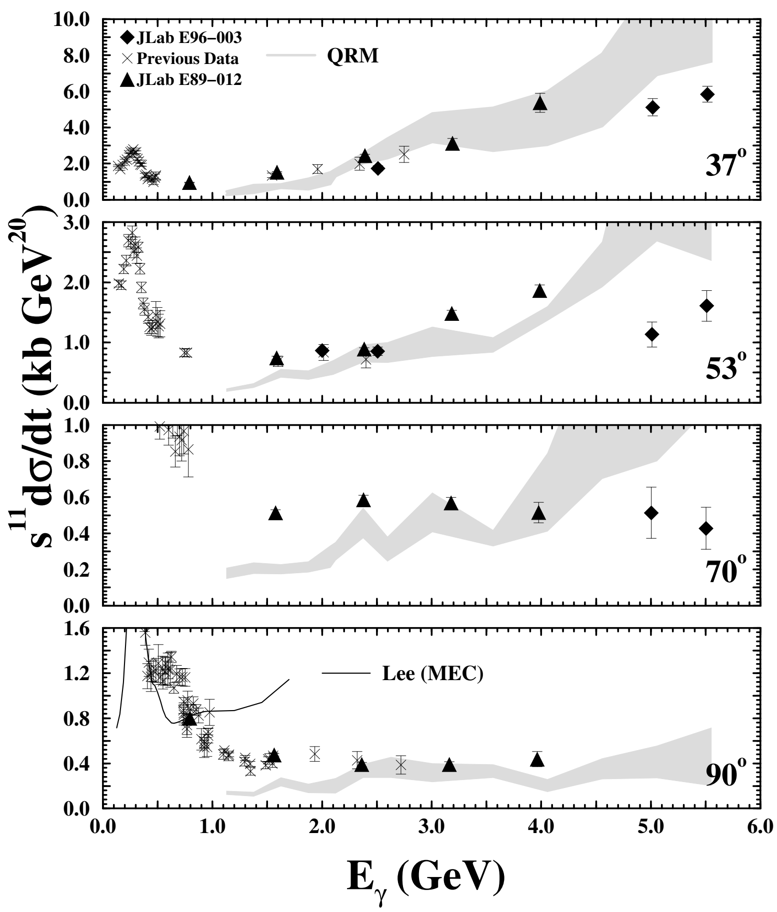

Figure 1: Data for deuteron photodisintegration as a function of the photon energy at four reaction angles. The darkened diamonds represent the E96-003 data. The darkened triangles represent the JLab E89-012 data [Bo98]. The crosses are all the other existing data [Ar84, Be95, Ch66, Cr96, Do76, Fr93, My61, Na88]. The solid line is a traditional meson-exchange calculation [Le88], and the shaded area is the quark rescattering model[Fr00]. These models have an absolute normalization. For the first time, evidence for scaling is observed at the forward reaction angles.

Ma73] predicts:

$$\frac{d\sigma}{dt} \propto s^{-11}. \tag{1}$$

This behavior has been observed at large angles, $\theta_{cm} = 70$ and $90°$ as shown in the figure. Here, $s^{11}d\sigma/dt$ is plotted as a function of E_γ. The new results [Sc01] shown as the diamonds in the figure are from experiment E96-003. These results indicate the first evidence for scaling at the forward angles and the highest energies. At 53° it appears that scaling sets in at photon energy of about 3 GeV, whereas at 37° there is the suggestion of scaling at 4 GeV. Because of the relatively large error limits and the relatively small energy region of the experiment, scaling cannot be claimed conclusively. An additional experiment which goes to higher energy would be necessary to confirm this surprising result.

The new quark rescattering model[Fr00] at the highest energy and especially at $\theta_{cm} = 53°$ is not in good agreement with the new data. Nevertheless the evidence for scaling at all the angles suggests that the GeV region is a "transition region" between meson-exchange models and pQCD.

References

[Ar84] J. Arends *et al.*,Nucl. Phys. A**412**, 509 (1984).

[Be95] J. E. Belz *et al.*, Phys. Rev. Lett.**74**, 646 (1995).

[Bo98] C. Bochna *et al.*, Phys. Rev. Lett.**81**, 4576 (1998).

[Br73] S. J. Brodsky and G. R. Farrar, Phys. Rev. Lett.**31**,1153 (1973).

[Br83] S. J. Brodsky and J. R. Hiller, Phys. Rev. C**28**, 475 1983.

[Ch66] R. Ching and C. Schaerf, Phys. Rev.**141**, 1320 (1966).

[Cr96] R. Crawford *et al.*, Nucl. Phys. A**603**, 281 (1996).

[Do76] P. Dougan *et al.*, Z. Phys. A**276**, 55 (1976).

[Fr00] L. L. Frankfurt *et al.*, Phys. Rev. Lett.**84**, 3045 (2000).

[Fr93] S. J. Freedman *et al.*, Phys. Rev. C**48**, 1864 (1993).

[Ho90] R. J. Holt, Phys. Rev. C**41**, 2400 (1990).

[Ko93] L. A. Kondratyuk *et al.*, Phys. Rev. C**48**, 2491 (1993).

[Le73] G. P. LePage and S. J. Brodsky, Phys. Rev. Lett.**31**, 1153 (1973).

[Le88] T.-S. H. Lee, Argonne National Laboratory Report No. PHY-5253-TH-88; T.-S.H. Lee, in *Proceedings of the International Conference on Medium and High Energy Nuclear Physics, Taipai, Taiwan, 1988* (World Scientific, Singapore, 1988), p.563.

[Ma73] V. Matveev *et al.*, Nuovo Cimento Lett.**7**, 719 (1973).

[My61] H. Myers *et al.*, Phys. Rev.**121**, 630 (1961).

[Na92] S. I. Nagornyi, YU. A. Kasatkin, and I.K. Kirichenko, Sov. J. Nucl. Phys. **55**, 189 (1992).

[Na88] J. Napolitano *et al.*, Phys. Rev. Lett.**61**, 2530 (1988).

[Sc01] E. Schulte *et al.*, preprint, 2000.

3.13 E97-006

Correlated spectral function and $(e, e'p)$ reaction mechanism

D. Rohe, I. Sick, Spokespersons
and
University of Basel, University of Hamptom, Jefferson Lab (Hall C), University of Virginia, Yerevan Physics Institute, Instituto Nazionale Fisica Nucleare Roma

3.13.1 Introduction

The purpose of experiment E97–006 is the measurement of the spectral function S(E_m,P_m) at high missing energy E_m and high missing momentum P_m. Assuming Plane Wave Impulse Approximation (PWIA), a direct measurement is possible via the (e,e'p) cross section, which factorizes into an e–p off shell cross section ([Fo83]) and the spectral function. Here the spectral function can be interpreted as the probability to find a proton with a certain E_m and P_m in the nucleus. For missing momenta less than the Fermi momentum of the nucleus ($\approx$ 250 MeV/c) and $E_m \leq 80$ MeV, the spectral function can be calculated via the Independent Particle Shell Model (IPSM). According to theory [Be94] the spectral function at high E_m, P_m (correlated region) is dominated by short–range correlations and is therefore of special interest. In this theory the spectral function was calculated for nuclear matter and extrapolated to nuclei of finite size using the Local Density Approximation (LDA).

To study the reaction mechanism, the experiment was performed both in parallel and perpendicular kinematics, where the initial momentum k_i of the nucleon inside the nucleus is parallel respectively perpendicular to the momentum transfer q. Because the Δ resonance as well as 2-body currents are of transverse character, it is believed that in parallel kinematics these processes will be suppressed. Further, from pure kinematical arguments it is clear that the (large) final momentum of the knocked-out proton is directly connected to a large initial momentum via p = k_i + q, whereas in the standard perpendicular or antiparallel kinematics the same final momentum can occur due to smaller initial momenta plus

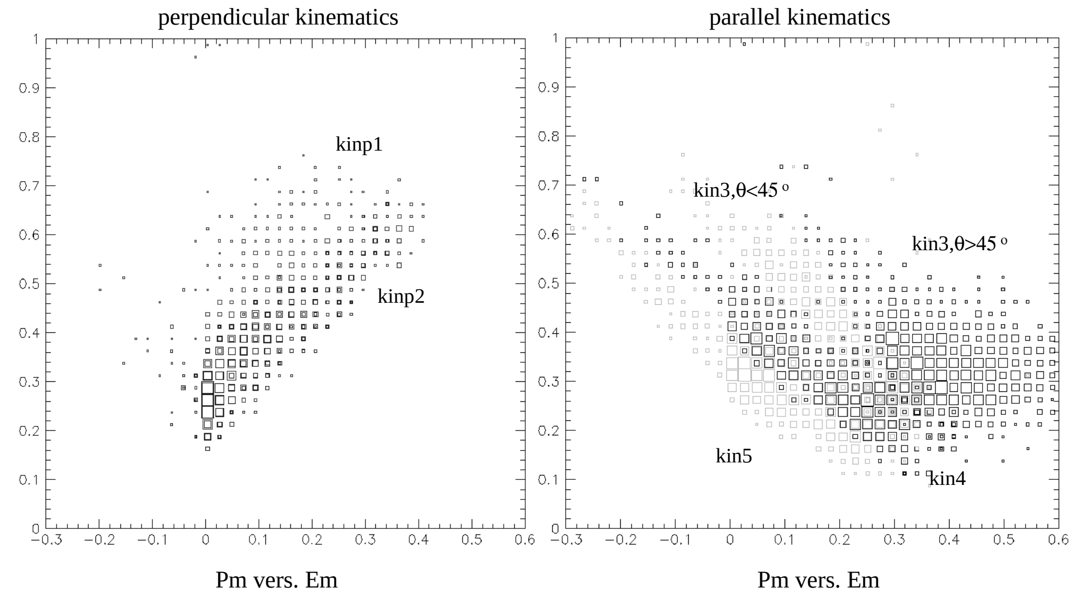

Figure 1: Covered P_m-E_m range of E97-006. Because there is no accidental subtraction applied, a substantial yield at negative E_m appears. The angle θ refers to the one between $\vec{k_i}$ and $\vec{q}$.

multiple scattering. These contributions then overwhelm the cross section due to the much larger spectral function. From this one concludes, that multistep processes are suppressed in parallel kinematics.

3.13.2 Experiment Status

The experiment was performed in summer of 1999 using the 3.2 GeV electron beam at TJNAF with a current between 10 to 60 μA. As targets C, Al, Fe and Au were used. The scattered electrons were detected in HMS and the protons in SOS in coincidence. Data were taken in three parallel and two perpendicular kinematics. The covered range in E_m, P_m is shown in Fig. 1. In addition to H_2–data for calibration purposes, data in quasi elastic kinematics at C were taken.

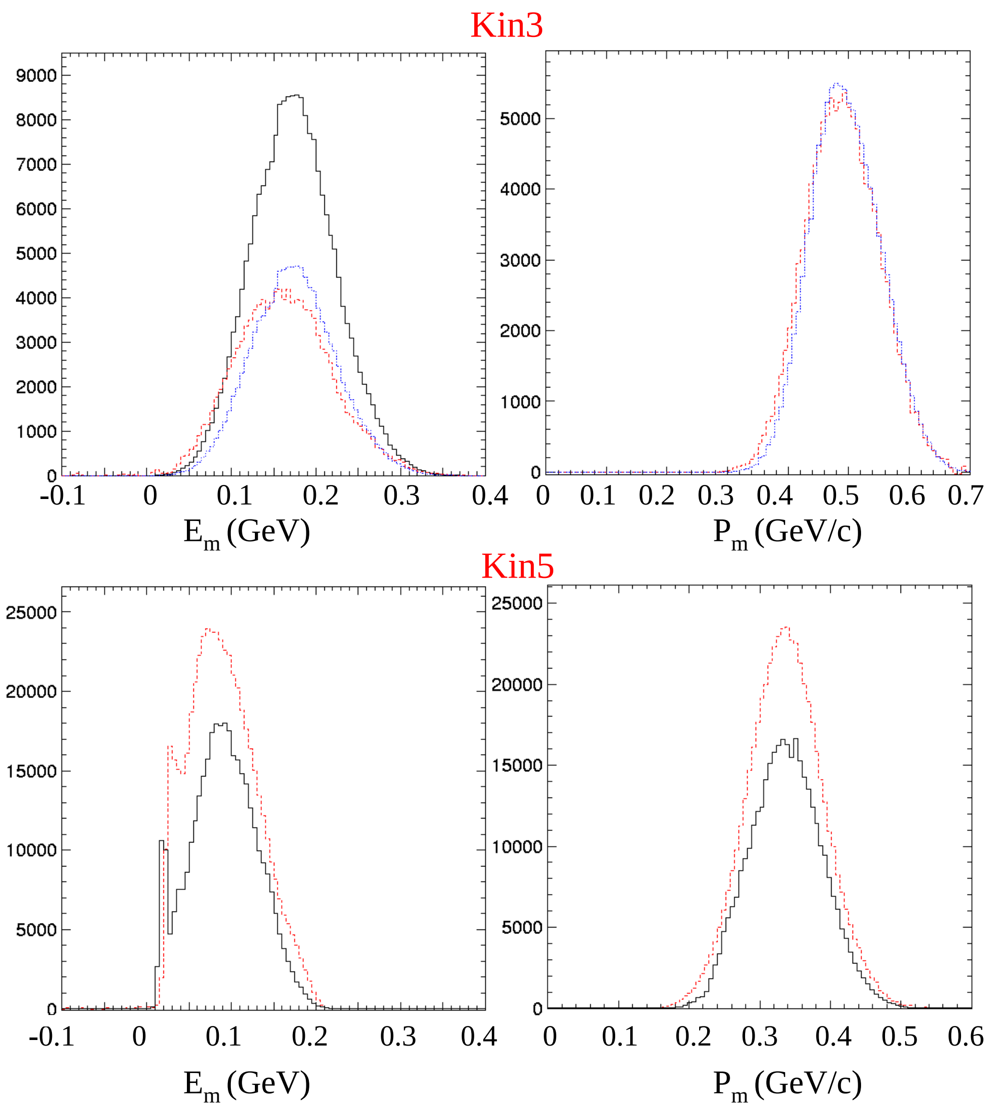

Figure 2: Comparison between the experimental yield (dashed) and the one obtained by the Hall C Monte Carlo simulation using the spectral function of O. Benhar (solid). Multiplying the yield based on the theoretical prediction with a "normalization" factor of 0.55 leads to the dotted curve. The "Δ-cut" (s. text) was applied to the data.

3.13.3 Preliminary Results

Comparing the yield obtained from quasi elastic scattering at C with the one predicted by the IPSM leads to the expected result: around 20 % of the yield is spread over the correlated region, which is not described in the IPSM. The spectral function is extracted from the data binned in (E_m, P_m) and corrected for radiative processes, which lead to events radiated in and out of a given (E_m, P_m) bin. The resulting spectral function is fed into the Monte Carlo simulation and after some iteration processes agreement between data and Monte Carlo spectra is obtained. The kinematics analyzed so far are kin3 and kin5. Especially kin3, where the correlated region covers a range of $0.3 < P_m < 0.7$ GeV/c, is influenced by the Δ- -resonance. The latter dies out with increasing missing momentum. It can —to some extent– - be separated from the correlated region by exploiting the fact that the Δ–region appeares at higher $\theta(\vec{k}, \vec{q})$ with respect to P_m than events belonging to the correlated region ("Δ-cut"). This is done in Fig. 2. Some features are remarkable: In the region of large $P_m (> 400$ MeV/c) the theory of [Be94] exceeds the data by a factor ≈ 2. In addition the average missing energy as well as the maximum of the spectral function with respect to E_m is shifted to lower E_m in the experiment. This means that the maximum of the spectral function does not appear at $\mathrm{E}_m = \mathrm{P}_m{}^2/(2M)$, where it is expected for pure short range correlations between two nucleons in the nucleus. The difference between theory and experiment increases with growing P_m. Going to lower P_m (< 400 MeV/c) the theory underestimates the data by a factor of 1.5. Despite this, the shape of the P_m-distribution is in both cases in good agreement with theory.

References

[Fo83] T. de Forest, Nucl. Phys. **A 392**, 232(1983)

[Be94] O. Benhar *et al.*, Nucl. Phys. **A579**, 493(1994)

3.14 E93-021

The Charged Pion Form Factor
H.P. Blok, G.M. Huber, and D.J. Mack

3.14.1 Introduction

Electromagnetic form factors are an excellent meeting place between experiment and theories of hadron structure. They also have a simple physical interpretation: for example, the charge form factor is the Fourier transform of the charge distribution. Of the experimentally accessible electromagnetic form factors of elementary hadrons, $F_\pi(Q^2)$, the charged pion form factor, stands out because the asymptotic normalization of the charged pion wave function is known from pion beta decay. Hence, there is an *absolute* prediction for F_π in the pQCD limit. Furthermore, because the charged pion contains only two valence quarks, the pQCD limit should be approached at relatively low Q^2. This means that NLO or NNLO calculations may eventually be directly comparable to data from an upgraded (12 GeV) JLab.

Due to the lack of a practical free pion target it is necessary, except at low Q^2, to use the virtual pions in the field of the proton. The longitudinal response at small $-t$ in $p(e,e'\pi^+)n$ is dominated by pion exchange and proportional to F_π^2. Using this technique, our collaboration studies $F_\pi(Q^2)$ at JLab at the highest feasible values of Q^2. Experiment 93-021 was the first phase in this program. Utilizing the maximum beam energy of 4 GeV available in 1997, we were able to perform measurements over the Q^2 range 0.5-1.6 (GeV/c)^2.

3.14.2 Preparations, Data Taking, and Status

Since control of systematic errors and Hall efficiency were important to us, the collaboration attempted to ensure that the detectors and magnets were in good working order and well understood and calibrated before the experiment. The collaboration replaced an inefficient mirror in the SOS gas cerenkov, had the HMS wire chambers rebuilt, gain-matched all the scintillating hodoscope channels, moved the HMS HV crates for easier access and added neutron shielding to reduce radiation damage. The 3C arc magnet power supply calibration was verified, and the arc magnets were put on the same hysteresis loop as the Accelerator Division field maps. Hall probe measurements by us before the run identified nonlinearities in the HMS quadrupole setting due to the neglect of residual fields; we modifed the HMS field setting program to take this into account. Cycling procedures for the HMS magnets were established. The largest configuration change was to pull the HMS quadrupole string back to achieve a smaller central angle of 10.5 degrees. A new collimator was installed and the new HMS optics matrix elements were determined. We also determined new optics matrix elements for the SOS, taking special care to account for saturation effects. Finally, we assisted Steve Wood in implementing the first use of an electronic logbook in Physics Division.

We successfully completed data taking for 93-021 in our first and only run in November-December 1997. Data were not only taken on Hydrogen but also on Deuterium for the purpose of reaction mechanism tests. A minor problem during the run was that the ESR was unable to provide sufficient cooling to operate both Hall A and Hall C cryotargets at the requested luminosities. More serious was the problem of radiation damage to equipment which had accumulated during the many months of high luminosity running of the previous experiment: the HMS quadrupoles' quench protection system was hypersenstive, tripping them off with virtually every angle and momentum change; and the VESDA system repeatedly shut down all detector power until the smoke sensor heads were replaced and properly calibrated. We were fortunately permitted to extend our final kinematic setting until nearly Christmas, marking the beginning of simultaneous 3 Hall operations at JLab.

3.14.3 Results

The data were analyzed at JLab, ODU, and the Vrije Universiteit. After reducing the data to separated differential cross sections $d\sigma/dt$, the longitudinal response $d\sigma_L/dt$ was compared to a recent Regge model of exclusive pion electroproduction.[1] This gauge-invariant model includes π-like and ρ-like Regge trajectories. For $d\sigma_L/dt$ at small $-t$ the ρ trajectory makes a negligible contribution, so $F_\pi(Q^2)$ can be determined as shown in Figure 1 from reference [2]. (Jochen Volmer received his Ph.D. for this work.[3]) Our values for F_π are far above

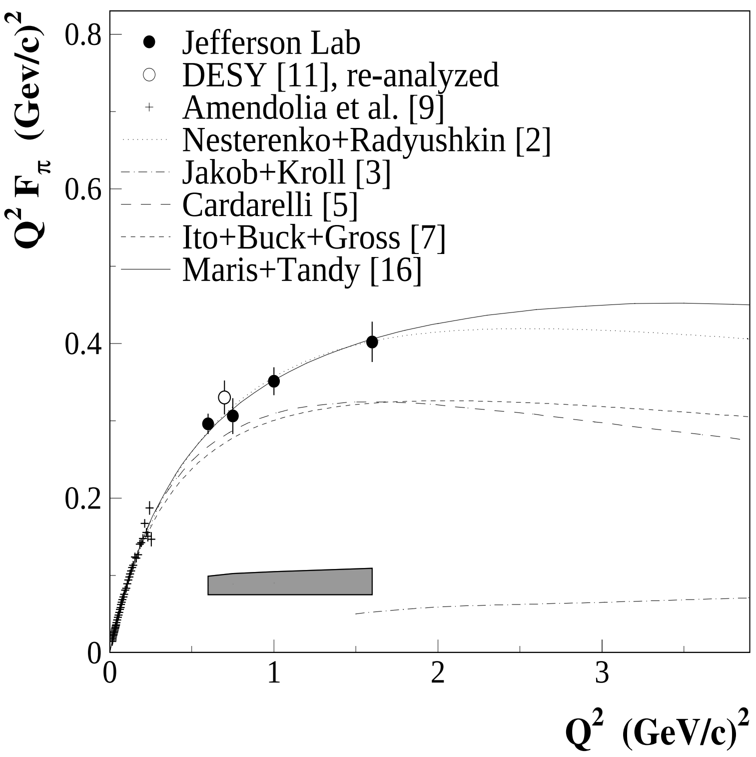

Figure 1: The modern F_π database, consisting of elastic $\pi + e$ measurements at low Q^2 from CERN and L-T separated pion electroproduction data from DESY and JLab at higher Q^2. From reference [2].

a pQCD calculation, and roughly double the prediction of an NLO pQCD calculation (not shown), highlighting the fact that at this Q^2 the soft contributions are still very important. Two calculations that include both soft and hard contributions[4, 5], and that were *not* fitted to the existing data set, describe our data quite well. The writing of a long paper has begun in which the experiment, data analysis, and cross sections will be discussed in detail.

We plan to finalize our results for the first ever *separated*, exclusive π^-/π^+ ratios on ^{2}H by early fall. These π^-/π^+ results highlight the different pion electroproduction reaction mechanisms in the longitudinal and transverse responses. The longitudinal ratios are consistent with pion pole dominance at small $-t$ (i.e., $\simeq 1$), a fact which helped guide our F_π analysis. The transverse response ratios are intriguing in that they show a rapid evolution with Q^2.

3.14.4 Upcoming Measurements

The Phase II F_π measurements in Experiment 01-004 were approved at PAC19 with A^- priority. Beam energies up to 5.25 GeV and the same HMS-SOS pair will be used. In this new experiment we will extend F_π to $Q^2 = 2.5$ (GeV/c)^2. A higher value of W will be used (2.22 GeV versus the previous 1.95 GeV), which has several benefits: it allows us to stay reasonably close to the pion pole at $Q^2 = 2.5$ (GeV/c)^2, and the model dependence of our F_π extraction via the Regge model may be smaller. To isolate the W dependence of the response functions, data will be taken at $Q^2 = 1.6$ (GeV/c)^2 at the higher value of W as well. Data for the separated π^-/π^+ ratio will also be taken. The experiment may be scheduled as early as the second half of 2002.

Longer term, no measurements above $Q^2 = 2.5$(GeV/c)^2 are possible until a new small angle, high momentum spectrometer companion to the HMS is built.

References

[1] M. Vanderhaeghen, M. Guidal, and J.-M. Laget, Phys. Rev. C **57** (1997) 1454; Nucl. Phys. **A627** (1997) 645.

[2] J. Volmer *et al.*, Phys. Rev. Lett. **86** 1713 (2001).

[3] Jochen Volmer, Ph.D. thesis, Vrije Universiteit, Amsterdam (2000), unpublished.

[4] V. A. Nesterenko and A. V. Radyushkin, Phys. Lett. **B115**, 410 (1982); A. V. Radyushkin, Nucl. Phys. **A532**, 141 (1991).

[5] P. Maris and P. C. Tandy, nucl-th/0005015